NGU Report 98.004
Onshore dating of Late Paleozoic through Mesozoic activities on the eastern and western proto-North Atlantic margins

NGU
Norges geologiske undersøkelse
Geological Survey of Norway

Postboks 3006 - Lade
7002 TRONDHEIM
Tlf. 73 90 40 11
Telefaks 73 92 16 20

REPORT

Report no.: 98.004	ISSN 0800-3416	Grading: Open

Title:
Onshore dating of Late Paleozoic through Mesozoic activities on the eastern and western proto-North Atlantic margins

Author: Elizabeth A. Eide & Trond H. Torsvik	Affiliates: Mobil, NFR, OD, Phillips, Statoil & UiO
County: Hordaland & Akershus	Kommune:
Map-sheet name (M=1:250.000)	Map-sheet no. and name (M=1:50.000)
Deposit name and grid-reference:	Number of pages: 134 Price: NOK 194,- Map enclosures:

Fieldwork carried out: 1996 and 1997	Date of report: 27.01.98	Project no: 2671.00	Person responsible:

Summary:

This report compiles results from six separate studies linked by the common fact that they address absolute dating of initiation and reactivation of brittle faults, dike emplacement and regional unroofing around the North Atlantic margin. The results from the study areas, western Norway, East Greenland and the Oslo Rift region, clearly demonstrate mutual and specific tectonic associations for the Late Paleozoic and Mesozoic that were only previously inferred from available data. Precise age data show very connected and correlatable histories for these marginal proto-North Atlantic zones for early Carboniferous, Permian, early Triassic and middle Jurassic times. These regions have been cited in the literature for their import in constraining offshore tectonic and basin development, but the new data provide, for the first time, very quantitative results to pinpoint and interpret these events.

The significant highlights include: 1) in East Greenland, the dating (paleomagnetic and ^{40}Ar-^{39}Ar) of Early Carboniferous lavas in previously 'Devonian' sedimentary basins; 2) in western Norway, the identification and quantification of a rapid cooling/unroofing event of latest Devonian-early Carboniferous age; 3) in western Norway, new ^{40}Ar-^{39}Ar age dating and re-classification of dike emplacement to distinct intervals in the Early Triassic and Middle Jurassic; 4) in western Norway, the dating, via paleomagnetic and ^{40}Ar-^{39}Ar methods, of two generations of brittle fault movements (Late Permian and Middle Jurassic ages); 5) also in western Norway, paleomagnetic dating of dikes yielding Late Permian poles that very closely correspond to the Late Permian poles for brittle fault movments in (4); 6) in the northern Oslo Rift region, identification and dating of the youngest (Early Triassic) dikes in the Oslo Graben and definition of slight apparent polar wander for Baltica from Permian through E. Triassic times.

Keywords: Western Norway	^{40}Ar-^{39}Ar geochronology	Paleomagnetics
East Greenland	Brittle faults	Dikes
Jurassic	Triassic	Carboniferous

CONTENTS

PREFACE

The interconnectedness of tectonic 'events' around the North Atlantic margin has been noted and discussed in both the onshore and offshore literature. Thus, the attempt to link tangible and visible onshore basin geometries, faults and extension-related dikes to their offshore counterparts is not new, but the degree to which these attempts have been based in quantitative facts is quite variable.

This report brings together six smaller 'chapters' each of which addresses a different aspect of the Late Paleozoic and/or Mesozoic history of part of the proto-North Atlantic margin. The studies were conducted in widely different areas (E. Greenland, western Norway, and the Oslo Rift region) but have revealed remarkably compatible, and some previously unknown, histories for various periods of the Late Paleozoic and Mesozoic evolution of the region. The work in this report represents the compiled onshore geologic work conducted during the course of this project and includes work/collaboration with the University of Oslo (Torgeir B. Andersen, Ebbe Hartz and Arild Andresen). The results here have, in various ways, been incorporated in the work/interpretations of the other reports in this series, both on- and offshore.

In western Norway, the literature had documented multiple faulting episodes, occurring in the ductile regime during exhumation of subducted Caledonian rocks, and subsequently, in the brittle regime as many of these earlier faults were transgressed and/or reactivated. The timing of these multiple faulting episodes has been somewhat open to interpretation, largely because of the technical difficulties in obtaining ages from fault rocks that have experienced several phases mechanical and chemical alteration. The **first chapter**, *'Absolute dating of brittle fault movements...'* (Eide et al., 1997) adresses absolute dating of brittle fault movements on the Dalsfjord fault in Sunnfjord, western Norway.

The study used a combination of paleomagnetic and ^{40}Ar-^{39}Ar dating techniques on two generations of brittle faults and obtained Late Permian (248-260 Ma) and Jurassic-Cretaceous (<163 Ma) ages for these fault activities. The resulting products were distinct, well-indurated fault breccias along, and partly cross-cutting, the older Dalsfjord fault. The latter is a feature that probably originated during extensional collapse of the western Norway region during and

immediately after Caledonian collision between Baltica and Laurentia. The complementary data we obtained for these younger brittle faulting events from the two dating techniques are useful because they allow us to locate western Norway (and Baltica) in both time and paleogeographic coordinates during the Late Paleozoic and middle Mesozoic.

Although brittle faults and fault breccias are appropriate to document dominantly extensional (or transtensional) movements in upper crustal levels, dikes can also be indicative of both paleostress environments and of the nature, timing and extent of an extensional 'episode'. When precise ages are combined with paleomagnetic poles derived from the same dikes, the resulting plate reconstructions can yield specific 'snapshots' of paleogeography and constrain the apparent polar wander paths for Late Palaeozoic and Mesozoic Euramerica as Pangea spasmodically stretched and eventually disaggregated.

In western Norway, several different occurrences of dikes had been mapped, analyzed and/or dated (e.g. Færseth et al., 1976, Skjerlie and Tysseland, 1981, Furnes et al., 1982 and Løvlie and Mitchell, 1982). These studies characterized at least one generation of continental tholeiitic basalt dikes within the nappes of western Norway (i.e. in the Sunnfjord area, between Nordfjord and Sognefjord) as well as a large group of NNW-to-N-trending alkaline dikes in the Sunnhordaland and Sotra areas (near Bergen). The emplacement ages of the dikes has remained somewhat enigmatic due either to evidence for chemical and/or mechanical alteration (in the case of some of the Sunnfjord dikes) or because of a fairly broad spread of K-Ar ages that did not immediately correlate with paleomagnetic data from the same rocks (in the case of the Sunnhordaland-Sotra dikes).

Chapters 2 and 3 of this report address the conundrums associated with these two groups of dikes in western Norway. Chapter 2, *'The age and tectonic significance of dolerite dykes in western Norway'*, (Torsvik et al., 1997) is a paleomagnetic study of the Sunnfjord dikes. The new data documented a Late Permian (250-270 Ma) emplacement/crystallization age for these dikes, previously assumed to be Devonian or older. Furthermore, the study showed the 'relative' dating power of dikes: the N-trending dikes intrude in an area complicated by younger E-W faults. The dikes show evidence for mild remagnetization in middle Mesozoic time; the degree of remagnetization increases with proximity of the dikes to the E-W faults

and thus constrains some fault motion to *post-date* Late Permian dike intrusion (i.e. probably of middle Mesozoic age). Connections between these younger faults and features traceable offshore are the subjects of discussion by Smethurst (1998).

On a similar track, Chapter 3 summarizes new ^{40}Ar-^{39}Ar age data from the Sunnhordaland and Sotra dikes in western Norway. These dikes intruded fairly pervasively during what was previously interpreted to be at least three pulsed, extensional episodes spanning from Late Carboniferous through to Middle Jurassic time. Our new isotopic data supplant this previous range of K-Ar ages from the rocks and confine dike emplacement to a brief interval in earliest Triassic and another in Middle Jurassic times.

The details in **Chapter 4**, '*The Oslo Rift: New paleomagnetic and $^{40}Ar/^{39}Ar$ constraints*' (submitted to *Geophysical Journal International* by Torsvik et al.), follow directly upon the results obtained from the Sunnhordaland-Sotra region and the brittle reactivation of the Dalsfjord fault. The initial research in this area was conducted in an effort to constrain some of the paleomagnetic information from the northern Oslo Rift region; the northern area was presumed less likely to have been affected by the reheating-remagnetization effects of the multiple intrusive pulses of Carboniferous-Permian ages further south in the Oslo Graben.

The dikes and the host limestones into which they intruded were dated paleomagnetically, and the dikes were then also dated with the ^{40}Ar-^{39}Ar method. The paleomagnetic data (pole) for these northern dikes was different from those obtained for the majority of Carboniferous-Permian intrusives further south in the Oslo Rift. ^{40}Ar-^{39}Ar dating of these dikes yielded concordant ages (overlapping between 238 to 246 Ma). The difference in pole positions between the northern dikes and the Carboniferous-Permian plutonic rocks in the remainder of the Oslo Graben could thus be attributed to slight apparent polar wander (APW) of the Oslo region between Carboniferous-Permian time to the Early Triassic. These dikes are the youngest recorded from the Oslo Rift region and correspond very well both to the ages from Sunnhordaland-Sotra dikes and the timing of the earliest brittle faulting event in the Dalsfjord area. Thus, the combination of data represent a picture of widespread and synchronous extension around the southern and western margins of Norway in latest Permian and early Triassic time.

Chapters 5 and 6 take the tectonic sequence further back in time to the Devonian and Early Carboniferous. The studies are illustrative in that the resulting data document a very early extensional phase, with some block uplift, immediately after the extensional collapse of the orogen and preceding amalgamation of Pangea. In Chapter 5, '*Early Carboniferous unroofing in western Norway and alkali feldspar thermochronology*' (Eide et al., in prep.), the special focus is on ^{40}Ar-^{39}Ar thermochronology of alkali feldspars taken from a profile through the main Nordfjord-Sogn extensional detachment zone in western Norway. The cooling histories for the feldspars, obtained by application of thermochronologic modelling of the Ar-data, are consistent in their recording a rapid cooling event in Early Carboniferous time (340-360 Ma) in the area. The high cooling rate, >15 cm/yr, recorded by the feldspars in these rocks had to be induced by some form of rapid block uplift in the area ('unroofing'). The unroofing 'event' itself probably occurred slightly prior to the actual cooling (due to time delay associated with relaxation of thermal gradients), and so could be as old as latest Devonian in age. The results suggest regional folding (inversion) in western Norway as causes for such pervasive unroofing of this area.

In a very related time period, **Chapter 6** '*Carboniferous ages for the East Greenland 'Devonian' basin...*' (Hartz et al., 1997) describes an exciting and rather controversial discovery in the Late Paleozoic sections of the E. Greenland basins. Hartz et al. again utilized a combination of paleomagnetics and ^{40}Ar-^{39}Ar geochronology to investigate a series of lavas in a section of the basins previously mapped as only 'Devonian'. Their paleomagnetic data from a stratigraphic seciton in a faulted basin indicate that the two stratigraphically lowermost intrabasinal angular unconformities are in fact, only one unconformity. This discovery reduced estimates of sediment thickness by ca. 2 km. Furthermore, the radiometric data from the lavas yielded Early Carboniferous (330-340 Ma) ages for rocks that overlie fossils previously considered Upper Devonian in age! These results trigger a need for complete joint stratigraphic, structural and geochronologic re-examination of these basins, especially since these rocks are used as templates to interpret offshore seismic data sections. The Early Carboniferous lavas could be related to crustal thinning and extension of similar age found in Spitsbergen and Scotland-Shetland, and are very close in time to the unroofing event (extension-related?) newly identified in western Norway (Chapter 5).

Although these six chapters do not propose a new concept by proposing onshore data/interpretations to interpret offshore features, they do provide some strikingly correlative and quantitative new data linking disparate regions through time. The amalgamation of Euramerica and eventually Pangea, as well as the subsequent dismemberment of Pangea, are thus seen to develop progressively through a series of distinct extension-related events of Early Carboniferous, Late Permian-Early Triassic and Middle Jurassic ages.

Trondheim, 25.01.98

Elizabeth Ann Eide
Senior Geologist (NGU)

Trond Helge Torsvik
Senior Geophysicist (NGU) and
Professor of Geodynamics (UiB)

SELECTED REFERENCES

Eide, E.A., Torsvik, T.H. & Andersen, T.B. (1997) Absolute dating of brittle fault movements: Late Permian and late Jurassic extensional fault breccias in western Norway. *Terra Nova* 9, 135-139.

Eide, E.A., Torsvik, T.H., Andersen, T.B. & Arnaud, N.A. (in prep.) Early Carboniferous unroofing in western Norway and alkali feldspar thermochronology.

Furnes, H., Mitchell, J.G., Robins, B., Ryan, P. & Skjerlie, F.J. (1982) Petrography and geochemistry of peralkaline, ultrapotassic syenite dykes of Middle Permian age, Sunnfjord, West Norway. *Norsk Geol. Tidsskr.* 62, 147-159.

Færseth, R.B., Macintyre, R.M. & Naterstad, J. (1976) Mesozoic alkaline dykes in the Sunnhordaland region, western Norway: ages, geochemistry and regional significance. *Lithos* 9, 331-345.

Hartz, E.B., Torsvik T.H. & Andresen A. (1997) Carboniferous age for the East Greenland 'Devonian' basin: Paleomagnetic and isotopic constraints on age, stratigraphy, and plate reconstructions. *Geology* 25, 675-678.

Løvlie, R. & Mitchell, J.G. (1982) Complete remagnetization of some Permian dykes from western Norway induced during burial/uplift. *Phys. Earth Plan. Int.* 30, 415-421.

Skjerlie, F.J. & Tysseland, M. (1981) Geochemistyr and Petrology of Dolerite Dykes of Probable Late Caldeonian age from the outer Sunnfjord region, West Norway. *Norges geol. unders. Bull.* 363, 25-43.

Smehurst, M.A. (1998) *Onshore-Offshore tectonic links in western Norway: An interpretation of magnetic and gravity fields.* NGU Report no. 98.006, 81 pages.

Torsvik, T.H., Andersen, T.B., Eide, E.A. & Walderhaug, H. (1997) The age and tectonic significance of dolerite dykes in western Norway. *J. Geol. Soc. Lond.* 154, 961-973.

Chapter 1

Published as:

Absolute dating of brittle fault movements: Late Permian and late Jurassic extensional fault breccias in western Norway

Eide, E.A., Torsvik, T.H. & Andersen, T.B.

in *Terra Nova* v. 9, pp. 135-139, 1997.

Absolute dating of brittle fault movements: Late Permian and late Jurassic extensional fault breccias in western Norway

Elizabeth A. Eide[1]*, Trond H. Torsvik[1,2] and Torgeir B. Andersen[3]

[1]*Geological Survey of Norway, PO Box 3006 Lade, N-7002 Trondheim, Norway,* [2]*Department of Solid Earth Physics, University of Bergen, N-5002 Bergen, Norway,* [3]*Department of Geology, University of Oslo, PO Box 1047 Blindern, 0316 Oslo, Norway*

ABSTRACT

$^{40}Ar/^{39}Ar$ geochronological and palaeomagnetic dating methods applied to fault breccias in western Norway have isolated two brittle reactivation episodes of the syn-post-Caledonian, extensional Nordfjord-Sogn Detachment. These events, of latest Permian and latest Jurassic–Early Cretaceous ages, demonstrate temporal relationships between development of chemical remanent magnetism and partial resetting of Ar isotopic systems during distinct breccia-forming episodes. A third event of Carboniferous age was also identified in the breccias with the $^{40}Ar/^{39}Ar$ technique and is a relict unroofing signature inherited from the fault wall-rocks. These brittle faults are significant time markers and become relevant to interpretations of offshore seismic data which attempt to place ages on faults that have undergone multiple reactivation episodes.

Terra Nova, 9, 135–139, 1997

Introduction

The potential of fault rocks to delimit the timing of tectonic events has advanced significantly since the quintessential fault-rock classification schemes of Sibson (1977) and Wise *et al.* (1984). Various isotopic dating methods can be applied to fault rocks to generate absolute ages of fault genesis and have been used with some success on mylonitic rocks in ductile fault zones (Lee, 1991; House and Hodges, 1994) as well as on pseudotachylites (Kelley *et al.*, 1994). Brittle fault rocks, because of their low-temperature nature and associated, 'open system' behaviour, are probably more difficult to date accurately with isotopic methods (Gibbons *et al.*, 1996).

We have utilized two different dating techniques to constrain the ages of fault breccia genesis in a reactivated detachment zone in western Norway (Fig. 1). Brittle fault breccias are viable materials for palaeomagnetic determination of the age of a fault-rock matrix that acquired a low-temperature, chemical remanent magnetic (CRM) signature, or the age of breccia clasts from fault wall-rocks that have acquired a partial thermochemical remanent magnetic (TRM) resetting signature (Fig. 2). We have addressed the hypothesis that, with control provided by palaeomagnetic and regional geological data, the $^{40}Ar/^{39}Ar$ geochronological method can accurately identify ages of fault brecciation in this multiply reactivated fault zone.

The circumstances for dating these brittle fault rocks were ideal as we had excellent tectonostratigraphic control (Osmundsen and Andersen, 1994; Brekke and Solberg, 1987), a shallowly dipping fault breccia, clear cross-cutting relationships between the breccia and the extensional detachment, and K-feldspar-bearing units in both hanging wall and footwall. The rocks were previously dated palaeomagnetically (Torsvik *et al.*, 1992), but the relatively large uncertainties associated palaeomagnetic ages (*c.* $\pm$ 10 Myr) encouraged us to reanalyse this earlier dataset and apply an independent dating technique ($^{40}Ar/^{39}Ar$) to the same rocks. The data illustrate complementary and supplementary powers of the two techniques when utilized in well-documented tectonostratigraphic settings.

Geological background

The Caledonian history of western Norway involved arc- and continental-collision and high-ultrahigh-pressure (HP-UHP) metamorphism as Baltican crust subducted beneath Laurentia from $\approx$ 450–410 Ma (Cuthbert *et al.*, 1983; Smith, 1984; Eide and Torsvik,

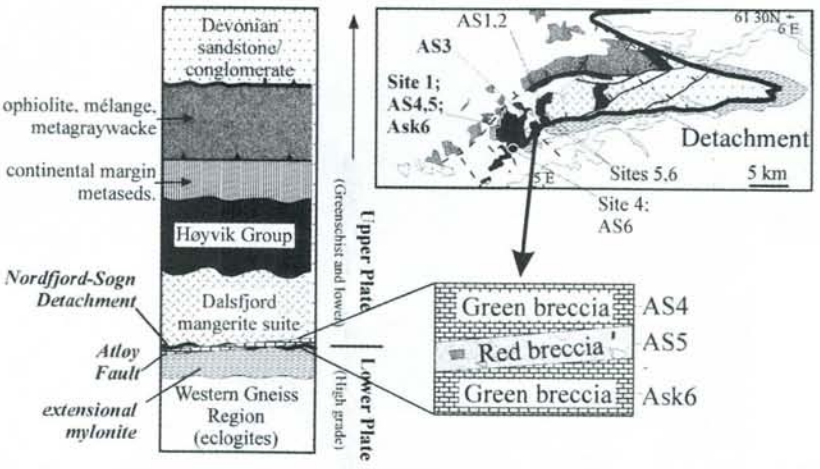

Fig. 1 Geological map and tectonostratigraphic column, modified after Osmundsen and Andersen (1994), showing relationships around the Nordfjord-Sogn Detachment (NSD) zone. High grade, eclogite-bearing basement of the Western Gneiss Region is overlain by weakly metamorphosed, allochthonous units with broadly Ordovician, white-mica cooling ages. On Atløy, the NSD was cut by two different brittle faults. Sample sites include those for $^{40}Ar/^{39}Ar$ dating ('AS' prefixes) and from the palaeomagnetic study of Torsvik *et al.* (1992) ('Site' prefixes).

Correspondence: Tel: + 47/73 90 4237; Fax: + 47/73 92 1620; E-mail: elizabeth.eide@ngu.no

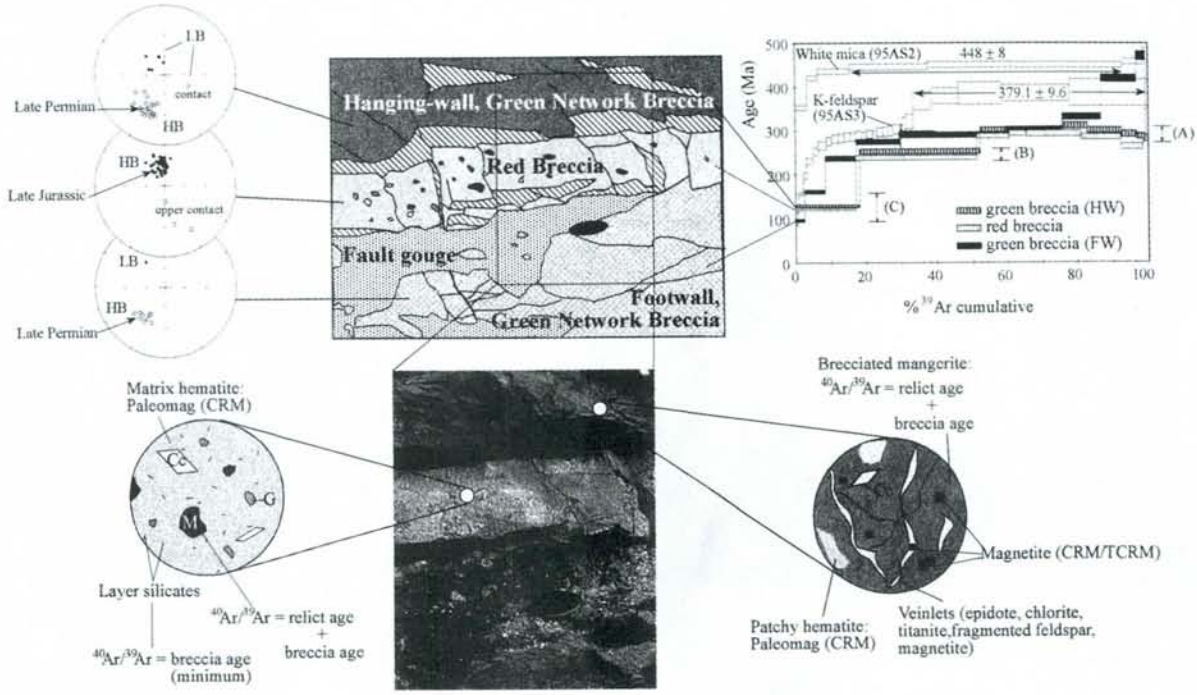

Fig. 2 Photograph and line drawing of the Atløy red and green fault breccias. Lower figure: application of the palaeomagnetic and ^{40}Ar/^{39}Ar dating techniques to fault rocks. Top left: HB and LB palaeomagnetic components from the three breccias. Note the dual polarity nature of the HB component in the red breccia. Top right: release spectra for the red and green breccias, a cycled, isothermal heating experiment from a mangerite feldspar, and white mica from the Upper Plate (see also Fig. 1). Age ranges (A), (B) and (C) correspond to separate thermochemical events (see text for details).

1996). Exhumation of deeply buried rocks by extensional collapse was accommodated by vertical shortening/horizontal stretching of the lower crust and large-scale, normal movement on a system of extensional detachments (Andersen and Jamtveit, 1990; Andersen *et al.*, 1991, 1994). Extensional shearing along the main Nordfjord–Sogn Detachment (NSD) is manifested as 2–3 km-thick extensional mylonites that juxtapose 'Lower Plate', eclogitic basement and 'Upper Plate', allochthonous rocks plus Devonian sedimentary basins (Fig. 1).

The NSD and extensional mylonite are folded (Roberts, 1983) and intersected by brittle faults, the most spectacular of which outcrops on the island of Atløy where a nearly flat-lying, fault-breccia zone cuts the NSD (Figs 1 and 2). The fault-breccia zone comprises a green network breccia and a cross-cutting red breccia. The latter is a 15–35 cm-thick package dipping $\approx 10°$ W and separates hanging wall (HW) from footwall (FW) green network breccias (Fig. 2) (Brekke and Solberg, 1987; Torsvik *et al.*, 1992). The HW green breccia reworked rocks of the Upper Plate Dalsfjord mangerite suite while the FW green breccia reworked both Upper Plate rocks and Lower Plate mylonites.

The nonbrecciated, Upper Plate, Dalsfjord mangerite-syenite contains microperthitic alkali feldspar, white mica, titanite, epidote, magnetite and ilmenite, orthopyroxene altered to chlorite, and minor calcite. The HW, green breccia comprises subangular feldspar clasts surrounded by veinlets with fine, feldspar fragments, chlorite, epidote, titanite, magnetite and fine, layer silicates (Fig. 2). The large clasts have subgrains and partially annealed fractures. The FW and HW green breccia are similar.

The red breccia comprises angular, mm- to cm-sized clasts in a fine-grained, brick-red matrix (Fig. 2). Rock clasts comprise greenish network-breccia fragments, calcite, minor layer silicates and oxides. Feldspar clasts occur either as masses of very fine, equigranular subgrains or coarse, twinned subgrain clusters, reminiscent of green-breccia clasts.

Summary of palaeomagnetic data

The magnetic mineralogies of both HW and FW green breccias comprise mainly magnetite, with accessory haematite and pyrrhotite. The FW breccia is dominated by high-temperature (HT) components with SSW declinations and negative inclinations (Fig. 2). This HT component, assigned a Late Permian age (250 Myr) by Torsvik *et al.* (1992), is sporadically overprinted by a younger, low-blocking (LB) component with NNW declinations and steep positive inclinations; the LB overprints are more pronounced in the HW than in the FW green breccia.

The red-breccia fabric is almost isotropic and has a haematite- and goethite-stained matrix with abundant pyrrhotite and accessory magnetite. NNW declinations with steep positive inclinations prevail (Fig. 2), but along the upper contact of the red breccia we notice a polarity shift; hence, cementation and fluid fluxes in the red breccia appear to cover a reversal of the Earth's magnetic field. The same LB (dual-polarity) component identified in the

green breccias is the principal high-blocking (HB) magnetization component in the younger red breccia; this HB component (Fig. 2) was assigned a late Jurassic–Early Cretaceous age (150 Myr) (Torsvik *et al.*, 1992). The stronger influence of LB components in the HW green breccia vs. the FW green breccia is attributed to expulsion of red-breccia fluids into the HW; the fluid infiltration is observed now as red patches in the upper green breccia close to the red-breccia contact. Analytical details, magnetic mineralogy and strain fabrics related to these palaeomagnetic data are presented in Torsvik *et al.* (1992).

$^{40}Ar/^{39}Ar$ data

We used furnace step-heating to analyse a red-breccia whole rock, HW and FW green-breccia whole rocks, K-feldspar clasts separated from the HW breccia, and white mica and K-feldspar separates from several Upper and Lower Plate units (Figs 1 and 2). Analyses were conducted at the Laboratoire de Géologie, Université Blaise Pascal et CNRS, Clermont-Ferrand, France with a protocol similar to Arnaud *et al.* (1993). Results and discussion of isothermal, cycled heating experiments and diffusion modelling of the K-feldspars will be presented elsewhere (Eide *et al.* in prep.). Ages are cited at the 1 σ confidence interval, with *J*-value error. Complete data tables are available from the authors.

Whole-rock fault-breccia data

The first two steps of the HW green-breccia spectrum comprise 52.2% of total $^{39}Ar_K$ gas and yield apparent ages of 129.5 ± 2.7 Myr and 253.2 ± 4.6 Myr, respectively (Fig. 2). The latter half of the spectrum gives a slightly disturbed group of semiconcordant steps with a weighted age of 296.2 ± 2.6 Ma (8 steps). Eleven steps from the FW green breccia define a pattern of ages which climb rapidly from 96.4 ± 2.5 Myr to a group of semiconcordant steps (steps 4 through 7; 58.4% of total $^{39}Ar_K$ gas) with a weighted age of 296.4 ± 2.8 Myr. Ages in the final 25% of the FW breccia spectrum climb rapidly to unrealistically high values (Fig. 2). The red-breccia release spectrum is identical to that of the HW green breccia and is characterized by an imprecise age of 286.6 ± 3.3 Myr in the upper temperature portion of the experiment (48.6% of gas, excluding the last step which comprised only air) and significantly younger first and second steps (122.2 ± 3.0 Myr and 238.3 ± 5.7 Myr) (Fig. 2).

The K/Ca ratios for the green HW and red breccias are similarly characterized by high initial values that drop and then climb in the higher-temperature portions of the experiments. K/Ca values drop again as the samples approach fusion (Fig. 3). The FW breccia exhibits a broadly similar pattern in the high-temperature, high-age steps, with a slightly lower initial K/Ca ratio compared to the other breccias. The Cl/K ratios for all three breccias are fairly low and exhibit a gradual increase through the high-age, high-temperature steps (Fig. 3).

Inverse isochron analysis of the red and HW green breccia data was not useful due to their highly radiogenic nature. Isochron analysis of the FW green breccia data clearly indicates excess Ar in the final four, high-temperature steps that yielded anomalously high ages.

White mica and K-feldspar

The spectrum for white mica from the Upper Plate Høyvik Group, overlying the mangerite, gives a plateau age of 448 ± 8 Myr (77% of $^{39}Ar_K$ released; sample AS2; Figs 1 and 2; Eide *et al.*, 1996). This age is within uncertainty of cooling ages from the same unit on Atløy and several other Upper Plate white micas (Andersen *et al.*, in press).

The spectra from isothermal, cycled heating experiments of K-feldspar separates from Upper and Lower Plate

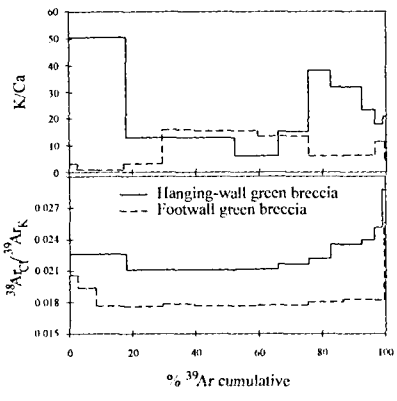

Fig. 3 K/Ca and $^{38}Ar_{Cl}/^{39}Ar_K$ ratios for whole-rock samples.

rocks (AS1, AS2, AS3, and AS6; Fig. 1) have identical release patterns, albeit with some intersample age differences related to partial, Late Permian resetting (Eide *et al.*, 1996; Eide *et al.* in prep.). An example spectrum (AS3), from immediately above the Atløy Fault defines three domains: a low-temperature domain of rapidly climbing ages (86.5–265.9 Myr), an intermediate-retentivity domain of semiconcordant-to-slightly increasing steps (292.6 ± 2.3 Myr, weighted age), and a high-temperature domain of concordant steps (379.1 ± 9.6 Myr, weighted age) (Fig. 2).

Discussion of $^{40}Ar/^{39}Ar$ data

The whole-rock spectra define three different age groups (ranges A, B and C, Fig. 2) corresponding to separate thermal episodes. Large volumes of Ar gas released in the whole-rock experiments resided in the K-feldspar clasts and distinguished inherited (relict, wall-rock) and new (brecciation-related) ages. Age range (A) (from ≈ 287 and 310 Ma) comprises the central group of semiconcordant ages in the FW breccia, the highest temperature portions of the HW green and red breccia spectra, and the intermediate domain in the K-feldspar (AS3). Age range (B) (from 238 to 253 Ma) represents a *minimum* resetting age and incorporates the second step in each of the red and HW green breccias, the concordant step from the FW breccia, and the downward cusp in the K-feldspar spectrum. Age range (C) (from 96 to 162 Ma) represents a *maximum* age range for the youngest resetting episode(s).

These three age groups document resetting of < 300 Myr old rocks (inherited age A) during one pervasive event older than 253 ± 5 Myr (the maximum of range B, Fig. 2). A less thorough resetting event, or events, occurred in sub-late-Jurassic times (range C, Fig. 2). The ages within (C) are indicative of partial Ar loss during at least two events: one more recent than 96 ± 3 Ma (perhaps associated with genesis of clay-rich fault gouge; see Fig. 2) and one event at least younger than 238 Ma and, most likely, younger than 163 ± 4 Ma (the maximum limit of range C). The latter event can be linked to the younger of two palaeomagnetic ages and probably dates the genesis of the red breccia (see 'Data comparison').

The higher, relative initial K/Ca ratios and low apparent ages in the first step of each whole-rock spectrum are attributable to outgassing of high-K phases with low Ar retentivity (Figs 2 and 3). The likely sources are fine-grained layer silicates in the rock matrices and low-retentivity, fine-grained portions of the K-feldspar clasts with some Cl-contribution from matrix chlorite. Genesis of the low-temperature layer silicates is linked to partial replacement of K-feldspar breccia clasts by quartz via the reaction:

$$6KAlSi_3O_8 + 4H_2O = 12SiO_2 + K_2Al_4(Si_6Al_2O_{20})[OH]_4 + 4KOH.$$

Thermal and diffusion modelling of the cycled, isothermal K-feldspar heating experiments from Upper and Lower Plates suggests that the Late Carboniferous age (≈ 287–310 Ma) of range (B) represents partial resetting of an early Carboniferous (350 Ma), rapid cooling event (Eide *et al.*, 1996). The high-retentivity portion (≈ 379 Ma) of the single-grain, K-feldspar experiment (Fig. 2) is neither present in the whole-rock experimental data nor in an analysed separate of K-feldspar HW clasts; the HT feldspar domain was destroyed during younger, grain-size reduction/brecciation events.

Data comparison and synopsis

Figure 4 synthesizes the $^{40}Ar/^{39}Ar$ and palaeomagnetic fault-rock ages in the context of an annotated Mid-Palaeozoic to Cretaceous apparent polar wander path (APWP) for Baltica/Europe. Group (B), whole-rock $^{40}Ar/^{39}Ar$ ages corroborate Late Permian, green-breccia palaeomagnetic ages of Torsvik *et al.* (1992) and fit closely to the APWP age of 260 Myr. The Late Permian palaeomagnetic age is interpreted as the time of CRM remanence acquisition during green-breccia formation at temperatures < 250 °C (Torsvik *et al.*, 1992) (Figs 2 and 4); the group (B) $^{40}Ar/^{39}Ar$ data document a strong resetting event older than 253 ± 5 Ma. The green-breccia forming event is thus constrained between ≈ 248 and 260 Ma. Regionally, extension-related dykes in western and southwestern Norway overlap in time with green breccia formation (Fig. 4; see also Torsvik *et al.*, in press).

Similarly, the palaeomagnetic data from the red breccia fall near the 98–144 Ma pole for Europe and overlap with data from extension-related dykes (Hinlopen) from Svalbard (Fig. 4). Torsvik *et al.* (1992) suggested the red-breccia data documented genesis of a late Jurassic, HB component, related to CRM acquisition during low-temperature haematite precipitation and red-breccia formation. Confidence in the red-breccia palaeomagnetic pole position is imparted by the dual-polarity nature of the HB component in the rock (LB component in the green breccia). The Group (C), whole-rock $^{40}Ar/^{39}Ar$ data constrain red-breccia genesis to be more recent than 162 Ma, with unique definition of the red-brecciation phase complicated by fault-gouge genesis after 96 Ma. The late Jurassic–Early Cretaceous age for red-breccia formation is likewise coincident with regional rifting and basin formation in the northern North Sea (Torsvik *et al.*, 1992; Færseth, 1996).

The fact that the HB component is only weakly developed in the HW green breccia (extracted as the LB component from the rock; see Fig. 2), and is nearly undeveloped in the FW green breccia, is due to the nearly horizontal orientation of the Dalsfjord Fault: warm fluids flowing through a fracture with this orientation would probably have percolated preferentially *upwards*, leaving very little haematite precipitate in the FW breccia. This implies that the Dalsfjord Fault orientation has not changed (rotated) significantly since the Early Cretaceous and again, reinforces the position of the red-breccia pole in Fig. 4.

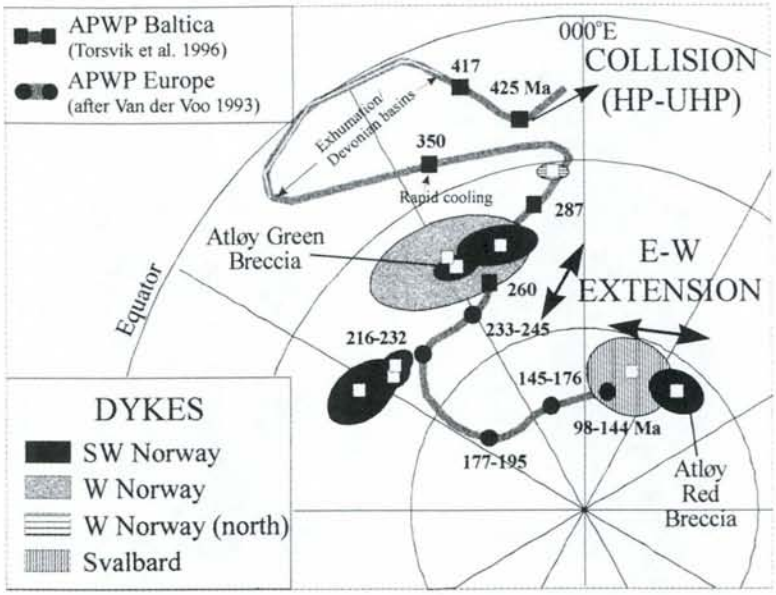

Fig. 4 Synopsis of palaeomagnetic and $^{40}Ar/^{39}Ar$ data on an annotated APWP for Baltica/Europe. Dark squares and circles on the APWP and adjacent numbers correspond to pole ages in Myr (after Torsvik *et al.*, 1996 and Van der Voo, 1993).

Of the two brittle faulting events, the latest Permian, green-breccia-forming episode was dominant. The magnetic component is unblocked only at high temperatures in both HW and FWs, and the most dramatic impact on the Ar-systematics of the whole-rock systems was effected during the green-brecciation activity. The magnitude of this latest Permian event takes on regional significance not only from broad inferences to early rifting events along the Baltica–Laurentia suture (e.g. Færseth, 1996), but even more directly from the numerous Late Permian mafic dykes exposed along the coast of western Norway (Fig. 4; Torsvik *et al.*, in press).

The common denominator in the brittle fault activity was infiltration of low-temperature fluids and cataclastic activity, manifested both as CRM signatures and Ar-resetting ages. We cannot state with absolute certainty that the Ar ages accurately date the time of CRM acquisition, given the fact that these two age-dating techniques are dependent upon very different properties of mineral systems; however, we emphasize that the palaeomagnetic and Ar data are remarkably consistent with one another and also with constraints provided by regional geology.

Acknowledgements

The authors thank Nicolas O. Arnaud for a very thorough review of an early version of the manuscript and two anonymous reviewers for useful comments. Research was supported by cooperative Mobil-Phillips-Statoil-NGU-NFR project funding to the authors and by a Nansen Fund grant and U.S.-Norway Fulbright Fellowship to EAE. This constitutes ONOFF contribution no. 2.

References

Andersen, T.B., Berry IV, H.N., Lux, D.R. and Andresen, A., 1997. The tectonic significance of pre-Scandian $^{40}Ar/^{39}Ar$ phengite cooling ages in the Caledonides of Western Norway. *J. Geol. Soc. London*, in press

Andersen, T.B. and Jamtveit, B., 1990. Uplift of deep crust during orogenic extensional collapse: A model based on field studies in the Sogn-Sunnfjord region of Western Norway. *Tectonics*, **9**, 1097–1111.

Andersen, T.B., Jamtveit, B., Dewey, J.F. and Swensson, E., 1991. Subduction and eduction of continental crust: major mechanisms during continent-continent collision and orogenic extensional collapse, a model based on the south Norwegian Caledonides. *Terra Nova*, **3**, 303–310.

Andersen, T.B., Osmundsen, P.T. and Jolivet, L., 1994. Deep crustal fabrics and a model for the extensional collapse of the Southwest Norwegian Caledonides. *J. Struct. Geol.*, **16**, 1191–1203.

Arnaud, N.O., Brunel, M., Cantagrel, J.M. and Tapponier, P., 1993. High cooling and denudation rates at Kongur Shan, eastern Pamir (Xinjiang, China) revealed by $^{40}Ar/^{39}Ar$ alkali feldspar thermochronology. *Tectonics*, **12**, 1335–1346.

Brekke, H. and Solberg, P.O., 1987. The geology of Atløy, Sunnfjord, western Norway. *Nor. Geol. U. Bull.*, **410**, 73–94.

Cuthbert, S.J., Harvey, M.A. and Carswell, D.A., 1983. A tectonic model for the metamorphic evolution of the Basal Gneiss Complex, Western South Norway. *J. Metamorph. Geol.*, **1**, 63–90.

Eide, E.A. and Torsvik, T.H., 1996. Palaeozoic supercontinental assembly, mantle flushing, and genesis of the Kiaman Superchron. *Earth Planet. Sci. Lett.*, **144**, 389–402.

Eide, E.A., Torsvik, T.H. and Andersen, T.B., 1996. Precise timing of multiple reactivation events on a Caledonian extensional detachment, Western Norway: What happens after exhumation? (abs.). *EOS, Trans. Am. Geophys. Un.*, **77**(46), F779.

Færseth, R.B., 1996. Interaction of Permo-Triassic and Jurassic extensional fault-blocks during the development of the northern North Sea. *J. Geol. Soc. London*, **153**, 931–944.

Gibbons, W., Doig, R., Gordon, T., Murphy, B., Reynolds, P. and White, J.C., 1996. Mylonite to megabreccia: Tracking fault events within a transcurrent terrane boundary in Nova Scotia, Canada. *Geology*, **24**, 411–414.

House, M.A. and Hodges, K.V., 1994. Limits on the tectonic significance of rapid cooling events in extensional settings: Insights from the Bitterroot metamorphic core complex, Idaho-Montana. *Geology*, **22**, 1007–1010.

Kelley, S.P., Reddy, S.M. and Maddock, R., 1994. Laser-probe $^{40}Ar/^{39}Ar$ investigation of a pseudotachylyte and its host rock from the Outer Isles thrust, Scotland. *Geology*, **22**, 443–446.

Lee, J., 1991. Incremental $^{40}Ar/^{39}Ar$ thermochronology of mylonitic rocks from the northern Snake Range, Nevada. *Tectonics*, **10**, 77–100.

Osmundsen, P.T. and Andersen, T.B., 1994. Caledonian compressional and late-orogenic extensional deformation in the Staveneset area, Sunnfjord, Western Norway. *J. Struct. Geol.*, **10**, 1385–1401.

Roberts, D., 1983. Devonian tectonic deformation in the Norwegian Caledonides and its regional perspectives. *Nor. Geol. U. Bull.*, **380**, 85–96.

Sibson, R.H., 1977. Fault rocks and fault mechanisms. *J. Geol. Soc. London*, **133**, 191–213.

Smith, D.C., 1984. Coesite in clinopyroxene in the Caledonides and its implications for geodynamics. *Nature*, **310**, 641–644.

Torsvik, T.H., Andersen, T.B. and Van Eide, E.A., 1997. The age and tectonic significance of dolerite dykes in Western Norway. *J. Geol. Soc. London*, in press.

Torsvik, T.H., Smethurst, M.A., Meert, J.G., Van der Voo, R., McKerrow, W.S., Brasier, M.D., Sturt, B.A. and Walderhaug, H.J., 1996. Continental break-up and collision in the Neoproterozoic and Palaeozoic—A tale of Baltica and Laurentia. *Earth Sci. Rev.*, **40**, 229–258.

Torsvik, T.H., Sturt, B.A., Swensson, E., Andersen, T.B. and Dewey, J.F., 1992. Palaeomagnetic dating of fault rocks: evidence for Permian and Mesozoic movements and brittle deformation along the extensional Dalsfjord Fault, western Norway. *Geophys. J. Int.*, **109**, 565–580.

Van der Voo, R., 1993. *Paleomagnetism of the Atlantic, Tethys and Iapetus Oceans.* Cambridge University Press, New York.

Wise, D.U., Dunn, D.E., Engelder, J.T., Geiser, P.A., Hatcher, R.D., Kish, S.A., Odom, A.L. and Schamel, S., 1984. Fault-related rocks: Suggestions for terminology. *Geology*, **12**, 391–394.

Received 9 April 1997; revised version accepted 19 September 1997

Chapter 2

Published as:

The age and tectonic significance of dolerite dykes in western Norway

Torsvik, T.H., Andersen, T.B., Eide, E.A. & Walderhaug, H.J.

in *J. Geol. Soc. London* v. 154, pp. 961-973, 1997.

Journal of the Geological Society, London, Vol. **154**, 1997, pp. 961–973, 10 figs, 2 tables. Printed in Great Britain

The age and tectonic significance of dolerite dykes in western Norway

TROND H. TORSVIK[1,3], TORGEIR B. ANDERSEN[2], ELIZABETH A. EIDE[1] & HARALD J. WALDERHAUG[3]

[1]*Geological Survey of Norway, PB 3006 Lade, N-7002 Trondheim, Norway*

[2]*Department of Geology, University of Oslo, PO Box 1047, 0316 Blindern, Oslo 3, Norway*

[3]*Institute of Solid Earth Physics, University of Bergen, Allegt. 41, N-5007 Bergen, Norway*

Abstract: Coast-parallel dykes in SW Norway, primarily of Permo-Triassic age, have been linked regionally to the early tectonic evolution of the Norwegian continental shelf. We demonstrate from palaeomagnetic data (mean declination=206.1°, inclination= −30.1°, α_{95}=11.8°) that dolerite dykes in the coastal Sunnfjord region of Western Norway and immediately west of the Devonian Basins are also of Permian (*c.* 250–270 Ma) age, and not lower- or pre-Devonian as previously advocated. The Sunnfjord dykes appear to be contemporaneous with dykes from SW Norway at Sotra (262 ± 6 Ma) and the oldest dykes from Sunnhordland (260–280 Ma), and geochemical data attest to a transition from sub-alkaline to alkaline magmatism at the dawn of the Mesozoic.

The Sunnfjord dykes are not simple records of E–W extension and magma intrusion, but instead represent significant mid–late Permian time markers within a complex zone of fault activation and rejuvenation. Late Mesozoic–Cenozoic magnetic overprinting (mean declination=348.6°, inclination= +68.9°, α_{95}=12°) and metamorphic alteration documented by these dykes are directly dependent upon proximity to major E–W brittle faults south of the Hornelen Devonian Basin, hence some motion and related fluid activity do post-date dyke intrusion. The E–W high-angle normal or oblique-slip faults can be regionally traced offshore to the Øygarden Fault Zone. Onshore, these faults truncate the Hornelen low-angle detachment, which in turn cuts folded Devonian strata. These observations, along with evidence for Permian and Late Jurassic–Cretaceous extension from the nearby Dalsfjord region, demonstrate important reactivation of a Late to post-Caledonian detachment and high-angle fault system in Western Norway.

Keywords: Norway, Permian, dykes, faults, reactivation.

Recent interpretation of seismic reflection data from offshore Western Norway (Fig. 1a) indicates that Permian extension was significantly greater and more regionally important than the Mesozoic (Jurassic–early Cretaceous) extension (Christiansson *et al.* 1995; Færseth *et al.* 1995). In onshore areas, Permian low-angle fault-rejuvenation in western Norway (Torsvik *et al.* 1992; Osmundsen 1996; Eide *et al.* 1997) and coast-parallel Permo-Triassic dykes in Southwest Norway (Færseth *et al.* 1976; Løvlie & Mitchell 1982) further attest to the importance of Late Palaeozoic rifting in the region (Fig. 1a).

Relatively abundant, coast-parallel, predominantly N–S-trending dykes, from the Sunnfjord area of Western Norway have also been noted since early mapping in the area commenced (Reusch 1881), but their age(s) and tectonic significance were never thoroughly investigated. The majority of these dykes were affected by E–W high-angle faults south of the Hornelen Devonian Basin (Fig. 1b); thus, Skjerlie & Tysseland (1981) interpreted the dykes as Lower Devonian or older because the faults were traditionally and regionally interpreted as primary controlling elements of Devonian sedimentation (Steel 1976; Norton 1986; Seranne & Seguret 1987). However, in more recent studies, these faults have been found to contain Late Palaeozoic and Mesozoic rejuvenation components (Torsvik *et al.* 1988, 1992; Wilks & Cuthbert 1994). The importance of establishing the age of the Sunnfjord dolerite dykes is therefore two-fold. First, they represent an important coast-parallel magmatic event which probably ties to the offshore tectonic development (pre-syn-rift?). Second, the dyke ages provide an important time-marker for subsequent faulting or rejuvenation of E–W high-angle structures in Western Norway.

Regional setting

The west Norwegian geological infrastructure is largely a product of the Scandian Orogeny that resulted from continental collision between Baltica and Laurentia and subsequent, extensional post-orogenic tectonics. In the Sunnfjord area, the continental collision can be accurately timed to the Mid-Silurian by the stratigraphic and deformational history of the Herland Group on Atløy (Fig. 1b) (Andersen *et al.* 1990). The collision hallmarks included high, pre-collision plate velocities (Torsvik *et al.* 1996), whole-scale subduction of Baltic continental crust and ensuing rapid Late Silurian–Lower Devonian exhumation of an orogen that contains high- and ultra-high pressure (HP–UHP) metamorphic rocks (Andersen *et al.* 1991, 1994; Dewey *et al.* 1993; Dobrzhinetskaya *et al.* 1995; Eide & Torsvik 1996). Extensional and erosional unroofing along the central parts of the orogen eventually resulted in formation of high-angle faults in the exhumed middle and upper crustal complexes. These faults subsequently controlled the formation of the Devonian Old Red Basins of Western Norway (Osmundsen & Andersen 1994) and were rooted in an array of lower-angle, extensional detachments that presently floor the eastern margins of the Devonian Basins (Andersen & Jamtveit 1990). The principal Nordfjord–Sogn Detachment

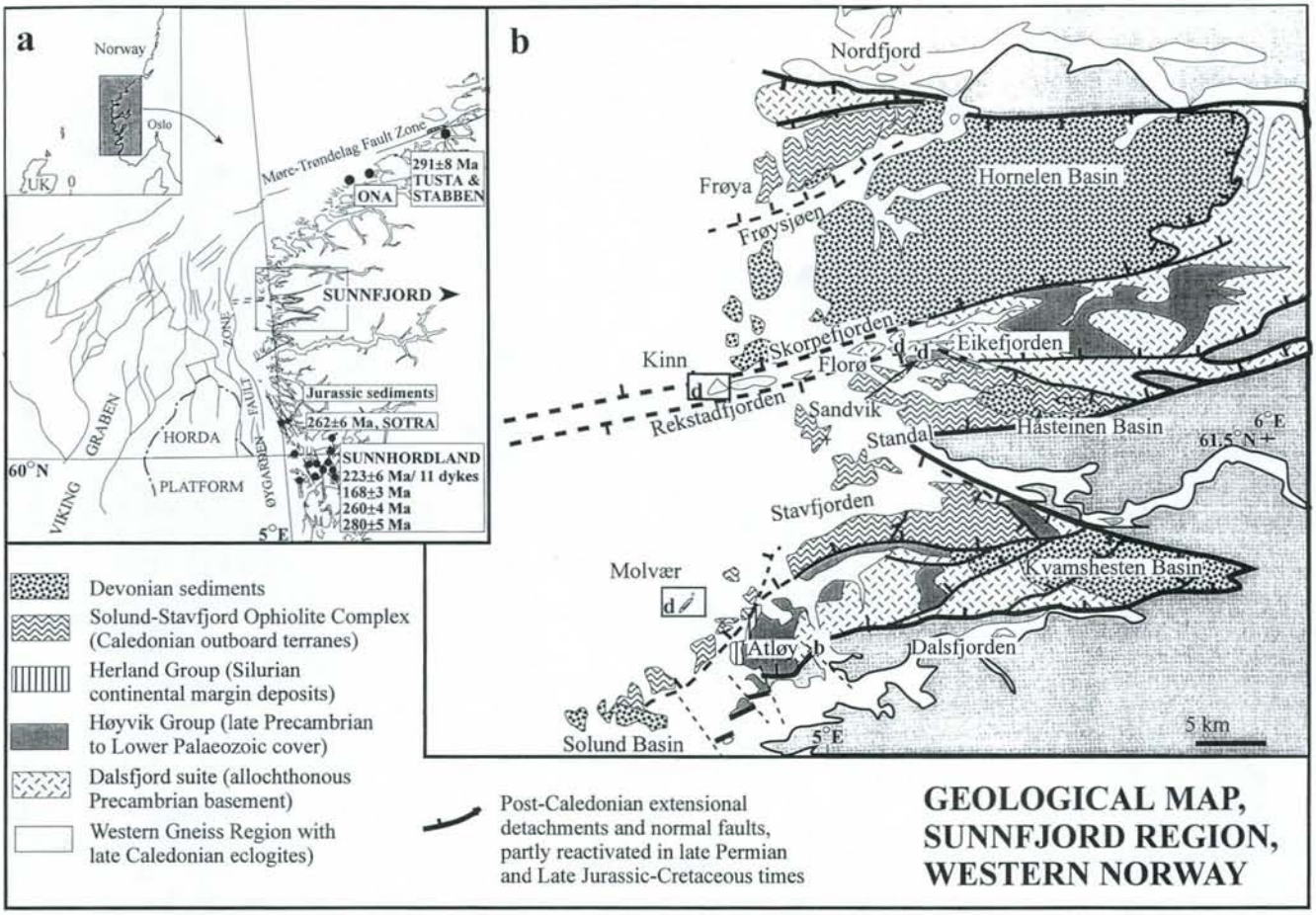

Fig. 1. (**a**) Sketch map of western Norway (see inset map for location in Norway), principal offshore structural elements and location of Permo-Triassic coast-parallel dykes. (**b**) Geological map of the Sunnfjord region, western Norway (see inset in a) and Sunnfjord dyke sampling localities (marked d). Fault-rock localities (Dalsfjord Fault) from the Atløy-Askvoll region (see text) are marked b.

(Norton 1986) juxtaposes the late-Caledonian HP rocks of the Lower Plate and low- to medium-grade Precambrian to Silurian allochthonous units of the Upper Plate (Fig. 1b) (Dewey *et al.* 1993; Andersen *et al.* 1994).

With the exception of the Håsteinen Basin which is mostly unconformable on its substrate, the Devonian Basins in western Norway are presently bounded by low-angle detachments to the east, reactivated faults along their northern and southern margins, and depositional unconformities to the west (Fig. 1b). Within the detachments and other major shear zones, kinematic indicators demonstrate top-west displacement; associated stretching lineations and magnetic fabrics have an E–W orientation (Chauvet & Seranne 1989; Swensson & Andersen 1991; Torsvik *et al.* 1992). Most of the penetrative deformation in the hanging- and footwalls of the detachments have been traditionally explained as syn-kinematic features related to post-orogenic extensional collapse (Seranne & Seguret 1987; Seguret *et al.* 1989). However, the structure of Devonian Basins, as well as their Upper and Lower Plate substrates, are dominated by inversion and E–W folding; these structures are arguably related to a phase of N–S shortening. Based on palaeomagnetic studies, Torsvik *et al.* (1988) demonstrated that N–S shortening continued into the Late Devonian and possible Early Carboniferous, although detailed structural studies in the footwall of the main detachment indicate that N–S shortening may have been related to sinistral transtensional deformation that had already begun in the Devonian (Krabbendam pers. com. 1996).

Sunnfjord dykes

The Sunnfjord dykes (Reusch 1881; Kolderup 1928; Kildal 1969; Skjerlie & Tysseland 1981) intrude the Late Precambrian and early Palaeozoic sequences of the basement and allochthons, but have not been observed to cut the Devonian Basins. Dykes trend 350°–060° (but mostly N–S) with steep WNW or vertical dips and vary in thickness from 0.1 to 10 m (Skjerlie & Tysseland 1981). Detailed sampling profiles from eight dykes and contacts at Molvær (Fig. 2a) and Kinn (Fig. 2b) were drilled in the field, whereas two dykes at Florø and Sandvik (Fig. 1b) were hand-sampled for logistic and archaeological reasons.

The Sunnfjord dykes have chemical compositions similar to continental tholeiites (Skjerlie & Tysseland 1981), but exhibit variable primary igneous textures and degrees of secondary alteration. Primary igneous textures appear to be logically correlated with dyke width and corollary differences in intrusive cooling rates, whilst secondary alteration depends upon the proximity of the dykes to the E–W Skorpe- and Rekstadfjorden Faults (Fig. 1b).

The least altered dykes occur on the Molvær isles (Figs 1b & 2a) where they intrude a highly deformed sequence of

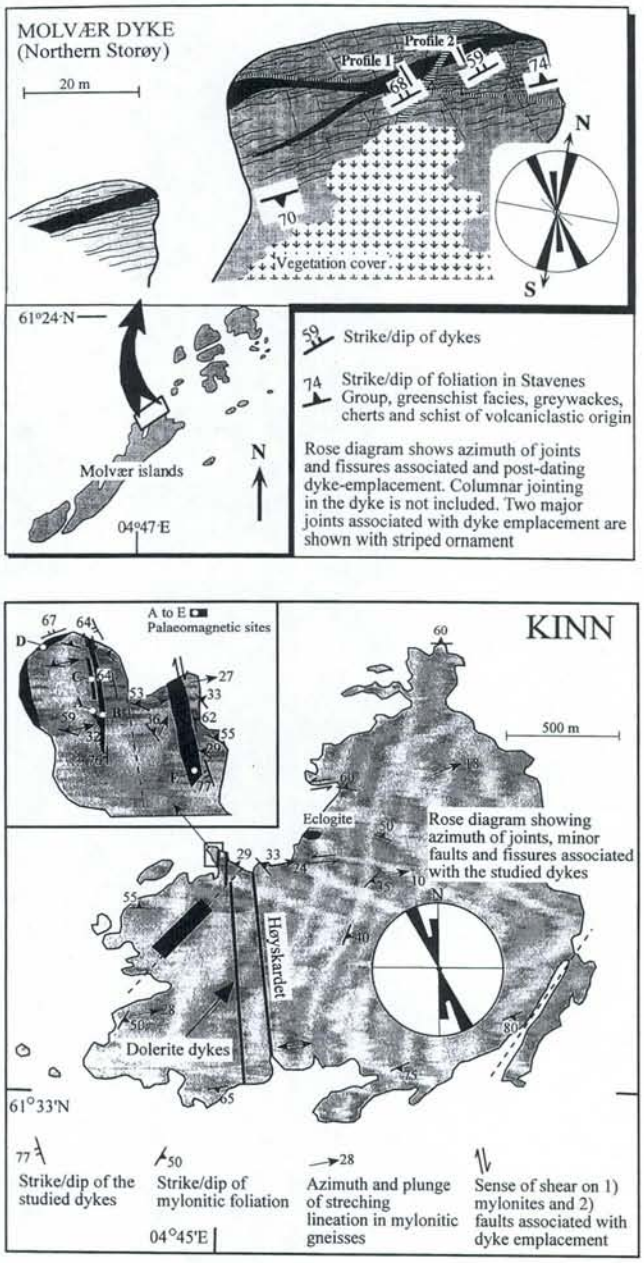

Fig. 2. Geological sketch map from (**a**) the Molvær isles and (**b**) Kinn (see Fig. 1b). Structural data from central and southern Kinn from Lutro (1991).

greenschist-facies schists, including meta-greywackes, graphitic schists, meta-cherts and meta-tuffaceous rocks of the Stavenes Group. The latter represents the volcano-sedimentary cover to the late Ordovician Solund–Stavfjord Ophiolite Complex (Furnes *et al.* 1990) both of which were obducted onto the Middle Silurian Herland Group during the initial stages of the Scandian orogeny (Andersen *et al.* 1990). The relationships between the Molvær dykes and the wall-rock structure indicate that dyke emplacement was partly controlled by the orientation of the main foliation of the Stavenes Group and a NNE-trending joint system that at least locally predates the Molvær dykes. A pre-existing, roughly E–W trending (0.1–0.5 m wide) zone of cataclastic brecciation controlled a 15 m long, E–W segment of the dyke (Fig. 2a). A separate set of NW-trending fractures apparently post-date the dykes at Molvær.

Except for jointing, the Molvær dykes are essentially unmetamorphosed and display glassy chilled margins and columnar jointing; both features indicate shallow intrusion levels and rapid cooling against the wall-rock. The dykes are hypocrystalline basalts with phenocrysts of plagioclase, clinopyroxene, and oxides in a groundmass that largely comprises grey-green, fresh glass. The opaque phases comprise abundant titanomagnetite and some accessory pyrite. Titanomagnetite grains range in size from the limit of optical resolution up to several hundred microns. Grain are elongated and often skeletal, indicative of fairly rapid cooling. Close inspection of the grains (Fig. 3a) shows that ilmenite lamellae are present on a very fine scale, indicating high-temperature oxidation to class II of Ade-Hall *et al.* (1971). The lamellae are closely spaced and always less than 1 μm in width, causing a partitioning which should have a marked effect on the domain state of the larger grains.

A basaltic dyke at Sandvik, just south of the Rekstadfjorden Fault (Fig. 1b), intrudes Late Precambrian quartzites and appears fresh in hand-specimen, but has undergone some low-grade metamorphic alteration. Plagioclase is pervasively pseudomorphed by sericite, while clinopyroxene is generally unaltered or may have minor epidote, biotite or amphibole replacement products. The dominant opaque phase is abundant class II titanomagnetite (Fig. 3b) with accessory pyrite. Slight to moderate low-temperature oxidation, with granulation and some replacement of opaque phases along grain edges is evident.

The Kinn dykes (Figs 1b & 2b) intrude highly deformed orthogneisses which locally preserve eclogite facies assemblages correlated with the Western Gneiss Region. Dyke margins are variably brecciated and in outcrop, these dykes are part of an intrusive network that comprises a large, coarse-grained gabbroic dyke- or sill-like mass with numerous, associated, narrow, branching aphanitic to porphyritic basaltic dykes. The main gabbro body (Site E in Fig. 2b) has a coarse-grained, subophitic texture, although clinopyroxene now occurs as sub- to euhedral grains with preserved cores replaced progressively or completely by amphibole. Coarse-grained opaque grains are typically up to several hundred microns in size. Titanomagnetite of high-temperature oxidation class II is again the dominant phase (Fig. 3c). The grains exhibit coarse ilmenite lamellae, and often contain smaller inclusions of pyrite. Low temperature alteration of individual titanomagnetite grains varies from slight to heavy, with replacement of oxides by non-opaque phases resulting in many cases. Fine-grained oxides occur on pseudomorphic amphibole.

The thinner basaltic Kinn dykes probably once had a texture similar to that of Molvær, but are now completely altered to lower greenschist facies. A glassy groundmass comprises amphibole and chlorite, in addition to amphibole pseudomorphs after clinopyroxene. Two distinct generations of oxides are present: (1) Primary titanomagnetite grains with maximum sizes in excess of 100 μm with well-developed ilmenite lamellae indicating high-temperature oxidation to class II (Fig. 3d). The lamellae pattern is on a coarser scale than e.g. the Molvær dykes. (2) A pervasive cross-hatched pattern of elongate magnetite particles, apparently formed during secondary metamorphism of the rock (Fig. 3e). The pattern is best seen in transmitted light (Fig. 3f), and secondary magnetite appears to follow microfractures.

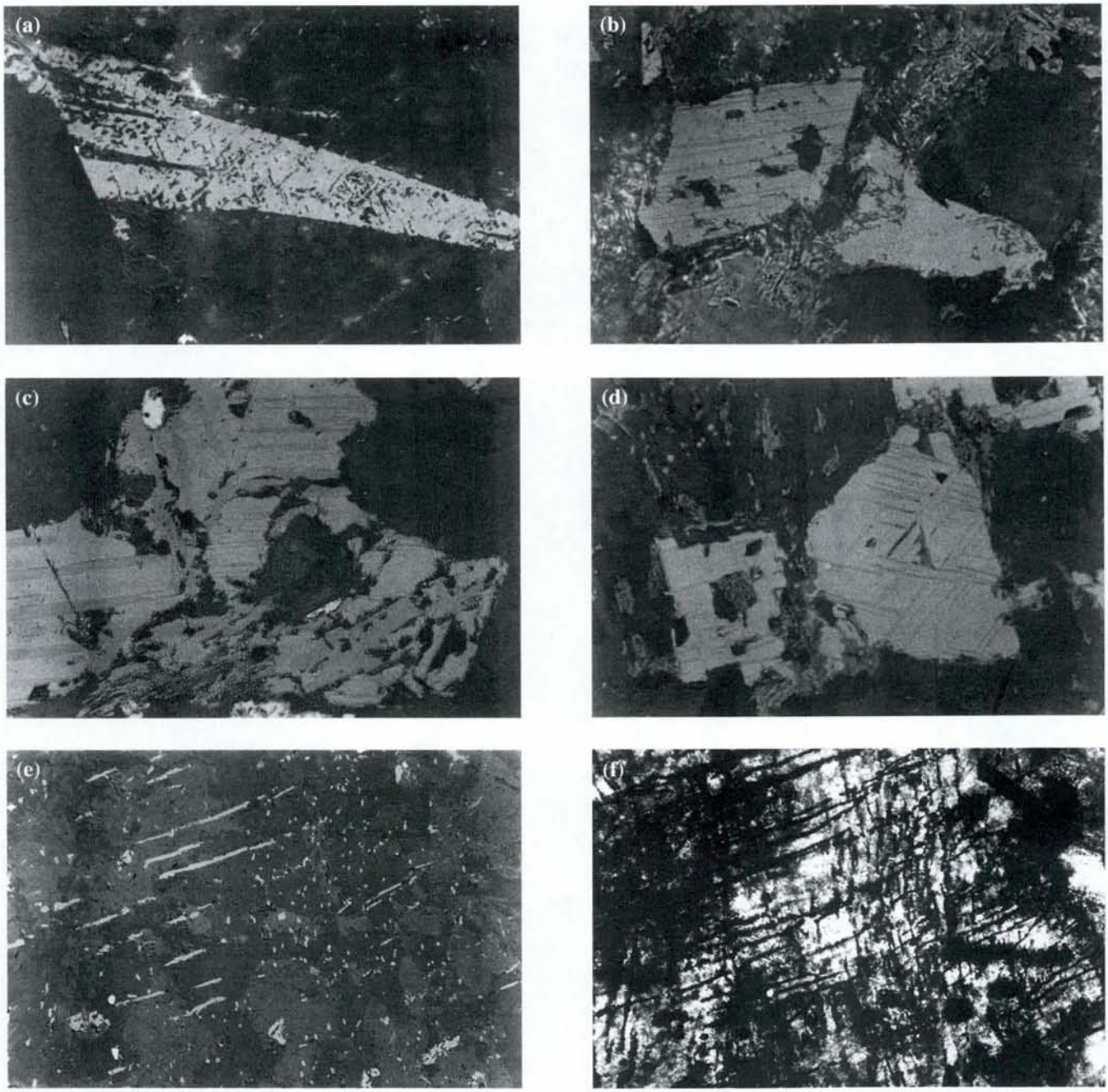

Fig. 3. Reflected light (a–e) and transmitted light (f) photomicrographs of opaque grains. See text for further descriptions. (**a**) Molvær dyke titanomagnetite (TM) grain. Frame width = 130 μm. Note very fine-scale ilmenite lamellae. (**b**) Sandvik dyke TM grain. Frame width = 130 μm. (**c**) Broad Kinn dyke TM grain (location E). Frame width = 325 μm. (**d**) Thinner Kinn dyke TM grain (location A). Frame width = 130 μm. (**e, f**) From same micrograph as (d) viewed in reflected and transmitted light, respectively, showing cross-hatched pattern of secondary magnetite. Frame width = 325 μm.

Palaeomagnetic experiments

The natural remanent magnetization (NRM) was measured with a JR5A magnetometer and remanence stability was tested by thermal and two-axis tumbler alternating field (AF) demagnetization. Characteristic remanence components were calculated using least squares analysis. NRM intensities and bulk-susceptibilities are listed in Table 1.

Thermo-magnetic analysis was performed on a horizontal translation balance, and all tested samples, independent of dyke alteration state or location within a single dyke, yield Curie-temperatures of 580°C, i.e. titanium-poor titanomagnetite or almost pure magnetite (Fig. 4a). Heating and cooling curves are practically identical and indicate minimal thermochemical alterations during the experiments.

Isothermal remanent magnetization (IRM) acquisition curves are dominated by magnetic phases which saturate in fields of 150–300 mT, and remanence coercive forces (H_{cr}) vary from 15 to 40 mT. High H_{cr} and probable pseudo-single domain (PSD) magnetite are observed from the pristine

Table 1. *Sampling details, mean NRM intensity and susceptibility and characteristic remanence components for the Sunnfjord dykes (mean sampling coordinates: 61.5°N and 4.8°E)*

	Strike/dip	Width (m)	NRM	Sus	Dec°	Inc°	*N*	α_{95}	*k*	Component
Molvær dykes										
Dyke A	232°/59°	2.0	495 ± 247	45 949 ± 4873	355.8	63.2	12	7.6	33.8	M-C
					220.1	−36.5	18	4.6	57.8	P
Dyke B	232°/59°	0.4	562 ± 97	35 281 ± 1837	329.8	73.8	3	17.5	50.8	M-C
					220.4	−20.6	6	23.7	8.4	P
Dyke C	232°/68°	0.6	1070 ± 388	36 019 ± 4259	213.3	−36.0	7	3.3	345.5	P
Contact schist			1.4 ± 0.9	529 ± 24	204.0	−28.6	6	2.9	550.0	P
Sandvik dyke	036°/90°	1.5	1507 ± 67	77 868 ± 5535	342.6	+73.2	13	10.1	17.8	M-C
					191.5	−32.8	8	8.2	46.7	P
Kinn dykes										
Dyke A	267°/63°	0.2	721 ± 250	55 862 ± 5117	069.0	+84.2	8	10.3	29.6	M-C
Dyke B	175°/64°	1.4	784 ± 219	53 927 ± 4699	030.4	+68.8	8	16.2	12.7	M-C
Dyke C	158°/70°	0.25	825 ± 227	57 577 ± 2738	038.7	+69.4	2	(38.4)	(44.4)	M-C
					188.3	−22.8	3	(56)	(5.9)	P
Dyke D	240/67°	3.5+	792 ± 129	52 754 ± 5220						
Dyke E	170°/77°	9.0	854 ± 109	59 868 ± 7297	342.8	+53.1	3	26.3	23.1	M-C
Contact gneiss			260 ± 118	13 162 ± 9706	357.0	+60.2	3	28.5	19.7	M-C
Florø dyke	010°/90°	2.3	4889 ± 695	81 331 ± 4361	299.7	+42.3	5	8.5	82.2	M-C
Combined					348.6	+68.9	9*	12.0	19.4	M-C
					206.1	−30.1	6*	11.8	33.3	P

NRM=natural remanent magnetization (mA/M); Sus=susceptibility (10^{-6} SI); Dec°, Inc°=mean declination and inclination; n=number of samples/sites*; α_{95}=95% cone of confidence; *k*=precision parameter; component interpretation: M-C, Mesozoic–Cenozoic; P, Permian.

Molvær dykes whilst the altered Kinn and Florø dykes show minimum values. This may partly indicate magnetite 'softening' with increased alteration, but properties of the magnetically harder Molvær dykes are clearly the result of smaller grains and finer lamella structure, i.e. due to primary mineralogic difference. Hysteresis analysis and saturation remanence to saturation magnetization (J_{rs}/J_s) and coercivity (H_{cr}/H_c) ratios show a clear trend towards a multidomain (MD) state from Molvær to Kinn dykes (Fig. 4b). J_{rs}/J_s is normally regarded as the best measure of grain size ranges, from 0.5 for uniaxial SD grains down to <0.02 for true MD magnetite (Dunlop 1986). Increasing titanium content raises the MS/PSD transition to 0.1. H_{cr}/H_c is theoretically between 1 and 2 for SD grains and increases with grain size. In practice true SD values for J_{rs}/J_s are very rare and in the Day diagram (Fig. 4b, Day *et al.* 1977), values most commonly fall in the PSD range. J_s values are around 1 $Am^2\ kg^{-1}$ for the Kinn, Florø and Molvær dykes and just below 2 $Am^2\ kg^{-1}$ for the Sandvik dyke, indicative of magnetite contents of *c.* 1% and 2% respectively.

Molvær dykes

The pristine Molvær dykes (Fig. 2) are characterized by two remanence components: (1) a low to intermediate unblocking component (denoted M-C) with northerly declinations and steep positive inclinations and, (2) a high unblocking component (denoted P) with SW declinations and negative inclinations (Fig. 5a; Table 1). Component P is characterized by discrete thermal unblocking between 560 and 580°C or by isolation in AF fields above 15–19 mT (Fig. 5b). Median destructive ($M_{1/2}$) AF fields range between 12 and 20 mT. In many instances the M-C component is not randomized before 550°C (Fig. 5a), but dyke margin samples and the baked contact schist (Fig. 5c) are less influenced by the M-C component. Maximum susceptibilities are recorded in the widest dyke A (Fig. 5d) and marginal samples show lower values than the interior and centre, which may attest to grain-size contrasts. However, titanomagnetite concentration and degree of high-temperature titanomagnetite oxidation are important

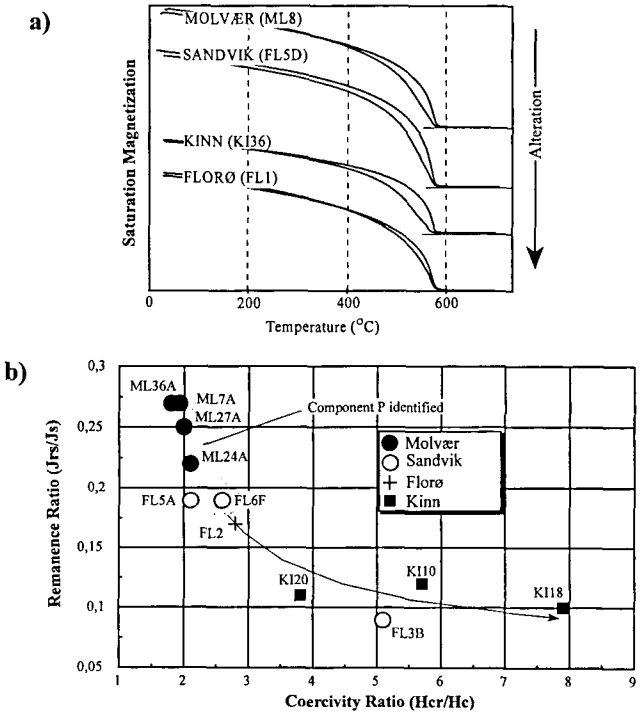

Fig. 4. (a) Thermomagnetic curves from the Sunnfjord dykes which are all identical with $T_c \approx 580$°C and reversible heating and cooling curves (b) J_{rs}/J_s and H_{cr}/H_c ratios. In the Day diagram, only the encircled samples with high J_{rs}/J_s and low H_{cr}/H_c reveal the P-component (probably primary Permian).

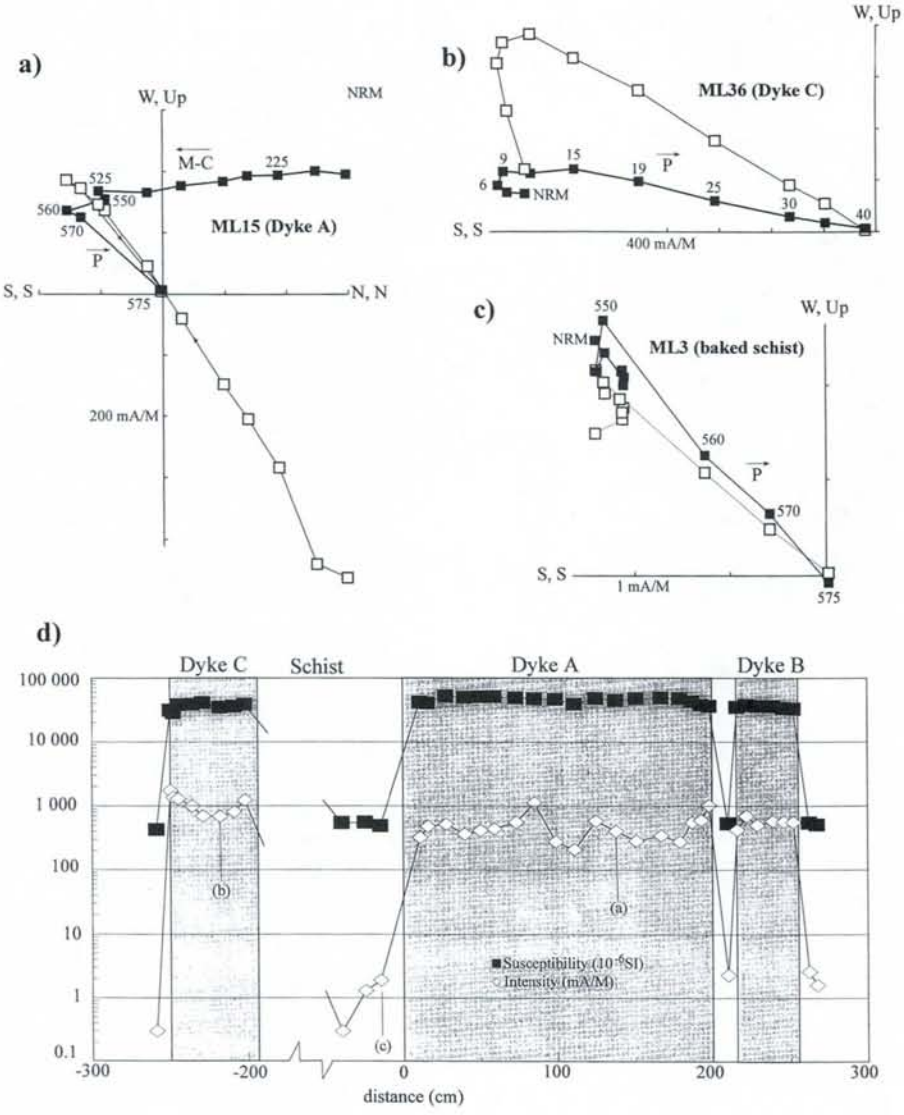

Fig. 5. Thermal (**a**) and alternating field (**b**) demagnetization of Molvær dyke samples and (**c**) thermal demagnetization of a baked contact sample. (**d**) Intensity and susceptibility profile (note logarithmic scale) through the tested dykes and contact (distance in centimetres). In orthogonal vector plots, solid (open) symbols represent projections onto the horizontal (vertical) plane.

factors. NRM intensities are also clearly influenced by overprints (M-C), but the narrow dyke C (Profile 2 in Fig. 2a), which is least affected by the M-C component, exhibits a pattern of high NRM with low susceptibility along the margins. This probably reflects a relatively undisturbed primary cooling pattern of a fine-grained margin and coarser-grained interior. The P component in the contact schist closely corresponds to the dyke components but schists sampled outside the baked region did not yield sensible palaeomagnetic results due to low intensity and viscous directional behaviour.

Sandvik dyke

The Sandvik dyke (Fig. 1b) is directionally more complex than the Molvær dykes. Most commonly the M-C component is identifiable whereas the P component is not isolated. Southerly directional trends show that the high unblocking component P is always present (identified in Fig. 6a), but 'stable end-directions' are often difficult to observe (Fig. 6b) due to the combined effect of overlapping unblocking-spectra and the fact that the P component often resides within an extremely narrow temperature interval (570–580°C). $M_{1/2}$ is considerably lower than the Molvær dykes, generally 1–5 mT, except in a subordinate number of samples where the P component was identified and $M_{1/2}$ was 10–12 mT.

Kinn dykes

These dykes were tested in considerable detail due their relatively complex textural characteristics (Fig. 3), but demagnetization behaviour is similar to, but less stable than those from Sandvik. All samples show pronounced southerly directional movement during demagnetization (Fig. 6b), but the high unblocking P component is difficult to isolate and only poorly identified in three samples from one dyke at temperatures above 550–570°C (Fig. 6c, Table 1). Low $M_{1/2}$ (2–4 mT) prevails, and the low to intermediate M-C components are comparable to those from Molvær and Sandvik (Fig. 7a).

Florø dyke

The Florø dyke has significantly higher NRM intensity (Table 1) and only M-C components are identified. A few

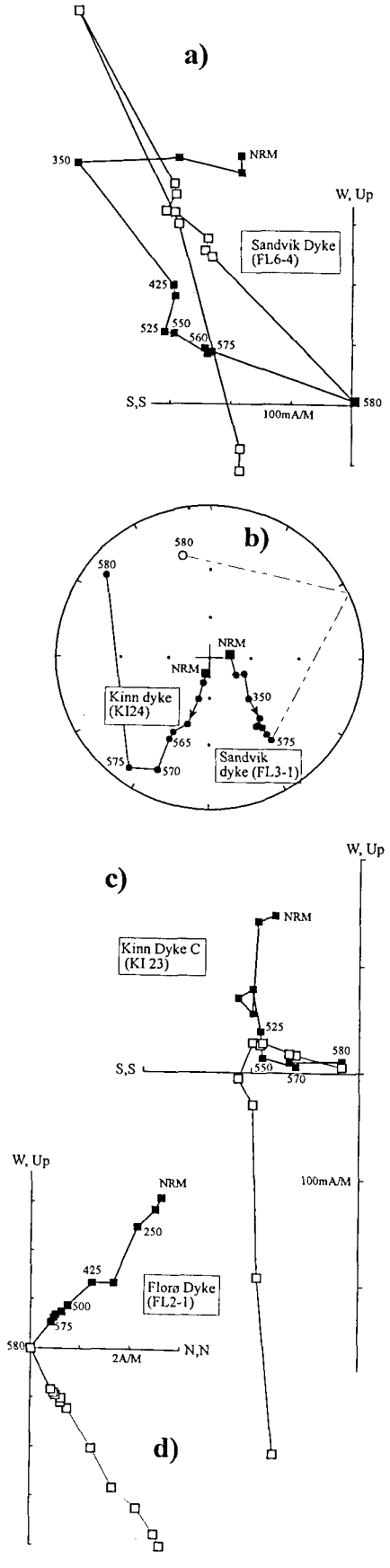

samples from this strongly altered dyke were thermally tested; they all show identical and almost uni-vectorial directional behaviour (Fig. 6d), but with somewhat more westerly declinations than M-C components from the other dykes (Fig. 7a).

Magnetic interpretation

Palaeomagnetic results from Sunnfjord dykes reveal a high unblocking component (P) with SSW declinations and negative inclinations, which is partially or entirely (Florø) overprinted by components (M-C) with N or NNW declinations and positive inclinations (Fig. 7a). Component P can be interpreted as mid–late Permian (*c.* 250–270 Ma) with a late Mesozoic–Cenozoic (M-C), probably Cretaceous or younger, overprint (Fig. 7a). The Sunnfjord dyke pole (P) is almost identical to fault-rocks ('green breccia' of Torsvik *et al.* 1992) from Atløy (Fig. 8), formed during low-angle faulting on the Dalsfjord Fault (Fig. 1b), and isotopically dated to 250–260 Ma (Eide *et al.* 1997). The Permian magnetic signature in the Sunnfjord dykes represents either a primary intrusion age or a regional overprint. We prefer the former explanation because extensive palaeomagnetic studies of the Devonian Basins and substrate (including an anorthosite locality 200 m from the Sandvik dyke; Site 25 in Torsvik *et al.* 1988) in the Sunnfjord area essentially yield pre-Permian magnetic ages.

Alteration and magnetic resetting of the Sunnfjord dykes is clearly related to movements along the prominent E–W faults south of the Hornelen Devonian Basin (Fig. 1b). Just south of the Rekstadfjorden Fault, at Sandvik, Permian directions are partially recovered whereas within the fault-zone, remagnetization prevails (Kinn), and at Florø (Fig. 1b) the Permian direction is entirely obliterated. These magnetic characteristics are represented by respective differences in mineralogy and degree of metamorphism, manifested first by primary igneous textural characteristics and grain sizes, and second, by the effects of subsequent metamorphic (hydrothermal) alteration on the magnetomineralogy. The M-C overprint plots near the present earth's magnetic field direction and may partly have a viscous and recent origin.

The Sunnfjord dykes all share a similar primary magnetic phase, i.e. abundant titanomagnetite of oxidation class II (Fig. 3) which explains the high Curie temperatures and unblocking temperatures. Differences in magnetic hardness partly arise from differences in grain-size and coarseness of the lamellae. The Molvær dykes show signs of fairly rapid cooling with commonly skeletal and very fine scale lamellae, while the broadest Kinn dyke (Dyke E) has the largest grains and coarsest lamellae. Varying degrees of low-temperature alteration of the primary titanomagnetite phase are evident in all dykes, and the thinner Kinn dykes (and Florø dyke) have a second significant magnetic phase (magnetite), clearly associated with later, lower greenschist-facies metamorphism (Fig. 3e & f).

A regional dyke perspective

Permo-Trassic dykes are observed in several areas in coastal western Norway, and the oldest dated dykes are located at

Fig. 6. Thermal demagnetization samples from the Sandvik (**a**, **b**), Kinn (**b**, **c**) and Florø dykes (**d**). In the stereoplot, closed (open) symbols denote positive (negative) inclination. See Fig. 5 for further legend.

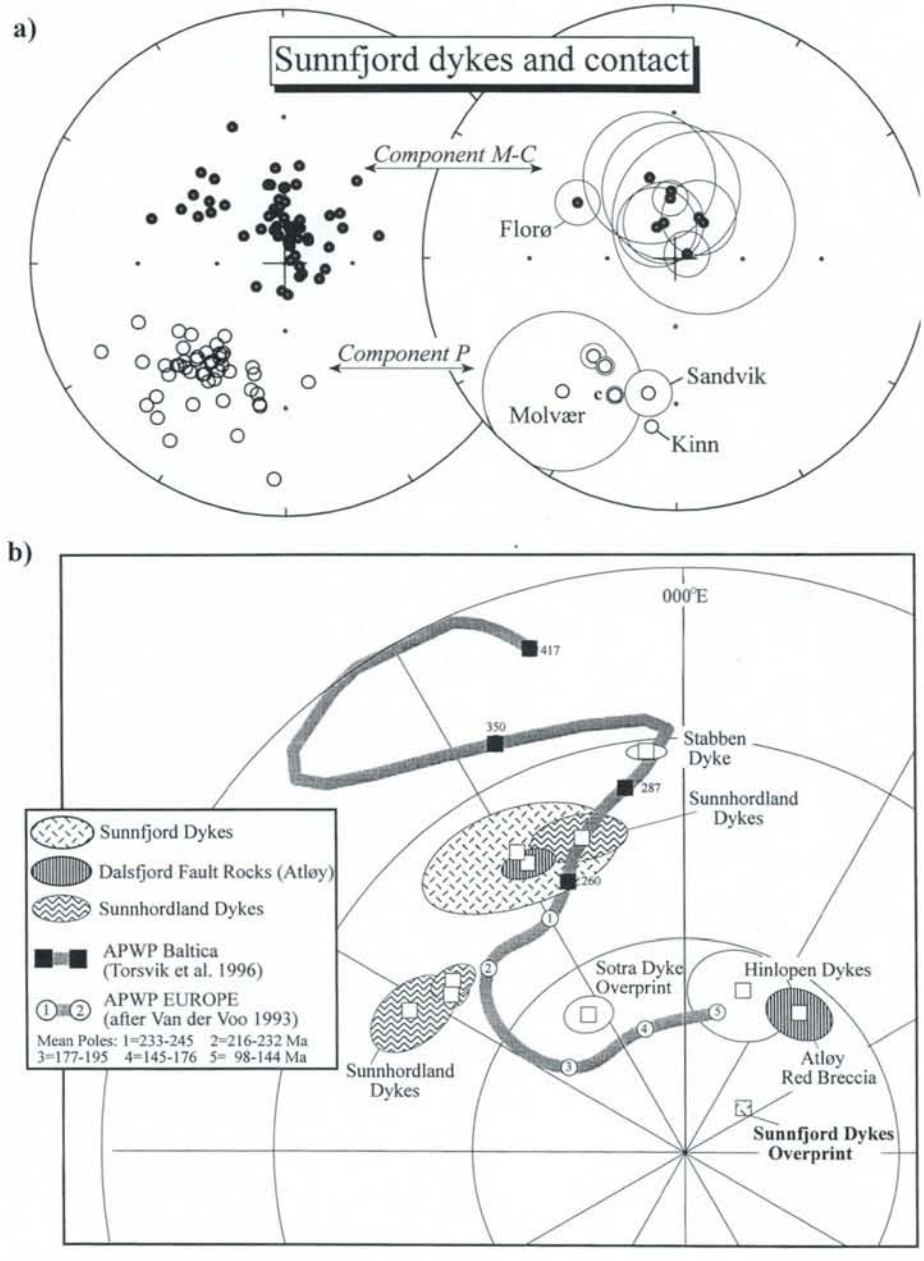

Fig. 7. (**a**) Characteristic remanence components from the Sunnfjord dykes, sample (left) and dyke-contact mean directions (right diagram with α_{95} confidence circles), respectively. (**b**) Apparent polar wander paths (APWP) for Baltica and Europe, selected poles from Western Norway (Table 2) and the Sunnfjord mean poles (component P and M-C, Tables 1–2). Sunnfjord M-C pole is shown without error confidence ellipses (d*p*/d*m*). For comparison, we also include a pole from the *c.* 145 Ma Hinlopen dolerites (Halvorsen 1989). Equal area polar projection.

Tustna-Stabben (Fig. 1a) and within the eastern part of the Møre Trøndelag Fault Zone. The palaeomagnetic pole from the E–W Stabben syenitic dykes (Sturt & Torsvik 1987) plots at the Lower Permian part of the Baltica APWP (Fig. 7b) and a Rb–Sr age of 291 ± 8 Ma obtained from the nearby island of Tustna (Råheim 1974) fits well with the magnetic age estimate. South of the Møre Trøndelag Fault Zone, N–S-trending basaltic dykes are observed on the island of Ona (Fig. 1a; Robinson pers. comm. 1995) but presently lack isotopic age constraints.

Isotopic age data are not yet available for the Sunnfjord dykes, but the palaeomagnetic data strongly suggest a mid-late Permian age (*c.* 250–270 Ma; Fig. 7a). Two ultrapotassic dykes from the same region (Dalsfjord area) are dated between 256–262 Ma (K/Ar whole rock; Furnes *et al.* 1982). These dykes, however, are highly altered with a strong magnetic fabric, and palaeomagnetic testing proved unsuccessful (Torsvik unpublished data 1992). Their unusual strike (E–W) and geochemistry are also markedly different from the sub-alkaline tholeiitic Sunnfjord dykes (Fig. 8b). Following Furnes *et al.* (1982) we regard it reasonable to conclude that the K/Ar whole rock ages from these dykes relate to strong hydrothermal alteration, probably linked to movement along the Dalsfjord Fault. The exact intrusion-crystallization age of these dykes is therefore uncertain.

Further southward along the coast, six concordant ages from two dykes on the island of Sotra (west of Bergen; Fig. 1a) yield a mean age of 262 ± 6 Ma (Fig. 8a; Løvlie & Mitchell 1982). Unpublished geochemical data suggest a continental tholeiitic affinity, conceivably similar to the Permian-aged Sunnfjord dykes (Furnes pers. comm. 1996). The palaeomagnetic data from the Sotra dykes, however, are clearly discordant with the Permian isotopic ages (Fig. 7b). The Sotra dykes are located along a major NNW–SSE lineament and the

Table 2. *Post-Carboniferous palaeomagnetic data from Western Norway (Figs 1 and 7b) that are discussed in the text*

Site Rock Unit (Geo.Lat., Geo.Long.)	Dec°	Inc°	α_{95}	Pole Lat.	 Long	d*p*	d*m*	Isotopic age	Magnetic age estimate	Ref.
NW Norway										
Stabben Dykes (63.3°N, 8.5°E)	192.0	−12.0	2.4	−32.1	354.4	1.0	2.0	291 ± 8 Ma (Rb/Sr)	Early Permian	1, 2
Central western Norway										
Sunnfjord Dykes (61.5°N, 4.8°E)	206.1	−30.1	11.8	−41.0	330.7	7.3	13.1		Mid–late Permian (Component P)	3
Sunnfjord Dykes (61.5°N, 4.8°E)	348.6	+68.9	12.9	−79.0	053.9	17.3	20.4		<Cretaceous (Component M-C)	3
Atløy 'green breccia' (61.3°N, 5°E)	205.0	−33.0	3.2	−43.2	331.5	2.0	4.0	253 ± 5 Ma ($^{40}Ar/^{39}Ar$)	Mid–Late Permian	4, 5
Atløy 'red breccia' (61.3°N, 5°E)	342.0	+58.0	3.2	−64.8	039.5	3.0	5.0	<130 Ma ($^{40}Ar/^{39}Ar$)	L. Jurrassic–E. Cretaceous	4, 5
SW Norway										
Sotra Dykes (60.0°N, 5°E)	019.5	+59.1	2.3	−66.0	325.0			262 ± 6 Ma (K/Ar)	Jurrasic ?	6
Sunnhordland Dykes (59.8°N, 5.5°E)	198.0	−27.0	5.8	−43.0	342.0			280–164 Ma (K/Ar)	Permian	7, 8
Sunnhordland Dykes (59.8°N, 5.5°E)	047.8	+48.9	5.0	−46.0	297.0				Triassic	7
Sunnhordland Dyke-UH (59.8°N, 5.5°E)	040.0	+48.0	2.5	−49.2	306.3			280 ± 5 Ma (K/Ar)	Triassic	9, 8
Sunnhordland Dyke-SA (59.8°N, 5.5°E)	041.0	+50.0	1.9	−50.2	303.8			223 ± 6 Ma (K/Ar)	Triassic	9, 8

Ref, References: 1, Sturt & Torsvik (1987); 2, Råheim (1974)-recalculated age from the Tustna dyke; 3, this study (Table 1); 4, Torsvik *et al.* (1992); 5, Eide *et al.* (1997); 6, Løvlie & Mitchell (1982); 7, Løvlie (1981); 8, Færseth *et al.* 1976-recalculated ages; 9, Walderhaug (1993).

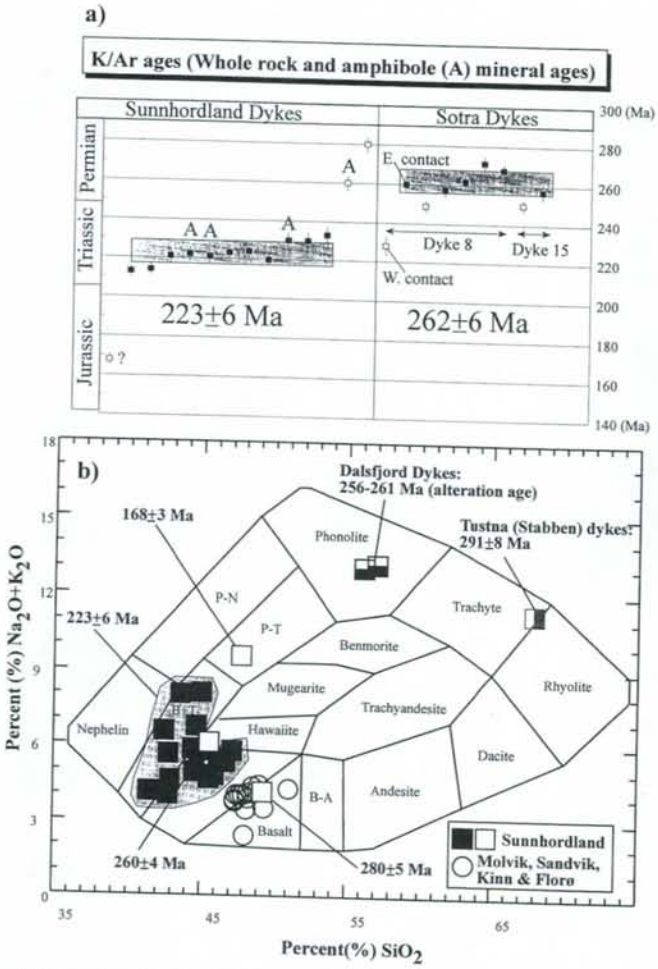

Fig. 8. (**a**) Recalculated K/Ar ages from 14 Sunnhordland dykes, Western Norway (after Færseth *et al.* 1976). Also included are K/Ar data from dykes (two profiles) from Sotra (Løvlie & Mitchell 1982). Concordant ages (with errors) are shaded. (**b**) Alkali–silica discrimination plot for the sub-alkaline Sunnfjord dykes (Molvær, Sandvik, Kinn & Florø; data from Skjerlie & Tysseland 1981), Sunnhordland dykes (mainly alkaline signature; data from Færseth *et al.* 1976). Also included for comparison, data from the Dalsfjord (Furnes *et al.* 1982) and Tustna dykes (Råheim 1974). B – A, basaltic andesite; B+T, basanite/tephrite; P – T, phonolitic tephrite; P – N, phonolitic nephelinite

palaeomagnetic pole probably represents a Jurassic remagnetization. In this respect it is important to note that faulted and fractured Jurassic sediments have recently been discovered in a fjord close to these dykes (Fossen 1997).

In the Sunnhordland region (Fig. 1b), Færseth *et al.* (1976) obtained 11 concordant K/Ar whole-rock and amphibole ages from alkaline-basaltic dykes that yielded a mean age of 223 ± 6 Ma (recalculated ages, this study; Fig. 8a). With the addition of a few 'outlying' ages (280 ± 5, 260 ± 4 and 168 ± 3 Ma), they argued for three intrusive events, i.e. Permian, Mid-Triassic and Jurassic. In our opinion, the composite 223 ± 6 Ma isotopic age fits with the bulk palaeomagnetic poles from these dykes (Løvlie 1981, Walderhaug 1993) since they plot near the 216–232 Ma mean pole for Europe (Van der Voo 1993; Fig. 7b). From some dykes, Løvlie (1981), found a poorly defined Permian direction (see pole in Fig. 7b) and this may validate the 260–280 Ma K/Ar ages.

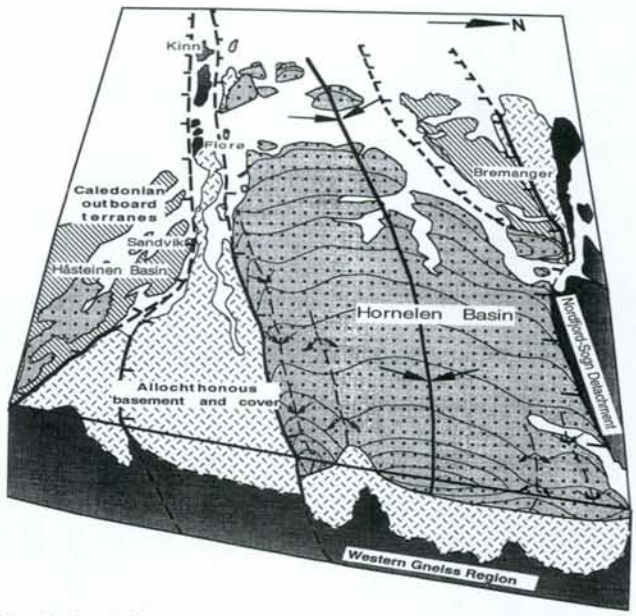

Fig. 9. Block diagram of the Hornelen Basin and substrate. The NNE–SSW section demonstrates age relationships between the basin-margin faults, Devonian basin fill, detachments and the regional east–west-trending folds in western Norway. Notice that the Nordfjord–Sogn Detachment capping the Western Gneiss Region is more intensely folded than the Hornelen Detachment. The low-angle and gently folded Hornelen Detachment truncates already folded Devonian sediments. The south-margin fault of the basin truncates all the other main structural elements in the area.

Færseth *et al.* (1976) noted that the 280 ± 5 Ma dyke differs in bulk- and rare earth element geochemistry from other Sunnhordland dykes; its sub-alkalic signature is comparable with the Sunnfjord dykes (Fig. 8b) and probably also to the Permian Sotra dykes. This argues for a Permian origin for some Sunnhordland dykes, although the 260 Ma Sunnhordland dyke does not follow the same chemical trend. The 168 Ma dyke age is troublesome since palaeomagnetic data from this dyke are similar to the 223 Ma dykes (Løvlie 1981; Walderhaug 1993) and new isotopic age data are clearly necessary to clarify the incongruities. On balance, available palaeomagnetic, isotopic and geochemical data from the entire group of dykes in Western Norway indicate probably two (mid–late Permian and mid-Triassic) intrusive events with subtle different magmatic signatures.

Conclusions

Palaeomagnetic data from the Sunnfjord dykes in coastal western Norway suggest a mid–late Permian (250–270 Ma) age and not Early Devonian or older age as argued by earlier workers. The primary remanent signature is carried by deuterically oxidized titanomagnetite (class II); the documented strong Late Mesozoic–Cenozoic overprinting and metamorphic alteration up to lower greenschist facies relate to proximity to major E–W shear zones and faults south of the Hornelen Devonian Basin. This leads to the conclusion that some of the motion and related hydrothermal fluid flow along the faults post-date dyke intrusion. The Sunnfjord dykes are thus not simple records of E–W extension and magma intrusion, but rather represent significant time markers within a complex zone of fault activation and rejuvenation. Mapping

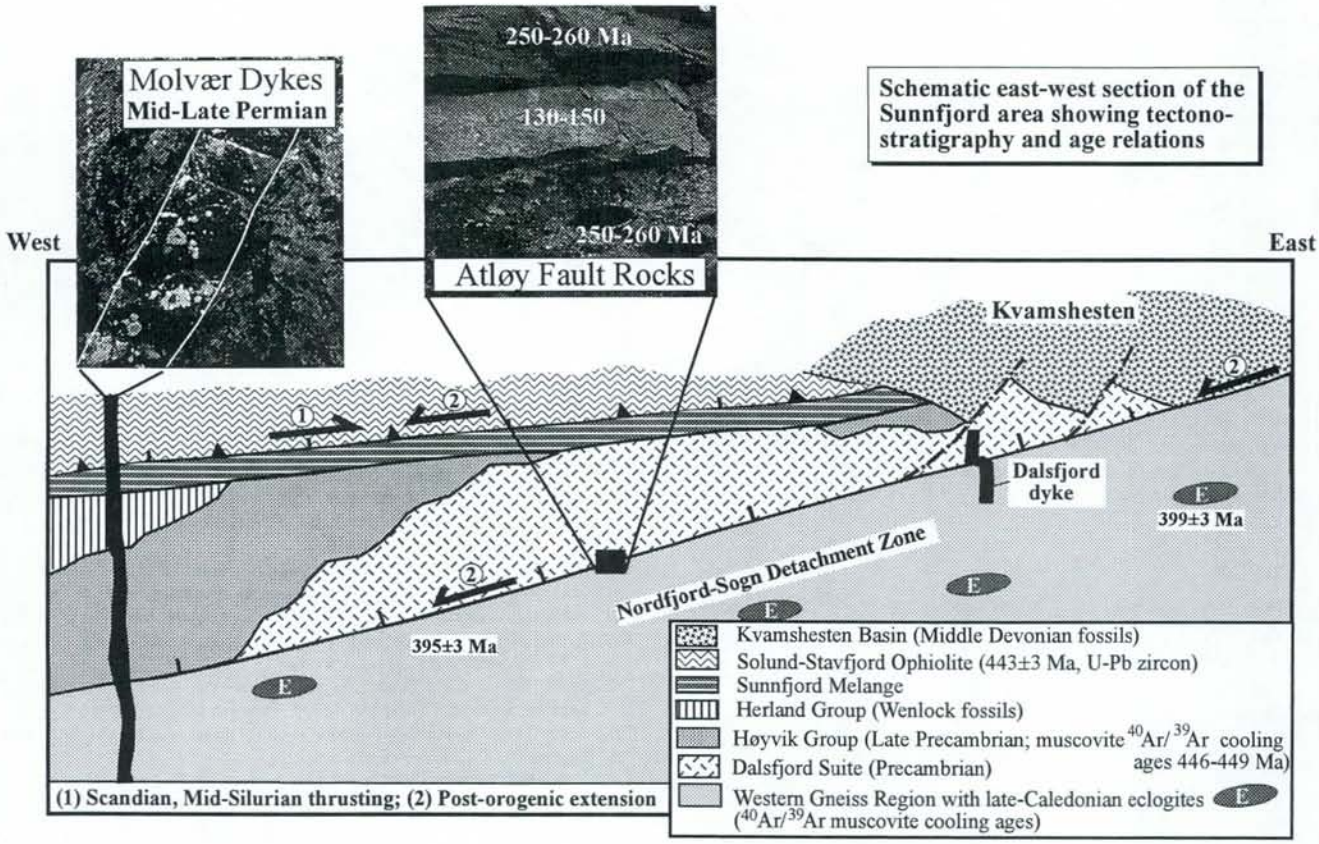

Fig. 10. Schematic (not to scale) east–west section of the Kvamshesten Devonian Basin and substrate. The profile illustrates the tectono-stratigraphy and the approximate position of the Molvær and Dalsfjord dykes. Notice that syn-depositional Devonian faults are truncated by the reactivated Nordfjord–Sogn Detachment, and that the Dalsfjord dyke is deformed by the fault. The relationship between the Molvær dykes and the main detachment can only be inferred from the relationships at Kinn, Florø and Sandvik. $^{40}Ar/^{39}Ar$ cooling ages of white micas are from Berry *et al.* (1993), Andersen *et al.* (1997) and Eide *et al.* (1997).

along the southern and eastern margin of the Hornelen Basin also shows that the south-margin fault of the basin truncates the east margin low-angle detachment, which in turn truncates the already folded youngest Devonian strata in the Hornelen Basin (Fig. 9). These observations of polyphase normal faulting reinforce previous analyses (Torsvik *et al.* 1988, 1992; Wilks & Cutbert 1994) and support the new palaeomagnetic data which demonstrate important reactivation of the Late to Post-Caledonian detachment and high-angle fault system in Western Norway. It is also noteworthy that the provenance for the Hornelen Devonian sediments is entirely from the Upper Plate lithologies (Nilsen 1968; Cuthbert 1991) and thus clearly demonstrates post-depositional rejuvenation of the main detachments and faults that presently bound the basins.

The importance of contractional and extensional rejuvenation of the Devonian on-shore structures in western Norway for the Late Palaeozoic and Mesozoic tectonic development of the offshore Horda Platform and the Viking Graben (Fig. 1a) is equivocal since correlation and integrated interpretation of the on- and off-shore structural features have hitherto been few and preliminary. Nonetheless, onshore tectonic models do serve as templates for understanding offshore structural geometries, and in our opinion the following sequence of Late Palaeozoic–Mesozoic events can be deduced from the onshore information.

(1) The Sunnfjord dykes are mid-late Permian in age and probably contemporaneous with the geochemically similar Sotra dykes (262 ± 6 Ma) and the oldest phase of magmatism in the Sunnhordland area (260–280 Ma). Collectively they attest to major Permo-Triassic rifting and a change from sub-alkaline (Permian) to alkaline (Triassic) magmatism.

(2) The Hornelen Basin is bounded by a shallow westward dipping detachment in the east and to the north and south by steep brittle E–W faults which cut the detachment (Fig. 9). These are post-depositional structures, although they probably lie close to the syn-sedimentary Devonian bounding faults. The E–W faults clearly affect the Permian aged Sunnfjord dykes and therefore record a protracted rejuvenation history and magnetic resetting during the Mesozoic–Cenozoic. Indeed, these faults are still seismically active.

(3) The E–W brittle faults can clearly be traced offshore to the Øygarden Fault Zone (Fig. 1a), the most extensive N–S structural element in offshore Norway, and probably representative of the main basin margin during Permo-Triassic and Jurassic extension (Færseth *et al.* 1995). Detailed offshore aeromagnetic studies which are underway will delineate if these E–W faults cut, or terminate at, the Øygarden Fault Zone.

(4) In the Dalsfjord region (Atløy, Fig. 1b) there is blatant onshore evidence for reactivation of the Nordfjord-Sogn Detachment (Fig. 10). Well-dated fault-rocks indicate that the Dalsfjord Fault, now flooring the Kvamshesten Devonian Basin, underwent periods of brittle low-angle (<15°) extensional reactivation during Permian and Upper Jurassic/Lower Cretaceous times (Torsvik *et al.* 1992; Eide *et al.* 1997).

Palaeomagnetic data from the oldest brittle fault rocks at Atløy (250–260 Ma) match the Sunnfjord dykes (Figs 7a & 8), and it thus appears that sub-alkaline magmatism and low-angle faulting were fairly contemporaneous, and in a predominantly E–W-oriented extensional stress field.

(5) South of the Solund Devonian Basin (Fig. 1), Færseth *et al.* (1995) argue that the Solund Fault (part of the Nordfjord-Sogn Detachment) continues offshore and represents a major structural barrier with opposing blocktilts. Although they find no direct evidence of post-Devonian faulting or reactivation, we observe that the Dalsfjord and probably also Solund Faults are 'young' tectonic features and the most important onshore faulting took place during the mid–late Permian times.

Financial support by the Geological Survey of Norway–Mobil Norway–Norwegian Research Council–Phillips–Statoil a.s. (T.H.T. & E.A.E.) and Norsk Agip–Norwegian Research Council (T.B.A.). ONOFF contribution no. 1.

References

Ade-Hall, J.M., Palmer, H.C. & Hubbard, T.P. 1971. The magnetic and opaque petrological response of basalts to regional hydrothermal alteration. *Geophysical Journal of the Royal Astronomical Society*, **24**, 137–174.

Andersen, T.B. & Jamtveit, B. 1990. Uplift of deep crust during orogenic extensional collapse: A model based on field studies in the Sogn-Sunnfjord region, W. Norway. *Tectonics*, **9**, 1097–1111.

——, Berry, H.N., Lux, D.R. & Andresen, A. 1997. The tectonic significance of pre-Scandian $^{40}Ar/^{39}Ar$ phengite cooling ages in the Caledonides of western Norway. *Journal Geological Society, London*, in press.

——, Jamtveit, B., Dewey, J.F. & Swensson, E. 1991. Subduction and eduction of continental crust: major mechanisms during continent-continent collision and orogenic extensional collapse, a model based on the south Norwegian Caledonides. *Terra Nova*, **3**, 303–310.

——, Osmundsen, P.T. & Jolivet, L. 1994. Deep crustal fabrics and a model for the extensional collapse of the southwest Norwegian Caledonides. *Journal of Structural Geology*, **16**, 1191–1204.

——, Skjerlie, K.P. & Furnes, H. 1990. The Sunnfjord Melange, evidence of Silurian ophiolite accretion in the West Norwegian Caledonides. *Journal of the Geological Society, London*, **147**, 59–68.

Berry, H.N., Lux, D.R., Andresen, A. & Andersen, T.B. 1993. $^{40}Ar/^{39}Ar$ dating of rapidly uplifted high-pressure rocks during late-orogenic extension in southwest Norway. *Abstract volume, GSA-Annual meeeting, Boston.*

Chauvet, A. & Seranne, M. 1989. Microtectonic evidence of Devonian extensional westward shearing in Southwest Norway. *In*: Gayer, R.A. (ed.) *The Caledonide Geology of Scandinavia*. Graham & Trotman, London, 245–254.

Christiansson, P., Odinsen, T., Berge, A.M., Faleide, J.I. & Gabrielsen, R.H. 1995. Crustal structure from deep seismic data in the northern north sea. *Terra Nova, abstracts supplement No. 1*, **7**, 55.

Cuthbert, S. 1991. Evolution of the Hornelen Basin, west Norway: new constraints from petrological studies of metamorphic clasts. *In*: Morton, A., Todd, S.P. & Haughton, P.D.W. (eds) *Developments in Sedimentary Provenence Studies*. Geological Society, London, Special Publications, **57**, 343–360.

Day, R., Fuller, M. & Schmidth, V.A. 1977. Hysteresis properties of titanomagnetite: grain size and compositional dependence. *Physics of the Earth and Planetary Interiors*, **13**, 260–267.

Dewey, J.F., Ryan, P.D. & Andersen, T.B. 1993. Orogenic uplift and collapse, crustal thickness, fabrics and metamorphic phase changes: the role of eclogites. *In*: Prichard, H.M., Alabaster, T., Harris, N.B.W. & Neary, C.R. (eds) *Magmatic Processes and Plate Tectonics*. Geological Society, London, Special Publications, **76**, 325–343.

Dobrzhinetskaya, L.F., Eide, E.A., Larsen, R.B., Sturt, B.A., Trønnes, R.G., Smith, D.C., Taylor, W.R. & Posukhova, T.V. 1995. Microdiamond in high-grade metamorphic rocks of the Western Gneiss Region, Norway. *Geology*, **23**, 597–600.

Dunlop, D.J. 1986. Hysteresis properties and their dependence on particle size: A test of Pseudo-Single-Domain remanence models. *Journal of Geophysical Research*, **91**, 9569–9584.

Eide, E.A. & Torsvik, T.H. 1996. Paleozoic Supercontinent assembly, Mantle flushing and genesis of the Kiaman Superchron. *Earth and Planetary Science Letters*, **144**, 389–402.

——, —— & Andersen, T.B. 1997. $^{40}Ar/^{39}Ar$ geochronologic and paleomagnetic dating of fault breccias; characterization of Late Palaeozoic and early Cretaceous fault reactivation in Western Norway. *Terra Nova*, in press.

Fossen, H. 1997. Advances in understanding the post Caledonian structural evolution of the Bergen area, West Norway. *Norsk Geologisk Tidsskrift*, in press.

Furnes, H., Mitchell, J.G., Ryan, P. & Skjerlie, F.J. 1982. Petrography and geochemistry of peralkaline, ultrapotassic syenite dykes of Middle Permian age, Sunnfjord, West Norway. *Norsk Geologisk Tidsskrift*, **62**, 147–159.

——, Skjerlie, K.P., Pedersen, R.B., Andesren, T.B., Stillman, C.J., Suthren, R., Tysseland, M. & Garmann, L.B. 1990. The Solund-Stavfjord Ophiolite Complex and associated rocks, west Norwegian Caledonides: Geology, geochemistry and tectonic environment. *Geological Magazine*, **28**, 209–224.

Færseth, R.B., Macintyre, R.M. & Naterstad, J. 1976. Mesozoic alkaline dykes in the Sunnhordland region, western Norway: ages, geochemistry and regional significance. *Lithos*, **9**, 331–345.

——, Gabrielsen, R.H. & Hurich, C.A. 1995. Influence of basement in structuring of the North Sea basin, offshore southwest Norway. *Norsk Geologisk Tidsskrift*, **75**, 105–119.

Halvorsen, E. 1989. A palaeomagnetic pole position of Late Jurassic/Early Cretaceous dolerites from Hinlopenstrete, Svalbard, and its tectonic implications. *Earth and Planetary Science Letters*, **94**, 398–408.

Kildal, E.S. 1969. *Geological map of Norway, bedrock Måløy*, map-sheet 20, 1:250 000. Geological Survey Norway.

Kolderup, N.H. 1928. *Fjellbygningen i kyststrøket mellom Nordfjord og Sognefjord*. Bergens Museums Årbok Naturvitenskaplig. Rekke, **1**.

Lutro, O. 1991. *Preliminary bedrock map of Florø*. Geological Survey of Norway.

Løvlie, R. 1981. Palaeomagnetism of coast-parallel alkaline dykes from western Norway; ages of magmatism and evidence for crustal uplift and collapse. *Geophysical Journal of the Royal Astronomical Society*, **66**, 417–426.

—— & Mitchell, J.G. 1982. Complete remagnetization of some Permian dykes from western Norway induced during burial/uplift. *Physics of the Earth and Planetary Interiors*, **30**, 415–421.

Nilsen, T. 1968. The relationship of sedimentation to tectonics in the Solund Devonian District of southwestern Norway. *Norges Geologiske Undersøkelse Bulletin*, **259**, 1–108.

Norton, M. 1986. Late Caledonian extension in western Norway: A response to extreme crustal thickening. *Tectonics*, **5**, 195–204.

Osmundsen, P.-T. 1996. *Late-orogenic structural geology and Devonian basin formation in Western Norway: A study from the hanging wall of the Nordfjord–Sogn Detachment in the Sunnfjord Region*. Dr. Scient thesis, University of Oslo, Norway.

—— & Andersen, T.B. 1994. Caledonian compressional and late-orogenic extensional deformation in the Staveneset area, Sunnfjord, Western Norway. *Journal of Structural Geology*, **16**, 1385–1401.

Reusch, H. 1881. Konglomerat-sandsteinsfelterne i Nordfjord, Søndfjord og Sogn. Nyt. *Magazin for Naturvidenskaberne*, **26**, 93–170.

Råheim, A. 1974. A Post Caledonian syenite porphyry dyke in the Western Gneiss Region, Tustna, Central Norway. *Norsk Geologisk Tidsskrift*, **54**, 139–147.

Seguret, M., Seranne, M., Chauvet, A. & Brunel, M. 1989. Collapse basins: A new type of extensional sedimentary basin from the Devonian of Norway. *Geology*, **17**, 127–130.

Seranne, M. & Seguret, M. 1987. The Devonian basins of western Norway:tectonics and kinematics of an extending crust: *In*: Coward, M.P., Dewey, J.F. & Hancock, P.L. (eds) *Continental Extensional Tectonics*. Geological Society, London, Special Publications, **28**, 537–548.

Skjerlie, F.J. & Tysseland, M. 1981. Geochemistry and petrology of dolerite dykes of probably Late Caledonian age from the outer Sunnfjord region, West Norway. *Norges Geologiske Bulletin*, **363**, 25–43.

Steel, R.J. 1976. Devonian basins of western Norway – sedimentary response to tectonism and to varying tectonic context. *Tectonophysics*, **36**, 207–224.

Sturt, B.A. & Torsvik, T.H. 1987. A Late Carboniferous palaeomagnetic pole recorded from a syenite sill, Stabben, Central Norway. *Physics Earth Planetary Interior*, **49**, 350–359.

Swensson, E. & Andersen, T.B. 1991. Contact relationships between the Askvoll group and basement gneisses of the Western Gneiss Region (WGR), Sunnfjord, W. Norway. *Norsk Geologisk Tidsskrift*, **71**, 15–27.

Torsvik, T.H., Sturt, B.A., Ramsay, D.M., Bering, D. & Fluge, P.R. 1988. Palaeomagnetism, magnetic fabrics and the structural style of the Hornelen

Old Red Sandstone, Western Norway. *Journal of the Geological Society, London*, **145**, 413–430.

——, ——, SWENSSON, E., ANDERSEN, T.B. & DEWEY, J.F. 1992. Palaeomagnetic dating of fault rocks: Evidence for Permian and Mesozoic movements and brittle deformation along the extensional Dalsfjord Fault, western Norway. *Geophysical Journal International*, **109**, 565–580.

——, SMETHURST, M.A., MEERT, J.G., VAN DER VOO, R., MCKERROW, W.S., BRASIER, M.D., STURT, B.A. & WALDERHAUG, H.J. 1996. Continental break-up and collision in the Neoproterozoic and Palaeozoic: A tale of Baltica and Laurentia. *Earth Science Review*, **40**, 229–258.

VAN DER VOO, R. 1993. *Paleomagnetism of the Atlantic, Tethys and Iapetus Oceans*. Cambridge University Press, Cambridge.

WALDERHAUG, H. 1993. Rock magnetic and magnetic fabric variations across three thin alkaline dykes from Sunnhordland, Western Norway: influence of initial mineralogy and secondary alterations. *Geophysical Journal International*, **115**, 97–108.

WILKS, W.J. & CUTBERT, S.J. 1994. The evolution of the Hornelen Basin detachment system, western Norway: implications for the style of late orogenic extension in the southern Scandinavian Caledonides. *Tectonophysics*, **238**, 1–30.

Received 20 January 1997; revised typescript accepted 7 April 1997.
Scientific editing by David Snyder

Chapter 3

Western Norway alkaline dikes: pinpoints for extension and rifting in the Early Triassic and Middle Jurassic

Eide, E.A., Torsvik, T.H., Walderhaug, H.J. & Løvlie, R.

to submit to *J. Geol. Soc. London*

3.1 INTRODUCTION

The distinct properties of dikes often make them ideal rock types to use as relative and absolute age markers, indicators of paleostress fields and tectonic regimes, and subjects for paleomagnetic data and paleogeographic reconstructions. In western Norway, exposures of several generations of predominantly alkaline dikes have been investigated over the last two decades by several research groups in order to determine dike ages and chemical derivations and thus, their significance for the extensional regimes they may represent.

Precise ages for dikes like these are of first order importance when attempting to correlate them with regional extension. Controversy over the actual ages, or range of ages, represented by the western Norway dikes has been evident in the literature and was propagated primarily by the large spread of ages determined previously for the rocks by the K-Ar total fusion method (ages ranged from 168 to 280 Ma) and the inconsistency of these K-Ar ages with paleomagnetic data from the same rocks. Clearly, the rocks had import for late Paleozoic and mid-Mesozoic extensional events offshore, but the precise timing of these events, as represented by the dikes, remains equivocal.

The ^{40}Ar-^{39}Ar geochronology method has certain advantages over the K-Ar method, especially in the more detailed information one is able to extract about the history of individual portions of a mineral or whole rock. The latter capacity enables the investigator to determine which parts of the mineral or whole rock may have been affected by episodes of Ar-loss or excess-Ar in a way that remains somewhat obtuse in a conventional K-Ar analysis. These advantages do not discredit all old K-Ar ages, but rather are a simple function of instrumental and technical advances made in the last decade with the newer, ^{40}Ar-^{39}Ar method; they require a critical, but open, view of old K-Ar ages, in addition to re-analysis of some samples with the newer technique in the case of very blatant controversies.

Our study demonstrates fairly clearly that the large range of ages of the western Norway dikes is an artefact of some disturbances in the Ar-sysematics of some of the dike rocks at different times, due to variable causes as discussed below. Further, the new data limit quite distinctly the ages of emplacement of these dikes to two episodes, one of Early Triassic and one of Middle Jurassic age.

3.2 GEOLOGIC SETTING AND PREVIOUS WORK

Dikes of the Sunnhordland and Sotra areas are the youngest igneous rocks in western Norway and follow dominantly NNW-trends (Fig. 1). The sets of NNW-trending faults and joints also abundant in the area are subparallel to some major structural features in the northern North Sea. For this reason, the dikes are important time and paleogeographic markers and may be 'smoking guns' to unravel extensional events on the continental shelf (see e.g. Færseth et al., 1976). The dikes in both areas are dominantly vertical with very sharp contacts to the surrounding country rocks. Some reactivation subsequent to dike emplacement is evident via development of calcite cements and brecciation in some of the dikes and dike fractures (Færseth et al., 1976).

The Sunnhordaland dikes comprise dominantly alkali-olivine basalts and may contain lherzolitic xenoliths; the latter were interpreted to be evidence for very rapid rise of fairly deep-seated magmas to shallow emplacement levels in the crust (Færseth, 1978). One dike observed to cross-cut an older dike generation (see also below) is notably olivine-absent and has a comparatively more alkaline nature than the other dikes. The cross-cutting relationship and the apparently more 'evolved' chemistry of this dike were in accord with its very young K-Ar age relative to other dikes analyzed from the Sunnhordaland area (see Færseth et al., 1976; Løvlie and Mitchell, 1982). Færseth et al. noted K-Ar age 'clusters' at ca. 280, 220 and 168 Ma (recalculated ages); they interpreted these age groups to correspond to at least three magmatic episodes of Early Permian, Late Triassic and Middle Jurassic age. Palaeomagnetic data from the same rocks (Løvlie, 1981) yielded somewhat variable results, but were interpreted to indicate possibly two intrusive events: one of Early-Mid Permian age, and another of Triassic/Jurassic age.

The Sotra dikes have chemical affinities to continental tholeiitic basalts (Løvlie and Mitchell, 1982) and are chemically similar the Molvær-Kinn dykes on the western margin of the Sunnfjord area (see discussion in Torsvik et al., 1997 and below; Fig. 1). Løvlie and Mitchell derived K-Ar whole-rock ages from the Sotra area that yielded a mean of 262 Ma. These age data were at odds with palaeomagnetic results that yielded Jurassic-Cretaceous ages (Løvlie and Mitchell, 1982).

Further north, peralkaline, ultrapotassic dikes in the Sunnfjord area (see Fig. 1) were dated by Furnes et al. (1982) by the K-Ar method and yielded Late Permian ages (256-261 Ma). The trend of these dikes is E-W, rather than N-S as in Sunnhordaland/Sotra, but the authors nevertheless suggested their resemblance in composition and time to the set of 'older' alkaline dikes near Bergen. Furnes et al. noted the possible temporal correlation of the Sunnfjord dikes with early, rift-related magmatism in the North Sea and to similarly-trending (E-W) dikes in the Orkneys (Fig. 1).

A recent palaeomagnetic study of several dolerite dike localities in the Sunnfjord region (Molvær-Kinn), west of the Devonian basins, indicates Permian (250-270 Ma) ages for the intrusion of these rocks. The latter dikes have generally N-S to NNE- trends, in general agreement with the dominant Sunnhordaland-Sotra trends. The geochemistry of the rocks is sub-alkaline to alkaline; the more alkaline (evolved) varieties apparently correspond to progressively younger dike generations (Skjerlie and Tysseland, 1981; Torsvik et al., 1997).

Palaeomagnetic ages from the Sunnhordaland and Sotra dikes are at odds with at least some of the K-Ar age data. Clearly, an explanation for these discrepancies must involve 1) resetting of the K-Ar ages, implying that palaeomagnetic poles of Triassic/Jurassic age are correct, with some weaker evidence for partially reset Permian poles, 2) remagnetization of the dikes at different intervals, implying that at least some of the K-Ar ages are correct, and/or 3) some combination of both (1) and (2), whereby some dikes experienced partial to complete resetting of one or both 'dating' techniques (K-Ar and paleomagnetics). Some of these possibilities have been previously discussed by Løvlie (1981) and Macintyre and Færseth (1982).

A summary plot of the previous K-Ar data from Sunnhordaland and Sotra is presented in Figure 2 (data from Færseth et al., 1976 and Løvlie and Mitchell, 1982). One age from a dike near Kvamshestern (Furnes et al., 1982) is also included in the figure. Visual analysis indicates one very young age (168 Ma) that corresponds to the most alkaline dike in the Sunnhordaland suite; as noted above, this young dike crosscuts an older dike generation. The largest cluster of K-Ar ages falls in the 211-233 Ma range and was interpreted to represent Late Triassic magmatism at ca. 220 Ma (Færseth et al., 1976). A group of older ages range

from ca. 260 to 280 Ma. We note that some of the ages derive from analysis of amphibole mineral separates and some from whole-rock analyses.

In order to address this problem of age discrepancies both within the K-Ar system and between K-Ar and paleomagnetic ages, we re-dated rocks from both Sunnhordaland and Sotra areas with the ^{40}Ar-^{39}Ar method. We selected rocks that were representive of the 'spread' in K-Ar ages; the re-analyzed rocks are marked with stars in Figure 2.

3.3 ^{40}Ar-^{39}Ar DATA

We analyzed three whole rocks from Sunnhordaland (SU4, SU9 and SU10) and one plagioclase mineral separate from a Sotra dike (3-96). Prior to ^{40}Ar-^{39}Ar furnace step-heating, clean samples were packed in Sn-foil and irradiated at the Siloé reactor in Grenoble, France. We used the ^{40}Ar-^{39}Ar analytical facility at Université Blaise Pascal et Centre National de la Recherche Scientifique, Clermont-Ferrand, France, with analytical protocol and irradiation parameters similar to Arnaud et al. (1993). Data are presented in Table 5.1 and Figures 3-5.

Sunnhordaland whole rock sample SU4 yielded a plateau age of 239 ± 4 Ma for 69% of the ^{39}Ar gas released in the experiment (Fig. 3a); the previous K-Ar age for this same sample was 222 ± 8 Ma. The spectrum is characterized by two unreasonably old, low temperature ages, the plateau, and four unreasonably high, high-temperature apparent ages. ('Temperature' in this context refers to the experimental temperature of the furnace during release of Ar-gas. See also Table 5.1). This 'saddle-shaped' spectrum is a typical expression of excess Ar in the sample and, indeed, this is borne out in the inverse isochron diagram (Fig. 3b). In the latter plot of the sample data, two different linear arrays are obvious: the lower, nearly horizontal data distribution comprises the four unreasonably high apparent ages observed at the upper end of the release spectrum (Fig. 3a). The other array defines a well-correlated line (MSWD = 0.59) indicating normal mixing between an atmospheric component of Ar and the radiogenic component which defines an age of 235 ± 5Ma, within uncertainty of the plateau age. We adopt the latter age, instead of the plateau age, in subsequent discussion of this sample.

The spectrum of the Sunnhordaland whole rock sample, SU9, was also characterized by a saddle-shape; the bottom of the saddle was slightly more irregular than the spectrum for SU4. An inverse isochron diagram of SU9 (Fig. 4; Table 5.1) reveals a similar excess-Ar problem in the highest and lowest temperature ends of the degassing experiment. When these points are eliminated from the regression (the gray boxes in Fig. 4), the resulting distribution is a linear array representing mixing between a nearly atmospheric component of Ar ($^{40}Ar/^{36}Ar$ = 326 ± 7) and a radiogenic component corresponding to an age of 241 ± 6 Ma (Fig. 4). The 'fit' to the line is not quite as good as that for SU4, so the scatter of data about the line cannot absolutely be attributed only to analytical errors. The previous K-Ar whole rock age for this sample was 280 Ma (Færseth et al., 1976)

The plagioclase separate from Sotra sample 3-96 (previously dated by whole-rock K-Ar at 262 Ma, Løvlie and Mitchell, 1982) yielded a very irregular spectrum with two low, initial ages and a series of roughly concordant-to-climbing age steps ranging between 282 and 328 Ma (Table 5.1). However, the inverse isochron diagram again isolates at least one group of excess-Ar components (in the high-temperature portion of the experiment). The line remaining after removal of these points from the regression is rather poorly correlated (MSWD = 5.0) and does not extract completely the excess-Ar component. Thus, the radiogenic intercept of 241 ± 11 Ma must be considered a maximum age for this sample.

The release spectrum from the whole-rock Sunnhordaland sample SU10 (see also Fig. 2) has a slightly undulating pattern (Fig. 5). A low-age, initial step is succeeded by a series of apparent ages (through fusion) that vary about ca. 160 Ma. A valid 'plateau' is not derived from these data, due primarily to the single low-age, low-volume step-down in the middle of the experiment. The weighted mean age for this sample (excluding the lowest one and highest two temperature steps) is 162 ± 3 Ma. An inverse isochron plot of these data was not useful as the data clustered in a single group very close to the ordinate (radiogenic) axis. Recall that this sample previously gave the youngest K-Ar age for the Sunnhordaland-Sotra dikes (168 Ma) (see Fig. 2).

3.4 INTERPRETATION AND REGIONAL SIGNIFICANCE

The new ^{40}Ar-^{39}Ar data are combined with the older K-Ar results in Figure 6. We interpret the 235 and 241 Ma ages for SU4 and SU9 to represent the crystallization ages of these samples. Portions of the whole rocks were quite clearly affected by excess-Ar that we were able to isolate through the inverse isochron diagrams. Excess Ar appears to be confined to the low-temperature, weakly bound parts of the whole rocks (most likely the slightly altered grain surfaces and/or glassy groundmass of the dikes) and to the high-temperature, more retentive portions of the rocks, corresponding to clinopyroxene and amphibole. Similarly, although the Sotra dike plagioclase (3-96) was also affected by excess Ar, we are confident that the 241 Ma age is a 'maximum' age for cooling of this sample and, because of its overlap with Sunnhordaland ages, we assume this age very nearly defines the timing of crystallization of the dike.

The younger dike, SU10, yielded an age of 162 Ma that we also interpret to document the crystallization of the dike. The spectrum, although slightly irregular, comprises a large gas volume with steps of very similar ages. The only evidence we see for Ar-loss in this sample is from the lowest-temperature, least retentive portion of the whole rock (first step in the spectrum). The age for this dike is similar within uncertainty to the original K-Ar age for this rock. Although the Early Triassic dikes dated in this study do show evidence for some alteration/disturbance post-dating crystallization, we could expect the youngest dikes in the area (e.g. the Mid-Late Jurassic dikes) to be *most likely* to retain their original ages; this reasoning follows from the fact that very few, if any, known thermal or fluid events occurred onshore subsequent to Jura-Cretaceous time. We note that Fossen and Dunlap (in review) suggest the age of this youngest dike to be ca. 220 Ma; they derive their age from ^{40}Ar-^{39}Ar analysis of an amphibole separate from the same whole rock dated in our study. Although we have not seen their data, we would tentatively propose that the 220 Ma amphibole age is a result of excess-Ar in the mineral system. In the case of the whole-rock analysis, the 'excess-Ar' in the amphibole becomes one of the mixing components in a homogeneous system comprising atmospheric, radiogenic and 'excess' Ar. Thus we support our claim that the 162 Ma age represents most closely the 'accurate' crystallization age of the dike.

Figure 6 demonstrates that the new data enable us to eliminate the very wide spread in older K-Ar ages. The rocks originally dated by whole-rock K-Ar methods at 222, 262 and 280 Ma (recalculated ages), can be reinterpreted to have crystallized in a fairly tight window between 235 and 241 Ma. This holds for both Sunnhordaland and Sotra areas. The K-Ar ages that were 'too old' can be reassessed with fair certainty to be the result of excess Ar that remained undetectable with the data derived through conventional K-Ar analysis. The 222 Ma K-Ar age which is now re-dated to 235 Ma, can best be interpreted to be a 'mixing age' between some episode of Ar-loss and excess-Ar. The Mid-Late Jurassic intrusive K-Ar age of 168 Ma is reasonably replicated and confirmed with the new whole rock ^{40}Ar-^{39}Ar age of 162 Ma.

The Early Triassic episode overlaps very precisely in time with ages from young dikes dated from the northern Oslo Rift (see Torsvik et al., in press and Chapter 4 of this Report) also by the ^{40}Ar-^{39}Ar method. Extension-related brittle faulting (248-260 Ma) in the Sunnfjord region of W. Norway (Torsvik et al., 1992; Eide et al., 1997) further enhances the picture of regional crustal extension along the southern and western Norway margin at the inception of the Mesozoic Era. The correlation of these events with the regional paleogeographic situation for this time period is illustrated in Figure 7. We note the excellent correspondence between the paleolatitudes deduced for southern Norway via our combined paleomagnetic and radiometric age data and the limits of the warm-water carbonates (25N) mapped from the offshore sedimentary record.

A similar correspondence in Mid-Late Jurassic time results when we compare our 162 Ma dike age with the timing of the second phase of brittle faulting in Sunnfjord (Torsvik et al., 1992; Eide et al., 1997) at <163 Ma, and the timing of emplacement of the Scania basalts in S. Sweden (178 Ma). Again, a regional picture of crustal extension, faulting and magma emplacement is generated for southern Scandinavia (Figure 8).

The importance of Late Permian-Early Triassic rifting and extension and of Middle-Late Jurassic rift and drift in the northern North Sea have certainly been noted in the literature (Færseth et al., 1997; Doré et al., 1997). This study refines these episodes both in time and space and quantifies very identifiable and distinct products (dikes) that can be used as analogues and time markers for similar offshore features.

3.5 REFERENCES

Arnaud N.O., Brunel, M., Cantagrel, J.M. & Tapponier, P. (1993) High cooling and denudation rates at Kongur Shan, eastern Pamir (Xinjiang, China) revealed by $^{40}Ar/^{39}Ar$ alkali feldspar thermochronology. *Tectonics* 12, 1335-1346.

Doré, A.G., Lundin, E.R., Fichler, C. and Olesen, O. (1997) Patterns of basement structure and reactivation along the NE Atlantic margin. *J. Geol. Soc. London* 154, 85-92.

Eide, E.A., Torsvik, T.H. & Andersen, T.B. (1997) Absolute dating of brittle fault movements: Late Permian and late Jurassic extensional fault breccias in western Norway. *Terra Nova* 9, 135-139.

Furnes, H., Mitchell, J.G., Robins, B., Ryan, P. & Skjerlie, F.J. (1982) Petrography and geochemistry of peralkaline, ultrapotassic syenite dykes of Middle Permian age, Sunnfjord, West Norway. *Norsk Geol. Tidsskr.* 62, 147-159.

Færseth, R.B. (1978) Mantle-derived lherzoilite xenoliths and megacrysts from Permo-Triassic dykes, Sunnhordaland, western Norway. *Lithos* 11, 23-35.

_____ (1996) Interaction of Permo-Triassic and Jurassic extensional fault-blocks during the development of the northern North Sea. *J. Geol. Soc. London* 153, 931-944.

Færseth, R.B., Macintyre, R.M. & Naterstad, J. (1976) Mesozoic alkaline dykes in the Sunnhordaland region, western Norway: ages, geochemistry and regional significance. *Lithos* 9, 331-345.

Færseth, R.B., Knudsen, B.-E., Liljedahl, T., Midbøe, P.S. & Søderstrøm, B. (1997) Oblique rifting and sequential faulting in the Jurassic development of the northern North Sea. *J. Struct. Geol.* 19, 1285-1302.

Løvlie, R. (1981) Palaeomagnetism of coast-parallel dykes from western Norway; ages of magmatism and evidence for crustal uplift and collapse. *Geophys. J. R. astr. Soc.* 66, 417-426.

Løvlie, R. & Mitchell, J.G. (1982) Complete remagnetization of some Permian dykes from western Norway induced during burial/uplift. *Phys. Earth Plan. Int.* 30, 415-421.

Macintyre, R.M. & Færseth, R.B. (1982) Comments on æPalaeomagnetism of coasat-parallel alkaline dykes from western Norway; ages of magmatism and evidence for crustal uplift and collapse' by R. Løvlie. *Geophys. J. R. astr. Soc.* 70, 539-542.

Rohrman, M., van der Beek, P. and Andriessen, P. (1994) Syn-rift thermal structure and post-rift evolution of the Oslo Rift (southeast Norway):New constraints from fission track thermochronology. *Earth Planet. Sci. Lett.* 127, 39-54.

Skjerlie, F.J. & Tysseland, M. (1981) Geochemistyr and Petrology of Dolerite Dykes of Probable Late Caldeonian age from the outer Sunnfjord region, West Norway. *Norges geol. unders. Bull.* 363, 25-43.

Torsvik, T.H., Sturt, B.A., Swensson, E., Andersen, T.B. and Dewey, J.F., 1992. Palaeomagnetic dating of fault rocks: evidence for Permian and Mesozoic movements and brittle deformation along the extensional Dalsfjord Fault, western Norway. *Geophys. J. Int.*, 109, 565-580.

Torsvik, T.H., Andersen, T.B., Eide, E.A. & Walderhaug, H. (1997) The age and tectonic significance of dolerite dykes in western Norway. *J. Geol. Soc. Lond.* 154, 961-973.

Verschure, R.H., Maijer, C. & Andriessen, P.A.M. (1989) Isotopic age determinations in South Norway: I. The Skår volcanic breccia, Greipstad, Vestagder. *Geol. Minj.* 68, 253-256.

Ziegler P. A. (1990) Geological Atlas of Western and Central Europe. *Shell Internationale Petroleum Maatschappij B.V.* 239 pp.

CAPTIONS

Figure 1. 'Onshore-offshore' map of western Norway showing locations of the major dike localities. Focus lies on Sunnhordaland-Sotra area (gray shading) with black dots representing the analysis localities of Færseth et al. (1976) and Løvlie and Mitchell (1982). The newly identified Jurassic sediments from the Bjørøy tunnel (Fossen et al., 1997) are also pinpointed. Other dikes discussed in the text include those from the Sunnfjord region (Mid-Late Permian dikes dated by Furnes et al., 1982 and Torsvik et al. 1997). The lineaments drawn from data of the Viking '93 aeromagnetic survey offshore are also shown. Details of the interpretations of these lineaments are presented in Smethurst (1998, this Report Series). A reconstruction for the N. Atlantic in the inset (upper left) of the figure illustrated the importance of the latest Permian-Early Triassic dikes dated in the current study with regard to influence on developing shelf structures.

Figure 2. Simple histogram of the K-Ar ages obtained for the Sunnhordaland-Sotra and Sunnfjord areas (Færseth et al., 1976; Furnes et al., 1982; Løvlie and Mitchell, 1982). Numbers on tops of the bars indicate the K-Ar ages for those rocks; bars with 'A' on the top represent K-Ar analyses of amphibole separates while all others are whole-rock analyses. Boxes with stars represent those samples redated in the present study; sample numbers in the present study are noted below each gray box. Note that the ages derived before 1979 have been recalculated using modern decay constants. Data display generated using NGUISO Isotopic Database and Analysis Package (Torsvik, 1998, this Report Series).

Figure 3. ^{40}Ar-^{39}Ar data from whole-rock analysis of SU4 (Sunnhordaland whole-rock). The previous K-Ar age was 222 Ma. (a) Age spectrum for the sample documents a plateau age of 239 ± 4 Ma (black boxes), with evidence for excess Ar components both in the low- and high-temperature ends of the spectrum. (b) Inverse isochron display of the same data reveals two distinct linear arrays. Gray boxes represent excess Ar components (low and high temperature steps removed in plateau calculation of (a)), while black boxes define a good fit of data about a line corresponding to mixing between an atmospheric component of Ar and an apparent age of 235 ± 5 Ma. We utilize the latter as the crystallization age of this sample (see text for details).

Figure 4. Inverse isochron display of ^{40}Ar-^{39}Ar data from whole-rock analysis SU9. Excess Ar components surmised from the spectrum for this sample are confirmed in this data presentation. When excess Ar components (gray boxes) are removed, the resulting linear array defines a nearly atmospheric intercept and a sample age of 241 ± 6 Ma. Previous K-Ar age for this sample was 280 Ma.

Figure 5. ^{40}Ar-^{39}Ar data from whole-rock analysis of SU10 (Sunnhordaland whole-rock). The data do not define a valid 'plateau', largely due to the single, low volume, low-temperature step (step 5). However, a simple mean age of 162 ± 4 Ma from these data (black boxes) is quite similar to the 168 Ma age for the same rock derived by Færseth et al. (1976). In the field, this dike crosscuts an older dike generation and has a distinctly more alkaline chemistry than others from Sunnhordaland.

Figure 6. Replicate of Figure 2 with new ^{40}Ar-^{39}Ar ages added from this study. The old K-Ar age 'spread' in the dike data is eliminated by the new analyses. Apparently 'older' Early Permian and 'younger' Late Triassic dikes converge instead to Early Triassic time. We interpret these new data to represent a single, focused pulse of extension-related magmatism in this area at the dawn of the Triassic; the spread in older K-Ar ages is a function of various reactivation events and/or original, partial-pressures of Ar that lead to excess Ar (or Ar loss) in some samples. Excess Ar is not as straightforward to detect with the K-Ar method as with the ^{40}Ar-^{39}Ar method. The Mid-Late Jurassic age previously derived for the crosscutting dike in Sunnhordaland by Færseth et al. (1976) is confirmed by the new analysis.

Figure 7. Early Triassic (243 Ma) paleoreconstruction for the North Sea region combining sedimentary facies distribution data of Ziegler (1990), paleomagnetic data from Torsvik et al. (1998) and ^{40}Ar-^{39}Ar data from the present study, Torsvik et al. (1998) and Eide et al. (1997). Some K-Ar ages for the Skår volcanic breccias of southern Norway (241 Ma, noted on figure) by Verschure et al. (1989) are also plotted. The data show a good match between paleolatitudes defined by Torsvik et al. (1998) and the expected northern limit of evaporites (25N) in NW Europe at this time. Furthermore, the new radiometric data demonstrate a consistent pattern of extension and magmatic activity along southern and western Norway at

this time, as Pangea continued its northward drift. Dike ages are supplemented by the timing of brittle fault activity in the Dalsfjord region (248-260 Ma, Eide et al., 1997).

Figure 8. Middle Jurassic (177- 164 Ma) paleogeographic reconstruction for the North Sea region, combining data as in Figure 7. Additions include the fission track (FT) data of Rohrman et al. (1994) for the Oslo Rift region. Again, the paleolatitudinal data from the Dalsfjord and Scania (S. Sweden) areas (Torsvik et al., 1992; Eide et al., in prep.) agree nicely with the limit of shallow-marine carbonates in the facies map (45N). The age data onshore (Dalsfjord fault rock, Sunnhordaland dike, Göbnehall dike (Eide et al., in prep.) demonstrate a consistent picture of extension and magmatism at this time period, corresponding also with some data available from offshore dating of volcanics (Ziegler 1990).

TABLE 3.1. ^{40}Ar-^{39}Ar data for four samples from Sunnhordaland and Sotra. Sunnhordaland samples included three whole rock alkaline basalts. Sotra samples was plagioclase separate.

1. Sample SU4 (Sunnhordaland 4), whole rock alkaline basalt; J = 0.0169700; wt = 5 mg
   Inverse isochron age = 235 ±5 Ma (use)
   Weighted mean plateau age = 239 ±4 Ma

T (°C)	$^{40}Ar/^{39}Ar$	$^{38}Ar/^{39}Ar$	$^{37}Ar/^{39}Ar$	$^{36}Ar/^{39}Ar$	^{39}Ar	$F^{39}Ar$	$\%^{40}Ar^*$	$^{40}Ar^*/^{39}K$	Age (Ma)	± 1σ
612	126.992	0.098	10.746	393.692	0.783	4.53	10.6	14.79	404.01	60.89
700	34.572	0.036	10.043	90.873	2.497	18.87	25.6	9.64	273.44	8.85
750	12.979	0.021	1.645	16.018	2.358	31.48	65.0	8.55	244.35	5.28
800	14.486	0.022	1.249	20.908	2.242	43.43	58.7	8.58	245.35	6.07
850	15.802	0.023	1.247	25.493	1.820	53.14	53.7	8.57	244.98	7.01
900	12.488	0.021	1.324	14.464	1.830	62.90	67.1	8.46	242.11	5.87
950	12.412	0.022	1.470	14.386	1.270	69.68	67.1	8.43	241.20	5.74
1000	9.875	0.020	1.603	6.911	1.409	77.22	80.7	8.07	231.63	7.02
1050	10.085	0.020	1.627	7.180	1.942	87.61	80.3	8.21	235.31	5.24
1100	10.596	0.021	3.453	7.644	1.100	93.58	81.1	8.84	252.23	5.60
1150	11.949	0.022	12.662	11.945	0.448	96.21	77.9	10.36	292.07	13.86
1200	44.308	0.038	35.414	40.593	0.062	96.67	78.6	48.69	1086.49	221.28
1400	21.002	0.021	13.674	20.365	0.562	100.00	76.1	17.95	479.76	8.47

2. Sample SU9 (Sunnhordaland 9), whole rock alkaline basalt; J = 0.0169800; wt = 5 mg
   Inverse isochron age = 241 ±6 Ma (use)
   No plateau age

T (°C)	$^{40}Ar/^{39}Ar$	$^{38}Ar/^{39}Ar$	$^{37}Ar/^{39}Ar$	$^{36}Ar/^{39}Ar$	^{39}Ar	$F^{39}Ar$	$\%^{40}Ar^*$	$^{40}Ar^*/^{39}K$	Age (Ma)	± 1σ
600	82.787	0.062	3.617	205.285	0.884	5.60	28.4	24.19	620.74	27.73
700	47.646	0.043	7.354	127.761	1.911	18.08	23.2	11.76	328.51	16.13
750	15.522	0.023	2.600	21.875	1.894	29.98	60.2	9.54	270.87	8.86
800	14.941	0.023	1.627	19.874	1.530	39.51	62.1	9.40	267.18	7.90
850	18.234	0.025	1.451	29.943	1.573	49.29	52.9	9.75	276.45	6.84
900	14.681	0.023	1.137	19.271	1.589	59.15	62.4	9.24	263.04	6.16
950	11.385	0.021	1.235	9.804	1.440	68.09	75.7	8.70	248.64	5.56
1000	10.377	0.020	1.623	7.219	1.687	78.60	80.8	8.49	243.06	5.25
1050	10.094	0.020	2.193	6.155	1.884	90.39	83.7	8.60	245.82	5.46
1200	14.189	0.021	16.065	13.187	1.176	98.69	80.4	13.09	362.17	7.57
1400	29.376	0.031	31.125	52.749	0.160	100.00	54.8	21.46	560.63	13.99

3. Sample 3-96 (Sotra 3), plagioclase; J = 0.0134900; wt = 5 mg
Inverse isochron age = 241 ±11 Ma (use), complicated by excess Ar.
No plateau age

T (°C)	$^{40}Ar/^{39}Ar$	$^{38}Ar/^{39}Ar$	$^{37}Ar/^{39}Ar$	$^{36}Ar/^{39}Ar$	^{39}Ar	$F^{39}Ar$	$\%^{40}Ar^*$	$^{40}Ar^*/^{39}K$	Age (Ma)	± 1σ
600	14.176	0.093	17.664	21.153	0.039	5.29	64.8	10.70	243.32	9.73
700	12.376	0.028	8.780	24.020	0.119	20.08	48.3	6.43	150.04	4.29
750	12.488	0.019	12.595	7.033	0.058	27.52	90.2	12.53	281.74	6.54
800	12.305	0.018	9.563	5.386	0.073	36.65	92.3	12.30	277.04	5.75
850	12.124	0.018	5.471	4.246	0.091	47.66	92.7	11.76	265.64	5.51
900	12.616	0.019	5.390	6.445	0.080	57.28	87.9	11.59	262.15	5.70
950	13.659	0.019	10.366	10.759	0.041	62.38	82.1	12.23	275.40	7.25
1000	13.336	0.020	17.947	11.034	0.050	69.12	84.7	13.20	295.67	6.26
1050	13.986	0.020	20.819	11.905	0.055	76.71	85.0	14.27	317.58	6.78
1100	14.580	0.020	19.452	13.398	0.044	82.73	82.0	14.17	315.53	7.59
1200	14.504	0.021	14.677	11.771	0.053	89.70	83.0	13.65	304.88	7.39
1400	22.168	0.026	12.528	33.322	0.080	100.00	60.1	14.80	328.48	8.60

4. Sample SU10 (Sunnhordaland 10), whole rock alkaline basalt; J = 0.0169700; wt = 5 mg
Inverse isochron age = 162 ±4 Ma (use)
Simple mean age = 162 ±4 Ma

T (°C)	$^{40}Ar/^{39}Ar$	$^{38}Ar/^{39}Ar$	$^{37}Ar/^{39}Ar$	$^{36}Ar/^{39}Ar$	^{39}Ar	$F^{39}Ar$	$\%^{40}Ar^*$	$^{40}Ar^*/^{39}K$	Age (Ma)	± 1σ
600	9.971	0.022	0.440	19.488	7.629	15.47	43.5	4.36	128.71	3.87
700	14.602	0.024	0.327	30.973	4.734	25.05	38.6	5.65	165.17	5.49
750	6.731	0.020	0.387	3.393	4.168	33.50	85.7	5.78	168.93	3.64
800	6.234	0.019	0.372	2.802	4.724	43.07	87.3	5.46	159.74	3.55
850	5.998	0.020	0.434	2.637	2.371	47.88	87.6	5.27	154.63	3.24
900	5.985	0.021	0.802	2.017	3.356	54.70	91.0	5.48	160.48	3.48
950	6.020	0.021	0.965	1.851	3.598	62.02	92.0	5.58	163.30	3.85
1000	6.101	0.021	1.267	2.086	4.540	71.29	91.3	5.63	164.62	3.52
1050	6.211	0.020	1.244	2.209	5.338	82.18	90.9	5.70	166.64	3.60
1100	6.123	0.019	1.156	2.438	4.030	90.40	89.6	5.54	162.01	3.60
1150	6.086	0.020	0.919	2.592	1.564	93.58	88.5	5.43	158.96	3.64
1200	6.674	0.021	1.147	3.351	0.483	94.57	86.5	5.82	170.04	4.38
1400	6.652	0.020	0.941	3.556	2.670	100.00	85.3	5.72	167.12	3.72

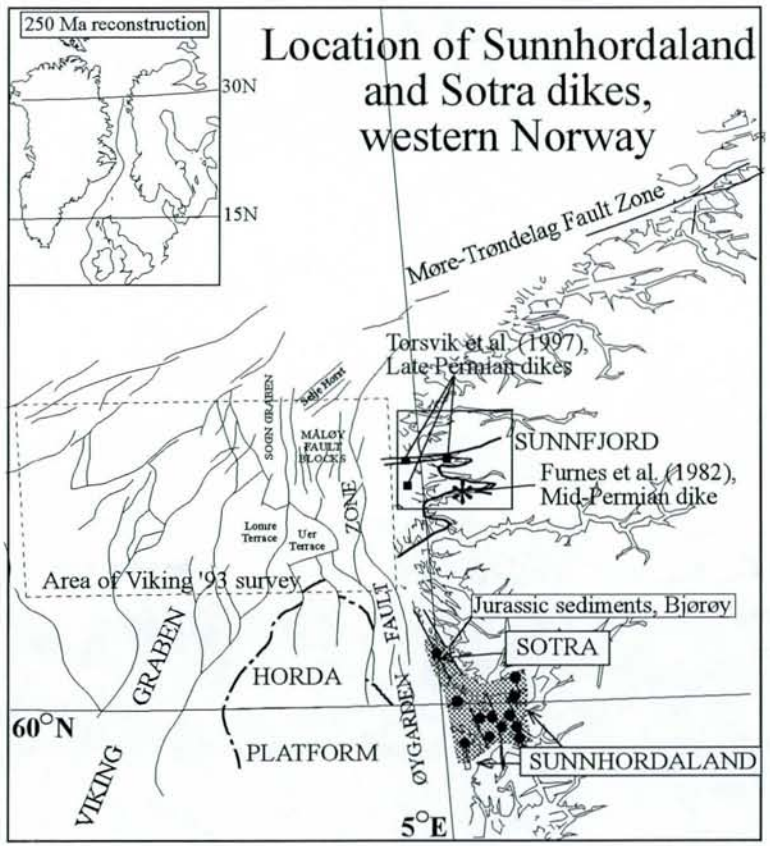
250 Ma reconstruction
30N
15N
Location of Sunnhordaland and Sotra dikes, western Norway
Møre-Trøndelag Fault Zone
Torsvik et al. (1997), Late-Permian dikes
SUNNFJORD
Furnes et al. (1982), Mid-Permian dike
Solje Horst
SOGN GRABEN
MÅLØY FAULT BLOCKS
Lonre Terrace
Ufr Terrace
ZONE
Area of Viking '93 survey
Jurassic sediments, Bjørøy
SOTRA
FAULT
GRABEN
HORDA
ØYGARDEN
60°N
PLATFORM
SUNNHORDALAND
VIKING
5°E

Figure 1

Original K-Ar ages for Sunnhordaland-Sotra dikes and Dalsfjord syenite dike

(Færseth et al., 1976; Furnes et al., 1982; Løvlie and Mitchell, 1982)

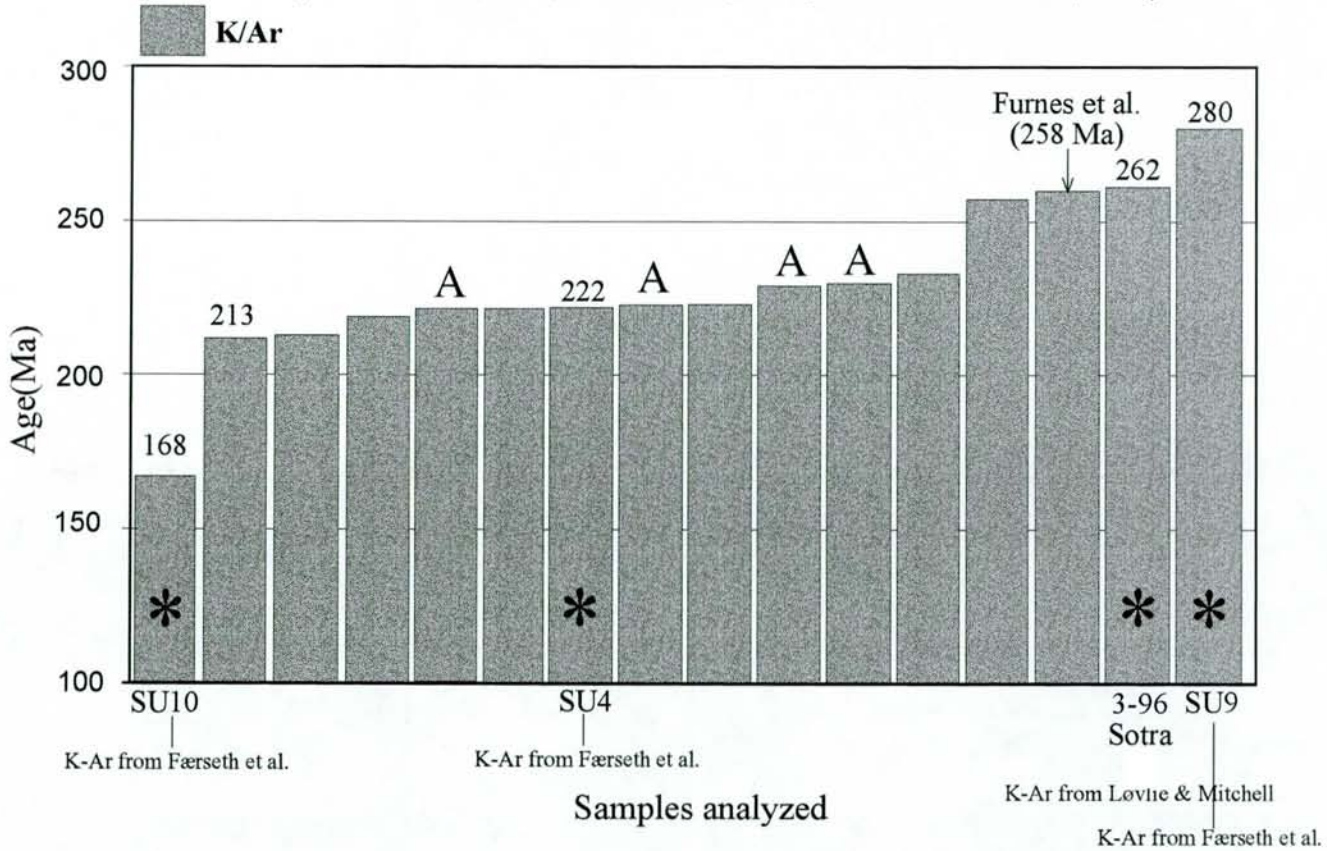

Figure 2

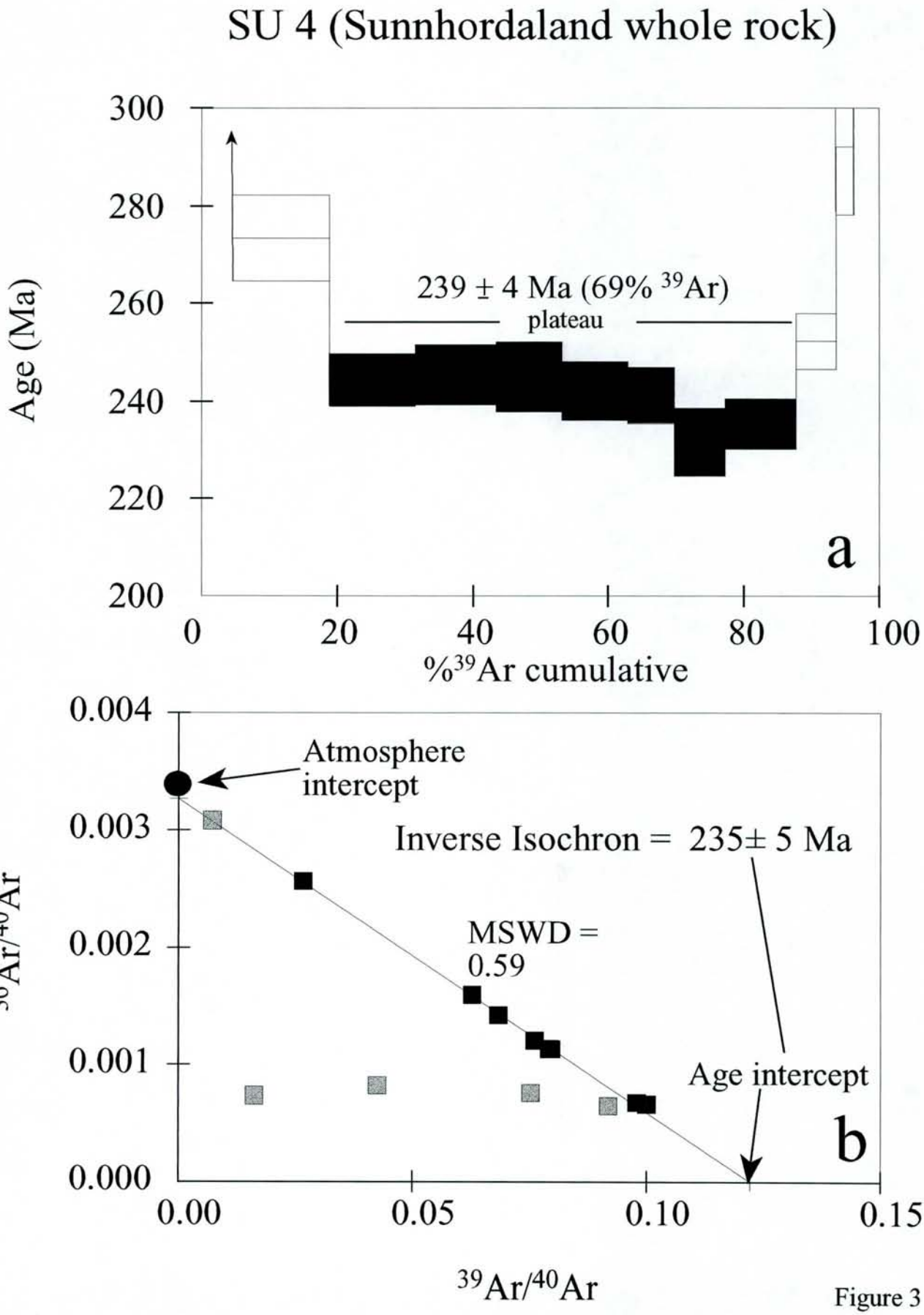
SU 4 (Sunnhordaland whole rock)
300
280
260
240
220
200
Age (Ma)
239 ± 4 Ma (69% 39Ar)
plateau
a
0
20
40
60
80
100
%39Ar cumulative
0.004
0.003
0.002
0.001
0.000
36Ar/40Ar
Atmosphere
intercept
Inverse Isochron = 235± 5 Ma
MSWD =
0.59
Age intercept
b
0.00
0.05
0.10
0.15
39Ar/40Ar

Figure 3

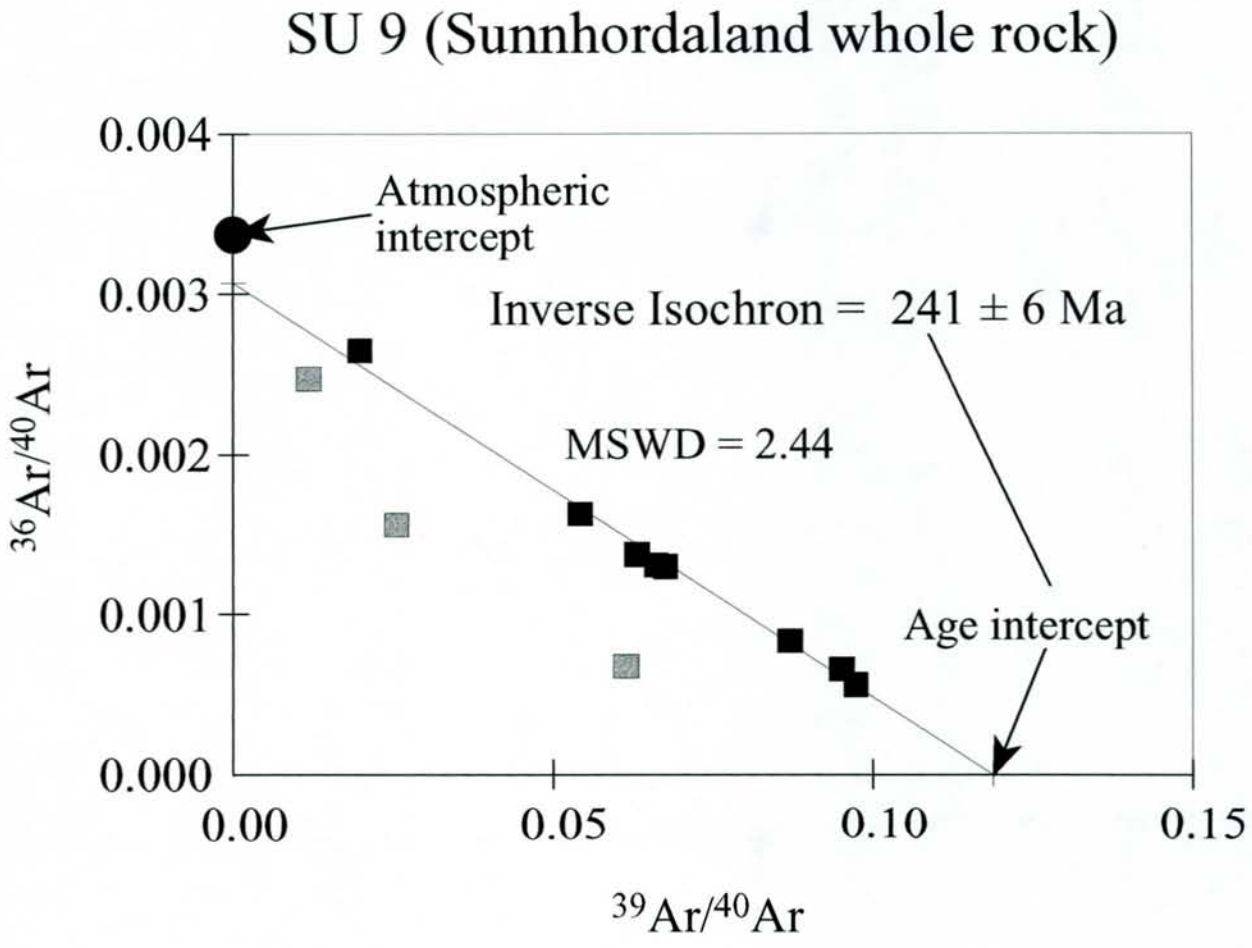
SU 9 (Sunnhordaland whole rock)
0.004
0.003
0.002
0.001
0.000
Atmospheric intercept
Inverse Isochron = 241 ± 6 Ma
MSWD = 2.44
Age intercept
0.00
0.05
0.10
0.15
$^{36}Ar/^{40}Ar$
$^{39}Ar/^{40}Ar$

Figure 4

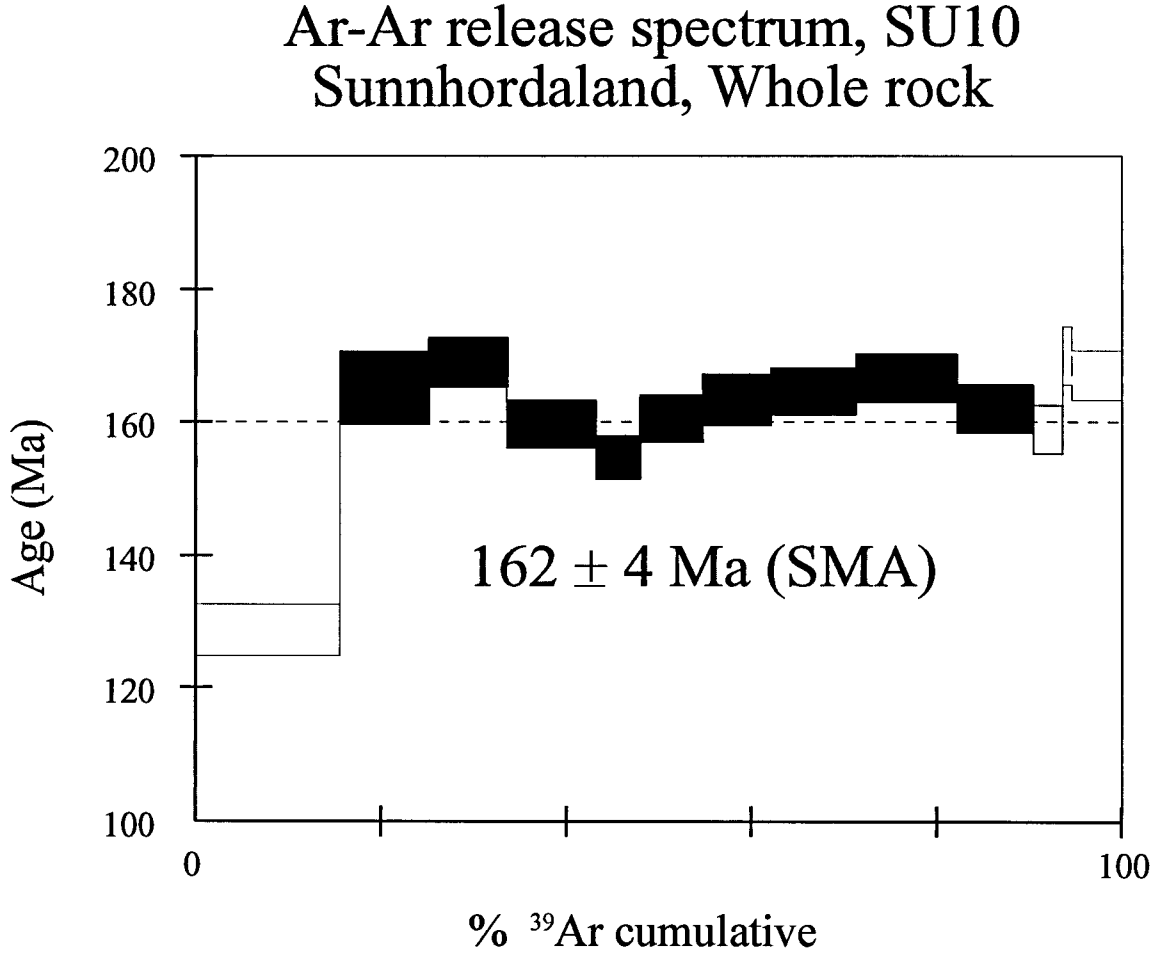

K-Ar = 168 Ma (Færseth et al., 1976)

Figure 5

Old K-Ar and new ^{40}Ar-^{39}Ar ages for Sunnhordaland-Sotra

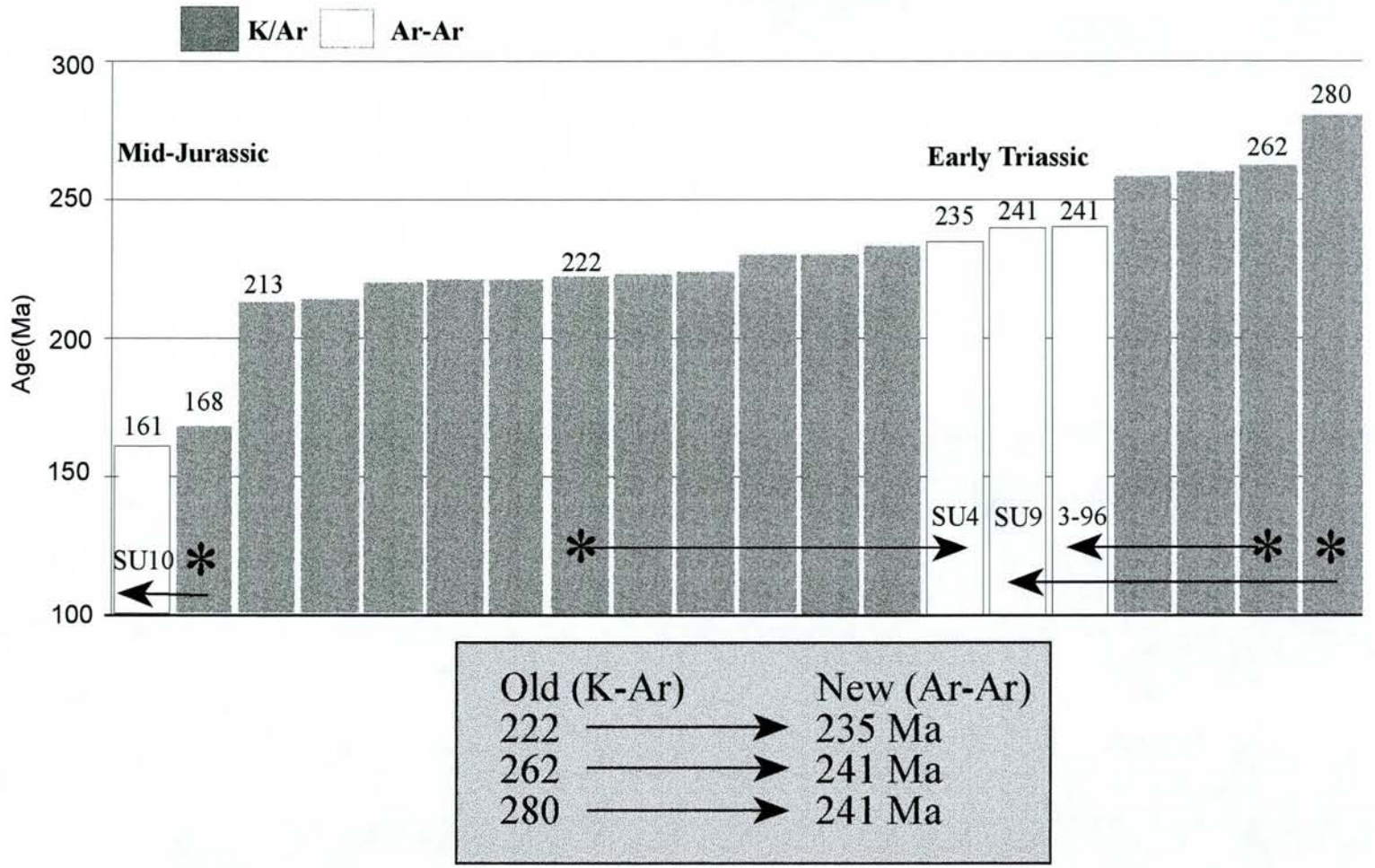

Figure 6

Early Triassic, Buntsandsstein, Palaeogeography (243 Ma)

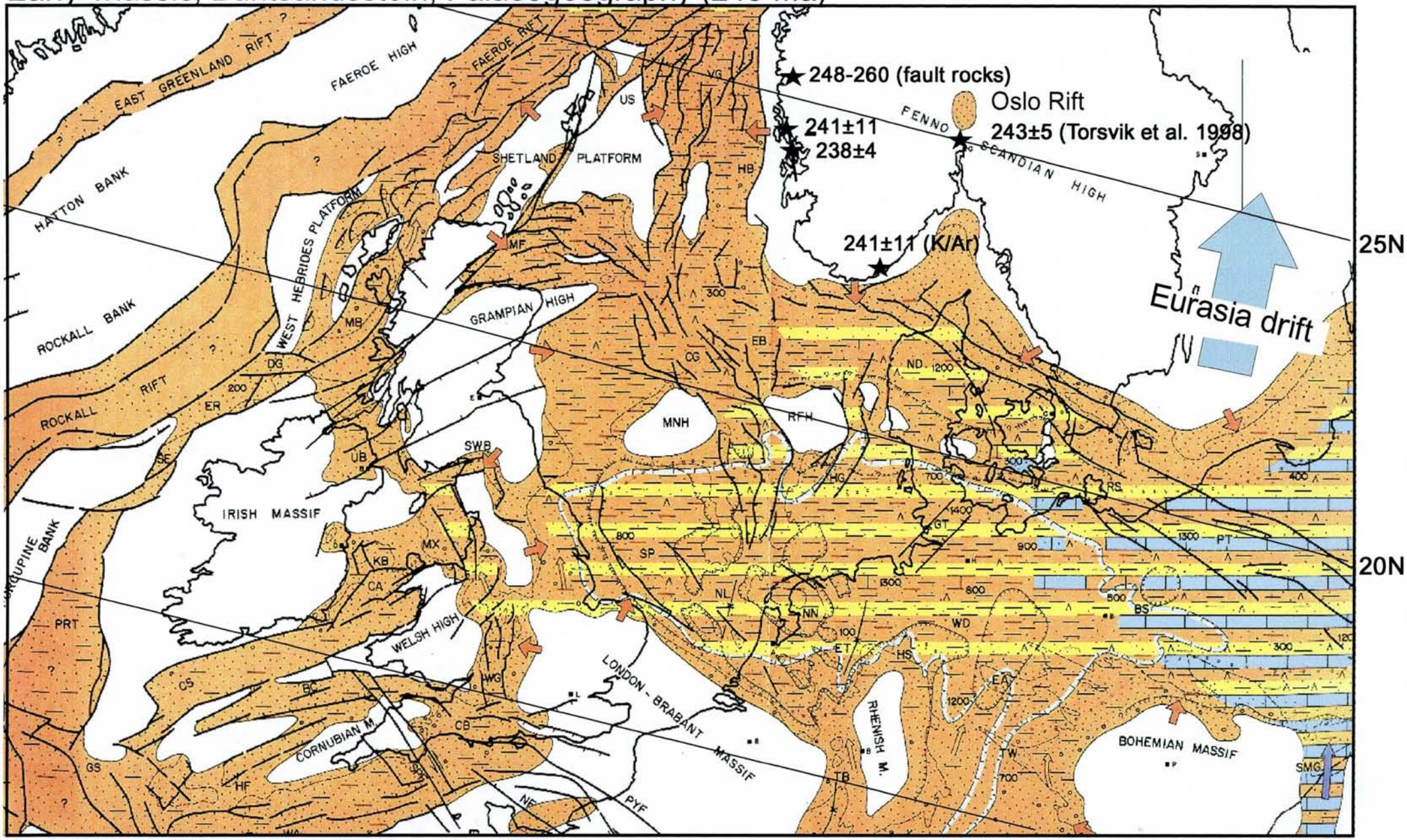

Continental, lacustrine

Deltaic, coastal and shallow-marine clastics

Cratonic, mainly low relief

Carbonates, mainly shallow-marine

★ Volcanics, local

Coal

Salt

Figure 7

Mid-Jurassic, Bajocian-Bathonian (176.5±4.0 -164.4±3.8 Ma), Palaeogeography

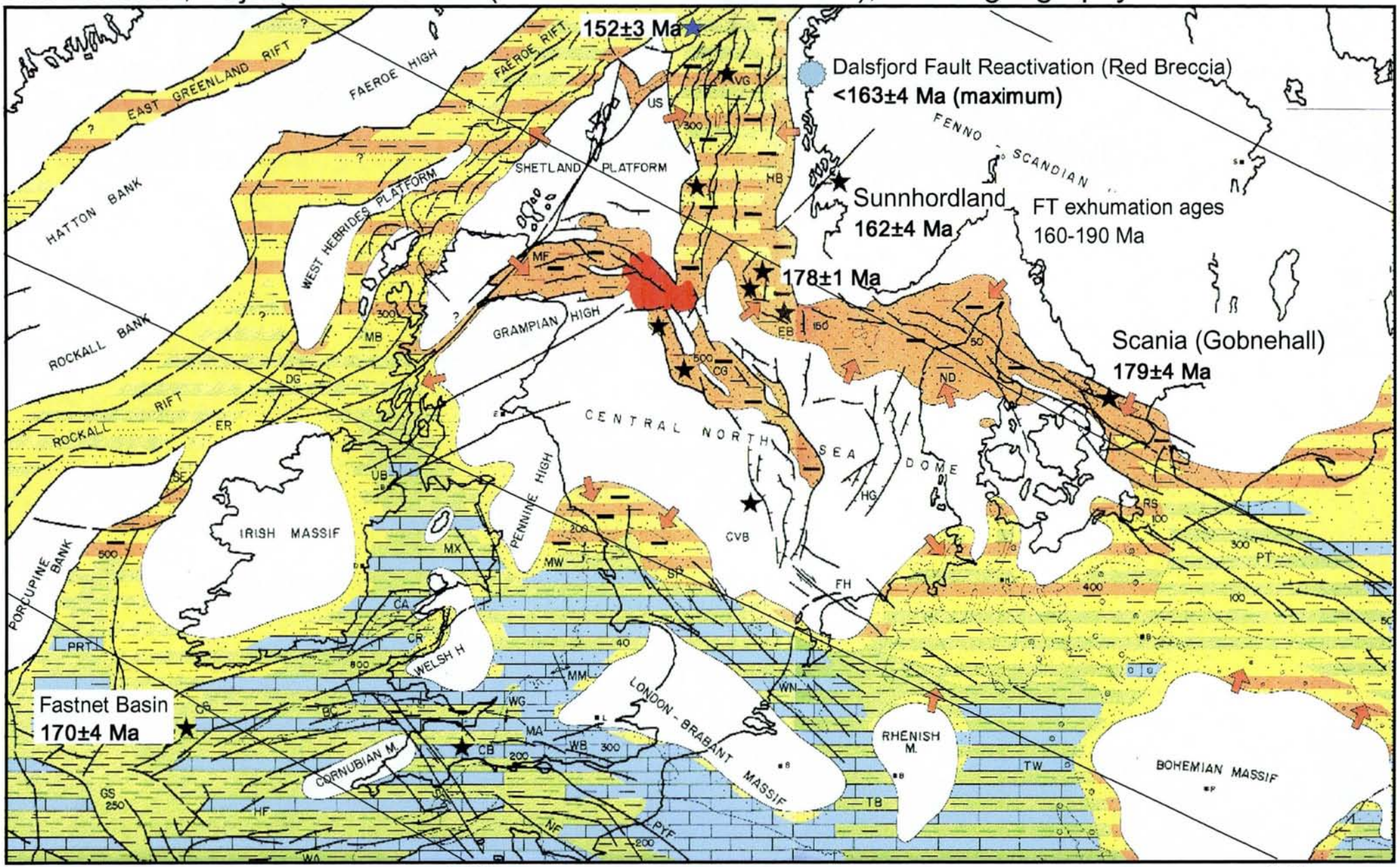

Continental, lacustrine
Deltaic, coastal and shallow-marine clastics
Shallow-marine, mainly shales
Carbonates, mainly shallow-marine
Cratonic, mainly low relief
Major extrusives
Volcanics, local
Coal

Figure 8

Chapter 4

Submitted as:

The Oslo Rift: New Palaeomagnetic and $^{40}Ar/^{39}Ar$ constraints

Torsvik, T.H., Eide, E.A., Meert, J.G., Smethurst, M.A. & Walderhaug, H.J.

Geophys. J. Int.

(23.01 submitted Geophys. J. International)

The Oslo Rift: New palaeomagnetic and $^{40}Ar/^{39}Ar$ age constraints

T.H. Torsvik[1,2], E.A. Eide[1], J.G. Meert[3], M.A. Smethurst[1] & H.J. Walderhaug[2]

[1]Geological Survey of Norway, P.B. 3006 Lade, N-7002 Trondheim (Norway)
[2] Institute of Solid Earth Physics, University of Bergen, Allegt. 41, N-5007 Bergen (Norway)
[3]Dept. of Geography and Geology, Indiana State Unversity, Terre Haute, IN 47809 (USA)

Abstract

$^{40}Ar/^{39}Ar$ whole-rock and plagioclase ages demonstrate that dioritic to monzonitic dykes from Bøverbru and Lunner belong to the youngest recorded magmatic activity in the Oslo Rift region (SE Norway). These dykes represent the terminal phase of rift and magmatic activity in the Oslo Graben at the dawn of the Triassic (246.2-238.3 Ma).

The Bøverbru and Lunner dyke ages are statistically concordant; the Bøverbru dyke, however, has an unusual palaeomagnetic signature and the new Early Triassic palaeomagnetic pole for Baltica (Eurasia) is exclusively based on the less complex Lunner dykes and contacts (palaeomagnetic pole: latitude=52.9°N, longitude=164.4°E, dp/dm=4.5°/7.3°).

The early Triassic (mean age:243±5 Ma (2σ)) palaeomagnetic pole is slightly different from the Upper Carboniferous-Permian (294-274 Ma) and Kiaman-aged poles from the Oslo Rift. The latter poles are concordant with the palaeomagnetic overprint signature of Palaeozoic sediments near the Oslo Rift.

Introduction and geology

The Oslo Rift system and its associated tract of intrusive rocks are fundamental Permo-Carboniferous features in southern Norway (Ramberg 1976, Ramberg & Larsen 1978, Neuman 1994, Sundvoll & Larsen 1994, Olaussen et al. 1994) (Fig. 1). Palaeomagnetically analysed rocks from the Oslo Graben show a predominance of reverse polarities (van Everdingen 1960, Douglass 1989) which comes as no surprise since the c. 310-240 Ma (Sundvoll & Larsen 1990, 1994) magmatic activity in the region partially overlaps with the Kiaman Reverse Superchron (KRS) (c. 311-262 Ma; Eide & Torsvik 1996 and references therein).

Although the rift-related rocks which intruded during the reverse-polarity superchron can be used to constrain palaeogeography, the rocks do not yield detailed information on the

specific ages of various magmatic episodes or tectonic regimes as related to the geomagnetic polarity time scale. Magmatic activity in the Oslo Rift did persist after the KRS and, as part of an ongoing regional palaeomagnetic and isotopic dating program in SE Norway, we present a detailed account of palaeomagnetic and $^{40}Ar/^{39}Ar$ experiments from some of these younger, rift-related rocks (analytical procedures described in Appendix 1). We focus in the northern part of the Oslo Rift region on dykes from the Bøverbru and Lunner areas (Fig. 1) and the Mjøsa Limestone rocks they intrude. The Upper Ordovician Mjøsa Limestone has been described in detail by Owen et al. (1990), Bjørlykke (1983), and Opalinski and Harland (1981), but to our knowledge, none of the investigated dykes at Bøverbru and Lunner (new 1995 road-cut) have been mentioned in the literature.

Following a Devonian-Early Carboniferous lacuna (subaerial exposure) for much of southern Norway, the rocks in the Oslo region experienced a continuous series of events related to final amalgamation of Pangea. The highlight of this Late Palaeozoic activity in the Oslo region includes N-S compression and related dextral transpression and transtension as Variscan tectonics advanced northward in continental Europe. Dextral transtension led to development of a purely extensional regime in the Oslo Rift system and the culmination of rifting and peak magmatic activity in the Oslo Graben (c. 279 Ma; Olaussen et al. 1994; Heeremans et al., 1996). The Latest Permian-Early Triassic period in the Oslo area has been described as the 'termination phase' of the evolution of the Oslo Rift system; this latest episode was associated with emplacement of small syenitic to granitic batholiths (Sundvoll and Larsen, 1994; Olaussen et al., 1994). The two study areas are free from these young batholithic intrusions (Fig. 1), and the only magmatic rocks previously described from this northern section of the Oslo Graben have been rhombporphyry (RP) rocks in the Lunner region (a dyke at Roa dated to 273±7 Ma; Rb-Sr, Sundvoll & Larsen 1993) and a NNW-SSE chain of gabbroic necks dated to 266±6Ma (K/Ar, Neuman et al. 1985). The RP dykes are outliers of the massive RP lavas extruded in the southern-central Oslo Graben during the peak rifting phase (Olaussen et al. 1994).

Palaeomagnetic experiments

Bøverbru dyke

The 1.3-1.4 m-wide Bøverbru diorite dyke cuts perpendicular to E-W-striking, steeply dipping- to overturned beds of the Upper Ordovician Mjøsa limestone. The limestone contacts with the dyke are baked in zones that extend 10-12 cm away from the contact; syn- or post-intrusion fluid influx along this contact is evident via mineralised veins and fractures and secondary alteration of the limestone. The chilled margins of the dyke are 12-15 cm wide, although the boundaries toward the more crystalline dyke interior are diffuse.

Typical demagnetization behavior for Bøverbru dyke and contact limestone samples is illustrated in Fig. 2a-d. High magnetic stability for baked limestone samples is reflected by almost univectorial demagnetisation behaviour (Fig 2b): reverse field-directions with southerly or SSW declinations and steep negative inclinations characterize the baked limestone. Away from the baked zone, we identify a normal polarity, low unblocking remanence component (LB) (<150-250°C, Fig. 2a). Curie-temperatures between 570-580°C and the unblocking temperature spectra suggest magnetite as the prime remanence carrier for the host limestone.

The natural remanent intensity (NRM) and susceptibility data for the Mjøsa limestone surrounding the dyke average 2mA/m and 95 (10^{-6} SI units). The baked samples have higher NRM intensity, increasing toward the dyke contact (up to 40 mA/m; Fig 2e). NRM and susceptibility values for dyke samples reach a maximum toward the center although we note a local minimum in the mid-section of the dyke. The demagnetisation data from the Bøverbru dyke are remarkable:

1. First, the fine-grained, chilled margin contact samples (<12-15 cm-wide zones) are characterized by reverse polarity high unblocking remanence components (HB) with steep negative inclinations and southerly declinations (Fig. 2c) that compare well with baked limestone directions (Fig. 2b). These data are distinct from the somewhat shallower directions observed in the non-baked Mjøsa limestone (Tables 1-2) and the 'transition limestone' ca. 72 centimeters away from the dyke contact (Fig. 2a), and thus indicate a partial positive contact test (see later discussion). Marginal dyke samples show a tight (quenched) directional clustering (HB, reverse polarity component) which is directionally comparable to contact limestone samples (Figs. 3a&b).
2. In contrast, the central and interior parts of the dyke are exclusively characterized by normal polarity, HB components with northerly declinations (Figs. 2d, 3a). This normal polarity

component is commonly identified as a LB component in marginal dyke samples (Figs. 2c & 3a).

Maximum thermal unblocking temperatures in the 550-580°C range suggest titanium-poor titanomagnetite (TM) or nearly pure magnetite as the bulk remanence carrier for both normal and reverse dyke sample directions. $M_{1/2}$ is typically around 35 mT with IRM saturation at around 300-350 mT for marginal samples. Lower $M_{1/2}$ (c. 10mT) and IRM saturation fields (200-250mT) for interior-central samples reflect the coarser grain-size in this part of the dyke. Thermomagnetic analyses, reveal distinct magneto-mineralogical differences (Fig. 4):

1. Marginal dyke samples (reverse polarity) are characterized by a combination of magnetite and maghaemite. During heating, saturation magnetization first increases and shows a kink at 150-170°C (cooling at 2-300°C produces a reversible phase), followed by inversion of maghaemite to a weaker magnetic phase at c. 350°C, and finally Curie-temperatures at around 580°C (Fig. 4a). The kink at 150-170°C (Fig. 4a - marginal samples) is a typical low-temperature TM (maghaemitization) phenomenon (Ade-Hall et al. 1979).
2. The interior and central parts of the dyke (normal polarity) show single Curie-temperatures at c. 580°C (Fig. 4b), indicative of titanium-poor TM. Reduced saturation magnetization after cooling indicates some oxidation.

Opaque mineralogy at the center of the dyke (Fig. 4d) is dominated by TM grains of up to 200μm in size. Grains show extensive evidence of low temperature alteration such as contraction cracks (maghemitization) and granulation. Minor amounts of pyrite are present as small inclusions in some of the grains. No high temperature exsolution features are observed, attesting to the fairly rapid cooling of the dyke. Near dyke margins (Fig 4c) maximum grain size decreases to c. 100μm, and numerous smaller grains ($d < 10\mu m$) appear. In addition to the same alteration features observed in the dyke interior, red staining around grain margins is evident under polarized light, suggesting formation of secondary hematite.

Lunner dykes (4 sites)

Dyke trends and nearly vertical dips at Lunner sites 4 and 1 (L4 and L1) are comparable with the structural orientation of the Bøverbu dyke, while dykes at Lunner sites 2 and 3 (L2

and L3) strike 200° (Table 1). Lunner dykes and the associated contact limestone show comparable directions with SSW declinations and intermediate, negative inclinations (Fig. 3c-d) and indicate a partial positive contact test. Limestone samples are essentially single-component (Fig. 5a) whilst dyke samples from Lunner dykes 1 and 4 (Figs. 3c & 5b) show minor, but often poorly defined LB components. Maximum unblocking temperatures are 550-565°C for both dyke and contact limestone. LB components are directionally smeared (Fig. 3c); hence we have not calculated a mean direction for LB components from the Lunner dykes.

Mjøsa Limestone (6 sites)

The regional magnetic signature of the Upper Ordovician (Caradoc) Mjøsa limestone was tested from six sites at the nearby Bøverbru and Hoen quarries (Table 2, Fig.1). The Mjøsa Limestone in the study area comprises a bioturbated limestone, with some dolomitisation; elsewhere in the northern Oslo Rift has a conglomeratic, bioclastic

All samples are dominated by steep positive LB components with northerly declinations and HB components with SSW declination and negative inclination (Fig. 6a). Directional stability for the high-temperature component was never observed above 500°C (Fig. 6b) at which point remanence intensity dropped below the instrument sensitivity levels.

$^{40}Ar/^{39}Ar$ experiments

Bøverbu dyke

Two cores were analyzed from Bøverbru. Sample M103 was drilled from the middle of the reverse-polarity, chilled dyke-margin (13 cm from west margin) and sample M106 was from the coarser-grained and normal-polarity dyke-center (88 cm from west margin). Analytical procedures are described in Appendix 1.

The chilled margin is aphanitic to slightly porphyritic with albitic feldspar phenocrysts in a groundmass of greenish-gray glass and feldspar microlites. Groundmass feldspar is fuzzy and occluded and the larger phenocrysts are often replaced by calcite and sericite. Minor chlorite alteration is evident. The coarse-grained dyke centre has a porphyritic, intersertal texture with coarse-grained clinopyroxene phenocrysts (augite, Table 3), coarse albitic feldspar (Table 3), minor amphibole and a groundmass of fine-grained plagioclase laths, amphibole needles, oxides, and minor interstitial glass. As with the other zones of the dyke, feldspars are slightly occluded and replaced by sericite and calcite. Chlorite occurs in numerous cracks in clinopyroxene and calcite replaces amphibole.

$^{40}Ar/^{39}Ar$ data from sample M103 (chilled margin) yield total fusion (TFA) and inverse isochron ages (242.0±5.3 Ma, 237.9± 8.1 Ma, respectively) within analytical uncertainty of one another, and nearly with uncertainty of the weighted mean plateau age (WMPA) (245.5±4.6 Ma) (Fig. 7; Table 4). The six-step release spectrum is characterised by four broadly concordant temperature steps that range in age from 240 to 252 Ma and represent 91.6% of the cumulative ^{39}Ar released. The large gas volume and slightly higher age of the fifth step in the plateau is responsible for the lack of age-overlap between the WMPA and the inverse isochron age. The Ar-release pattern for M106 (dyke centre) comprises eight-steps three of which are concordant at 242.5±4.6 Ma in the middle temperature range (38.4% of cumulative ^{39}Ar); these steps are preceded by two low-age concordant steps and succeeded by a stair-step increase in apparent ages until fusion (Fig. 7, Tables 3-4).

The K/Ca and $^{38}Ar_{Cl}/^{39}Ar_K$ plots (Fig. 7) indicate progressive Ar release from different mineral phases in the whole rocks. The first steps in both spectra, with lowest apparent ages, are consistent with degassing from slightly altered, fine-grained, low-K groundmass that has undergone some Ar loss. In the case of M106, these low ages are also Cl-correlated and may indicate contribution from the chlorite alteration on the pyroxenes in the sample. The central portions of each spectra, comprising the broadly concordant steps (in M106) or the plateau steps (in M103) yield gas from relatively high-K phases with minimal Cl-content that we attribute to degassing of groundmass, fine-grained feldspar and later, feldspar phenocrysts over furnace temperatures of ca. 900-1100°C. The final steps indicate exhaustion of K-bearing phases and increased release from Cl- and Ca-correlated Ar-components. In the case of the chilled margin (M103), the latter effect is restricted to a very low volume final (fusion) step comprising mostly air, while M106 shows definite effects of degassing from Ca- and Cl-rich amphibole and clinopyroxene phenocrysts (Fig. 7).

Lunner dykes

The Lunner 1 sample, LU1, is a pale gray, cryptocrystalline to slightly porphyritic rock with phenocrysts of fine- to medium-grained alkali feldspar, oxides, rare biotite, and some groundmass glass. Coarse feldspar laths are somewhat mottled due to replacement by sericite(?), but appeared fairly fresh and pink to pink-translucent when separated. Lunner sample, LU4, has a similar appearance to the Bøverbru dyke, with gray-green color and feldspar phenocrysts, but it lacks clinopyroxene. The rock is cryptocrystalline with some large

albitic feldspar phenocrysts in a matrix of equigranular feldspar, oxides, minor glass and chlorite (see Table 3).

The $^{40}Ar/^{39}Ar$ release spectrum for LU1 (Fig. 8) defines a plateau of 237.2±4.4 Ma (62.3% of ^{39}Ar gas). The plateau is preceded by two initial, low temperature, low-age steps, and succeeded by three, rising, apparent ages that reach a maximum of 267 Ma at fusion (1400°C). The steps in the plateau itself exhibit a slight, consistent increase with increasing experimental temperature (Fig. 8a). On an inverse isochron, the plateau steps cluster as a very radiogenic group of points with with poor correlation to an ordinate intercept 241.4±8.4 Ma and an abscissa intercept ($^{40}Ar/^{36}Ar$ ratio) of 235±60 (atmospheric value = 295.5). The alkali feldspar separate (LU1A, from rock LU1) defines a plateau of 246.2±4.6 Ma for 58.6% of ^{39}Ar released (Fig. 8b). Two initial, low-age, low-volume steps are Cl-correlated, while the central and final portions of the pattern indicate Ar-gas derived from the K-rich feldspar.

Sample LU4 yielded a plateau age of 238.3±4.5 Ma for 65.9% of ^{39}Ar gas released, and is similiar within uncertainty to LU1 (Fig. 8). The 238.2±4.6 Ma inverse isochron age (also excluding the first and final four temperature steps) is indistinguishable from the plateau age, is well-correlated (MSWD = 0.23) and yields a $^{40}Ar/^{36}Ar$ value of 282±8.

The high, but distinctly variable K/Ca ratios for the 'rising' plateau portion of whole-rock analysis LU1 suggest Ar was released from at least two K-bearing phases: a very high-K phase (higher temperatures in the furnace heating experiment) and a phase with slightly less K (middle temperature portion of the plateau) (compare e.g., to K/Ca ratios for Bøverbru and LU4, Figs. 7 and 8c). The release of Ar from two different high-K reservoirs in LU1 corresponds to presence of both alkali feldspar and biotite in the rock, and probably documents the different closure temperatures of these minerals over the ca. 10 m.y. age range represented in the plateau. The feldspar separate , LU1A, confirms the 'mixed' age of the whole rock analysis, as well as the fact that the feldspar is the more retentive phase (i.e. releases its gas at higher temperatures) of the two in the rock.

Albitic feldspar is the dominant K-bearing phase in LU4, corresponding to Ar-gas release during analysis at temperatures between 750 and 1000°C. The excluded, lowermost temperature step is a product of degassing weakly bound Ar gas at grain surfaces. The excluded (from calculation) high temperature steps in LU4 represent exhaustion of the feldspar gas and commencement of degassing a different, high-Ca phase that we presume to be altered glassy groundmass.

Interpretation and discussion

Bøverbru and Lunner dykes

We consider the plateau age of 245.5±4.6 Ma (sample M103) to date the crystallisation age of the Bøverbru dyke. The age of 242.5±4.6 Ma for the plagioclase-generated portion of M106 (dyke centre) is within uncertainty of the WMPA for M103 and should be expected, since this single dyke obviously cooled quickly. We nonetheless discount the reliability of the data from the M106 (dyke centre) sample because the majority of the the gas release was governed by the effects of excess-Ar containing components (pyroxene and amphibole). We interpret the plateau ages of 246.2±4.6 Ma (LU1A, alkali feldspar) and 238.3±4.5 Ma (LU4, whole rock) to represent the time of crystallisation of the Lunner dykes. Despite differences in chemistry (and hence mineral compositions), the Lunner ages and the Bøverbru M103 age are concordant at the 95% confidence level and we cite a weighted mean age of 243.3±2.6 Ma (i.e. early Triassic) for their crystallization to simplify subsequent discussion (see Table 5).

The mean palaeomagnetic directions from the Lunner dykes and their high-stability contact limestone are reasonably grouped, and show on average, steeper inclinations (c.-45°) than the Mjøsa overprints (c.-35°). The latter is concordant with data from the Upper Carboniferous-Permian Oslo Graben lavas (274-294 Ma) (van Everdingen, 1960). Hence, the early Triassic age (243 Ma) obtained for the Lunner dykes is reflected by marginally steeper palaeomagnetic inclinations (Fig. 9). Given the complicated Bøverbru palaeomagnetic signature (see below) we base our new early Triassic palaeomagnetic pole (243 Ma) entirely on the Lunner dykes and contacts (Fig. 10, Table 6). Based on the Lunner data we calculate a palaeolatitude of 27°N for the Oslo region at c. 243 Ma; this fits well with lithofacies indicators, and as an example, the main outcrop of Zechstein evaporates (Ziegler 1990) plots between 17-23°N in our palaeomagnetically controlled reconstruction (Fig. 10b).

Complex Bøverbru dyke remagnetization

The reverse direction for the Bøverbru dyke has a somewhat steeper inclination than the Lunner dykes. A partial positive contact test may indicate that the dyke was intruded in a reverse polarity field, but we also show that the central parts of the dyke record a normal polarity field. The unusual antipodal magnetic characteristic for the Bøverbru dyke is most likely the result of remagnetisation of the central parts of the dyke:

The normal polarity Bøverbru inclinations in the dyke center-interior resemble LB components from the dyke margin and the regional LB components in the Mjøsa Limestone and hence suggest that a same Jurassic-or-younger, thermochemical or viscous overprint strongly affected the coarse-grained interior-central parts of the dyke and is further observed as a LB component in marginal samples. We propose the following series of events as an explanation for the observed magnetic signature of the dyke:

- an original, 243 Ma reverse magnetization during intrusion-crystallisation of the dyke and preserved in the dyke chilled margin and limestone baked contact, followed by
- a Jurassic-or-younger magnetic resetting that preferentially affected the coarse-grained and less stable dyke center.

However, it is also possible that the partial positive contact test may be an artifact of post-dyke fluid influx along the dyke-limestone contact which is evident via mineralized veins and fractures and secondary alteration of the host limestone. Low-temperature alteration/maghaemitization, relating to fluids, is recognized throughout the dyke (Fig. 4c-d), and at a certain time this may have led to complete remagnetization of the dyke and the contact limestone in a reverse field direction. This maghaemitization process enhanced magnetic stability differences, as marginal grains were effectively subdivided by shrinkage cracks while central grains retained larger (PSD/MD) magnetite regions which were more easily remagnetized in a younger normal polarity field. Hence, we are inclined to argue that both the margin (reverse) and interior-center (normal) magnetizations could be of secondary origin.

Mjøsa limestone

The Cambro-Silurian sequences in the vicinity of the Oslo rift show a strong Permian magnetic overprint which we relate to extensive magmatism and fluid-development during evolution of the Oslo Rift system. This is exemplified by a negative fold-test (95% confidence level) from the Mjøsa Limestone (HB component), where *in-situ* directions (Fig. 9c-d) and hence, palaeomagnetic poles are virtually indistinguishable from those of the Oslo Graben/Ringerike Lavas (274-294 Ma; Fig. 10, compare poles OGL=Oslo Graben Lavas, RL=Ringerike Lavas and MS-1=Mjøsa HB component). Similar magnetic overprinting is observed from the Silurian Ringerike Sandstone (Table 6 & Fig. 10, pole RS=Ringerike Sandstone overprint), but primary Silurian directions in these red-beds were also recovered above 600°C (Douglass 1989). Northwards and away from the Oslo Rift, but toward the

'Caledonian' front, the Permian overprint in the Mjøsa Limestone vanishes (Perroud et al. 1992; Torsvik et al., in progress).

LB components from the Mjøsa limestone fail a fold-test at the 95% confidence level; and probably represent Jurassic or younger remagnetization (Fig. 10; pole MS-2). The proposed Jurassic-to-younger resetting of the Mjøsa Limestone and probably also the Bøverbru dyke center (Figs. 9 and 10) can be tied to established tectonic events in the area. Post-rift evolution of the Oslo Rift system, constrained by fission track thermochronology (Fig. 9f), is interpreted to entail post-rift (i.e. post-Permian) exhumation of 3-4 km; furthermore, the exhumation was differential, but continuous, from the central part to the northwest part of the Oslo Graben during Triassic through Jurassic time (Rohrmann et al. 1994). The low-temperature (100-300°C) hydrothermal fluid circulation associated with this exhumation process (Rohrman et al. 1994) would be consistent with the magnetic resetting characteristics we observe in the dykes and the limestones, but were probably neither focused nor intense enough to cause significant resetting of the Ar-systematics of the dykes.

Conclusions

(1) The Lunner and Bøverbru dykes are dated to 243±5 Ma (2σ error) and represent the youngest radiometrically dated dykes in the Oslo Rift area, intruded during the final, curtailed throes of magmatic activity in the graben whilst the Oslo Rift was located at 27°N. The dykes differ in age from the main, Oslo Graben lava pulse (274-294 Ma) and demonstrate a minor APW from Permian to early Triassic times.

(2) The dual-polarity magnetic signature of the Bøverbru dyke, demonstrably of the same intrusion age as those from Lunner is a complex Mesozoic remagnetization phenomenon.

(3) Extensive Oslo Rift magmatism and fluid-development remagnetised the Mjøsa Limestone in the Hadeland area at around 274-294 Ma, but further to the north, and some 25 km away from the main Oslo Rift magmatism, the Permian remagnetisation is absent (Torsvik et al, in progress).

(4) The Mjøsa Limestone has also undergone, at least locally, a younger thermo-chemical remagnetisation event, probably of Jurassic-to-younger age, which is demagnetised at temperatures below 150-300°C.

Acknowledgment

Financial support by Mobil, NFR, NGU, Phillips and Statoil. ONOFF contribution no. 4

References

Ade-Hall J. M., Palmer H. C. & Hubbard T. P., 1971. The magnetic and opaque petrological response of basalts to regional hydrothermal alteration. Geophys. J. R. astr. Soc. 24, 137-174.

Arnaud N.O., Brunel, M., Cantagrel, J.M. & Tapponier, P., 1993. High cooling and denudation rates at Kongur Shan, eastern Pamir (Xinjiang, China) revealed by $^{40}Ar/^{39}Ar$ alkali feldspar thermocronology. Tectonics, 12, 1335-1346.

Bjørlykke, K., Subsidence and tectonics in Late Precambrian and Palaeozoic sedimentary basins of Southern Norway. Nor. geol. Unders. Bull., 380, 159-172.

Cebula, G. T., M. J. Kunk, H. H. Mehnert, C. W. Naeser, J. D. Obradovich, and J. F. Sutter (1986) The Fish Canyon Tuff, a potential standard for the ^{40}Ar-^{39}Ar and fission-track dating methods (abs.). *Terra Cognita* **6**, Proceedings from ICOG VI, 139-140.

Douglass, D.N., 1989. Palaeomagnetics of Ringerike Old Red Sandstone and related rocks, southern Norway:implications for pre-Carboniferous seperation of Baltica and British Terranes. Tectonophysics, 148, 11-27.

Eide E. A. & Torsvik T. H., 1996. Paleozoic supercontinental assembly, mantle flushing, and genesis of the Kiaman Superchron. Earth Plan. Sci. Lett. 144, 389-402.

Heeremans M., Larsen B. T. & Stel H., 1996. Paleostress reconstruction from kinematic indicators in the Oslo Graben, southern Norway: new constraints on the mode of rifting. Tectonophys. 266, 55-79.

Maluski, H. (1995) Argon 40-argon 39 dating: Principles and applications to minerals from terrestrial samples. In: *Nuclear Methods of Dating*. Kluwer Academic, Hingham, Mass: 325-352.

Neumann E.-R., 1994. The Oslo Rift: P-T relations and lithospheric structure. Tectonophys. 240, 159-172.

Neumann, E.-R., Larsen, B.T., & Sundvoll, B., 1985.. Compositional variations among gabbroic intrusions in the Oslo Rift. Lithos, 18, 35-59.

Olaussen S., Larsen B. T. & Steel R., 1994. The Upper Carboniferous-Permian Oslo Rift: Basin fill in relation to tectonic development. In: Pangea: Global Environments and Resources. Can. Soc. Petrol. Geol. Mem. 17, 175-197.

Opalinski P. R. & Harland T. L., 1981. The Middle Ordovician of the Oslo Region, Norway, 29. Stratigraphy of the Mjøsa Limestone in the Toten and Nes-Hamar areas. Nor. Geol. Tidsskr. 61, 59-78.

Perroud, H., Robardet, M. & Bruton, D.L., 1992. Palaeomagnetic constraints upon the palaeogeographic position of the Baltic Shield in the Ordovician. Tectonophysics, 201, 97-120.

Ramberg, I.B., 1976. Gravity interpretation of the Oslo Graben and associated igneous rocks. Nor. geol. unders. Bull., 325, 193pp.

Ramberg, I.B. & Larsen, B.T., 1978. Tectonomagmatic Evolution. In Dons. J.A. & Larsen, B.T. (eds.) The Oslo paleorift. A review and Guide to Excursions. Nor. geol. unders. Bull., 337, 55-73.

Rohrmann M., Van der Beek P. and Andriessen P., 1994. Syn-rift thermal structure and post rift evolution of the Oslo Rift (southeast Norway): New constraints from fission track thermochronology. Earth Plan. Sci. Lett. 127, 39-54.

Sundvoll B. & Larsen B. T., 1990. Rb-Sr isotope systematics in the magmatic rocks of the Oslo Rift. Nor. geol. unders. Bull., 418, 27-46.

Sundvoll B. & Larsen B. T., 1993. Rb-Sr and Sm-Nd relationships in dyke and sill intrusion in the Oslo Rift and related areas. Nor. geol. unders. Bull. 425, 25-41.

Sundvoll B. & Larsen B. T., 1994. Architecture and early evolution of the Oslo Rift. Tectonophys. 240, 173-189.

Torsvik, T.H., Smethurst, M.A., Meert, J.G.,Van der Voo, R. & McKerrow, W.S., Brasier, M.D., Sturt, B.A. & Walderhaug. H.J., 1996. Continental break-up and collision in the Neoproterozoic and Palaeozoic: A tale of Baltica and Laurentia. Earth Sci. Rev., 40, 229-258.

Van Everdingen, R.O., 1960. Palaeomagnetic analysis of Permian extrusives in the Oslo Region, XVII Skr. Nor. Vidensk. Akad. Oslo, 1, 1-80.

Van der Voo, R., 1993. Paleomagnetism of the Atlantic, Tethys and Iapetus Oceans. Cambridge University Press, New York, 411pp.

Ziegler, P.A., 1990. Geological atlas of Western and Central Europe 1990. Shell, 239 pp.

Table 1 Palaeomagnetic results from Bøverbru and Lunner dykes

Site/Area	Pol	Dec°	Inc°	N	α_{95}	k	Comment
Bøverbru Quarry:							
B2 Bøverbru dyke	N	359.8	+70.3	46	5.6	14.95	HB Interior, LB margin
(130-140cm, 152/86)	R	198.3	-72.6	14	3.4	141.5	HB margin
B3 Contact Limestone (0-40 cm)	N	356.3	+49.5	6	11.7	33.79	LB
	R	188.5	-60.3	25	2.2	169.6	HB
B4 Limestone (0.72-4 meters)	N	354.8	+59.2	9	7.1	54.25	LB
(Transitional)	R	197.8	-40.1	11	6.7	47.71	HB
Lunner dykes (width, strike/dip):							
L1 (85 cm, 140/84)	R	199.1	-48.3	6	10.9	38.5	HB
Contact Limestone	R	197.7	-42.7	3	7.7	259.5	HB
L2 (350cm, 200/80)	R	205.2	-45.5	6	8.9	58.1	HB
Contact Limestone	R	202.2	-42.6	7	3.6	278.6	HB
L3 (120cm, 200/81)	R	200.3	-31.1	3	23.8	28.0	HB
Contact Limestone	R	202.9	-40.4	2	26.2	93.1	HB
L4 (67 & 153cm, 152/90)	R	176.2	-44.5	5	12.2	40.0	HB
Contact Limestone	R	191.3	-47.5	8	3.7	227.5	HB

Dec°/Inc°=mean declination/inclination; N=number of samples; α_{95}=95 percent confidence circle; k=precision parameter; HB=high un-blocking component; LB=low un-blocking component. Pol=magnetic polarity; N/R=normal/reverse polarity

Table 2 Site-mean directions from the Upper Ordovician (Caradoc) Mjøsa Limestone

Area/ Site	Bedding Strike/Dip	Pol	*In-situ* Dec°	Inc°	N	α_{95}	k	100% unfolded Dec°	Inc°	Comment
Bøverbru Quarry (60.7°N & 10.7°E):										
B1	090/93	N	026.1	+58.2	6	5.0	178.7	165.1	+25.3	LB
		R	196.1	-39.3	8	3.9	206.3	342.3	-45.2	HB
Moen Quarry (60.7°N & 10.7°E):										
M1	081/75	N	022.4	+65.7	10	5.9	67.2	155.8	+35.1	LB
		R	196.8	-36.4	9	5.9	76.6	308.7	-58.6	HB
M2	106/76	N	340.2	+66.0	5	10.5	54.4	212.4	+32.8	LB
		R	203.3	-34.9	5	11.0	49.8	359.8	-68.1	HB
M3	114/77	N	342.2	+68.8	4	10.4	79.2	219.9	+28.2	LB
		R	194.2	-32.2	7	7.1	72.7	047.5	-68.8	HB
M4	110/77	N	024.4	+60.1	4	13.5	47.0	197.0	+42.8	LB
		R	199.9	-33.9	7	2.8	476.8	020.2	-69.1	HB
M5	113/60	N	347.0	+69.5	3	6.0	427.7	220.1	45.5	LB
		R	207.2	-29.9	6	11.5	34.9	292.5	-86.4	HB
Mean LB										
B1, B3-B4*, M1-M5		N	002.9	63.3	8#	7.6	54.0	188.7	36.6	LB
						15.8	*13.2*	*(unfolded parameters)*$		
Mean HB										
B1,B4*, M1-M5		R	199.4	-35.3	7#	3.9	237.3	015.4	-72.7	HB
						23.1	*7.8*	*(unfolded parameters)*$		

*from Table 1
N=samples/sites#; $Statistically negative fold-test at the 95 percent confidence level. Cf. Table 1 for further details.

Table 3 Representative electron microprobe analyses of feldspar (fsp) and clinopyroxe (cpx) from Bøverbru and Lunner (LU) dykes. 'R' = analysis of grain rim; 'C' = analysis of grain core. Feldspars are albitic, with slightly higher K2O in grain cores than rims; clinopyroxene in Bøverbru is augitic.

Oxide	**Bøverbru fsp (R)**	**Bøverbru fsp (C)**	**LU4 fsp (C)**	**LU4 fsp (R)**
SiO_2	66.89	66.23	66.34	67.38
Al_2O_3	20.97	21.65	20.72	20.27
FeO	0.26	0.4	0.95	0.75
CaO	0.44	0.58	1.47	0.94
Na_2O	10.85	10.16	10.55	11.02
K_2O	0.7	1.27	0.28	0.16
BaO	0	0	0.03	0.03
Total	100.11	100.29	100.34	100.55

Oxide	**Bøverbru cpx**
SiO_2	47.47
TiO_2	1.88
Al_2O_3	7.78
MgO	12.79
FeO	7.54
MnO	0.11
CaO	21.49
Na_2O	0.63
K_2O	0.00
Cr_2O_3	0.23
NiO	0.00
Total	99.92

Table 4 $^{40}Ar/^{39}Ar$ furnace step-heating data

a) Bøverbru Dyke, sample M103 Whole Rock (J=0.0067, weight=12.85 mg): 13 cm from west contact (chilled margin)

Temp °C	$^{40}Ar/^{39}Ar$	$^{38}Ar/^{39}Ar$	$^{37}Ar/^{39}Ar$	$^{36}Ar/^{39}Ar$ (10^{-3})	^{39}Ar (10^{-14}moles)	$F^{39}Ar$ released	$\%^{40}Ar^*$	$^{40}Ar^*/^{39}Ar$	Age (Ma)	± 1σ Ma
700	21.008	0.054	0.948	23.070	1.00	7.95	66.86	14.44	166.62	4.24
800	25.019	0.052	13.688	19.345	0.87	14.82	81.77	21.29	240.54	4.27
900	23.662	0.047	0.368	7.002	0.83	21.48	88.99	21.68	244.70	4.22
1000	23.839	0.062	0.216	10.000	3.39	48.56	87.31	20.97	237.17	3.80
1100	28.023	0.123	0.635	19.783	6.38	99.53	79.53	22.37	252.00	5.22
1150	82.702	0.000	0.000	196.743	0.06	100.00	2.52	25.65	286.07	16.49

b) Bøverbru Dyke, sample M106 Wole Rock (J=0.00676, weight=13.0 mg): 88 cm from west contact (centre)

Temp °C	$^{40}Ar/^{39}Ar$	$^{38}Ar/^{39}Ar$	$^{37}Ar/^{39}Ar$	$^{36}Ar/^{39}Ar$ (10^{-3})	^{39}Ar (10^{-14}moles)	$F^{39}Ar$ released	$\%^{40}Ar^*$	$^{40}Ar^*/^{39}Ar$	Age Ma	± 1σ Ma
700	30.209	0.196	2.877	37.844	0.12	4.95	62.92	19.57	224.19	5.46
800	22.688	0.071	14.078	16.814	0.07	7.94	79.87	19.62	224.66	5.54
900	23.934	0.055	4.163	7.964	0.11	12.34	88.24	22.15	251.71	6.14
1000	24.414	0.047	0.304	11.023	0.36	27.07	85.74	21.22	241.84	5.54
1050	22.668	0.060	0.379	5.341	0.47	46.42	91.29	21.13	240.89	5.13
1100	24.595	0.116	0.910	5.731	0.72	75.75	91.78	23.02	260.92	5.55
1200	29.330	0.180	3.329	10.575	0.57	99.11	87.79	26.70	299.33	6.00
1400	120.499	0.249	70.931	352.760	0.02	100.00	15.92	28.38	316.66	48.32

Table 4 (cont'd)

c) Lunner Dyke 1, sample LU1A Alkali feldspar (J=0.016980, weight=5.0 mg)

Temp °C	$^{40}Ar/^{39}Ar$	$^{38}Ar/^{39}Ar$	$^{37}Ar/^{39}Ar$	$^{36}Ar/^{39}Ar$ (10^{-3})	^{39}Ar (10^{-14}moles)	$F^{39}Ar$ released	$\%^{40}Ar^*$	$^{40}Ar^*/^{39}Ar$	Age Ma	± 1σ Ma
600	30.234	0.058	0.068	85.145	0.520	4.15	18.3	5.54	162.29	13.15
700	37.762	0.042	0.110	102.927	0.527	8.36	21.0	7.92	227.66	9.61
750	10.260	0.019	0.015	5.327	2.530	28.55	84.9	8.71	248.86	5.39
800	10.157	0.020	0.016	5.181	0.890	35.66	85.2	8.65	247.24	5.79
850	9.786	0.019	0.009	4.636	1.241	45.57	86.2	8.44	241.53	5.62
900	9.700	0.019	0.007	4.400	1.361	56.43	86.8	8.42	241.05	5.24
950	9.923	0.019	0.012	4.429	0.797	62.79	87.0	8.63	246.80	5.58
1000	10.16	0.019	0.010	4.594	0.525	66.98	86.8	8.82	251.86	5.64
1050	9.388	0.019	0.009	3.822	0.533	71.23	88.1	8.28	237.20	4.48
1100	9.423	0.019	0.007	4.012	0.539	75.53	87.6	8.25	236.65	4.49
1200	9.704	0.019	0.006	4.466	1.702	89.12	86.6	8.40	240.63	4.52
1400	10.601	0.019	0.067	5.088	1.363	100.00	86.1	9.13	259.98	6.02

d) Lunner Dyke 1, sample LU1 Whole Rock (J=0.016970, weight=5.0 mg)

Temp °C	$^{40}Ar/^{39}Ar$	$^{38}Ar/^{39}Ar$	$^{37}Ar/^{39}Ar$	$^{36}Ar/^{39}Ar$ (10^{-3})	^{39}Ar (10^{-14}moles)	$F^{39}Ar$ released	$\%^{40}Ar^*$	$^{40}Ar^*/^{39}Ar$	Age Ma	± 1σ Ma
600	7.132	0.019	0.144	6.187	9.644	14.57	74.9	5.35	156.71	3.48
700	10.138	0.020	0.058	11.327	10.025	29.7	67.6	6.85	198.52	4.67
750	9.481	0.019	0.021	4.762	8.012	41.79	85.4	8.10	232.26	4.89
800	8.776	0.019	0.016	2.353	3.775	47.48	92.2	8.09	232.08	4.87
850	8.823	0.018	0.014	2.368	3.176	52.28	92.2	8.13	233.21	5.00
900	9.019	0.019	0.016	2.876	2.748	56.42	90.7	8.18	234.54	4.99
950	8.980	0.018	0.014	2.773	3.581	61.83	91.0	8.17	234.29	4.89
1000	9.069	0.018	0.01	2.788	5.238	69.73	91.0	8.26	236.54	4.89
1050	9.260	0.019	0.01	3.261	6.214	79.10	89.7	8.31	237.99	5.09
1100	9.225	0.018	0.011	2.683	5.039	86.71	91.5	8.44	241.55	5.32
1150	9.159	0.018	0.014	1.988	3.496	91.98	93.7	8.58	245.20	5.42
1200	9.604	0.019	0.023	3.185	1.428	94.14	90.3	8.68	247.84	5.33
1400	10.213	0.018	0.03	2.762	3.884	100.00	92.1	9.41	267.29	5.51

e) Lunner Dyke 4, sample LU4 Whole Rock (J=0.016970, weight=5.0 mg)

Temp °C	$^{40}Ar/^{39}Ar$	$^{38}Ar/^{39}Ar$	$^{37}Ar/^{39}Ar$	$^{36}Ar/^{39}Ar$ (10^{-3})	^{39}Ar (10^{-14}moles)	$F^{39}Ar$ released	$\%^{40}Ar^*$	$^{40}Ar^*/^{39}Ar$	Age Ma	± 1σ Ma
700	18.451	0.026	2.789	38.221	3.913	11.04	40.9	7.72	221.98	6.22
750	12.916	0.022	0.324	16.767	1.098	14.07	62.5	8.09	232.07	5.52
800	11.903	0.022	0.351	12.773	0.948	16.69	69	8.24	236.09	5.11
850	12.581	0.022	0.341	15.067	1.19	19.98	65.4	8.25	236.39	5.36
900	11.788	0.021	0.355	12.392	2.179	26.01	69.7	8.24	235.99	5.66
950	9.939	0.02	0.354	5.77	3.815	36.56	83.3	8.31	237.91	5.27
1000	9.342	0.019	0.386	3.867	4.213	48.22	88.2	8.27	236.8	5.02
1050	9.551	0.02	0.475	4.622	6.935	67.42	86.2	8.27	236.86	4.89
1100	10.317	0.02	0.914	6.746	3.425	76.93	81.6	8.48	242.47	5.03
1150	10.465	0.021	0.86	6.437	2.593	84.13	82.6	8.71	248.66	5.23
1200	12.825	0.021	0.86	9.234	0.587	85.76	79.5	10.27	289.79	6.36
1300	11.961	0.021	0.97	8.467	1.987	91.28	79.9	9.64	273.27	5.93
1400	13.194	0.021	0.794	10.908	3.14	100	76.4	10.14	286.47	6.96

Table 5 $^{40}Ar/^{39}Ar$ isotopic ages (1σ including error in J)

				Isochron Analysis				Age Spectrum			
Dyke	Sample	Mineral	Total Fusion Age±1σ	N	MSWD	$^{40}Ar/^{36}Ar$ Intercept ±1σ	Age±1σ	N	^{39}Ar (%)	Age±1σ	Utilised Age±1σ
Bøverbru	M103	WR	242.0±5.3	4	2.0	350±53	237.9±8.1	4	91.6	245.5±4.6	**245.5±4.6**
Bøverbru	M106	WR	265.6±5.1	-	----	----------	----------	(3	38.4	242.5±4.6)	
Lunner 1	Lunn1	WR	221.2±4.2	10	5.48	235±60	241.4±8.4	9	62.3	237.2±4.4	
Lunner 1	Lunn1a	PLG	241.8±4.6	12	16.29	282±11	240.8±4.8	6	58.6	246.2±4.6	**246.2±4.6**
Lunner 4	Lunn4	WR	243.7±4.6	7	0.23	282±8	238.2±4.6	7	65.9	238.3±4.5	**238.3±4.5**
										Weighted Mean	**243.3±2.6**

Table 6 Overview and interpretation of selected palaeomagnetic data from the Oslo Rift area

Code*	Formation	Location Lat.	Long.	Dec°	Inc°	α_{95}	N	VGP Lat.	Long.	dp/dm	Age (±2σ) or Comment
Primary data: Oslo Rift magmatic rocks:											
LU	Lunner dykes and contacts	60.3	10.6	197.1	-43.2	5.9	8	52.9	164.4	4.5/ 7.3	243±5 Ma (Tables 1 & 5)
RL	Ringerike Lavas (B1-RP7-RP10)	60.0	10.25	204.0	-33.0	13.4	3	44.6	157.4	8.6/15.2	281±4 Ma Rb-Sr (tilt corrected)
	(Ages: 276±6, 281±6 & 291±8)										
OGL	Oslo Graben Lavas	59.5	10.5	204.0	-36.0	1.5	27	47.0	157.0	1.0/ 1.7	281±2 Ma Rb-Sr (tilt corrected)
	(Ages: 274±3, 276±6, 277±3, 278±5, 278±12, 278±8, 279±9, 280±7, 281±6, 281±4, 284±7, 288±9, 288±7, 290±4, 291±8, 291±18, 292±20 & 294±6)										
Secondary data:											
Permian overprints related to main Oslo Rift magmatic pulse (code RL and OGL)											
MS-1	Mjøsa Limestone	60.5	10.7	199.4	-35.3	3.9	7	46.7	163.5	2.6/ 4.5	*In-situ* HB data (Table 2)
RS	Ringerike Sandstone	60.0	10.25	207.0	-36.0	2.9	19	45.6	152.7	2.0/ 3.4	
Jurassic-or-younger overprint related to thermo-viscous exhumation											
MS-2	Mjøsa Limestone	60.5	10.7	002.9	+63.3	7.6	8	74.2	183.1	9.5/12.0	*In-situ* LB data (Table 2)

*see fig. 10; Lat./Long.=latitude/longitude; VGP=virtual palaeomagnetic pole; dp/dm=semi-axis.....
Cf. Table 1 for further details.

APPENDIX 1: Experimental and analytical procedures

The Natural remanent magnetisation (NRM) was measured on a 2G Squid and a JR5A spinner magnetometer. Remanence stability was tested by progressive thermal (MMTD60), and to a minor extent alternating field (AF), demagnetisation (2-axis tumbler). Characteristic remanence directions were determined using the least square regression analysis implemented in the SIAPD computer program (available at http://www.ngu.no/geophysics). Thermomagnetic analysis was performed on a horizontal translation balance.

Prior to $^{40}Ar/^{39}Ar$ furnace step-heating, clean Bøverbru ('M') and Lunner ('LU') whole rock (M103, M106, LU1 & LU4) and plagioclase (LU1A) fractions (180-250 μm) were packed in Sn-foil and irradiated at the Siloé reactor in Grenoble, France. We used the $^{40}Ar/^{39}Ar$ analytical facility at Université Blaise Pascal et Centre National de la Recherche Scientifique, Clermont-Ferrand, France, with analytical protocol and irradiation parameters similar to Arnaud et al. (1993). Samples were step-heated using a radio frequency furnace with temperature calibration (±10°C) by an optical pyrometer. Each 25 minute heating step was gettered for 5 minutes prior to inlet and samples were degassed at 400°C for 25 minutes before the analysis. Mineral compositional data are reported in Table 3; $^{40}Ar/^{39}Ar$ data are reported in Tables 4-5 and Figures 7-8. The two Bøverbru samples were irradiated separately from the three Lunner samples (on different days); thus, we incorporate the interlaboratory uncertainty in J-value (2%) when making inter-locality age comparisons (Table 5 and text), but we do not include the J-value error when tabulating the Bøverbru or Lunner data alone (Table 4). We cite uncertainties at the 1σ level. Plateaus were defined as comprising three or more contiguous steps that overlap at the 95% confidence level and together constitute more than 50% of the total experimental gas. Individual steps were 'weighted' by both length (gas volume) and individual age uncertainty (IAAA software, integrated analysis of argon-argon data, is available at http://www.ngu.no/geophysics. Monitor minerals were the Fish Canyon Tuff feldspar (27.4 Ma, Cebula et al. 1986) and the Caplongue hornblende (344.5 Ma, Maluski 1996).

FIGURE CAPTIONS

FIGURE 1

Geological sketch map of the Oslo Rift (SE Norway), sampling areas (this study) and those of Douglass (1989) and van Everdingen (1960).

FIGURE 2

(a-d) examples of thermal demagnetization from the Bøverbru dyke and the host Mjøsa limestone. (e) NRM intensity and susceptibility variations through the Bøverbø dyke and host Mjøsa limestone. Contact and dyke sampled in two profiles; note some difference in NRM intensity across the dyke. Magnetic polarity based on high unblocking components (HB); note that dyke margin is of reverse polarity whilst dyke center-interior is of normal polarity. In vector-diagrams, open (closed) symbols denote points in the vertical (horizontal) plane.

FIGURE 3

Characteristic remanence components from Bøverbru dyke (a) and host limestone contact and transition (b). (c,d) remanence components from Lunner dykes and limestone contacts.
In stereo-plots (a,c), open (closed) symbols denote negative (positive) inclinations. HB/LB=high/low unblocking remanence components.

FIGURE 4

Thermomagnetic analysis of samples from the Bøverbru dyke margin (A) and center (B).
(1) Kink at 150-180°C (irreversible creation of a magnetic phase with higher saturation magnetization); (2) inversion of maghaemite to a weaker (haematite) magnetic phase at T>350°C; (3) magnetite T_c c. 580°C.
(C) Reflected light micrograph from margin of Bøverbru dyke (frame width=330μm). Note presence of numerous small TM grains as well as larger grains with distinct low temperature alteration features.
D) Reflected light micrograph for center of Bøverbru dyke showing TM grains with low temperature alteration features (frame width = 330μm)

The Bøverbru dyke constitutes TM grains with different grain size differences. Low-temperature alteration/maghemitization proceeded from surface inward in grains, affecting smaller grains with higher surface/volume ratio more, giving stronger maghaemite signature at margins as observed on J_s-T curves. This effect also might further enhance stability

differences, as marginal grains are effectively subdivided by shrinkage cracks while central grains retain larger (PSD/MD) magnetite regions. Heating for J_s-T curves invert maghaemite (both centrally and marginally) to hematite, leaving only magnetite signature on J_s-T curves on cooling. Reduction in J_s during cooling is always higher for marginal samples.

FIGURE 5

Examples of thermal demagnetization from Lunner dyke 4, baked limestone (a) and dyke margin (b).

FIGURE 6

Characteristic remanence components (a) and example of thermal demagnetization (b) for the Mjøsa limestone.

FIGURE 7

$^{40}Ar/^{39}Ar$ release spectra and K/Ca and Cl/K ratios for two whole rock samples from the Bøverbru dyke. Sample M103 derives from the dyke margin and M106b from the coarse-grained dyke center. The release spectrum for M103 yields a plateau age of 245.5±4.6 Ma (steps 2 through 5). Both spectra and their elemental ratios demonstrate release of Ar-gas from different phases in the whole rocks: plagioclase dominates the Ar-release pattern for both rocks, but the spectrum for M106b is much more complicated by the presence of excess Ar in coarse-grained amphiboles and clinopyroxenes. Temperatures indicated in labels on the spectra correspond to those measured during the furnace step-heating experiment.

FIGURE 8

a) Whole-rock $^{40}Ar/^{39}Ar$ release spectrum and element ratios for Lunner dyke LU1. The data define a statistically valid plateau age of 237.2±4.4 Ma, but we note the slight but progressive rise in the steps with increasing temperature. The elemental ratios reveal that this results from degassing of two high-K phases during the experiment: biotite at slightly lower temperatures and K-feldspar at higher temperatures. This phenomenon is revealed in the spectrum in b) a pure alkali feldspar separate from the same rock which yields a plateau age of 246.2±4.6 Ma. c) Whole-rock release spectrum and elemental ratios for Lunner dyke LU4. This sample contained only alkali feldspar as a high-K phase and yields both a plateau and inverse isochron

within analytical uncertainty (238.3 Ma). Portions of the spectra used to calculate cited plateau ages are in black.

FIGURE 9

Site-mean directions from Bøverbru-Lunner dykes (a), contact/baked limestone (b) and the regional Mjøsa limestone (c). Also shown mean directions from the Ringerike lavas, 276-291 Ma (E: after Douglass et al. 1989) and site-mean directions from the Oslo Graben Lavas, 274-294 Ma (D: after van Everdingen). (F) frequency distribution of post-Permian, apatite-zircon fission track ages, Oslo Rift area.

FIGURE 10

(A) Palaeozoic apparent polar wander path for Baltica (Torsvik et al. 1996) extended with that of stable Europe (Van der Voo 1993) from early Triassic times. Poles (Table 6) derived from the present study (MS-1=Mjøsa Limestone HB; MS-2=Mjøsa Limestone LB; LU=Lunner dykes & contacts) are plotted along with 'primary' igneous poles from the Oslo igneous (RL=Ringerike Lavas (large errors since only 3 sites) and OGL=Oslo Graben Lavas). Also included a palaeomagnetic overprint pole from the Ringerike Sandstone (RS). Note the concordance between MS-1 & RS (magnetic overprints) and OGL & RL, which suggest regional remagnetization between 294-274 Ma (see text)

(B) Early Triassic (243 Ma) reconstruction using the mean Lunner pole. Equal area projections.

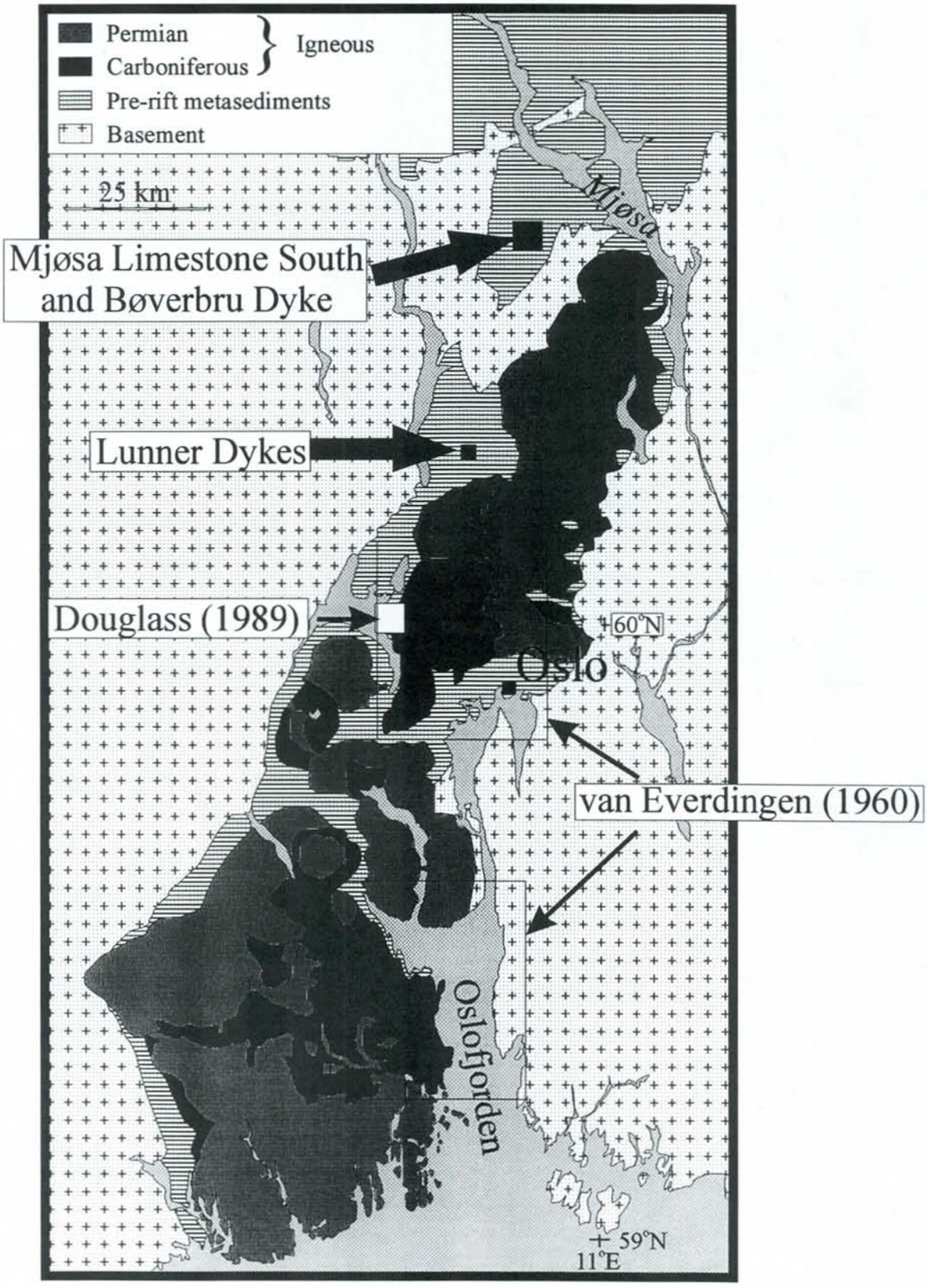

Figure 1 (Torsvik et al.)

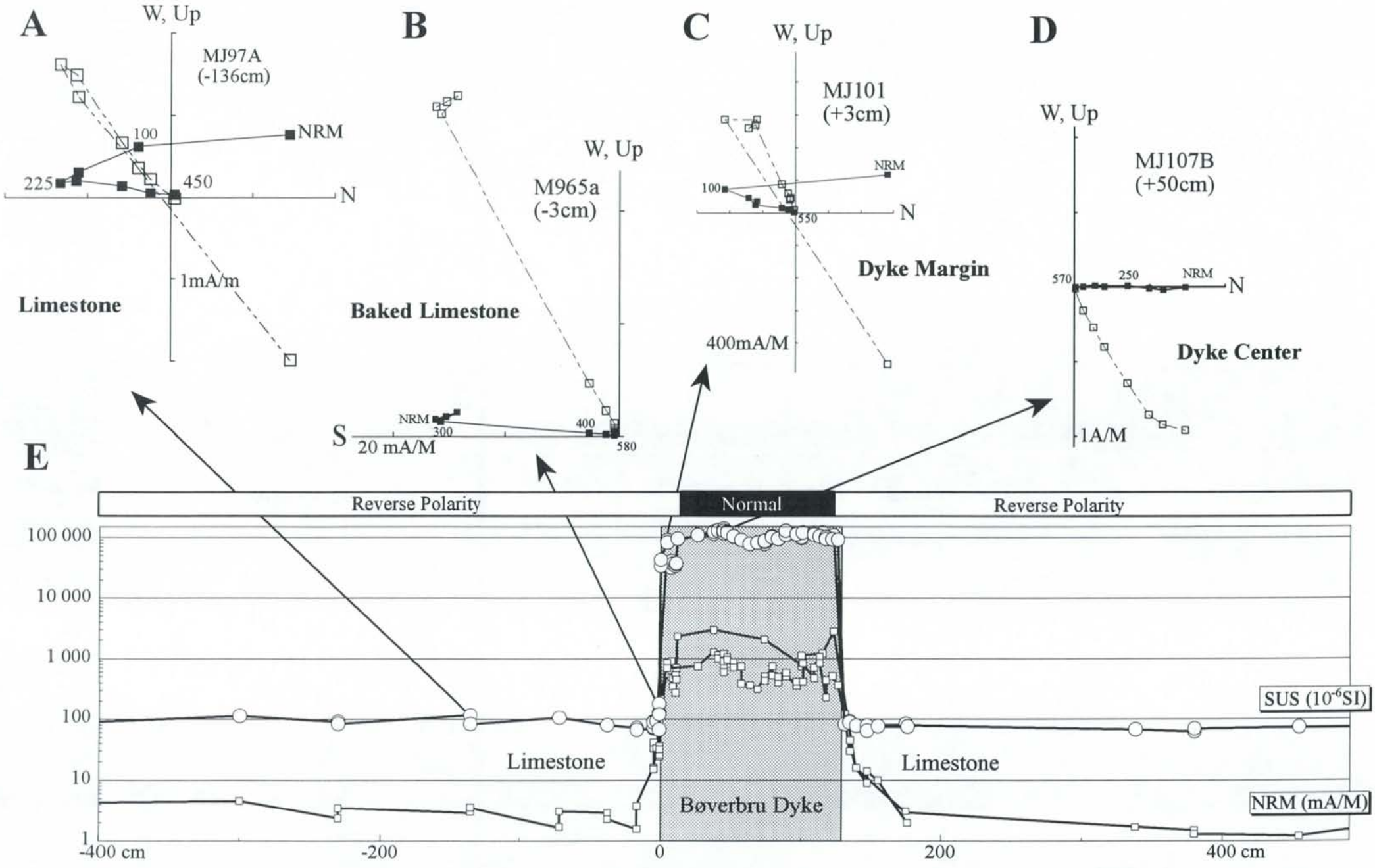

Figure 2 (Torsvik et al.)

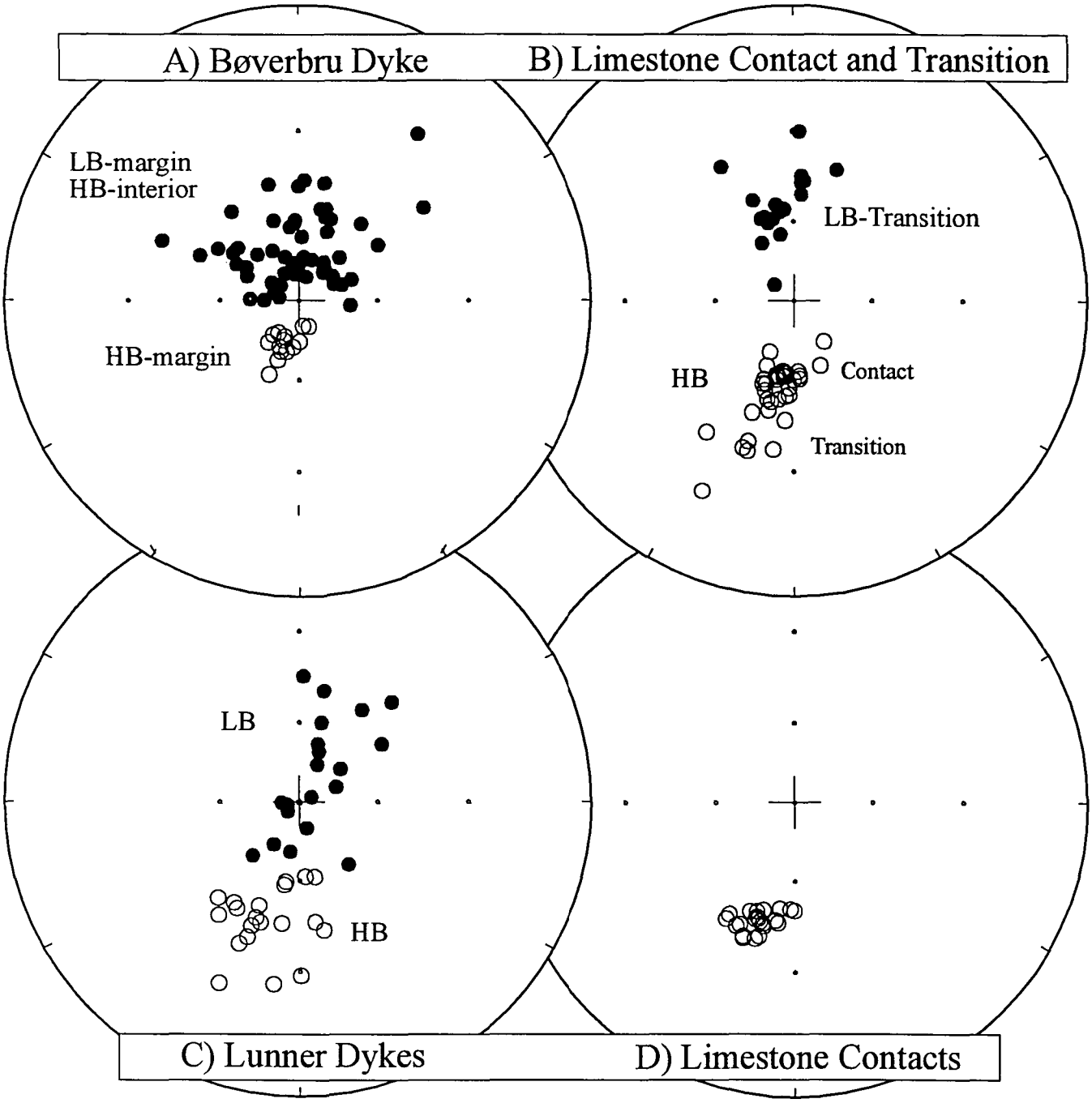

Fig. 3 (Torsvik et al.)

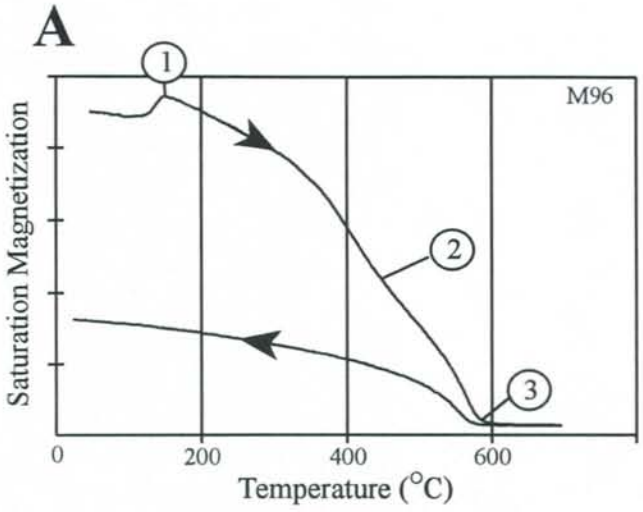

Dyke Margin (Reverse Polarity)

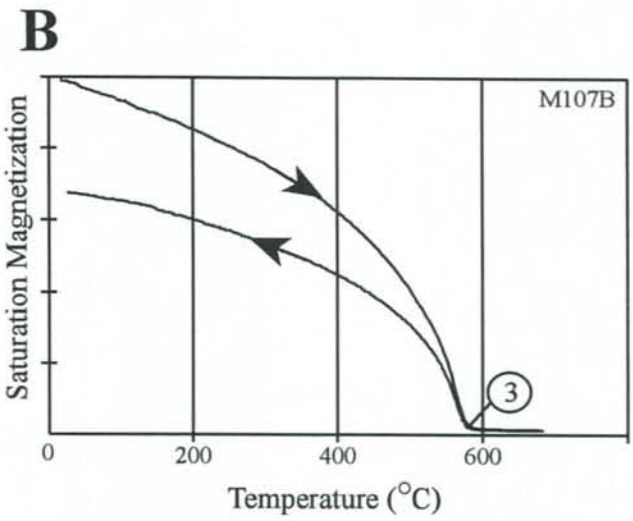

Dyke Centre (Normal Polarity)

C

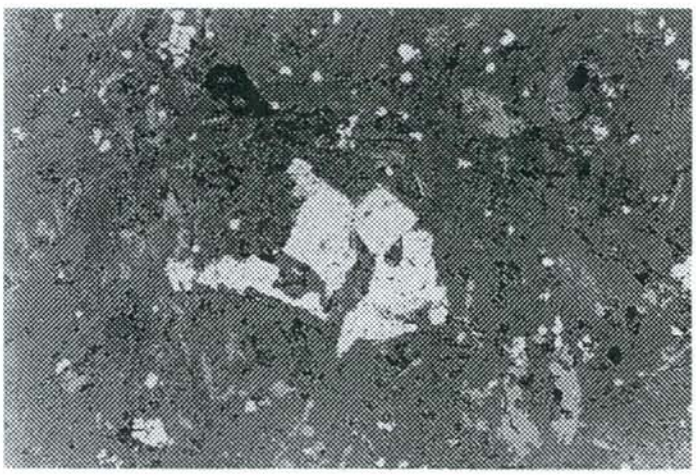

D

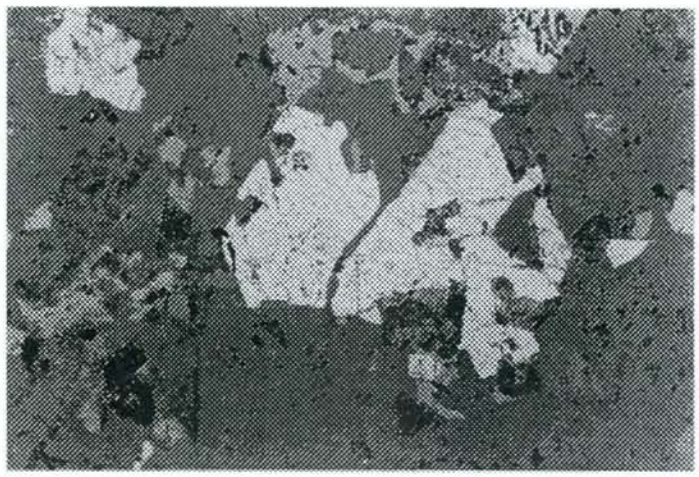

Figure 4 (Torsvik et al.)

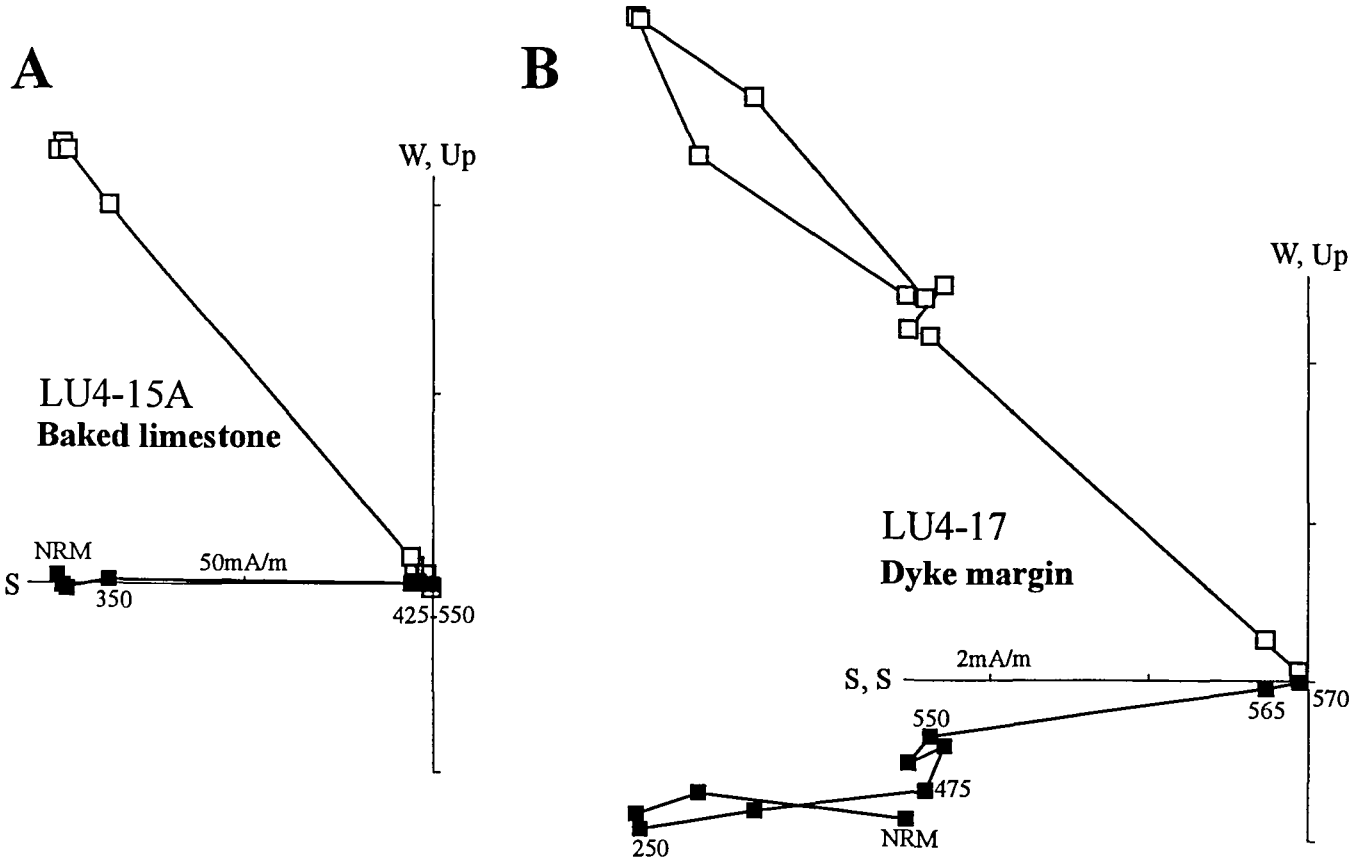

Figure 5 (Torsvik et al.)

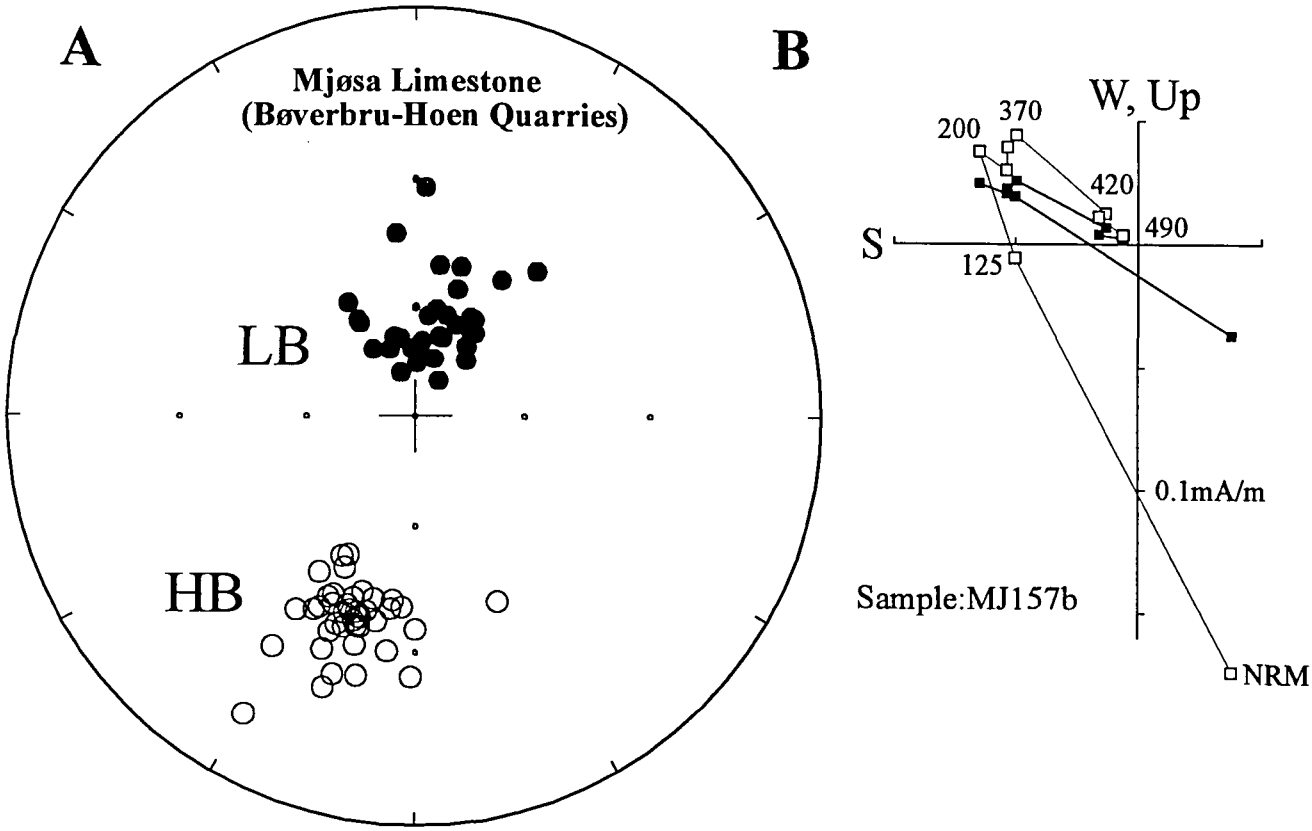

Figure 6 (Torsvik et al. 97)

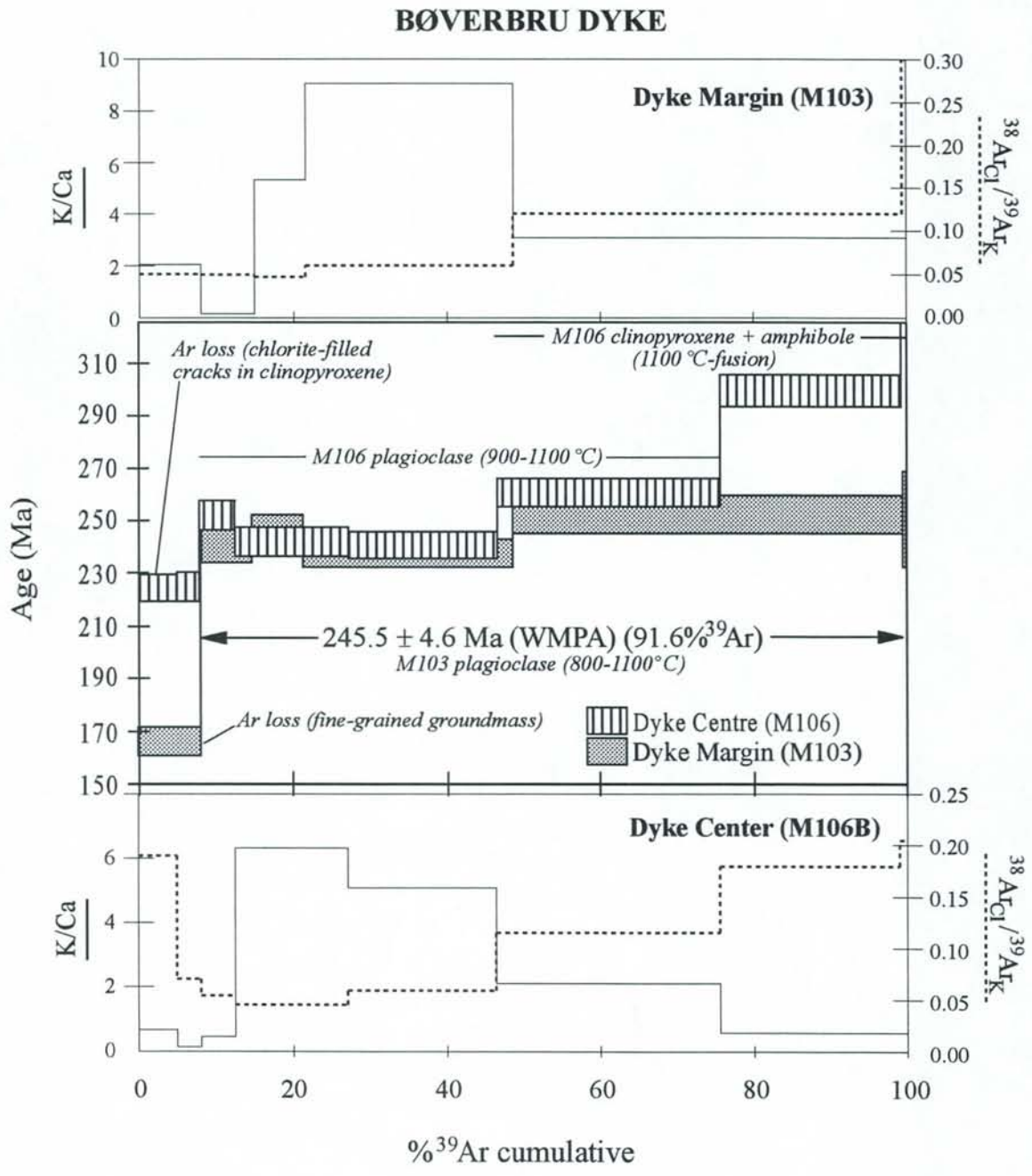

Figure 7 (Torsvik et al.)

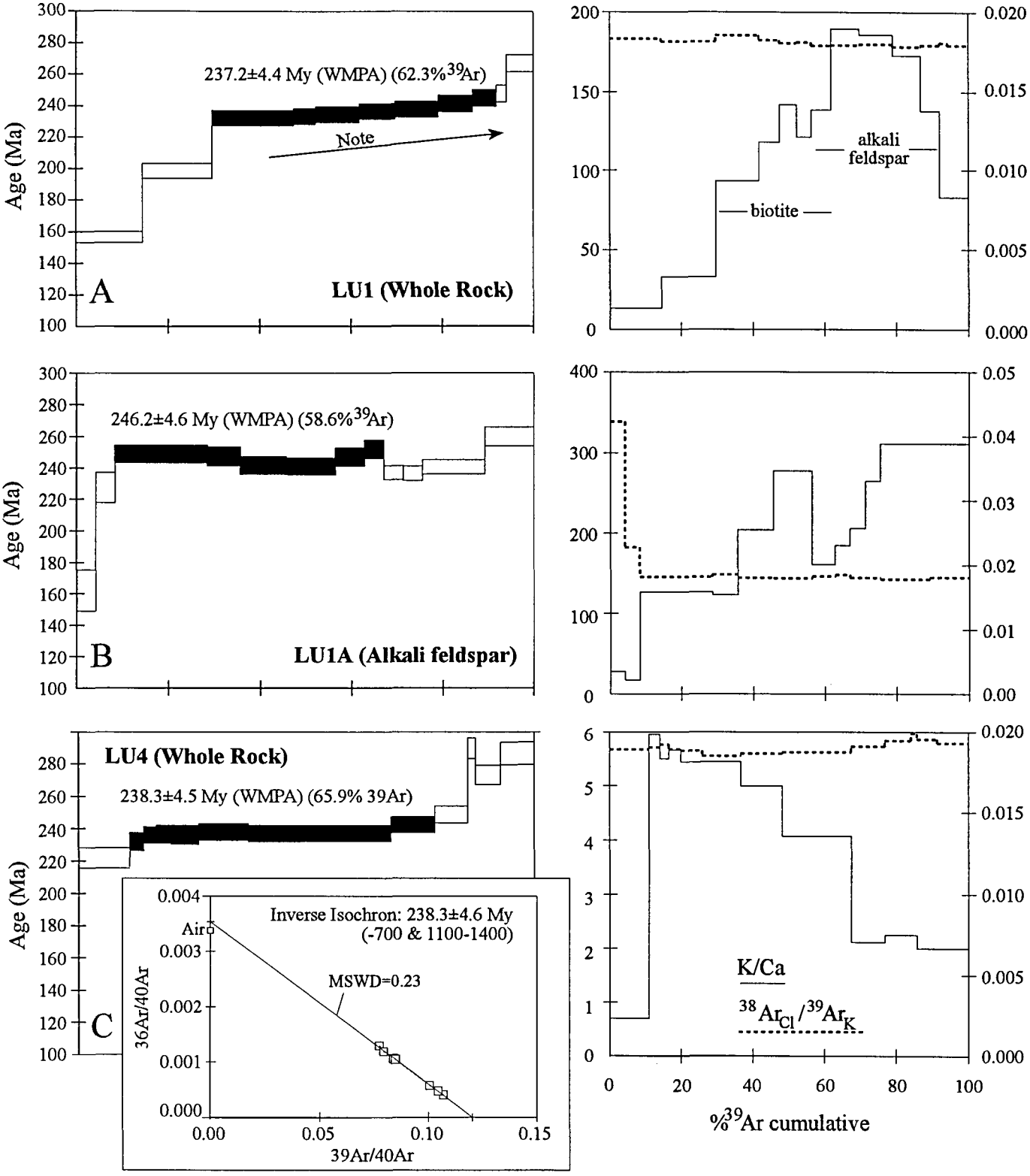

Figure 8 (Torsvik et al.)

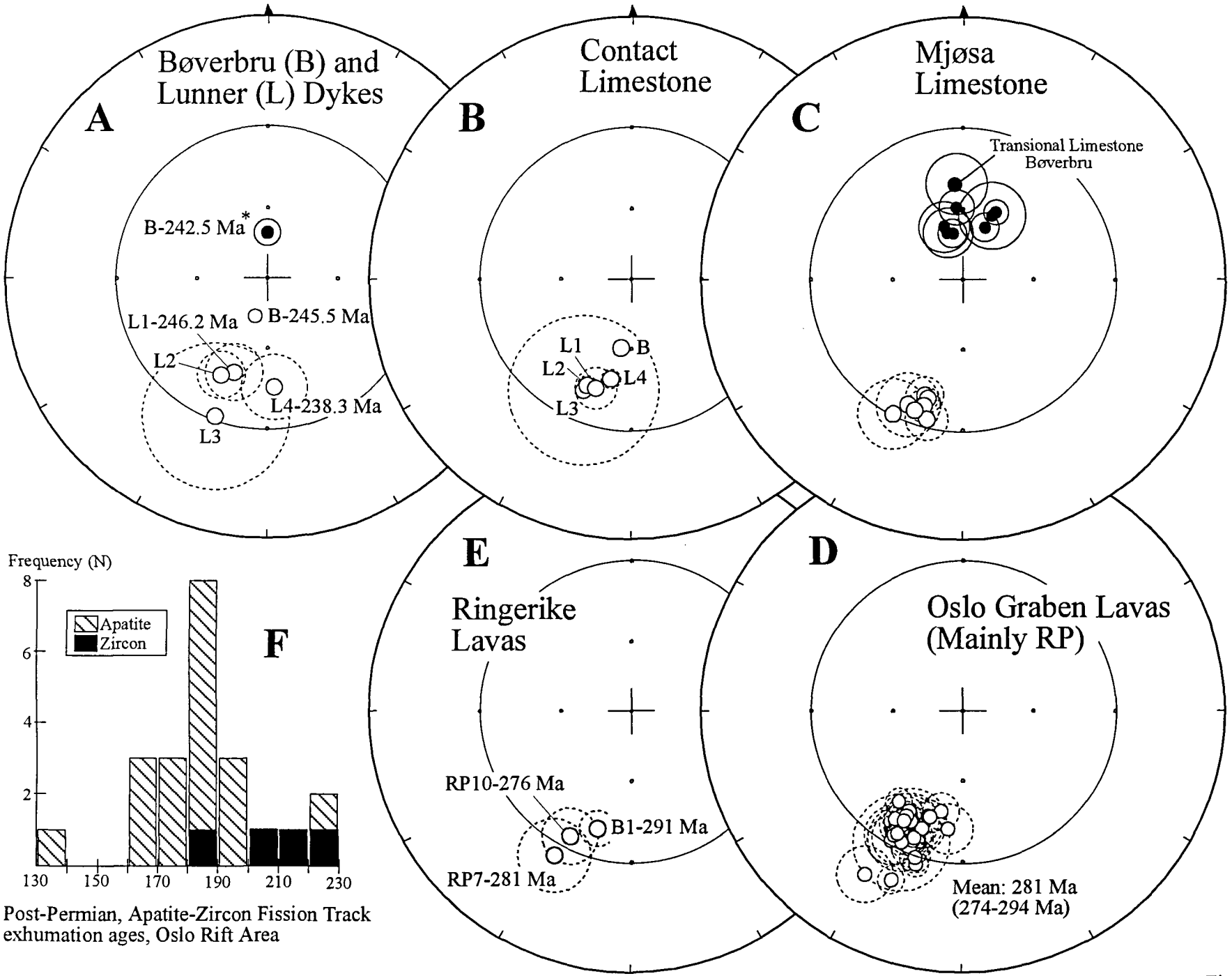

Post-Permian, Apatite-Zircon Fission Track exhumation ages, Oslo Rift Area

Figure 9 (Torsvik et al.)

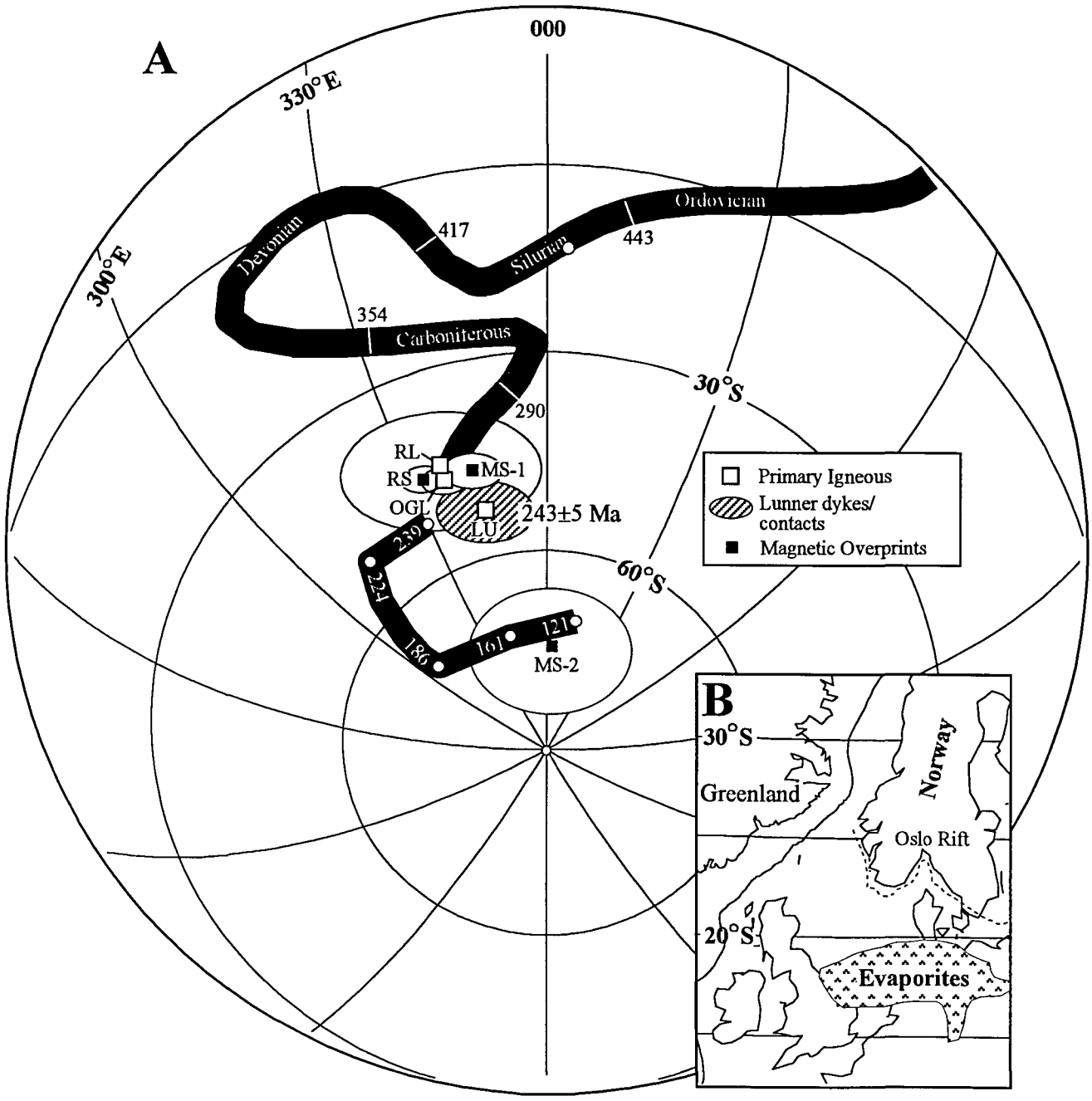

Figure 10 (Torsvik et al.)

Chapter 5

Early Carboniferous unroofing in western Norway and alkali feldspar thermochronology

Eide, E.A., Torsvik, T.H., Andersen, T.B. & Arnaud, N.O.

to submit to *J. Geophys. Res.*

5.1 ABSTRACT

$^{40}Ar/^{39}Ar$ thermochronologic data from an extensional detachment zone in western Norway document punctuated, late Paleozoic through Mesozoic tectonothermal activity in an area surrounding a major, syn-post-Caledonian extensional detachment. $^{40}Ar/^{39}Ar$ mica ages of 448 ± 8 Ma, 420 ± 8 Ma, and 392 ± 7 Ma from the hanging wall nappe, the detachment mylonite, and the footwall, high-grade basement, respectively, indicate maintenance of a low geothermal gradient during, and immediately after, Caledonian collision and progressive removal of >50 km of crustal overburden. Diffusion and thermal modeling of alkali feldspars sampled in a profile through the detachment zone best replicate laboratory Ar-release patterns when feldspars comprise three or four diffusion domains, each with differing activation energies that range from high- to intermediate- to low- closure temperatures. These domains correspond to distinct, regional changes in late Palaeozoic cooling rates: 1) slow cooling at 0.5-2.2°C/m.y. from ca. 410 to 360 Ma; 2) *rapid* cooling at ≥15°C/m.y. in Early Carboniferous time (360-340 Ma); 3) slow cooling at 0.4-1.7°C/m.y. after c. 310 Ma, with subsequent partial Ar-loss and/or thermal resetting in Late Jurassic-Early Cretaceous and Tertiary times.

The Early Carboniferous rapid cooling event recorded by the feldspars links the western Norway continental margin to Early Carboniferous unconformities and similarly-aged episodes of regional extension, basin inversion and igneous activity now documented in East Greenland, the British Isles and Svalbard. We attribute the Early Carboniferous rapid cooling event in western Noway to an episode of unroofing. Unroofing was a consequence of increased topography and erosion; movement of the rocks toward the surface (higher topography) was probably triggered by thermal underplating, probably in latest Devonian time. The feldspar modeling results, based upon 'mulidomain theory', thus have tenable links to a series of regionally recorded geologic events and support the judicious application of diffusion and thermal modeling of Ar-Ar alkali feldspar data from areas with well-constrained tectonostratigraphy and other, independent means of age control.

5.2 INTRODUCTION

The post-Caledonian evolution of the northern North Atlantic region has been derived in large part by linking the post-Caledonian onshore histories of eastern Laurentia, Avalonia, Baltica and Barentsia with offshore seismic and well data (Fig. 1). The post-Caledonian evolution of western Baltica has been a somewhat peripheral actor in developing these tectonic models because of its paucity of onshore, post-Devonian rocks. Available chronologic markers for post-Caledonian, onshore western Baltica presently comprise a few absolute ages from young, brittle faults and Late Permian dikes, the occurrence of Jurassic sediments in isolated pockets, and tectonothermal information available from the Permo-Carboniferous Oslo Rift region (Fig. 1) (Løvlie, 1981; McIntyre and Færseth, 1982; Bøe and Bjerkli, 1989; Torsvik et al., 1992; Sundvoll and Larsen, 1994; Rohrman et al., 1995; Torsvik et al., 1997; Eide et al., 1997). These geographically and chronologically discontinuous pieces of information contrast with well-exposed Late Paleozoic and Mesozoic sediments, volcanic rocks and fault-basins on East Greenland, Svalbard and the British Isles (Haszeldine, 1984; Steel and Worsley, 1984; Ziegler, 1990; Coward, 1993; Braathen et al., 1997; Hartz et al., 1997). The thermotectonic history of Baltica is an obvious, but relatively unconstrained, player in models of the post-Caledonian history of the North Atlantic.

The thermal history of the exposed Baltican crust can be used as a proxy for (missing) post-Devonian rocks onshore and may be tracked via judicious application of thermochronology. $^{40}Ar/^{39}Ar$ alkali feldspar thermochronology and thermal and diffusion modeling of Ar-feldspar data have been used successfully elsewhere to document cooling and unroofing histories and ages of fault motions (e.g. Lovera et al., 1989; Copeland et al., 1991; Arnaud et al., 1993). Nonetheless, use of cooling histories modeled from Ar-feldspar data remains a contentious method in tectonic analysis due to ongoing debate about mechanisms of Ar diffusion in feldspars and the inherent assumptions necessary to extrapolate the laboratory modeling results to natural feldspar behavior (Lovera et al., 1989, 1990; Foland and Xu, 1990; Villa, 1994; Arnaud and Kelley, 1997).

Notwithstanding, and in part because of, these arguments, we have applied thermal and diffusion modeling to Ar-Ar data from isothermal, cycled heating experiments on alkali feldspars from western Norway following the method of Lovera et al. (1989; 1991), and

assuming 'multidomain theory' for Ar distribution in the feldspar samples. The rocks derive from a tightly constrained tectonostratigraphic profile through a major extensional detachment and the resulting data are significant for two reasons: 1) they document a heretofore unknown, rapid cooling event during, or just preceding, Early Carboniferous time (ca. 360 Ma) in western Norway, and 2) they are most easily and reasonably explained to represent Ar release from several (three to four) diffusion domains of varying sizes and activation energies in the feldspars. The age data and cooling histories are very consistent with events of similar age previously documented in the Barents Sea region, East Greenland and Britain and promote multidomain, volume diffusion as a viable physical process governing Ar transport and storage in some natural alkali feldspars.

5.3 GEOLOGIC SETTING

The samples were taken from a profile through the Nordfjord-Sogn Detachment Zone (NSDZ) in the Sunnfjord region of western Norway (Figs. 1 & 2). The Caledonian history of the area involved a subduction-collision sequence between a rapidly moving Baltican continent and nearly stationary Laurentia in Late Ordovician to Late Silurian (c. 450-420 Ma) times; this process generated high-to-ultrahigh pressure (HP-UHP) rocks in the subducted Baltican crust (western Norway) and HP rocks in the allochthonous nappes now exposed on both Laurentian and Baltican margins (Torsvik et al., 1996; Eide & Torsvik, 1997; Andersen et al., 1998; Hartz, 1998). Exhumation of the deeply subducted Baltican crust has been ascribed to extensional collapse along a series of detachments, possibly aided by slab delamination (Andersen et al., 1991, 1994; Dewey et al., 1993).

Exhumation and associated top-to-the-west extension in Early-Middle Devonian times in western Norway was coeval with deposition of fluvial-alluvial clastic sediments in basins initiated on the allochthonous nappes (Hossack, 1984; Osmundsen and Andersen, 1994; Osmundsen et al., in review). The syn-post-collisional crustal thinning and top-west transport juxtaposed the HP, eclogite-bearing basement of the Western Gneiss Region with middle and upper crustal allochthonous constituents and Devonian basins, and is now manifested by the 2-3 km-thick extensional mylonite of the NSDZ (Figs. 1 and 2).

As background to this study, we point to some anomalous tectonostratigraphic relationships in this collision-extension-exhumation scenario that have remained unclarified in the literature and indicate significant, but enigmatic, post-Caledonian activity in western Norway. First, the Devonian Basins are now in contact with both high- and low-pressure units, despite the fact that the clasts of the basin sediments sourced exclusively from a high crustal level source (see Fig. 1) (Cuthbert, 1991; Osmundsen et al., in review). Second, the entire tectonostratigraphy, including the Devonian Basins, is folded along E-W trending axes into a broad, anti- and syn-formal series (Roberts, 1983; Chauvet and Seranne, 1994; Osmundsen and Andersen, 1994; Torsvik et al., 1986) (Fig. 1). Third, parts of the folded Devonian sediments are apparently metamorphosed to lower greenschist facies. Fourth, several generations of brittle faults cutting the area and have been classified as either syndepositional (in the Devonian Basins), Late Permian and related to similarly-aged mafic dikes occurring along near-shore western Norway (Fig. 1), or 'Mesozoic and younger' and related to the general east-west extensional regime active during offshore basin development and opening of the North Atlantic (Torsvik et al., 1992; Osmundsen, 1996; Hartz & Andresen, 1997; Osmundsen et al., in review). The chronology of these events and their implications for post-Caledonian Baltica have been partially resolved by the Ar- feldspar studies in western Norway.

5.4 SAMPLE DESCRIPTION

The focus on Late Paleozoic and younger events in western Norway necessitated use of thermochronologic methods with low closure temperatures since the region was not heated above c. 400°C since Middle Devonian time; much of the Upper Plate, in fact, remained below 400°C since the Early Silurian (Andersen et al., 1998). We utilized the advantage of low Ar-closure temperatures for slowly cooled alkali feldspars (c. 400° to 150°C; Arnaud et al., 1993) to track the cooling histories of the rocks in a profile through the NSDZ. We have established that the structurally highest and lowest samples were isolated from the influence of advective heating or fluids associated with Permian and Mesozoic reactivation of the NSDZ (Eide et al., 1997) (Fig. 2). In addition to alkali feldspars, we also analysed white micas, biotite and amphibole from the same or associated rocks to establish boundary constraints (temperatures and times) for the alkali feldspar thermal and diffusion modeling.

The samples included rocks from the hanging wall of the NFD, the detachment mylonite and the decompressed lower crustal rocks and constitute, from structurally uppermost to lowermost (Fig. 2): alkali feldspar and white mica from the Høyvik Group (AS2a, b), two alkali feldspars from the Dalsfjord Mangerite Suite (AS1 and AS3), alkali feldspar and white mica from the detachment mylonites (AS6a,b), and white mica (BA1), alkali feldspar (BA3), biotite (T97) and barroisitic amphibole (4000.011) from several basement gneiss lithologies in the eclogite-bearing rocks (Fig. 2). Brittle fault rocks from the fault on Atløy, cross-cutting the detachment, have also been dated with the Ar-Ar method (Eide et al., 1997). The structural and temporal relationships between the various tectonostratigraphic units are described in Brekke and Solberg (1987), Osmundsen and Andersen (1994), and Andersen et al. (1998) (see also Fig. 2). All feldspar mineral chemistry data were obtained on the Cameca Camebax microprobe at the Mineralogical-Geological Museum in Oslo.

5.4.1. Høyvik Group

The Høyvik Group is a meta-psammitic unit which unconformably overlies the Dalsfjord Suite and is unconformably overlain by the Silurian (Wenlock) Herland Group marine sedimentary package (Fig. 2) (Brekke and Solberg, 1987; Andersen et al., 1990). Quartz is characterized by undulatory extinction and sutured grain boundaries while alkali feldspar porphyroclasts have weakly undulatory extinction and smoothly curved grain boundaries; tabular phengites are gently kinked to undeformed. Textural features are interpreted to suggest one episode of white mica growth and deformation at temperatures from 400-450°C slightly prior to 448 Ma ($^{40}Ar/^{39}Ar$ cooling ages for phengite in the rocks) (Andersen et al., 1998).

Sample AS2 derives from the lowermost section of the Høyvik Group, ca. 50 m above the unconformable contact with the Dalsfjord Suite (Fig. 2). The rock constitutes an alkali feldspar-quartz-phengite-oxide gneiss with accessory titanite and pyrite and late, minor chlorite. The foliation is defined by thin layers of fairly coarse-grained phengite separating quartzofeldspathic bands. Feldspar porphyroclasts in the sample are microperthitic, coarse-grained and asymmetrically flattened; subgrain development is evident on grain rims and fine oxide inclusions occur in grain cores. Chemically the feldspars comprise microcline hosts ($Or_{97-98}Ab_{2-3}$) with exsolved, albite rods or beads (Or_1Ab_{99}).

5.4.2. Dalsfjord Suite

The bulk of the Dalsfjord Suite is a crystalline unit of (presumed) Precambrian age and comprises mangeritic syenite gneiss with minor granitic gneiss, anorthosite and younger non-gneissose gabbros (Brekke and Solberg, 1987). A late, greenschist facies overprint pervades the sequence and the lowermost 50 m of the unit is brecciated in proximity to the brittle, Dalsfjord Fault at Atløy (Brekke and Solberg, 1987; Eide et al., 1997) (Fig. 2). One sample (AS1) was taken ca. 20 m below the unconformable contact with the Høyvik Group (Fig. 2). A second Dalsfjord Suite sample (AS3), was taken from ca. 50 m above the brittle fault on Atløy.

Sample AS1 contains microcline, plagioclase, quartz, and oxides with accessory garnet and, in thin veins or pockets, a secondary, greenschist facies assemblage of titanite, white mica, chlorite, biotite. The quartzofeldspathic mineral textures indicate partially-recovered strain via subgrain zone development around alkali feldspar rims, strained twins in plagioclase, and polygonal quartz rinds around the coarsest alkali feldspar porphyroblasts. Plagioclase feldspars are antiperthitic and clouded with fine-grained white mica, titanite and/or epidote grains, related to the greenschist facies recrystallisation. Alkali feldspar hosts have a composition of $Or_{95-97}Ab_{3-5}$ with some exsolved albite strings and rods ($Or_{1-3}Ab_{97-99}$).

Sample AS3 has a mineral assemblage similar to AS1 but is much more deformed (both ductiley and brittley). Grain boundaries are generally serrated and irregular and the quartzofeldspathic minerals exhibit extensive subgrain growth. Microperthite is slightly turbid and plagioclase porphyroblasts are clouded by fine-grained inclusions of white mica. Late Permian and Late Jurassic-Early Cretaceous brittle activity along the Atløy Fault was accompanied by brittle fracturing of the rock and associated very low-greenschist facies mineralization in thin veinlets (Torsvik et al. 1992; Eide et al., 1997). Feldspar hosts with composition Or_{96-99} have fine (<20 μm) albite lamellae.

5.4.3. The Nordfjord-Sogn Detachment and mylonites

The low- to medium-grade, highly strained rocks occur in the footwall of the detachment. The mylonitic to ultramylonitic foliation is punctuated by smeared, alkali feldspar augen. Sample AS6 was taken from ca. 50 m below the tectonic contact with the Upper Plate units

(Fig. 1) and comprises alkali feldspar, quartz and phengite, with minor oxides in a mylonite matrix. No mineral chemistry data were obtained from this unit.

5.4.4. Western Gneiss Region units

Regionally, these rocks are a blend of granitic, granodioritic and tonalitic gneisses, eclogites, and partially metamorphosed mafic igneous rocks (anorthosites, gabbros and garnet-pyroxenites). The eclogite-bearing gneisses in Sunnfjord have been described by Cuthbert (1985) and Cuthbert and Carswell (1990). Samples BA1 and BA3 from the small island of Bårdsholmen are part of a Precambrian granulite facies complex (1000 ± 10 Ma, Gromet & Andersen, 1994) metamorphosed to eclogite facies during Caledonian collision, and subsequently retrogressed to amphibolite facies during exhumation (Engvik et al., in prep.). Sample BA1 is from an eclogite facies quartz-felsite comprising blue quartz, phengite, epidote, zoisite and accessory zircon; garnet, omphacite, rutile, paragonite, biotite and Cl-rich amphibole may also occur (Andersen et al., 1994; Engvik et al., in prep.). The quartz-rich rock is fairly massive with a weak planar fabric imparted by aligned, coarse-grained phengites. Phengites appear fresh and undeformed except for very thin, slightly recrystallized grain rims.

Leucocratic granulite (BA3) comprises quartz, orthoclase, fine-grained white mica, and accessory oxides, epidote and Cl-rich amphibole; biotite forms after white mica. Garnet and hypersthene also occur in some examples (Engvik et al., in prep.). The rock has a strong planar fabric where both quartz and feldspar are flattened along the foliation plane. Variably sized quartz grains have serrated boundaries and undulatory extinction, while coarser feldspar porphyroblasts have irregular extinction zones (partially healed subgrain regions). Feldspars have rare, very fine-grained mica inclusions. Mesoperthite from BA3 has composition $Or_{90}Ab_{10}$ (Engvik et al., in prep.).

Biotite 95T97 was separated from a pegmatite filling a top-west shear zone in Lower Plate, tonalitic basement gneisses. The pegmatite comprised the assemblage biotite, albite and quartz. Barroisitic amphibole (4000.011) was separated from a monomineralic vein cutting an eclogite body.

5.5. $^{40}Ar/^{39}Ar$ GEOCHRONOLOGY

5.5.1. Analytical procedures

High purity mineral separates for $^{40}Ar/^{39}Ar$ analysis were prepared by standard crushing, cleaning and separating techniques; sample size fractions and weights, and irradiation details are presented in Table 1. We used the $^{40}Ar/^{39}Ar$ analytical facility at Laboratoire de Géologie, Université Blaise Pascal et Centre National de la Recherche Scientifique, Clermont-Ferrand, France with analytical protocol similar to Arnaud et al. (1993). Data are reported at the 1σ confidence level; plateau and isochron ages are reported including uncertainty in J-value (about 2%), while individual steps are cited without J-value uncertainty. Data reduction included standard corrections for interfering isotopes from nuclear interactions, extraction blanks, mass discrimination and decay of ^{37}Ar. Statistical analysis of the data with the IAAA97 (Integrated Ar-Ar Analysis '97) software package for Windows 95 (Torsvik et al., 1997) includes: 1) plateau determination by weighting both age uncertainty (vertical axis) and length (^{39}Ar gas volume, horizontal axis) of individual steps in the age spectrum and 2) a 'good' fit for inverse isochrons determined by a MSWD with an F-variate critical value <1 (Dalrymple and Lanphere, 1969; Roddick et al., 1980). The heating schedule for feldspars followed that proposed by Lovera et al. (1991) (see also Table 2). Feldspar diffusion and thermal modeling followed the programs of Lovera et al. (1989) and Lovera (1990), adapted to IAAA97. All samples were degassed at 400°C for 25 minutes prior to analysis. Data are reported in Tables 1 and 2. Release spectra are presented in Figure 2; inverse isochrons discussed in text for micas and amphibole are presented in Figure 3; Figure 4 shows diffusion and thermal modeling results for the feldspars.

5.5.2. White micas

The release spectrum for AS2b white mica (NSD hanging-wall) is characterized by increasing apparent ages over the first 20% of ^{39}Ar released before reaching a plateau age of 448 ± 8 Ma (77% of the total ^{39}Ar) (Fig. 2) (see also Eide et al., 1997). The final two temperature steps represent <2% of the gas. Inverse isochron analysis did not yield a good line fit to the very radiogenic data. The plateau age is within (2σ) analytical uncertainty of cooling ages obtained from other Høyvik Group white micas from the island of Atløy and the mainland (Andersen et al., 1998). K/Ca and Cl/K ratios and petrographic examination indicate the gas

evolved from a fairly homogenous, high-K muscovite, in accord with results of Andersen et al. (1998) (Table 1).

The release spectrum for AS6b phengite from a high level in the detachment mylonites yields a plateau age of 420 ± 8 Ma that constitutes 95% of gas released (Table 1; Fig. 2). As with sample AS2b, the K/Ca and Cl/K ratios indicate Ar-release from a homogeneous, high-K white mica.

Phengite BA2 from the eclogite-bearing basement yields a saddle-shaped spectrum with a saddle-low of 450 ± 10 Ma (at c. 70% completion) that climbs toward 487 ± 18 Ma at fusion (Table 1; Fig. 2). In the inverse isochron, the first three steps show a 'reverse' (positive slope) correlation, a typical distribution for an excess Ar component. The remaining data cluster too closely to the ordinate to provide a useful regression. The Cl/K ratios for the sample are low and constant. The K/Ca ratios are high, but variable: highest values in the early, old portions of the saddle drop dramatically in the latter half of the analysis (Table 1).

5.5.3. Biotite

Pegmatitic biotite (T97) from the decompressed lower crustal rock sof the WGR yields a somewhat irregular spectrum with apparent ages rising during the first 3% of gas released toward the plateau age of 395 ± 7 Ma (for 54.4% ^{39}Ar gas) (Fig. 2). The apparent age subsequently drops to 374 Ma and climbs in the remainder of the experiment to an apparent age of 408 Ma at fusion. Inverse isochron analysis yielded an array with reasonable spread between atmospheric and radiogenic components, but a poor fit to the data partly due to a high-temperature group of points with apparent excess Ar. A poorly-correlated line through all the datapoints yields an age of 394 ± 8 Ma with an $^{40}Ar/^{36}Ar$ ratio below atmospheric value (295.5) (Fig. 3a). An isochron correlated through only through those data used in the plateau calculation yields an age of 399 ± 7 Ma, still with a 'poor' fit and abcissa intercept below an atmospheric value. The Cl/K ratios are low and constant. The K/Ca ratios were high and variable, exhibiting a saddle 'low' where the apparent age drops slightly in the central portion of the experiment (Table 1).

5.5.4. Amphibole

Barroisitic amphibole from the eclogite fracture yields a saddle-shaped spectrum with apparent ages falling from unrealistically high values (807 Ma) to a saddle-low of 387 Ma, before climbing to an age of 426 Ma at fusion. The central portion of the 'saddle' yields a plateau age of 392 ± 7 for 71% of the gas (Fig. 2). Inverse isochron analysis demonstrates excess Ar components, isolated in the first five temperature increments, and a second excess Ar 'array' in the upper temperature steps; a fit of a line to the remaining data (those comprising the plateau) yields a poorly-correlated line, corresponding to an age of 398 ± 10 Ma with a nearly atmospheric intercept (301 ± 44) (Fig. 3b). The five temperature increments used in both isochron and spectrum calculations are those over which amphibole most commonly degasses (900-1100°C). K/Ca and Cl/K ratios are quite constant except for the earliest temperature steps (corresponding to the anomalously high ages) (Table 1).

5.5.5. Mica and amphibole data interpretation

The low-age, low-volume apparent ages for white micas AS2b and AS6b characterize degassing of slightly reset, low retentivity portions of grain rims at low extraction temperatures; these probably correspond to the slightly recrystallized grain margins visible in thin section (see above). The samples otherwise represent homogeneous micas that cooled through 448 ± 8 Ma and 420 ± 8 Ma (AS2b and AS6b, respectively) at temperatures between 370°C and 400°C. The 400°C maximum is constrained by the analysis of ductile deformation textures (Andersen et al., 1998); the 370°C minimum is constrained by the feldspar modeling results (see below). The K/Ca and age spectrum patterns for white mica (BA1) from Bårdsholmen indicate degassing of two different white mica phases (in addition to phengite, paragonite has been described from some Bårdsholmen lithologies by Engvik et al., in prep.) and/or of excess Ar in an inhomogeneous phengite. No geological age significance is attached to the apparent ages from this sample.

The biotite release spectrum and K/Ca ratios (T97; Figs. 2 and 3a) indicate Ar released from inhomogeneous biotite grains; this is most likely an original (chemical or structural) feature, based on the coarse, euhedral and undeformed appearance of the grains, but could also be attributed to slightly uneven degassing of biotites under high vacuum (e.g. Gaber et al., 1988). The plateau age of 395 ± 7 Ma is interpreted as the cooling age for these pegmatite minerals

through closure temperatures between ca. 300 and 350°C (McDougall and Harrison, 1988). The spectrum for the amphibole fracture-filling (4000.011) is likewise somewhat disturbed. The very high ages in the early part of the spectrum are certainly attributable to excess Ar (Fig. 3b), but the central portion of the spectrum yields a plateau age of 392 ± 7 Ma. This age is interpreted only as a *maximum* age for the cooling of the minerals, since it lies in the hollow of a saddle attributed to excess Ar. This cooling age must represent closure to Ar below temperatures from 450 to 500°C which is the interpreted maximum range for retrograde amphibolite facies conditions experienced by the eclogite facies rocks. Excess Ar may have been derived directly from the surrounding eclogite body during depressurization and/or dewatering of the surrounding gneisses during exhumation.

5.6 ALKALI FELDSPAR $^{40}Ar/^{39}Ar$ THERMOCHRONOLOGY

5.6.1. Data

Release spectra, Cl/K ratios, and Arrhenius plots from cycled, isothermal heating experiments from the five feldspar samples have very similar patterns, albeit with some intersample apparent-age variations at specific sections of the heating schedules (Figs. 2 & 4; Table 2). The basic release spectrum patterns in Figure 2 define: 1) a set of low-temperature, low-volume steps (<8% of ^{39}Ar gas) with ages that rise rapidly from <100 Ma to 2) a tightly-clustered, semi-concordant or slightly rising group of ages that range either from ca. 290 up to 360 Ma (AS2a and BA3) and comprise 12-20 % of the total gas, with a fairly abrupt transition to 3) a group of high-temperature, high-volume (60-80% of the gas total) steps usually defining Early-Middle Devonian plateau ages. Individual steps corresponding to the middle group of broadly 'Carboniferous' ages comprise relatively small gas volumes elicited during the isothermal portion of the furnace heating experiments. We draw attention also to the concave-downward cusp that is characteristic of the change from the low-temperature, rapidly rising age group to the semi-concordant, 'Carboniferous' age group (Fig. 2). The Cl/K ratios are typically very high in the first two, low temperature steps of the feldspar analyses and fall to variable, but low, values for the remainder of the isothermal portion of each experiment; these values vary subtley in the high-temperature sections of the experiments (Table 2). On Arrhenius diagrams the data define three different groups: the low- and high-temperature groups have broadly similar, negative slopes, while the middle group defines a distinct, sub-horizontal line with $\log(D_o/r^2)$ values ranging from -5 to -6 (Fig. 4).

The release spectrum from the structurally highest sample, AS2a (Høyvik Group; phengite from the same rock = 448 Ma, see above), climbs from an apparent age of 79 Ma to 298 Ma within the first 3.4% of ^{39}Ar gas released (Fig. 2). The middle group of semi-condordant ages ranges from 298 to 350 Ma. In the upper part of the monotonically increasing portion of the heating schedule, the apparent ages reach a semi-plateau of 418 ± 9 Ma that comprises 70.8% of the ^{39}Ar gas (Table 2).

Apparent ages from feldspar AS1 (Dalsfjord Suite, structurally below AS2a) (Table 2; Fig. 2), climb from 101 ± 4 Ma to 289 ± 11 Ma within the first 4.1% of ^{39}Ar released. A group of semi-concordant ages (isothermal steps) then rise gradually to 326 ± 12 Ma. At the shift to the monotonic temperature schedule, ages rise again to reach a semi-plateau in the high-temperature/fusion portion of the experiment with an integrated age of 393 ± 28 Ma (48% of the gas volume). Uncertainties in the upper temperature steps of this experiment were larger than in the other samples due to an unusually high, high-temperature machine blank on the day of analysis.

The release spectrum from the structurally-lower Dalsfjord Suite sample (AS3) has a pattern nearly identical to AS1, except that all apparent ages are offset to lower values. The ages climb from 86 Ma to 276 Ma during the first 2.5% of ^{39}Ar released. The remaining isothermal temperature steps define a group of semi-concordant ages that rise gradually 320 Ma. The final, high temperature part of the experiment yields a plateau at 380 ± 7 Ma for 66.7% of the gas volume (Table 2; Fig. 2).

Feldspar from the mylonite (AS6a) yields a release pattern representing, broadly, four segments. Rapidly rising ages from 61 to 267 Ma (5.8% of the evolved gas) reach a group of semi-concordant ages ranging from 286 to 320 Ma for 13.7% of gas released. The final isothermal steps (three steps at 800°C) and the subsequent five cycled, monotonically increasing steps, define a more rapidly rising group of ages from 334 to 379 Ma over 16.7% of the experiment. The majority of gas is released during final melting and fusion in two steps with an integrated age of 425 ± 8 Ma (63.8% of the gas).

The early part of the release spectrum for sample BA3 (gneiss, Lower Plate) exhibits rising ages grouped in low-volume, semi-plateau pairs at 93 and 260 Ma and comprising 2.4% of the evolved gas (Fig. 2, Table 2). The gas-release theme common to the other feldspars is repeated during the bulk of the isothermal steps which define a group of semi-concordant steps ranging in age from 347 to 376 Ma (ca. 17% of the gas). The final 80% of the gas released in the high temperature portion of the experiment yields discordant ages rising from 382 to an unrealistic 636 Ma at fusion.

5.6.2. Feldspar modeling results and interpretation

In the modeling exercises, Ar-diffusion was assumed to follow the Arrhenius relationship $D = D_0 exp^{-E/RT}$ in feldspars comprising several diffusion domains of differing sizes, activation energies (E) and frequency factors (Dodson, 1973; Lovera et al., 1989; Harrison et al., 1991). All variables are defined in Table 4. We followed the modeling procedure described in Lovera et al. (1991) and assumed a plane slab geometry throughout the exercises. To obtain the diffusion parameters for each domain, we generated first, synthetic Arrhenius plots to compare to the observed Arrhenius diagram (see Fig. 4). For these initial runs, the number of domains and the domain volume fraction were based on visual evaluation of the release spectra, while intial E and frequency factors were determined by the slope and intercept of a line through the low-temperature leg of the laboratory Arrhenius distribution. Frequency factors and E for the other domains were selected intuitively for the first iteration and revised in subsequent runs after visual evaluation of the model fit to the data. We attempted with each sample to maintain the smallest possible number of domains that achieved a reasonable fit in order to avoid making numerous assumptions about the 'unseen' diffusion structures of the feldspars; we were able to model all the feldspars reasonably by using either three or four diffusion domains, although trial runs did indicate nearly 'perfect' fits in some samples by using five or six domains.

Once an acceptable fit was achieved to the Arrhenius diagram, the diffusion data were plotted on the log (r/r_o) diagram (Richter et al., 1991) because only this presentation of the model data is insensitive to the heating schedule of the experiment; thus, this diagram can provide the least adulterated representation of the fit of the modeled Ar-diffusion parameters to the real (laboratory) diffusion data (Lovera et al., 1991). Misfits between the laboratory and the

synthetic log (r/r_o) data were addressed iteratively. The accepted fits are presented in Figure 4a-e. For reasons discussed below, misfits of the synthetic models to the highest temperature portions of the log (r/r_o) plots were given less priority than achieving good fits in the lower-temperature portions of the experiments.

Finally, diffusion parameters from the accepted log (r/r_o) plots were used to calculate closure temperatures and cooling histories for each domain in the sample. We utilized the cooling age and (assumed) closure temperature of the white micas analysed in this study for the initial (upper) boundary conditions for the thermal modeling runs and selected cooling rates and starting temperatures for each domain in the sample (Table 4). The unique cooling histories generated from these inputs were then evaluated by generating a synthetic age spectrum from the model cooling history and comparing this result to the observed age spectrum (Fig. 4a-e). Misfits to the observed spectrum were addressed by changing the cooling rates for the affected domain(s) until a visually acceptable match between synthetic and laboratory spectra was obtained.

Domain 1 in all the feldspars corresponds to the lowest-temperature portion of the heating experiments, represented on the release spectra by the group of rapidly increasing, small volume temperature steps (Figs. 2 and 4). Domains 2 and 3 correspond to the bulk of the isothermal heating steps, represented on the release spectra by the group of tightly clustered, semi-concordant data yielding broadly 'Carboniferous' ages. Domain 4 (or 3 in sample AS2) corresponds to the high-temperature, large gas-volume steps that generally yield Early-Middle Devonian plateau ages.

Activation energies for the various domains increased from Domains 1 through 4. Domain 1, the smallest, low-volume domain, had E between 34.7 and 36 kcal/mol. Domains 2-3 had slightly higher E, ranging usually from 37.3 to 40 kcal/mol, but in the case of BA3, reaching E as high as 47.6 kcal/mol. The large gas-volume Domain 4 (or 3 for AS2) had E between 49 and 50 kcal/mol. Frequency factors, logically, exhibited the opposite relationship to the domain sizes: Domain 1 maintains the highest frequency factors (4.8 to 6.3 sec^{-1}), and Domain 4 (or 3), the lowest (3.2 to 3.67 sec^{-1}). Clearly, the high volume, high temperature domains tended to dominate the model fits to both Arrhenius and age spectra plots; however,

since the 'volume diffusion' properties of Ar in feldspar are not valid above the melting temperatures of orthoclase (ca. 1150°C; Richter et al., 1991; Lovera et al., 1991), we ignored poor fits in the upper portions of the log (r/r_o) plots in instances where fitting those high-temperature data compromised good fits in the lower-temperature portions of the heating experiments (Fig. 4a-e). This is not to say that we believe the cooling histories for the high temperature domains are invalidated, but rather that these upper temperature histories do not conform strictly to the premises of the modeling exercises (see also discussion below).

The cooling history patterns were very similar for each of the feldspar samples (Fig. 5) whereby Domains 1 and 4 (or 3) achieved best fits when slow cooling rates were used: 0.4 to 1.7°C/m.y. for Domain 1 and 0.6 to 2.2°C/m.y. for Domain 4 (or 3) (Fig. 5, Table 4). The middle Domains 2-3 fit the observed data only when rapid cooling rates were applied. We found generally that all fits for Domains 2-3 were better at cooling rates above 15°C/m.y; the fits for several of the samples (AS1, AS2 and AS3) were better when rates between 20 and 50 °C/m.y. were used (Table 4, Fig. 5). The model fits did not improve greatly, nor did they collapse, when rates up to 100 °C/m.y were used. However, due to ongoing discussion related to the realistic ability to utilize and assess cooling rates and paleogeotherms (e.g., Manckelow and Grasemann, 1997), we allocate the more conservative, minimum rate of 15 °C/m.y for Domains 2-3; this value is nonetheless an order of magnitude higher than that recorded by the feldspars either during Domain 1 or 3 cooling periods.

Some workers who apply multi-domain theory to feldspar modeling prefer to use a single E for all the domains in a single sample by reasoning that Ar sites in the same feldspar should ideally be governed by the same diffusion properties at the scale of the grain size, and thus, should be related by the same E. We find equally valid reasoning that, given the assumption of different domains of different sizes in the same feldspar, the physical capacity to diffuse Ar into or out of a small site should require less energy (lower E) than to do so with a larger site (higher E). In a more quantitative way, we tested these two possibilities by modeling the feldspars with the same domains and domain sizes, but instead held the E constant for each domain; the results from these runs showed first, that the cooling histories are not dramatically affected by the choice of activation energy or frequency factors, and second, that

a better fit to all of the observed data was achieved using different Es for different domains in the same feldspar. This conforms to similar findings of Harrison et al. (1991).

The initial assumption of several diffusion domains in the feldspars, intuitively sensible from the 'compartmentalization' observed in the Ar release-spectrum patterns, as well as the departure from linearity of the Arrhenius diagrams (see Lovera et al., 1989), was borne out by the diffusion and thermal model fits. Most importantly, as discussed below, the very different cooling rates obtained in these modeling runs have a logical relationship to independent, regional, geologic events.

In Figure 5, the onset of the rapid cooling episode in each of the feldspars, represented by Domains 2-3, occurs at a slightly different time period. Those feldspars located structurally (tectonostratigraphically) farthest from the Dalsfjord and Atløy Faults yield the *oldest* ages for onset of the rapid cooling event, while those closest to the fault yield the *youngest* ages. We attribute this difference not to represent real differences in the age of onset of this rapid cooling 'event', but rather to partial resetting of the Ar systems in those rocks closest to the reactivated fault. This fault zone was brittley reactivated at least twice, in Late Permian and Latest Jurassic-Early Cretaceous times (Torsvik et al., 1992; Eide et al., 1997). We suggest that the Lower Plate basement (BA3) and the Høyvik Group (AS2a) feldspars were isolated from the fluids and/or frictional heating associated with these younger fault reactivation/resetting events. These two samples, with very similar ages of onset for the rapid cooling event thus record most accurately the timing of the event—i.e. in Early Carboniferous time, between 340 and 360 Ma (Fig. 5).

What physical manifestation can we place on the domains in each of these feldspar samples given that similar cooling histories are produced in feldspars from very different rocks with different degrees of deformation? First, the high temperature domain corresponds to very retentive sites for Ar in the feldspar lattice; these sites are characterized by high K- and low Cl-contents and apparent ages (except for BA3) very much in keeping with post-Caledonian cooling of the feldspars (corresponding to exhumation in Early-Middle Devonian times). The Es for these high-temperature domains are within the ranges suggested for single domain, high purity orthoclase feldspars in other studies (Foland, 1974; Arnaud and Kelley, 1997), and

we suggest that Ar released from these sites corresponds to that retained in the original feldspar following cooling after continental collision, thrusting and metamorphism. The low temperature, Domain 1 was more difficult to model, because of the small volume of gas it represents (see e.g., Fig. 5d), but it is nonetheless evident that the Ar in these sites is slightly Cl-correlated and is representative of partial resetting of the Ar-isotopic system in the feldspar at some younger time(s). We suggest that Domain 1 represents one or more of several, less retentive sites in fluid inclusions, in cracks, in subgrains and other strain-induced features (especially those samples taken in close proximity to the fault zone) and/or the albite lamellae. The nature of the middle Domains 2-3 sites are more speculative and we can only propose that these represent some original part of the feldspar lattice that remained open to diffusion of radiogenic Ar until Early Carboniferous times. We reason that the middle domain is a K-related site and not an anion site from the fact that the same release patterns and relative proportions of radiogenic and reactor-induced Ar are produced from different samples.

We interpret the model diffusion parameters and cooling rates to represent 3 to 4 domains in the feldspars that increase in size and retentivity with increase in closure temperature; the largest domains thus closed earliest to Ar and, as regional temperatures dropped, progressively smaller domains were isolated to diffusion of Ar. This process is mimicked in the laboratory by releasing weakly held Ar from the smallest diffusion domains at the lowest experimental temperatures, and progressively exhausting Domains 2-4 via combination of isothermal and cycled heating until the sample was fused.

5.7. REGIONAL IMPACT

The Early Carboniferous rapid cooling event identified in this study has three potential explanations: 1) thermal relaxation following a magmatic event, or 2) a response to unroofing (or exhumation) from a warm to a relatively cooler crustal level. We lack any evidence in western Baltica for magmatic activity at that time, so we favor the second, tectonic/erosion unroofing situation for the western Norway region at this time; however, we note (see discussion below) that the unroofing may have been induced by thermal underplating that was never achieved surface expression in the form of igneous rocks.

Approach of a crustal unit toward the surface can be accomplished by tectonic exhumation, fault-controlled footwall uplift accompanied by increased rates of erosion, or increased topography and erosion (caused, e.g., by folding). We briefly examine each of the three mechanisms.

The rocks in this area underwent 'tectonic exhumation' during and immediately after continental collision in early-middle Devonian time, as demonstrated by a variety of structural, kinematic and geochronologic data (see Andersen et al., 1991). By the Early Carboniferous, the geologic evidence in western Norway implies that this post-collision, exhumation period was completed and thus, sudden 'unroofing' in the area must have another cause.

Fault-controlled footwall uplift is sometimes invoked in sedimentary basin modeling to clarify basin thermal histories. In the case of western Norway, some form of footwall uplift in Early Carboniferous time would have required a regional normal fault or fault system. Presently, only the Øygarden Fault Zone emerges as a candidate to affect this sort of crustal movement. Based upon current estimates of depth-to-basement on both sides of the fault zone, interpretations of the ØFZ geometries (seismics) and estimates of apparent ages/thicknesses of sedimentary packages on the western side of the fault (Osmundsen, pers. comm.), any activity/initiation of the Øygarden Fault Zone in Early Carboniferous time is unlikely.

We thus implicate increased topography and erosion to account for the rapid cooling recorded in these rocks. We suggest tentatively that increased topography was caused by regional thermal underplating possibly accompanied by regional folding/metamorphism (along E-W axes) of the both detachment and the basal sediments in the Devonian basins of western Norway (see 'Introduction' for details). The timing of our Early Carboniferous cooling event fits well with relative time constraints previously suggested for this folding episode (Torsvik et al., 1986, e.g.). However, if folding can indeed be pinpointed to Latest Devonian-Early Carboniferous times, it must also (in western Norway) have been accompanied by regional unroofing. This follows from the fact that folding alone cannot accomplish the cooling response we observe in the rocks because fold geometries predict variable cooling rates depending upon a rock's position within the fold sequence (e.g., rocks within a synform

would move relatively downward compared to those positioned in the antiform). Thermal underplating in this area would not necessarily have resulted in extensive melting and magma production primarily because the lithosphere in western Norway (western Baltica) was and has remained very thick. Thus, emplacement of a deep-seated thermal anomaly could invoke unroofing without production of the 'usual' magmatic products.

A minimum calculation of the quantity of crustal overburden unroofed/eroded during this rapid cooling episode mandates knowledge of three parameters: 1) starting/ending temperatures of the rocks, 2) the cooling rate and 3) the geothermal gradient. We know (1) and (2) but have no real control on (3), so we must calculate the amount of denuded overburden for a range of possible geothermal gradients. We can assume over the duration of the cooling 'event' (1 to 5 m.y.) that the geothermal gradient did not change, and what we effectively calculate is 'instantaneously' unroofed rocks. For the purposes of these calculations, we use only the temperatures and cooling rates for samples AS2 and BA3, since they were unaffected by younger reactivation events. Values in Table 3 indicate that AS2 (upper plate) cooled at a rate of 50°C in 1-2 m.y.; during its most rapid cooling episode, BA3 cooled at a rate of 95°C in ca. 5 m.y., within the same range as AS2. Table 4 lists the amount of overburden unroofed in the crustal column above BA3 and AS2, assuming the widest reasonable range of geothermal gradients possible for the crust at that time. The lowest geothermal gradient (10°C/km) is an absolute minimum for this system; this is a reasonable gradient we can estimate for the area after rapid subduction following Iapetus closure in early Silurian time and eclogite-facies metamorphism of Silurian-early Devonian age.

The actual geothermal gradient by Late Devonian time had almost certainly begun toward higher values as the crust decreased thickness and began to re-equilibrate. The highest geothermal gradient used in this exercise is a 'normal' crustal geothermal gradient (25°C/km), and is the absolute maximum we can anticipate for the crust in this area at that time; we have no evidence for extensive melting of the crust in the area from Silurian time onward, so higher geotherms are not justified. The crust had probably not completely equilibrated (recovered) from the very low geotherms of the collisional event by Early Carboniferous time, so an estimated geothermal gradient between 10 and 25°C/km is realistic.

A minimum of ca. 4 km of overburden must have been removed from the column of rock above sample BA3 (WGR) over a period of 5 m.y. in order to generate/maintain the rapid cooling profile we observe in the feldspars (assuming a crust with a 'normal' geotherm). This translates to a smoothed unroofing rate of 0.8 mm/yr. The column of unroofed material increases if we apply colder geothermal gradients. The same calculation for the NSD hanging-wall (AS2) yields 2 km of unroofed material in 1 m.y. for the most conservative (high, 'normal') geothermal gradient. It is tempting to suggest that the two-km difference between the minimum unroofing estimates for upper and lower plate rocks (i.e. 2 km) is real. We know that these rocks were at higher crustal levels than those in the WGR at that time; however, the actual vertical (structural) distance between these two rock units in the tectonostratigraphic package for that time period is impossible to reconstruct accurately. We thus cite 2 to 4 km as a conservative minimum estimate for the quantity of unroofed material from this area during that brief time period. This would translate to ca. 500 m of acutal 'uplift' of the crustal package. Implicit in our discussion is the fact that, although the 'cooling event' was Early Carboniferous in age, the actual movement of the crustal package toward the surface must have begun slightly earlier (Latest Devonian time?) due to the inherent delay in onset of thermal relaxation.

Reginally, latest Devonian and early Carboniferous folding, faulting and magmatic activities are well-documented. In the United Kingdom, folds in the Devonian ORS of the Orcadian and East Shetland basins have presumed Latest Devonian ages. This activity was followed by block faulting in central England and Scotland and thick Lower Carboniferous sedimentary basin fill, as well as initiation of alkaline and tholeiitic volcanism of Tournaisian age (Midland Valley region). Plutonic activity on Shetland of early Carboniferous age (Torsvik et al., 1989) appears to have followed closely upon folding of Devonian strata in the ORS. Similarly on Spitsbergen, Early Carboniferous faulting and basin formation succeeded Late Devonian folding of ORS sediments (Harland et al., 1984; Braathen et al., 1995). On East Greenland, a recently identified major Early Carboniferous unconformity (pre-336 Ma) in a formerly 'Devonian' basin (Hartz et al., 1997), attests to a tectonically induced erosional (or non-depositional) episode in the area. A major sedimentary hiatus of latest Devonian-early Carboniferous age has also been described for the northern Siberian platform (Nishikin et al., 1996). Events of similar age in southern and western Norway should thus not be unexpected,

but were not recognized previously simply because of the lack of rocks younger than Middle Devonian in the area. The only tools with by which to 'see' events of this age are those like feldspar thermochronology which can document younger, cooler thermal histories and radiometric dating to obtain absolute ages on young, brittle fault motions.

Various postulates for the tectonic regime responsible for this Late Devonian-Early Carboniferous folding, faulting, magmatism and/or erosion have been suggested: e.g., a system incorporating shear along major NE-trending faults (Great Glen, Møre-Trøndelag, e.g.); back-arc extension related to subduction of Rheic Ocean as the European Massifs and Gondwana moved progressively north to collide with Euramerica; docking of Siberia from the East. At this time, we lack strong evidence to support one or several of these activities, and it may be that one tectonic event alone cannot account for the apparently widespread, late Devonian-early Carboniferous activity in the North Atlantic region.

5.8. OFFSHORE IMPLICATIONS

The regional importance of the *lack of* Carboniferous and younger rocks on the eastern side of the North Atlantic has, until now, been severely minimized. These new Ar data have implications for late Paleozoic unroofing/erosion of rocks overlying western Norway and Devonian folding. Calculations for the amount and timing of North Sea extension are also necessarily affected. Unroofing of continental western Norway could provide some of the northerly clastic source areas demanded by paleocurrent constraints in Mid-Late Carboniferous sedimentary basins in and around the United Kingdom.

5.9. REFERENCES

Andersen, T. B. & Jamtveit, B. (1990) Uplift of deep crust during orogenic extensional collapse: A model based on field studies in the Sogn-Sunnfjord region of Western Norway. *Tectonics* 9, 1097-1111.

Andersen T. B., Jamtveit B., Dewey J. F., & Swensson E. (1991) Subduction and eduction of continental crust; major mechanisms during continent-continent collision and orogenic extensional collapse. *Terra Nova* **3**: 303-310.

Andersen T. B., Osmundsen P-T. & Jolivet L. (1994) Deep crustal fabrics and a model for the extensional collapse of the southwest Norwegian Caledonides. *J. Struct. Geol.* **16**: 1191-1203.

Andersen, T.B., Berry IV, H.N., Lux, D.R. & Andresen, A. (1998) The tectonic significance of pre-Scandian $^{40}Ar/^{39}Ar$ phengite cooling ages in the Caledonides of Western Norway. *J. Geol. Soc. London* 155, 297-310.

Arnaud, N.O. & Kelley, S.P. (1997) Argon behaviour in gem-quality orthoclase from Madagascar: Experiments and some consequences for $^{40}Ar/^{39}Ar$ geochronology. *Geochim. Cosmochim. Acta* 61, 3227-3255.

Arnaud, N.O., Brunel, M., Cantagrel, J.M. & Tapponier, P. (1993) High cooling and denudation rates at Kongur Shan, eastern Pamir (Xinjiang, China) revealed by $^{40}Ar/^{39}Ar$ alkali feldspar thermochronology. *Tectonics* 12, 1335-1346.

Brekke., H. & Solberg, P. O. (1987) The geology of Atløy, Sunnfjord, western Norway. Norsk Geol. Unders. Bull. 410: 73-94.

Braathen A., Bergh, S.G. & Maher, H.D., Jr. (1995) Structural outline of a Tertiary Basement-cored uplift/inversion structure in western Spitsbergen: Kinematics and controlling factors. *Tectonics* 14, 95-119.

Bøe, R. & Bjerkli, K. (1989) Mesozoic sedimentary rocks in Edøyfjorden and Beitstadfjorden, central Norway: implications for the structural history of the Møre-Trøndelag fault zone. *Marine Geol.* 87, 287-299.

Chauvet, A. & Séranne, M. (1994) Extension-parallel folding in the Scandinavian Caledonides: implications for late-orogenic processes. *Tectonophys.* 238, 31-54.

Coward, M.P. (1993) The effect of Late Caledonian and Variscan continental escape tectonics on basement structure, Paleozoic basin kinematics and subsequent Mesozoic basin

development in NW Europe. In: (Parker, J.R., ed.) *Petroleum Geology of Northwest Europe: Proceedings of the 4th Conference.* The Geological Society, London, pp. 1095-1108.

Cuthbert, S.J. (1985) *Petrology and tectonic setting of relatively low temperature eclogites and related rocks in the Dalsfjord area, Sunnfjord, west Norway.* Ph. D. University of Sheffield.

_____ (1991) Evolution of the Devonian Hornelen Basin, western Norway: new constraints from petrological styudies of metamorphic clasts. In: (Morton, A.C., Todd, S.P. & Haughton, P.D.W., eds.) *Developments in sedimentary provenance studies.* Geol. Soc. London Sp. Pub. 57, 343-360.

Cuthbert, S.J. & Carswell, D.A. (1990) Formation and exhumation of medium-temperature eclogites in the Scandinavian Caledonides. In: (Carswell, D.A., ed.), *Eclogite facies rocks.* Blackie & Son Ltd, 180-203.

Dewey, J.F., Ryan, P.D. & Andersen, T.B. (1993) Orogenic uplift and collapse, crustal thickness, fabrics and metamorphic phase changes: the role of eclogites. In: Alabaster, H.M., Harris, N.B.W. & Neary, C.R. (eds) *Magmatic processes and plate tectonics*, Geol. Soc. London, Sp. Pub. 76, 325-343.

Eide, E.A. and Torsvik, T.H. (1996) Palaeozoic supercontinental assembly, mantle flushing, and genesis of the Kiaman Superchron. *Earth Plan. Sci. Lett.*, 144, 389-402.

Eide, E.A., Torsvik T.H. & Andersen, T.B. (1997) Absolute dating of brittle fault movements: Late Permian and late Jurassic extensional fault breccias in western Norway. *Terra Nova*, 9, 135-139.

Engvik, A., Austrheim, H. & Andersen, T.B. (in prep.) Eclogitization and amphibolitization of Precambrian rocks from the south side of Dalsfjorden, Sunnfjord, SW Norway.

Foland, K.A. (1974) ^{40}Ar diffusion in homogeneous orthoclase and an interpretation of Ar diffusio nin K-feldspar. *Geochim. Cosmochim. Acta* 38, 151-166.

Foland, K.A. & Xu, Y. (1990) Diffusion of ^{40}Ar and ^{39}Ar in irradiated orthoclase. *Geochim. Cosmochim. Acta* 54, 3147-3158.

Gromet, L.P. & Andersen, T.B. (1994) Eclogite inclusions in granite gneisses: preservation of Precambrian intrusive relations in the eclogitized crust of Sunnfjord, SW Norway (abs.). Geol. Soc. Am. Abs. Progs.

Harrison, T.M., Lovera, O.M. & Heizler, M.T. (1991) ^{40}Ar/^{39}Ar results for alkali feldspars containing diffusion domains with differing activation energy. *Geochim. Cosmochim. Acta* 55, 1435-1448.

Hartz, E.H. (1998*) Late orogenic evolution of the East Greenland and Scandinavian Caledonides.* Unpubl. Ph.D. dissertation, University of Oslo, Norway. 161 pp.

Hartz, E.H. & Andresen, A. (1997) From collision to collapse: Complex strain permutations in the hinterland of the Scandinavian Caledonides. *J. Geophy. Res.* 102, 24,697-24,711.

Hartz, E.H., Torsvik, T.H. & Andresen, A. (1997) Carboniferous age for the East Greenland 'Devonian' basin: Paleomagnetic and isotopic constraints on age, stratigraphy, and plate reconstructions. *Geology* 25, 675-678.

Haszeldine, R.S. (1984) Carboniferous North Atlantic palaeogeography: stratigraphic evidence for rifting, not megashear or subduction. *Geol. Mag.* 121, 443-463.

Hossack, J.R. (1984) The geometry of listric growth faults in the Devonian basins of Sunnfjord, W. Norway. *J. Geol. Soc. London* 141, 629-637.

Lovera, O.M. (1990) Computer programs to model ^{40}Ar/^{39}Ar diffusion data from multidomain samples. *Computers & Geosciences* 18, 789-813.

Lovera, O.M., Richter, F.M. & Harrison, T.M. (1989) The $^{40}Ar/^{39}Ar$ thermochronometry for slowly cooled samples having a distribution of diffusion domain sizes. *J. Geoph. Res.* 94, 17,917-17,935.

Lovera, O.M., Richter, F.M. & Harrison, T.M. (1991) Diffusion domains determined by ^{39}Ar released during step heating. *J. Geoph. Res.* 96, 2057-2069.

Løvlie, R. (1981) Palaeomagnetism of coast-parallel dykes from western Norway; ages of magmatism and evidence for crustal uplift and collapse. *Geophys. J. R. astr. Soc.* 66, 417-426.

Løvlie, R. & Mitchell, J.G. (1982) Complete remagnetization of some Permian dykes from western Norway induced during burial/uplift. *Phys. Earth Plan. Int.* 30, 415-421.

Macintyre, R.M. & Færseth, R.B. (1982) Comments on æPalaeomagnetism of coasat-parallel alkaline dykes from western Norway; ages of magmatism and evidence for crustal uplift and collapse' by R. Løvlie. *Geophys. J. R. astr. Soc.* 70, 539-542.

McDougall, I. & Harrison, T.M. (1988) Geochronology and Thermochronology by the $^{40}Ar/^{39}Ar$ Method. New York, Oxford University Press. 215 p.

Nikishin, A.M., Ziegler, P.A., Stephenson, R.A., Cloetingh, S.A.P.L., Furne, A.V., Fokin, P.A., Ershov, A.V., Bolotov, S.N., Korotaev, M.V., Alekseev, A.S., Gorbachev, V.I., Shipolov, E.V., Lankreijer, A., Bembinova, E.Yu & Shalimov, I.V. (1996) Late Precambrian to Triassic history of the East European Craton: dynamics of sedimentary basin evolution. *Tectonophys.* 268, 23-63.

Osmundsen, P-T. (1996) *Late-orogenic structural geology and Devonian basin formation in Western Norway: A study from the hanging wall of the Nordfjord-Sogn Detachment in the Sunnfjord Region.* Unpubl. Ph.D. dissertation, University of Oslo, Norway. 168 p.

Osmundsen, P.T. and Andersen, T.B. (1994) Caledonian compressional and late-orogenic extensional deformation in the Staveneset area, Sunnfjord, Western Norway, *J. Struct. Geol.* 10, 1385-1401.

Roberts, D. (1983) Devonian tectonic deformation in the Norwegian Caledonides and its regional perspectives. *Nor. Geol. U. Bull,* 380, 85-96.

Roddick, J.C., Cliff, R.A. & Rex, D.C. (1980) The evolution of excess argon in Alpine biotites—A $^{40}Ar/^{39}Ar$ analysis. Earth Plaet. Sci. Lett. 48, 185-208.

Rohrman, M., van der Beek, P. & Andriessen, P. (1994) Syn-rift thermal structure and post-rift evolution of the Oslo Rift (southeast Norway):New constraints from fission track thermochronology. *Earth Planet. Sci. Lett.* 127, 39-54.

Steel, R.J. & Worsley, D. (1984) Svalbard's post-Caledonian strata—an atlas of sedimentational patterns and paleogeographic evolution. *Petrol. Geol. of Northwest European Margin.* Graham & Trotman, London. pp. 109-135.

Sundvoll, B. and Larsen, B.T. (1994) Architecture and early evolution of the Oslo Rift. *Tectonophys.* **240**, 173-189.

Torsvik T H, Sturt B A, Ramsay D M, Kisch H J & Bering D (1986) The tectonic implications of Solundian (Upper Devonian) magnetization of the Devonian rocks of Kvamshesten, western Norway. *Earth Plan. Sci. Lett.* 80, 337-347.

Torsvik, T.H., Sturt, B.A., Swensson, E., Andersen, T.B. and Dewey, J.F., 1992. Palaeomagnetic dating of fault rocks: evidence for Permian and Mesozoic movements and brittle deformation along the extensional Dalsfjord Fault, western Norway. *Geophys. J. Int.*, 109, 565-580.

Torsvik, T.H., Andersen, T.B., Eide, E.A. & Walderhaug, H. (1997) The age and tectonic significance of dolerite dykes in western Norway. *J. Geol. Soc. Lond.* 154, 961-973.

Villa, I. (1994) Multipath Ar transport in K-feldspar deduced from isothermal heating experiments. *Earth Plan. Sci. Lett.* 122, 393-401.

Ziegler P. A. (1990) Geological Atlas of Western and Central Europe. *Shell Internationale Petroleum Maatschappij B.V.* 239 pp.

5.10. CAPTIONS

Figure 1. Regional and local geology map for western Norway study area. (a) Study area relative to the Western Gneiss Region (WGR) onshore and basement lineaments offshore, including project study area (Viking '93). Major faults are shown in thick black lines. Gray zones onshore denote areas with Late Paleozoic and Mesozoic dikes. (b) Sample localities (black dots) cross a tectonostratigraphic profile through the Nordfjord-Sogn Detachment Zone (NSDZ). Key to patterns in Figure 2. Patterns and shaded units to west of NSDZ are allochthonous while light gray to the East denotes basement.

Figure 2. Tectonostratigraphic section through the NSDZ as in Figure 1b. Modified after Osmundsen & Andersen (1994). All 40Ar/39Ar samples derive from profile through the NSDZ. Age spectra contain corresponding mineral and sample number. Note that some samples (AS2 and AS6) yielded both mica and feldspar sample ages. High errors on some of the high temperature steps in the feldspar spectra are due to high, high-temperature blanks since some analyses were done very shortly after reloading the furnace. See text for details.

Figure 3. Inverse isochron diagrams for the biotite and amphibole samples from the WGR basement, corresponding to respective age spectra in Fig. 2 (lower right corner). (a) Biotite from pegmatite filling a small shear zone yields a relatively poorly correlated fit of the data to a line with an (impossible) intercept less than atmospheric value when all data are included. Utilizing only those data comprising the plateau age (Figure 2), yields an upper intercept of nearly atmospheric value, but a worse correlation of the data to the line. The ordinate intercept of 394 ± 8 Ma is within uncertainty of the plateau age of 395 ± 7 Ma. The isochrons and consistency of the K/Ca and Cl/K ratios do not lead us to think this sample contains excess Ar. (b) Amphibole from a monomineralic vein filling an eclogite shows two clear data distributions. One distribution (white boxes) comprises a low-temperature series of excess Ar components, while the remaining higher temperature steps (where amphiboles normally degas during step-heating) define a mixing line between an atmospheric component of Ar and a radiogenic component with an age of 398 ± 10 Ma.

Figure 4. Age spectra and modeling results for alkali feldspars from the Detachment profile. Upper diagram in each figure (a-e) comprises the laboratory spectrum (duplicated from Figure

2) and the corresponding 'best-fit' modeled spectrum (dotted line). The lower diagram in each figure comprises the laboratory $\log(r/r_o)$ vs. ^{39}Ar cumulative plot for each sample and the corresponding $\log(r/r_o)$ curve generated through the diffusion and thermal modeling runs. Number of diffusion domains used in the modeling is also indicated for each sample. We note that the upper portions of the experiments were very difficult to model due to the breakdown of the feldspar structure (melting) above furnace temperatures of 1100°C. We thus focused on model fits to the lower-temperature sections of the spectra. See text for details.

Figure 5. Cooling curves generated by data derived from modeling in Figure 4 and displayed in Table 3. Color-coding in upper left corner of the graph is a schematic representation of the tectonostratigraphic levels with corresponding feldspar sample cooling curves plotted. We note the 'starting' points in the runs (control from white mica ages from three of the same rocks where we also analyzed feldspars). The upper temperature, older domains are best modeled via slow cooling (0.5-2.2°C/m.y.) from the time of blocking of white micas below ca. 400oC. All feldspars subsequently exhibit the same, very dramatic break in slope, albeit at slightly different times, that corresponds to very rapid cooling of the feldspars (at rates of 15-50°C/m.y.). The rapid cooling episodes are followed by another period of slow cooling (0.4-1.7°C/m.y.) and/or partial Ar-loss until the rocks reached surface levels. Close inspection of the age differences at the onset of the rapid cooling (vertical portions of the curves) reveals that the two 'oldest' rapid cooling episodes (pink and blue curves) correspond to the uppermost (Høyvik Group) and lowermost (basement) feldspar samples in the profile. Investigation of the map locations of these samples in Figure 1b shows that they are very far from the NSDZ. The 'youngest' rapid cooling onset corresponds to the feldspar sampled within the detachment mylonite, and very close to brittle faults with known ages of activity in the Late Permian and Late Jurassic (see Eide et al., 1997). We thus interpret these apparent differences in age of onset of the rapid cooling event to represent instead different degrees of post-cooling resetting in Late Permian and/or Mesozoic times as the Detachment was alternately reactivated. The samples farthest from the detachment (BA3, blue, and AS2, pink) were not reset and thus represent most accurately the timing of onset of the rapid cooling episode (i.e. between 340 and 360 Ma).

Such consistency in modeling results from feldspars representing different tectonostratigraphic levels and rock types supports strongly the cooling rates defined by the curves. The onset of rapid cooling in the Early Carboniferous in western Norway is contemporaneous with other faulting episodes and unconformities around the North Atlantic margin. The cause for rapid cooling in western Norway is attributed to topographic/erosive response to a thermal pulse/underplating beneath Baltica in latest Devonian time.

Table 5.1. $^{40}Ar/^{39}Ar$ data from white micas, biotite and amphibole, western Norway

Phengite, AS2b, Upper Plate; J = 0.0067644; wt. = 1.2 mg

Temp °C	$^{40}Ar/^{39}Ar$	$^{38}Ar/^{39}Ar$	$^{37}Ar/^{39}Ar$	$^{36}Ar/^{39}Ar$ (10^{-3})	^{39}Ar (10^{-14}moles)	$F^{39}Ar$ released	$\%^{40}Ar^*$	$^{40}Ar^*/^{39}Ar$	Age (Ma)	± 1σ
700	34.615	0.086	0.074	9.222	0.25	3.28	91.68	31.86	352.09	5.71
800	39.514	0.028	0.011	2.643	0.24	6.43	97.64	38.72	419.72	5.44
850	40.908	0.021	0.002	1.769	0.68	15.31	98.58	40.38	435.64	6.58
900	41.690	0.021	0.000	0.906	1.69	37.53	99.30	41.42	445.59	6.63
950	42.098	0.021	0.000	0.626	1.80	61.18	99.51	41.91	450.27	6.44
1000	42.014	0.021	0.001	0.531	2.39	92.62	99.58	41.85	449.75	6.34
1100	43.529	0.022	0.019	2.934	0.44	98.39	97.79	42.65	457.32	6.59
1200	61.280	0.025	0.224	53.771	0.06	99.14	72.90	45.19	481.15	8.64
1400	141.747	0.095	0.057	378.955	0.07	100.00	19.71	28.07	313.63	33.27

Phengite, AS6b, Upper Plate; J = 0.0067000; wt. = 2.8 mg

Temp °C	$^{40}Ar/^{39}Ar$	$^{38}Ar/^{39}Ar$	$^{37}Ar/^{39}Ar$	$^{36}Ar/^{39}Ar$ (10^{-3})	^{39}Ar (10^{-14}moles)	$F^{39}Ar$ released	$\%^{40}Ar^*$	$^{40}Ar^*/^{39}Ar$	Age (Ma)	± 1σ
700	36.500	0.027	0.046	3.991	0.29	2.61	93.66	35.35	383.48	6.51
800	38.489	0.023	0.010	1.371	0.16	4.06	92.82	38.09	410.09	7.67
850	39.467	0.023	0.006	1.902	0.53	8.88	96.61	38.92	418.00	6.79
900	39.802	0.023	0.003	1.480	2.37	30.45	98.45	39.37	422.37	6.15
950	39.602	0.023	0.003	0.711	4.09	67.74	99.19	39.40	422.60	5.91
1000	39.265	0.023	0.028	0.502	2.99	94.97	99.21	39.12	419.99	5.99
1050	39.497	0.023	0.105	1.650	0.42	98.80	95.74	39.04	419.14	6.18
1100	42.646	0.027	0.667	15.165	0.07	99.46	76.18	38.35	412.57	7.30
1200	63.043	0.042	1.299	111.249	0.03	99.77	38.11	30.97	340.18	12.69
1400	415.680	0.285	0.592	1394.640	0.03	100.00	2.55	11.31	131.77	106.46

Phengite, BA1, Lower Plate; J = 0.0188300; wt. = 9.45 mg

Temp °C	$^{40}Ar/^{39}Ar$	$^{38}Ar/^{39}Ar$	$^{37}Ar/^{39}Ar$	$^{36}Ar/^{39}Ar$ (10^{-3})	^{39}Ar (10^{-14}moles)	$F^{39}Ar$ released	$\%^{40}Ar^*$	$^{40}Ar^*/^{39}Ar$	Age (Ma)	± 1σ
600	13.603	0.022	0.008	9.208	0.14	0.13	80.10	10.90	336.69	7.92
650	14.320	0.020	0.003	4.407	0.33	0.43	90.82	13.00	395.16	8.10
700	14.749	0.019	0.001	2.873	0.45	0.84	94.10	13.88	418.86	8.31
750	14.749	0.019	0.002	2.450	0.41	1.22	94.93	14.00	422.17	8.52
800	14.802	0.018	0.002	2.080	0.42	1.61	95.67	14.16	426.45	8.59
850	15.512	0.019	0.001	2.597	2.44	3.84	94.90	14.72	441.41	8.76
900	16.046	0.018	0.000	0.824	12.98	15.74	98.28	15.77	469.09	11.30
950	15.677	0.018	0.000	0.357	30.64	43.82	99.10	15.54	462.94	9.47
1000	15.218	0.018	0.001	0.267	26.31	67.93	99.25	15.10	451.55	9.54
1050	15.158	0.018	0.001	0.276	18.10	84.51	99.23	15.04	449.88	10.44
1100	15.255	0.018	0.003	0.101	12.74	96.18	99.56	15.19	453.80	9.55
1150	15.770	0.018	0.002	0.000	2.89	98.83	99.76	15.73	468.11	10.14
1200	16.242	0.016	0.005	0.000	0.84	99.60	99.77	16.21	480.46	9.65
1400	28.083	0.024	0.001	39.996	0.44	100.00	58.57	16.45	486.73	17.88

Table 1. cont'd.

Biotite, T97, Lower Plate; J = 0.0188300; wt. = 2.93 mg

Temp °C	$^{40}Ar/^{39}Ar$	$^{38}Ar/^{39}Ar$	$^{37}Ar/^{39}Ar$	$^{36}Ar/^{39}Ar$ (10^{-3})	^{39}Ar (10^{-14}moles)	$F^{39}Ar$ released	$\%^{40}Ar^*$	$^{40}Ar^*/^{39}Ar$	Age (Ma)	± 1σ
600	39.690	0.039	0.011	111.962	0.14	0.52	18.10	7.18	228.92	5.68
650	21.224	0.025	0.008	34.080	0.75	3.20	53.26	11.30	348.17	9.10
700	15.712	0.020	0.005	11.441	1.36	8.09	78.65	12.36	377.41	8.22
750	14.367	0.019	0.004	5.915	1.13	12.15	87.80	12.61	384.48	8.19
800	13.809	0.019	0.003	3.327	1.36	17.03	92.75	12.81	389.78	7.96
850	13.391	0.018	0.002	0.907	4.74	34.06	97.76	13.09	397.53	8.46
900	13.293	0.018	0.002	0.797	4.02	48.51	97.98	13.03	395.72	8.18
950	13.678	0.019	0.005	1.742	2.53	57.60	96.04	13.14	398.75	10.62
1000	12.703	0.018	0.004	1.482	2.41	66.26	96.33	12.24	374.07	7.85
1100	12.931	0.018	0.002	0.713	7.28	92.41	98.11	12.69	386.46	7.96
1200	13.534	0.018	0.002	0.086	1.99	99.56	99.54	13.47	407.86	9.13
1400	63.975	0.048	0.000	179.281	0.12	100.00	18.67	11.95	366.04	64.78

Amphibole, 4000.011, Lower Plate; J = 0.0188300; wt. = 14.91 mg

Temp °C	$^{40}Ar/^{39}Ar$	$^{38}Ar/^{39}Ar$	$^{37}Ar/^{39}Ar$	$^{36}Ar/^{39}Ar$ (10^{-3})	^{39}Ar (10^{-14}moles)	$F^{39}Ar$ released	$\%^{40}Ar^*$	$^{40}Ar^*/^{39}Ar$	Age (Ma)	± 1σ
600	42.529	0.062	4.285	45.448	0.02	0.32	69.94	29.94	806.59	21.38
700	39.577	0.049	2.369	24.606	0.03	0.84	82.48	32.76	866.87	21.38
750	23.511	0.033	1.493	17.025	0.01	1.11	79.49	18.73	545.01	25.77
800	22.153	0.028	1.724	16.538	0.01	1.31	78.97	17.54	514.86	31.41
850	23.854	0.030	2.130	20.793	0.04	2.10	75.47	18.06	528.11	13.06
900	17.338	0.035	3.156	17.123	0.06	3.29	72.99	12.72	387.26	12.26
950	15.464	0.044	6.047	8.924	0.14	6.10	86.99	13.58	410.68	9.74
1000	13.954	0.034	10.007	5.442	0.56	17.52	95.69	13.56	410.18	9.06
1050	12.542	0.024	10.407	3.555	1.37	45.30	99.90	12.73	387.60	8.60
1100	12.646	0.021	9.497	3.140	1.43	74.31	100	12.84	390.79	8.83
1150	13.812	0.022	10.663	3.155	0.90	92.63	100	14.17	426.65	9.56
1200	13.948	0.022	10.925	3.564	0.28	98.41	100	14.22	427.99	13.31
1400	80.074	0.066	11.461	238.135	0.08	100.00	15.16	12.35	377.27	73.21

Prior to irradiation the mineral fractions were packed in Sn-foil and irradiated at the Siloé reactor of Commissariat à l'Energie Atomique in Grenoble, France. Monitor minerals (one at the top and one at the base of the quartz vial) were the Fish Canyon Tuff feldspar (27.4 Ma) and the Caplongue hornblende (344.5 ± 0.5 Ma). Irradiation parameters (flux, salts, and shielding) were calculated after Arnaud et al. (1993). In addition to the double vacuum resistance heating furnace (for feldspar analyses, Table 5.2), we used a radio frequency furnace for white mica, biotite and amphibole analyses. The latter furnace has regular temperature calibration by means of an optical pyrometer correlated to precise furnace power output. Temperatures for both furnaces are known at ±10°C for each step with 25 minute step duration and 5 minutes gettering for all micas and amphibole.

Table 5.2. K-feldspar Ar-release and diffusion data.
K-feldspar AS2A, Upper Plate; J = 0.0068510; wt. = 4 mg

Temp °C	$^{40}Ar/^{39}Ar$	$^{38}Ar/^{39}Ar$	$^{37}Ar/^{39}Ar$	$^{36}Ar/^{39}Ar$ (10^{-3})	^{39}Ar (10^{-14} moles)	$F^{39}Ar$ cumulative	$\%^{40}Ar^*$	$^{40}Ar^*/^{39}Ar$	Age (Ma)	± 1σ
402	519.255	0.388	0.000	1825.169	0.01	0.11	-1.94	-10.08	0.00	0.00
403	83.950	0.078	0.000	266.860	0.03	0.37	7.77	6.52	78.88	11.97
449	29.366	0.033	0.000	49.915	0.06	0.93	50.58	14.85	174.83	7.04
449	29.378	0.030	0.000	30.557	0.05	1.43	69.71	20.48	236.87	8.32
508	29.183	0.025	0.000	17.759	0.12	2.54	82.23	24.00	274.59	6.27
504	36.183	0.030	0.000	34.212	0.09	3.40	72.48	26.22	298.08	6.80
563	31.948	0.025	0.026	12.351	0.17	5.05	88.68	28.33	320.05	6.91
563	32.112	0.024	0.000	9.998	0.12	6.24	90.85	29.18	328.74	7.38
614	32.020	0.024	0.146	8.017	0.19	8.04	92.67	29.68	333.92	7.44
614	33.051	0.025	0.000	9.018	0.15	9.51	91.97	30.40	341.30	7.41
664	31.610	0.023	0.352	4.872	0.18	11.21	95.53	30.21	339.38	7.15
664	32.044	0.024	0.000	2.573	0.12	12.35	97.55	31.26	350.09	7.80
706	32.636	0.024	0.000	5.481	0.12	13.50	95.02	31.01	347.54	7.20
706	30.828	0.024	0.862	2.169	0.09	14.34	98.12	30.29	340.17	7.98
757	31.884	0.024	0.981	3.069	0.10	15.27	97.40	31.10	348.48	7.28
757	32.612	0.027	0.836	6.204	0.07	15.96	94.63	30.90	346.42	8.66
802	31.838	0.024	0.736	3.809	0.09	16.77	96.65	30.80	345.45	7.67
802	30.413	0.024	1.311	3.550	0.08	17.55	96.93	29.54	332.47	8.27
801	32.128	0.025	0.000	2.846	0.07	18.19	97.32	31.27	350.15	10.34
802	34.724	0.030	0.830	5.554	0.14	19.52	95.50	33.20	369.74	12.97
698	116.081	0.053	0.000	0.000	0.00	19.53	99.97	116.04	1055.4	166.38
754	41.913	0.025	0.000	0.000	0.01	19.58	99.91	41.88	455.04	25.98
801	33.410	0.027	0.075	0.073	0.03	19.84	99.85	33.36	371.37	15.19
857	34.976	0.026	0.518	0.000	0.08	20.64	100.04	35.02	387.95	7.52
907	34.778	0.027	0.262	0.995	0.16	22.21	99.14	34.49	382.70	8.50
953	35.416	0.026	0.000	1.161	0.28	24.88	98.94	35.04	388.18	8.12
1001	37.429	0.027	0.000	1.974	0.46	29.23	98.37	36.82	405.81	8.26
1050	37.840	0.027	0.137	1.955	0.79	36.81	98.44	37.26	410.13	8.27
1105	39.140	0.027	0.119	2.000	1.27	48.93	98.45	38.54	422.73	8.75
1150	38.744	0.026	0.092	2.485	1.89	66.98	98.07	38.00	417.44	8.50
1201	39.372	0.026	0.127	2.596	2.42	90.11	98.03	38.60	423.32	8.72
1401	45.251	0.030	0.282	24.675	1.03	100.00	84.17	38.10	418.43	9.01

Temp	Time	f	D/r^2	1000/T	$-\log(D/r^2)$	$\log(r/r_o)$
402	25	0.11	6.08E-10	1.481	9.216	0.301
403	25	0.37	6.75E-09	1.479	8.170	-0.210
449	25	0.93	3.83E-08	1.385	7.416	-0.058
449	30	1.43	5.14E-08	1.385	7.289	-0.122
508	20	2.54	2.90E-07	1.280	6.538	0.089
504	30	3.40	2.21E-07	1.287	6.656	0.111
563	20	5.05	9.15E-07	1.196	6.039	0.311
563	30	6.24	5.86E-07	1.196	6.232	0.408
614	20	8.04	1.68E-06	1.127	5.775	0.565
614	30	9.51	1.13E-06	1.127	5.948	0.651
664	20	11.21	2.30E-06	1.067	5.638	0.833
664	30	12.35	1.18E-06	1.067	5.929	0.979
706	20	13.50	1.93E-06	1.021	5.713	1.128
706	30	14.34	1.03E-06	1.021	5.989	1.266
757	20	15.27	1.79E-06	0.971	5.748	1.428
757	30	15.96	9.44E-07	0.971	6.025	1.567
802	20	16.77	1.75E-06	0.930	5.758	1.661
802	30	17.55	1.16E-06	0.930	5.937	1.751
801	40	18.19	7.48E-07	0.931	6.126	1.840
802	120	19.52	5.48E-07	0.930	6.261	1.913
698	30	19.53	1.29E-08	1.030	7.889	2.168
754	30	19.58	9.36E-08	0.974	7.029	2.053
801	30	19.84	4.42E-07	0.931	6.354	1.955
857	30	20.64	1.41E-06	0.885	5.851	1.961
907	30	22.21	2.94E-06	0.847	5.532	2.012
953	30	24.88	5.49E-06	0.816	5.261	2.055
1001	30	29.23	1.03E-05	0.785	4.988	2.091
1050	30	36.81	2.18E-05	0.756	4.661	2.090
1105	30	48.93	4.53E-05	0.726	4.344	2.100
1150	25	66.98	1.17E-04	0.703	3.931	2.023
1201	30	90.11	2.72E-04	0.678	3.566	1.977

K-feldspar, AS1, Upper Plate; J = 0.0068510, wt. = 4 mg

Temp °C	$^{40}Ar/^{39}Ar$	$^{38}Ar/^{39}Ar$	$^{37}Ar/^{39}Ar$	$^{36}Ar/^{39}Ar$ (10^{-3})	^{39}Ar (moles 10^{-14})	$F^{39}Ar$ cumulative	$\%^{40}Ar^*$	$^{40}Ar^*/^{39}Ar$	Age (Ma)	± 1σ
400	18.094	0.050	0.002	33.082	0.06	0.19	46.77	8.46	101.68	4.09
400	17.351	0.031	0.000	10.803	0.07	0.43	81.73	14.18	167.27	5.18
450	19.466	0.030	0.001	8.560	0.08	0.67	87.06	16.95	198.16	4.68
500	22.106	0.026	0.011	4.852	0.54	2.42	93.47	20.66	238.86	4.49
500	23.774	0.023	0.003	2.297	0.22	3.12	97.04	23.07	264.74	11.57
550	25.789	0.023	0.004	1.504	0.31	4.14	98.17	25.32	288.54	10.63
550	26.831	0.021	0.007	0.842	0.33	5.20	98.95	26.55	301.49	5.85
600	27.473	0.023	0.012	1.201	0.43	6.59	98.60	27.09	307.12	13.12
600	27.291	0.022	0.006	0.446	0.27	7.45	99.39	27.13	307.50	11.31
650	28.126	0.022	0.001	1.198	0.41	8.79	98.63	27.74	313.91	11.29
650	27.548	0.021	0.000	0.225	0.25	9.60	99.63	27.45	310.83	10.96
700	27.932	0.022	0.001	1.172	0.40	10.89	98.65	27.55	311.97	12.83
700	27.823	0.022	0.004	0.363	0.24	11.66	99.49	27.68	313.28	11.77
750	28.331	0.022	0.001	0.701	0.35	12.79	99.15	28.09	317.53	10.81
750	28.469	0.021	0.000	0.399	0.27	13.67	99.46	28.32	319.87	10.45
800	28.757	0.022	0.001	1.199	0.34	14.77	98.66	28.37	320.45	12.40
800	28.963	0.022	0.000	0.888	0.27	15.63	98.98	28.67	323.51	12.18
800	29.088	0.022	0.000	0.364	0.21	16.31	99.51	28.94	326.37	13.30
800	28.983	0.022	0.000	0.000	0.36	17.49	99.87	28.95	326.37	11.88
700	42.275	0.023	0.000	31.739	0.01	17.52	78.14	33.03	368.05	37.71
750	31.876	0.019	0.000	0.547	0.02	17.60	99.39	31.68	354.36	17.70
800	30.188	0.022	0.000	0.000	0.07	17.82	99.88	30.15	338.77	6.75
850	29.671	0.023	0.000	0.794	0.20	18.46	99.10	29.40	331.09	18.41
900	29.884	0.023	0.001	1.501	0.42	19.83	98.42	29.41	331.17	17.71
950	30.366	0.024	0.001	1.920	0.73	22.20	98.04	29.77	334.88	19.22
1000	31.322	0.025	0.001	2.272	1.36	26.59	97.78	30.63	343.62	20.05
1050	32.740	0.025	0.001	2.281	2.65	35.18	97.87	32.04	358.03	18.43
1150	35.842	0.027	0.001	2.613	5.15	51.86	97.78	35.05	388.23	32.54
1200	36.210	0.027	0.000	2.222	8.31	78.78	98.12	35.53	393.02	28.10
1400	36.750	0.027	0.000	2.298	6.55	100.00	98.09	36.05	398.16	30.32

Temp °C	Time (min)	f	D/r^2	1000/T (K^{-1})	$-\log(D/r^2)$	$\log(r/r_o)$
400	20	0.19	2.33E-09	1.486	8.633	0.106
400	30	0.43	6.46E-09	1.486	8.190	-0.116
450	20	0.67	1.76E-08	1.383	7.756	0.102
500	20	2.42	3.53E-07	1.294	6.452	-0.172
500	30	3.12	1.69E-07	1.294	6.771	-0.013
550	20	4.14	4.83E-07	1.215	6.316	0.092
550	30	5.20	4.33E-07	1.215	6.363	0.116
600	20	6.59	1.07E-06	1.145	5.971	0.214
600	30	7.45	5.30E-07	1.145	6.276	0.366
650	20	8.79	1.43E-06	1.083	5.846	0.414
650	30	9.60	6.49E-07	1.083	6.188	0.585
700	20	10.89	1.73E-06	1.028	5.762	0.607
700	30	11.66	7.55E-07	1.028	6.122	0.787
750	20	12.79	1.82E-06	0.978	5.741	0.809
750	30	13.67	1.01E-06	0.978	5.996	0.937
800	20	14.77	2.05E-06	0.932	5.689	0.976
800	30	15.63	1.15E-06	0.932	5.940	1.101
800	40	16.31	7.13E-07	0.932	6.147	1.205
800	120	17.49	4.32E-07	0.932	6.364	1.313
700	30	17.52	5.07E-08	1.028	7.295	1.373
750	30	17.60	1.20E-07	0.978	6.919	1.398
800	30	17.82	3.48E-07	0.932	6.459	1.360
850	30	18.46	1.00E-06	0.890	5.998	1.306
900	30	19.83	2.29E-06	0.853	5.640	1.287
950	30	22.20	4.34E-06	0.818	5.362	1.296
1000	30	26.59	9.36E-06	0.786	5.029	1.265
1050	30	35.18	2.31E-05	0.756	4.636	1.193
1150	30	51.86	6.34E-05	0.703	4.198	1.199
1200	30	78.78	1.84E-04	0.679	3.734	1.068

K-feldspar, AS3, J = 0.0068510, wt. = 4 mg

Temp °C	$^{40}Ar/^{39}Ar$	$^{38}Ar/^{39}Ar$	$^{37}Ar/^{39}Ar$	$^{36}Ar/^{39}Ar$ (10^{-3})	^{39}Ar (moles 10^{-14})	$F^{39}Ar$ cumulative	$\%^{40}Ar^*$	$^{40}Ar^*/^{39}Ar$	Age (Ma)	± 1σ
400	12.089	0.039	0.004	16.843	0.14	0.58	59.29	7.17	86.48	2.04
400	11.598	0.031	0.017	5.585	0.08	0.91	85.73	9.94	118.89	5.94
450	14.227	0.025	0.001	3.045	0.30	2.14	93.53	13.31	157.40	3.07
450	17.439	0.023	0.007	1.908	0.23	3.09	96.62	16.85	197.08	7.26
500	20.428	0.022	0.004	1.467	0.48	5.06	97.74	19.97	231.30	7.16
500	22.177	0.022	0.004	0.643	0.33	6.42	98.99	21.95	252.78	9.10
550	23.431	0.022	0.003	0.740	0.56	8.73	98.93	23.18	265.90	9.33
550	24.193	0.022	0.003	0.000	0.36	10.20	99.85	24.16	276.29	9.23
600	24.788	0.022	0.001	0.500	0.47	12.13	99.26	24.61	281.04	9.61
600	24.812	0.022	0.003	0.000	0.38	13.70	99.85	24.78	282.84	9.41
650	25.188	0.022	0.002	0.280	0.46	15.57	99.53	25.07	285.94	9.54
650	25.098	0.022	0.002	0.000	0.34	16.96	99.85	25.06	285.86	9.31
700	25.472	0.022	0.002	0.282	0.42	18.70	99.53	25.35	288.94	10.00
700	25.200	0.021	0.002	0.000	0.33	20.04	99.85	25.16	286.93	9.31
750	25.791	0.022	0.003	0.344	0.42	21.76	99.47	25.65	292.10	9.24
750	25.428	0.022	0.002	0.000	0.31	23.01	99.85	25.39	289.33	10.18
800	26.218	0.022	0.007	0.442	0.43	24.76	99.37	26.05	296.29	9.79
800	26.221	0.022	0.004	0.000	0.36	26.24	99.86	26.18	297.66	11.02
800	26.378	0.022	0.003	0.000	0.31	27.50	99.86	26.34	299.31	10.68
800	26.744	0.023	0.003	0.000	0.54	29.73	99.86	26.71	303.13	10.83
700	23.852	0.006	0.005	0.000	0.01	29.77	99.85	23.82	272.66	18.94
750	25.837	0.023	0.004	0.000	0.03	29.91	99.86	25.80	293.63	7.76
800	27.231	0.023	0.005	0.000	0.09	30.28	99.86	27.19	308.22	6.06
850	27.838	0.023	0.005	0.000	0.25	31.31	99.87	27.80	314.53	15.18
900	28.528	0.024	0.009	0.447	0.48	33.29	99.42	28.36	320.35	16.17
1000	33.400	0.027	0.007	1.612	1.27	38.50	98.49	32.90	366.67	20.04
1050	34.783	0.028	0.007	2.132	1.89	46.24	98.12	34.13	379.06	18.40
1100	35.382	0.029	0.005	2.323	2.93	58.28	97.99	34.67	384.49	25.33
1150	35.318	0.027	0.003	1.988	4.71	77.63	98.26	34.70	384.82	19.05
1200	35.323	0.027	0.002	1.740	5.45	100.00	98.47	34.78	385.58	30.77

Temp °C	Time (min)	f	D/r^2	1000/T (K^{-1})	$-\log(D/r^2)$	$\log(r/r_o)$
400	20	0.58	2.18E-08	1.486	7.661	0.014
400	30	0.91	2.14E-08	1.486	7.669	0.018
450	20	2.14	2.47E-07	1.383	6.608	-0.050
450	30	3.09	2.16E-07	1.383	6.666	-0.021
500	20	5.06	1.05E-06	1.294	5.977	0.038
500	30	6.42	6.81E-07	1.294	6.167	0.133
550	20	8.73	2.29E-06	1.215	5.640	0.223
550	30	10.20	1.21E-06	1.215	5.917	0.361
600	20	12.13	2.82E-06	1.145	5.549	0.491
600	30	13.70	1.77E-06	1.145	5.753	0.593
650	20	15.57	3.59E-06	1.083	5.445	0.718
650	30	16.96	1.98E-06	1.083	5.704	0.847
700	20	18.70	4.06E-06	1.028	5.392	0.942
700	30	20.04	2.26E-06	1.028	5.646	1.069
750	20	21.76	4.70E-06	0.978	5.328	1.137
750	30	23.01	2.45E-06	0.978	5.611	1.278
800	20	24.76	5.48E-06	0.932	5.261	1.308
800	30	26.24	3.29E-06	0.932	5.483	1.419
800	40	27.50	2.22E-06	0.932	5.654	1.504
800	120	29.73	1.39E-06	0.932	5.857	1.606
700	30	29.77	1.09E-07	1.028	6.963	1.728
750	30	29.91	3.54E-07	0.978	6.450	1.698
800	30	30.28	9.86E-07	0.932	6.006	1.681
850	30	31.31	2.75E-06	0.890	5.561	1.645
900	30	33.29	5.59E-06	0.853	5.253	1.662
1000	30	38.50	1.63E-05	0.786	4.787	1.730
1050	30	46.24	2.86E-05	0.756	4.543	1.742
1100	30	58.28	5.49E-05	0.728	4.260	1.725
1150	30	77.63	1.42E-04	0.703	3.849	1.634

K-feldspar, AS6A, mylonite; J = 0.0068510, wt = 4.3 mg

Temp °C	$^{40}Ar/^{39}Ar$	$^{38}Ar/^{39}Ar$	$^{37}Ar/^{39}Ar$	$^{36}Ar/^{39}Ar$ (10^{-3})	^{39}Ar (moles 10^{-14})	$F^{39}Ar$ cumulative	$\%^{40}Ar^*$	$^{40}Ar^*/^{39}Ar$	Age (Ma)	± 1σ
400	13.257	0.068	0.001	28.130	0.13	0.50	38.18	5.06	61.50	1.71
400	11.653	0.036	0.000	10.937	0.09	0.85	72.46	8.44	101.46	3.19
450	13.116	0.031	0.002	6.930	0.19	1.59	84.39	11.07	131.87	2.67
450	16.434	0.028	0.000	5.211	0.15	2.21	90.58	14.89	175.19	7.74
500	19.001	0.027	0.002	3.806	0.27	3.28	93.99	17.86	208.25	8.35
500	21.456	0.026	0.000	1.973	0.21	4.13	97.16	20.85	240.84	11.18
500	23.849	0.024	0.002	1.718	0.41	5.75	97.76	23.31	267.33	9.80
550	25.215	0.023	0.000	0.445	0.22	6.64	99.34	25.05	285.73	12.69
600	26.267	0.023	0.001	0.722	0.44	8.38	99.06	26.02	295.95	13.76
600	27.040	0.023	0.001	0.370	0.35	9.76	99.47	26.90	305.11	14.33
650	27.523	0.023	0.001	0.539	0.44	11.51	99.30	27.33	309.63	14.08
650	27.694	0.023	0.001	0.000	0.32	12.78	99.87	27.66	313.03	15.49
700	27.781	0.023	0.002	0.533	0.46	14.61	99.31	27.59	312.33	16.56
700	28.026	0.023	0.001	0.002	0.29	15.76	99.87	27.99	316.47	15.63
750	28.167	0.023	0.002	0.520	0.34	17.12	99.33	27.98	316.38	17.26
750	28.255	0.023	0.002	0.010	0.27	18.21	99.86	28.22	318.83	18.29
800	28.618	0.024	0.003	0.721	0.32	19.47	99.14	28.37	320.44	19.21
800	29.854	0.024	0.002	0.514	0.34	20.81	99.38	29.67	333.81	10.49
800	29.852	0.025	0.001	0.387	0.28	21.92	99.50	29.70	334.16	17.31
800	30.595	0.026	0.000	0.153	0.56	24.15	99.73	30.51	342.47	16.83
750	31.265	0.020	0.026	0.000	0.03	24.26	99.89	31.23	349.80	6.77
800	32.050	0.024	0.000	0.000	0.15	24.86	99.88	32.01	357.73	6.54
850	32.263	0.023	0.001	0.985	0.22	25.73	99.00	31.94	357.00	10.74
900	32.688	0.027	0.005	1.087	0.57	27.99	98.92	32.34	361.01	10.46
950	33.297	0.027	0.004	1.111	0.86	31.43	98.92	32.94	367.09	11.03
1000	34.466	0.029	0.003	1.164	1.19	36.16	98.91	34.09	378.68	11.76
1200	37.821	0.034	0.002	1.865	12.02	84.04	98.47	37.24	409.99	13.93
1400	39.896	0.032	0.000	2.953	4.01	100.00	97.76	39.00	427.23	8.33

Temp °C	Time (min)	f	D/r^2	1000/T (K^{-1})	$-\log(D/r^2)$	$\log(r/r_o)$
400	20	0.50	1.62E-08	1.486	7.789	0.035
400	30	0.85	2.06E-08	1.486	7.686	-0.016
450	20	1.59	1.19E-07	1.383	6.924	-0.037
450	30	2.21	1.02E-07	1.383	6.990	-0.004
500	20	3.28	3.83E-07	1.294	6.417	0.022
500	30	4.13	2.75E-07	1.294	6.560	0.094
500	20	5.75	1.05E-06	1.294	5.980	-0.196
550	30	6.64	4.81E-07	1.215	6.318	0.248
600	20	8.38	1.71E-06	1.145	5.768	0.217
600	30	9.76	1.10E-06	1.145	5.960	0.313
650	20	11.51	2.44E-06	1.083	5.613	0.356
650	30	12.78	1.34E-06	1.083	5.872	0.486
700	20	14.61	3.29E-06	1.028	5.483	0.486
700	30	15.76	1.51E-06	1.028	5.820	0.655
750	20	17.12	2.93E-06	0.978	5.534	0.688
750	30	18.21	1.69E-06	0.978	5.773	0.807
800	20	19.47	3.11E-06	0.932	5.507	0.834
800	30	20.81	2.36E-06	0.932	5.627	0.894
800	40	21.92	1.55E-06	0.932	5.810	0.985
800	120	24.15	1.12E-06	0.932	5.950	1.055
750	25	24.26	2.83E-07	0.978	6.548	1.195
800	45	24.86	8.58E-07	0.932	6.066	1.113
850	25	25.73	2.28E-06	0.890	5.641	1.046
900	25	27.99	6.38E-06	0.853	5.195	0.956
950	25	31.43	1.07E-05	0.818	4.971	0.966
1000	25	36.16	1.67E-05	0.786	4.777	0.981
1200	25	84.04	3.71E-04	0.679	3.431	0.682

K-feldspar, BA3, Lower Plate; J = 0.0188300, wt. = 7.65 mg

Temp °C	$^{40}Ar/^{39}Ar$	$^{38}Ar/^{39}Ar$	$^{37}Ar/^{39}Ar$	$^{36}Ar/^{39}Ar$ (10^{-3})	^{39}Ar (moles 10^{-14})	$F^{39}Ar$ cumulative	$\%^{40}Ar^*$	$^{40}Ar^*/^{39}Ar$	Age (Ma)	± 1σ
400	190.120	0.137	0.035	649.166	0.01	0.01	0.96	1.83	61.04	27.98
400	20.307	0.031	0.013	60.225	0.03	0.02	13.82	2.81	92.89	18.35
450	6.001	0.020	0.027	10.849	0.11	0.06	47.00	2.82	93.35	4.18
450	4.986	0.019	0.022	5.915	0.19	0.13	64.89	3.24	106.70	3.91
500	5.127	0.018	0.019	2.839	0.53	0.34	83.25	4.27	139.48	2.81
500	5.623	0.018	0.016	1.286	0.63	0.58	92.73	5.21	168.97	3.39
550	8.798	0.018	0.011	1.808	3.66	1.99	93.63	8.24	260.15	4.85
550	8.628	0.018	0.014	0.978	1.07	2.40	96.30	8.31	262.25	5.50
600	10.476	0.018	0.014	1.147	2.46	3.35	96.48	10.11	314.31	6.55
600	10.510	0.018	0.013	0.564	2.07	4.15	98.10	10.31	320.10	6.49
650	11.984	0.018	0.013	1.124	3.78	5.60	96.98	11.62	357.04	7.38
650	11.144	0.018	0.012	0.392	3.03	6.77	98.66	10.99	339.46	6.82
700	11.761	0.018	0.011	0.662	5.11	8.73	98.06	11.53	354.55	7.17
700	11.397	0.018	0.011	0.259	3.72	10.16	99.02	11.29	347.62	7.04
750	11.816	0.018	0.013	0.516	5.30	12.20	98.43	11.63	357.26	7.19
750	11.672	0.018	0.013	0.253	4.67	14.00	99.06	11.56	355.37	7.34
800	12.066	0.018	0.013	0.731	5.22	16.01	97.95	11.82	362.51	7.60
800	11.726	0.018	0.013	0.185	4.35	17.68	99.24	11.64	357.43	7.33
800	11.928	0.018	0.012	0.266	3.67	19.10	99.05	11.81	362.39	7.42
800	12.156	0.018	0.012	0.342	6.71	21.68	98.89	12.02	368.11	7.68
700	12.590	0.017	0.000	1.019	0.14	21.73	97.36	12.26	374.65	9.22
750	12.145	0.019	0.013	0.283	0.43	21.90	99.03	12.03	368.28	7.72
800	12.545	0.018	0.011	0.640	1.59	22.51	98.23	12.32	376.46	7.71
850	12.945	0.018	0.009	1.272	5.39	24.58	96.87	12.54	382.42	7.81
900	12.821	0.018	0.010	0.976	11.26	28.92	97.51	12.50	381.37	8.87
1000	13.517	0.018	0.010	0.947	27.05	39.33	97.70	13.21	400.65	8.81
1050	13.896	0.018	0.013	1.300	42.54	55.70	97.03	13.48	408.17	8.79
1100	14.924	0.018	0.011	1.074	36.87	69.89	97.67	14.58	437.56	9.53
1150	15.658	0.018	0.004	1.163	45.81	87.52	97.61	15.28	456.30	9.65
1200	15.195	0.018	0.002	0.871	28.85	98.62	98.09	14.90	446.28	9.79
1400	24.018	0.018	0.003	5.170	3.59	100.00	93.60	22.48	636.83	13.09

Temp °C	Time (min)	f	D/r^2	1000/T (K^{-1})	$-\log(D/r^2)$	$\log(r/r_o)$
400	20	0.01	2.04E-12	1.486	11.690	0.223
400	30	0.02	1.28E-11	1.486	10.893	-0.175
450	20	0.06	2.22E-10	1.383	9.653	0.059
450	30	0.13	6.17E-10	1.383	9.210	-0.163
500	20	0.34	6.36E-09	1.294	8.196	0.073
500	30	0.58	9.65E-09	1.294	8.015	-0.017
550	20	1.99	2.37E-07	1.215	6.625	-0.060
550	30	2.40	7.92E-08	1.215	7.101	0.178
600	20	3.35	3.57E-07	1.145	6.447	0.429
600	30	4.15	2.60E-07	1.145	6.585	0.498
650	20	5.60	9.28E-07	1.083	6.032	0.737
650	30	6.77	6.29E-07	1.083	6.201	0.822
700	20	8.73	1.99E-06	1.028	5.700	1.034
700	30	10.16	1.18E-06	1.028	5.928	1.147
750	20	12.20	2.99E-06	0.978	5.525	1.363
750	30	14.00	2.06E-06	0.978	5.687	1.444
800	20	16.01	3.94E-06	0.932	5.404	1.681
800	30	17.68	2.46E-06	0.932	5.609	1.783
800	40	19.10	1.70E-06	0.932	5.770	1.864
800	120	21.68	1.15E-06	0.932	5.940	1.949
700	30	21.73	1.02E-07	1.028	6.993	1.680
750	30	21.90	3.17E-07	0.978	6.500	1.850
800	30	22.51	1.18E-06	0.932	5.927	1.942
850	30	24.58	4.26E-06	0.890	5.371	2.009
900	30	28.92	1.01E-05	0.853	4.995	2.136
1000	30	39.33	3.10E-05	0.786	4.509	2.449
1050	30	55.70	6.79E-05	0.756	4.168	2.526
1100	30	69.89	8.76E-05	0.728	4.057	2.699
1150	30	87.52	1.98E-04	0.703	3.703	2.734
1200	30	98.62	4.96E-04	0.679	3.305	2.733

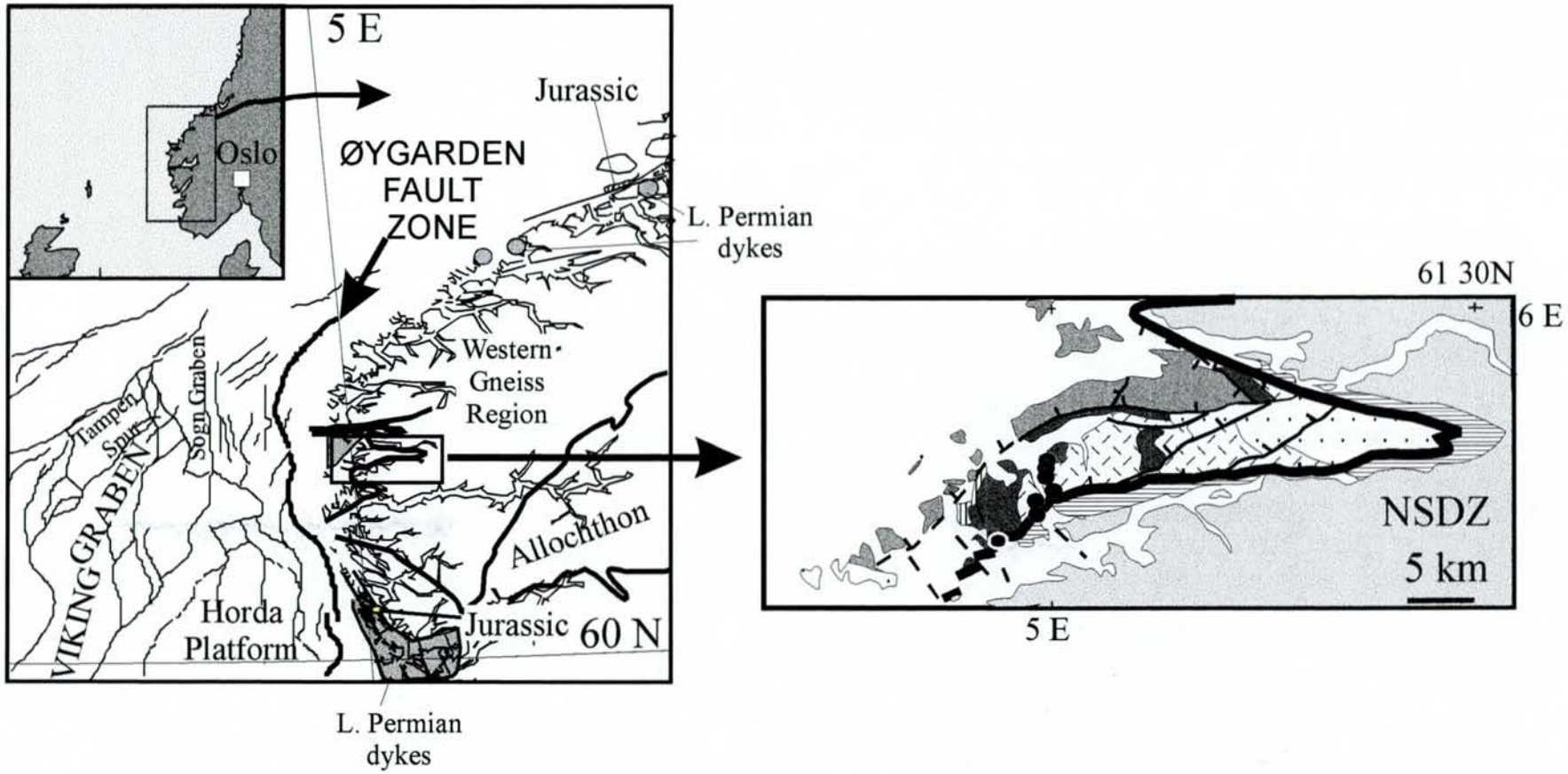
5 E
Jurassic
Oslo
ØYGARDEN
FAULT
ZONE
L. Permian
dykes
61 30N
6 E
Western
Gneiss
Region
Tampen
Spur
Sogn Graben
VIKING GRABEN
Allochthon
NSDZ
5 km
Horda
Platform
Jurassic
60 N
5 E
L. Permian
dykes

Figure 1a,b

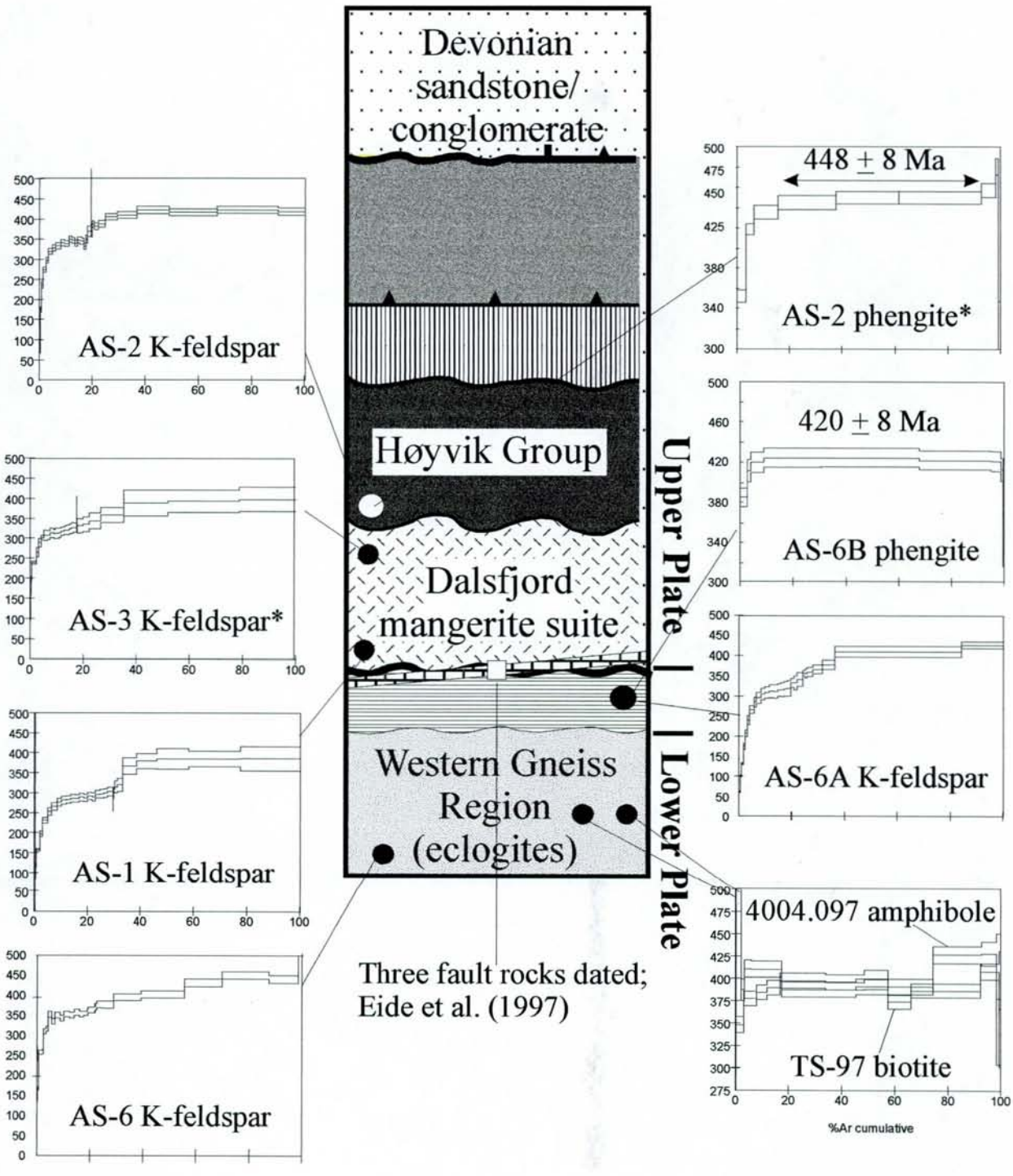
Devonian sandstone/ conglomerate
Høyvik Group
Dalsfjord mangerite suite
Western Gneiss Region (eclogites)
Upper Plate
Lower Plate
Three fault rocks dated; Eide et al. (1997)
AS-2 K-feldspar
AS-3 K-feldspar*
AS-1 K-feldspar
AS-6 K-feldspar
448 ± 8 Ma
AS-2 phengite*
420 ± 8 Ma
AS-6B phengite
AS-6A K-feldspar
4004.097 amphibole
TS-97 biotite
%Ar cumulative

Figure 2

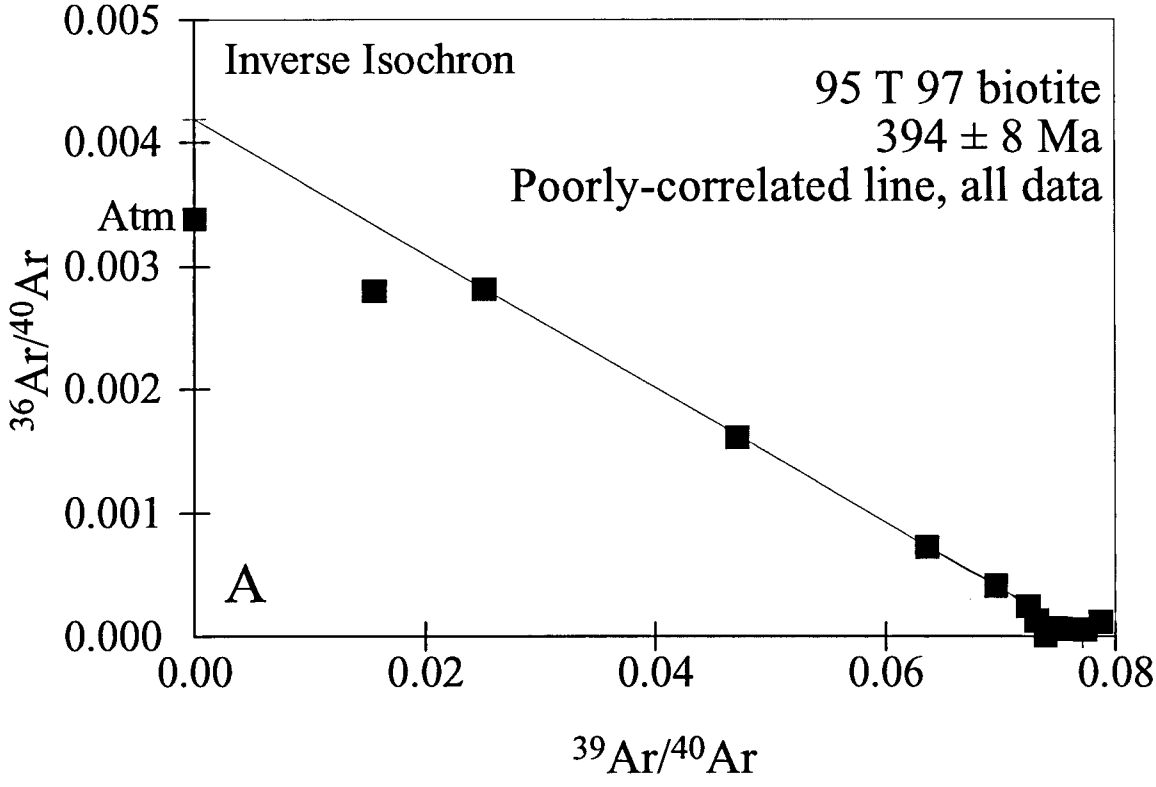
Inverse Isochron
95 T 97 biotite
394 ± 8 Ma
Poorly-correlated line, all data
Atm
A
0.005
0.004
0.003
0.002
0.001
0.000
0.00
0.02
0.04
0.06
0.08
36Ar/40Ar
39Ar/40Ar

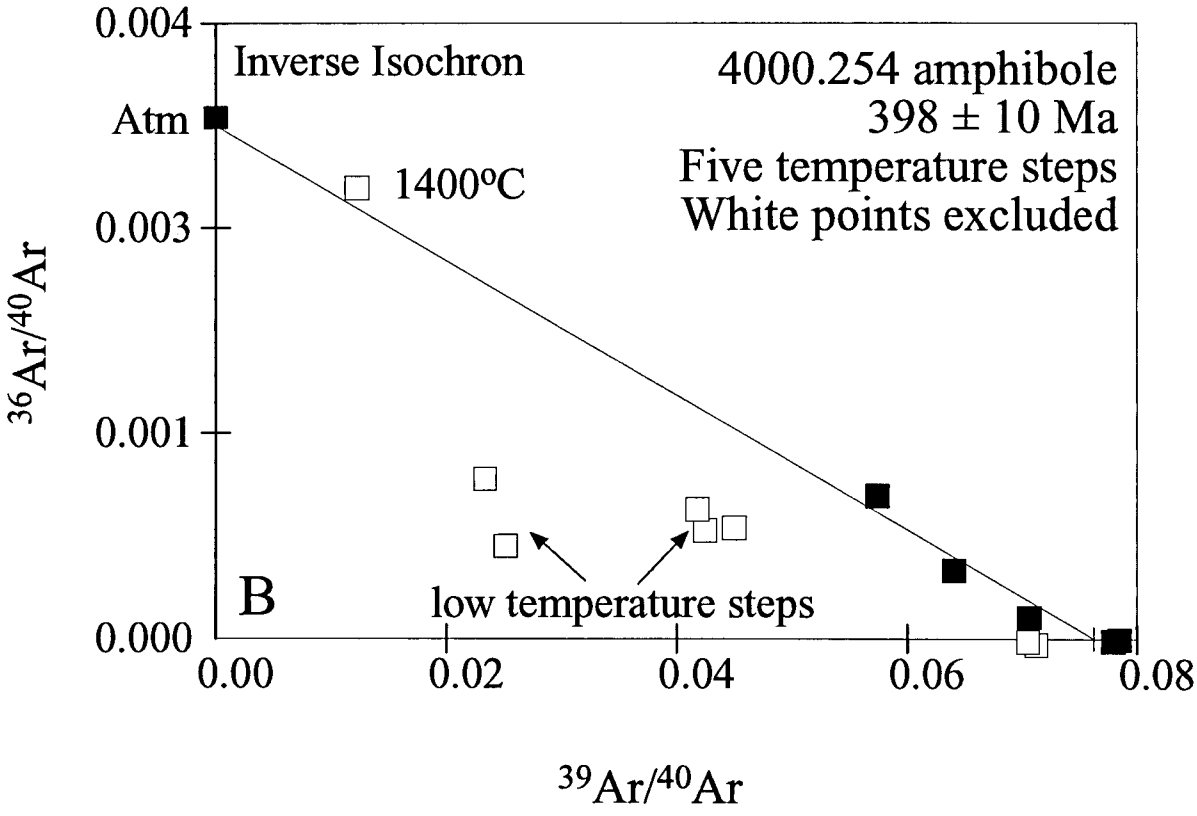
Inverse Isochron
4000.254 amphibole
398 ± 10 Ma
Five temperature steps
White points excluded
1400°C
Atm
B
low temperature steps
0.004
0.003
0.001
0.000
0.00
0.02
0.04
0.06
0.08
36Ar/40Ar
39Ar/40Ar

Figure 3

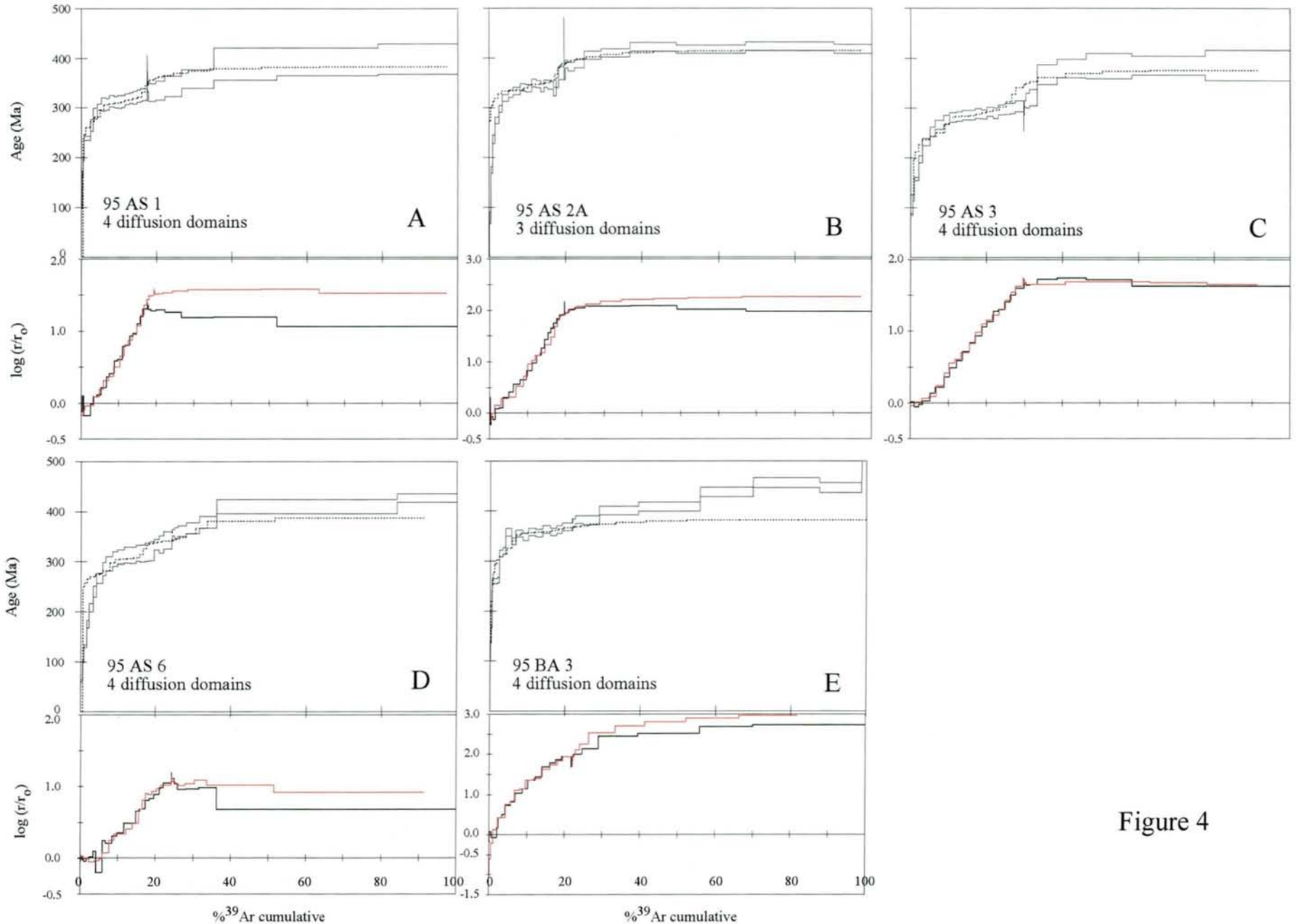
Age (Ma)
log (r/r$_o$)
95 AS 1
4 diffusion domains
A
95 AS 2A
3 diffusion domains
B
95 AS 3
4 diffusion domains
C
95 AS 6
4 diffusion domains
D
95 BA 3
4 diffusion domains
E
%^{39}Ar cumulative
%^{39}Ar cumulative

Figure 4

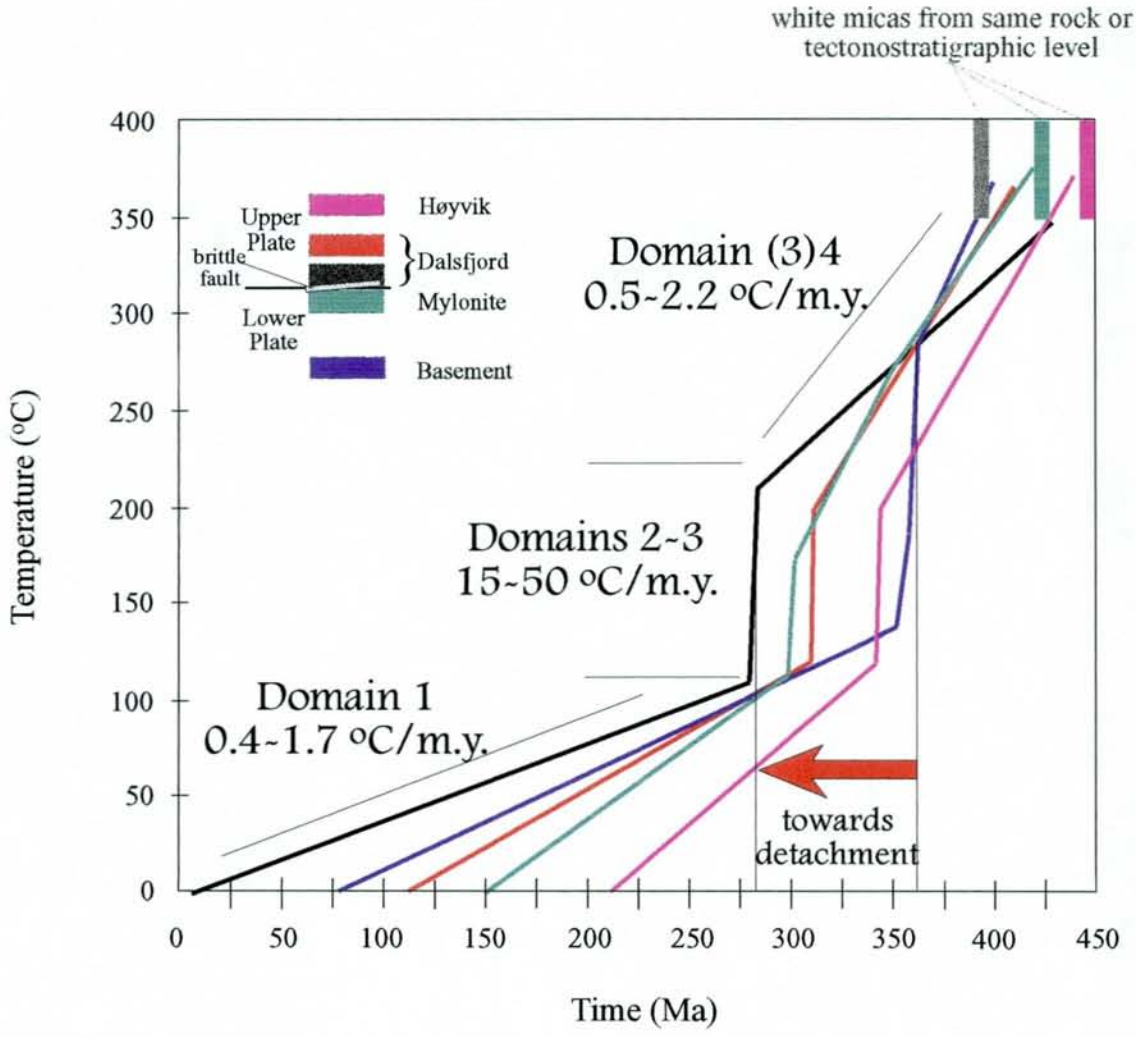
white micas from same rock or tectonostratigraphic level
Upper Plate
brittle fault
Lower Plate
Høyvik
Dalsfjord
Mylonite
Basement
Domain (3)4
0.5-2.2 °C/m.y.
Domains 2-3
15-50 °C/m.y.
Domain 1
0.4-1.7 °C/m.y.
towards detachment
Temperature (°C)
Time (Ma)
0
50
100
150
200
250
300
350
400
450

Figure 5

Chapter 6

Published as:

Carboniferous age for the East Greenland 'Devonian' Basin: Paleomagnetic and isotopic constraints on age, stratigraphy, and plate reconstructions.

Hartz, E.H., Torsvik, T.H. & Andresen, A.

in *Geology* v. 25, 675-678, 1997

Carboniferous age for the East Greenland "Devonian" basin: Paleomagnetic and isotopic constraints on age, stratigraphy, and plate reconstructions

SPECIAL REPORT

E. H. Hartz* Department of Geology, University of Oslo, Box 1047, 0316 Oslo, Norway

T. H. Torsvik NGU, Box 3006 Lade, N-7002 Trondheim, Norway, *and* Institute of Solid Earth Physics, University of Bergen, N-5002 Bergen, Norway

A. Andresen Department of Geology, University of Oslo, Box 1047, 0316 Oslo, Norway

ABSTRACT

New paleomagnetic and isotopic data from East Greenland indicate that this classical "Devonian" basin was partly formed in Carboniferous. The basin preserves a stratigraphically linked magnetic reversal pattern of primary character. Paleomagnetic data indicate that the two stratigraphically lowermost intrabasinal angular unconformities, identified on each side of the basin, in fact correlate as one unconformity. This implies a 2 km reduction of the estimated basin thickness, and thus that the unconformity represents a major depositional hiatus. Successions below the unconformity are taken to be Devonian (Givetian) in age, on the basis of correlation with paleomagnetic reference poles. However, we argue that the overlying strata are Carboniferous, rather than Devonian, in age, on the basis of a ca. 336 Ma $^{40}Ar/^{39}Ar$ extrusive age for a basalt flow and paleomagnetic data. A Carboniferous age for the strata has significant implications for vertebrate evolution; fossils of a terrestial tetrapod, *Ichthyostega*, are found above the unconformity. *Ichthyostega* is regarded as the earliest fossil of an animal known to walk on land; however, our data suggest that these dry footsteps are much younger than previously believed. Our results are also significant for plate reconstructions. Paleomagnetic data indicate that the lower part of the basin was deposited at low southerly latitudes. Sediments above our Early Carboniferous unconformity were deposited approximately at lat 4°N, indicating that the continent had drifted northward. A minor pole-longitude misfit between Devonian and Carboniferous poles from East Greenland and North America implies (1) a closer pre–Labrador Sea Greenland–North America fit; (2) counterclockwise block rotations (10°–15°) of the study area; or (3) a combination of both. The East Greenland "Devonian" basin formed along the Caledonian spine of Euramerica, and counterclockwise block rotation may have occurred between sinistral faults resulting from continued relative movement between Baltica and Laurentia during Devonian and Carboniferous time.

INTRODUCTION

The East Greenland "Devonian" basin formed as an intramontane supradetachment basin (Hartz and Andresen, 1995) within the Caledonian orogen (Bütler, 1959; Haller, 1971). Devonian deposits generally are in large north-south–trending grabens, most recently suggested to be controlled by major left-lateral faults (Larsen and Bengaard, 1991). Herein we report the first paleomagnetic data from the East Greenland Devonian deposits. These data cast doubts on the proposed Devonian age of the entire basin sedimentary succession and challenge traditional facies correlations across the basin.

GEOLOGIC SETTING AND PALEOMAGNETIC SAMPLING

Devonian deposits unconformably overlie Late Proterozoic to Ordovician sedimentary rocks and, in some localities, overlie Precambrian gneiss (Fig. 1A; Bütler, 1959). Basin fill is estimated to be >8 km thick and consists mainly of coarse terrestrial clastics and minor fine-grained lacustrine deposits (Olsen and Larsen, 1993). Bütler (1959) reported that the stratigraphy of the basin can be divided into the following four series: the Basis series, suggested to be late-Middle Devonian (Givetian); the late Givetian to Frasnian Kap Kolthoff series; the early Famennian Kap Graah series; and the Famennian Celsius Bjerg series. Each series is separated by angular unconformities, and the ages are identified on the basis of vertebrate fossils (Jarvik, 1961; Friend et al., 1983).

In a reexamination of the lithostratigraphy of the basin, Olsen and Larsen (1993) divided the deposits into four new groups based on sedimentary facies correlations. Their revised stratigraphy combines rocks across marked angular unconformities, however, which we find awkward. We therefore favor the stratigraphic subdivision proposed by Bütler (1959). Our studies have focused on paleomagnetic and isotopic sampling of the Basis, Kap Kolthoff, and Kap Graah series in two

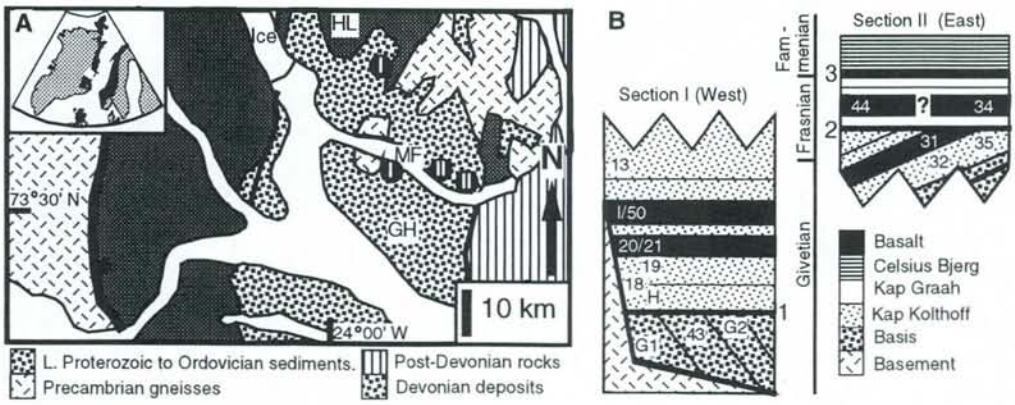

Figure 1. A: Map of field area in East Greenland. Location is marked by white box in index map, where black marks extent of Caledonides before opening of North Atlantic Ocean. Thin lines—faults; thick lines—fjord region detachment zone; black circles—sample locations; MF—Moskusoksefjord; HL—Hudson Land; GH—Gauss Halvø (I/II marks section I and II, each compiled from two localities). B: Simplified stratigraphic column of Devonian deposits in Moskusoksefjord is after Bütler (1959). Numbers within columns refer to sampling sites. Thin lines mark bedding and thick lines mark unconformities (1, 2, and 3).

*E-mail: ebbe.hartz@geologi.uio.no.

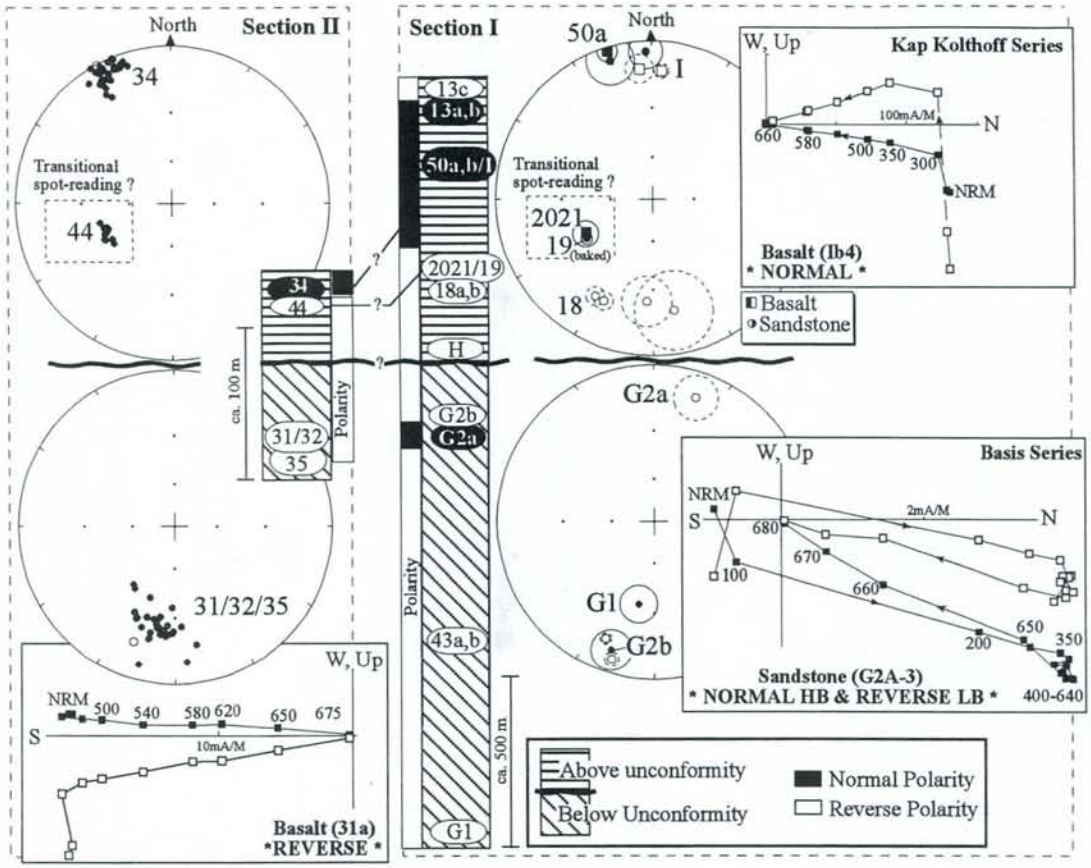

Figure 2. Examples of thermal demagnetization, approximate sampling positions, magnetostratigraphy, and suggested paleomagnetic correlation between sections I and II. Note that unconformities in two sections are correlated rather than placing section II on top of section I, i.e., introducing second unconformity (Fig. 1B). In Zijderveld diagrams, solid symbols represent points in horizontal plane, open symbols represent points in vertical plane. In stereoplot, closed symbols represent positive inclinations, open symbols represent negative inclinations. All data are shown in bedding-corrected coordinates. Section II stereoplots show individual sample directions, whereas section I stereoplots, for reasons of simplicity, are shown as site-mean directions with α_{95} confidence circles.

TABLE 1. MEAN DIRECTIONS OF EAST GREENLAND "DEVONIAN" BASIN (LAT. 73.7°N, LONG. 23.7°W)

	In-situ					Bedding corrected			
S/P	Dec	Inc	N	α_{95}	k	Dec	Inc	α_{95}	k
Above unconformity:									
I/N	353.1	-1.4	5	16.9	21.5	352.6	-2.4	11.7	43.4
I/R	193.5	-21.9	4	21.8	18.7	192.4	-20.6	21.3	19.6
II /N	333.9	3.8	33*	1.7	213.3	333.5	4.8	1.7	213.3
C/M	358.8	8.6	10	14.6	11.9	358.1	7.6	13.4	14.0
Paleomagnetic south-pole:									
Latitude = 20.1°S, Longitude = 338.3°E, dp/dm = 6.8°/13.5°									
Below unconformity:									
I/N	020.4	6.1	11*	9.7	23.3	019.1	-10.5	9.7	23.3
I/R	194.7	-3.0	4	28.0	11.7	197.7	6.1	24.6	14.9
II/R	176.3	13.5	3	6.4	377	190.5	22.5	7.7	256.6
C/M	188.5	3.0	8	14.6	15.4	195.2	13.0	11.6	23.9
Paleomagnetic south-pole:									
Latitude = 9.1°S, Longitude = 321°E, dp/dm = 6°/11.8°									
Anomalous basalt sites:									
Combined I (44), II (20 and 21/ baked sandstone 19); cf. Figs. 2 & 3 and text									
	244.1	40.8	3	13.3	87.5	243.7	42.0	11.7	111.5

Note: S/P = Section and polarity (C/M = Combined/ Mixed)
Dec/Inc = mean declination/ inclination.
N = number of sites (or samples *) (total number of samples included in statistics = 374).
α_{95} = 95% confidence circle.
k = precision parameter.
dp/dm = semi-axis of the 95% confidence ovals.

sections across two previously defined intrabasinal unconformities (Fig. 1, A and B).

Section I

The Basis series represents the oldest Devonian deposits in East Greenland (Fig. 1B; Bütler, 1959). The unit is only exposed in west-central Moskusoksefjord (Fig. 1A) and consists of conglomerates interfingering with red sandstones which dip 35° to 70° eastward (sites G1, 43, and G2). The Kap Kolthoff series is between the first and second intrabasinal unconformities, and the lowermost part of this series was sampled in east-central Moskusoksefjord (Fig. 1A, sites H, 18, and 19). The stratigraphically highest of these sites (site 19) was sampled directly below a 10-m-thick basalt flow (sites 20 and 21). A second basalt flow located 250 m stratigraphically above the first basalt was also sampled in two sites (sites 1 and 50). In the upper part of the Kap Kolthoff series, a red conglomeratic sandstone, the Snehvide Formation of Olsen and Larsen (1993), was sampled at two localities at east-central Dybendal (Fig. 1A, site 13).

Section II

In eastern Moskusoksefjord, the Basis and Kap Kolthoff series are mapped as conformable and are separated from the Kap Graah series by an angular unconformity (Fig. 1B; Bütler, 1959). Sandstone and basalts of the Kap Kolthoff series were sampled in three sites (Fig. 1B; sites 31, 32, and 35). Basalts within the lowermost Kap Graah

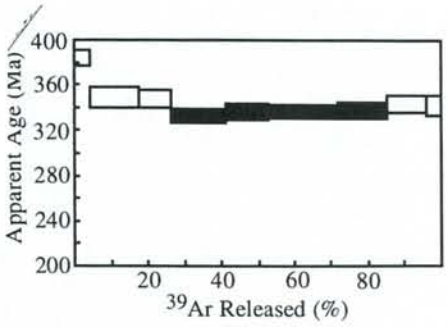

Figure 3. Furnace step-heating spectra for plagioclase from lowermost basalt in Kap Graah series (site 44). Shaded steps (4–7, 59.1% of released ^{39}Ar) define near-plateau age of 335.6 ± 3.1 Ma (2σ confidence level, including J-value). These steps all yield >90% radiogenic ^{40}Ar.

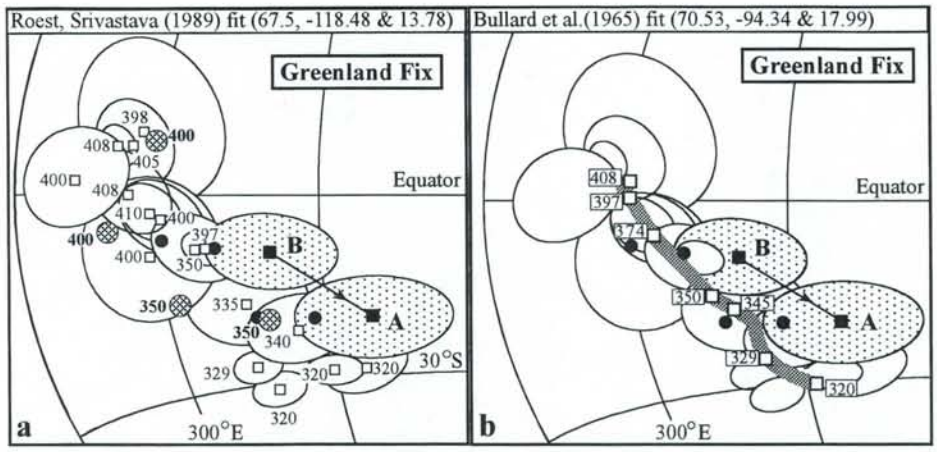

Figure 4. a: Devonian and Carboniferous poles from Laurentia (North America and Scotland; open squares with 95% confidence ovals) and Baltica (patterned larger circles with bold age numbers) in North American coordinates (Bullard et al., 1965, fit, lat 88°N, long 27°W, Euler angle = –38°) and subsequently rotated into Greenland coordinates (Labrador Sea closed) using fit of Roest and Srivastava (1989). Reference poles 410–320 Ma were listed in Torsvik et al. (1996) (except entry 20 in Table 1). b: As in a, but using Bullard et al. (1965) fit for Labrador Sea reconstruction (Euler pole and rotation angle calculated from their Greenland-Europe and Europe–North America fits). For diagram simplicity, only Laurentia error ellipses and smooth spline path derived from Laurentia and Baltica data (smoothing parameter = 200; graded according to Q-factor; cf. procedure in Torsvik et al., 1996) are shown. In both fits, Greenland poles plot to east but overlap with Devonian and Carboniferous poles. Misfit is best reduced with original Bullard et al. (1965) fit. Misfit can also be reduced by invoking local block rotations on vertical axes for poles B (below unconformity) and A (above unconformity). Black circles indicate effect of compensating for local counterclockwise rotations about vertical axis in 10° and 20° steps. Note that pole A is in much better correspondence with Early Carboniferous poles than previously claimed Devonian (Frasnian) age.

series were sampled directly above this locality (Fig. 1B, site 34). The lowest basalt horizon in the Kap Graah series was also sampled 10 km farther northwest (site 44). Within the ~10-m-thick basalt horizon, thin (<5 cm) layers of sand are discernible, indicating that some basalt horizons may include more than one flow.

PALEOMAGNETIC RESULTS

The natural remanence magnetization (NRM) was measured with a JR5A (Trondheim) and a 2G Squid (Ann Arbor) magnetometer. The NRM stability of 430 samples was tested by stepwise thermal demagnetization (MMTD60 furnace), and ancient remanence components were isolated using a least square algorithm.

In section I, at least four polarity transitions are identified, and in two red sandstone units (G2 and 13) both polarities occasionally were identified in individual samples (Fig. 2, site G2A). Characteristic remanence components in red sandstones are carried by hematite; this is also commonly the case for the basalts (Fig. 2), which are typically of high-temperature deuterically oxidized (class II–III) character, remanence being carried by low-titanium titanomagnetites and hematite. Sites below the Basis–Kap Kolthoff unconformity (section I) are dominated by reverse polarity directions and south-southwest declinations and positive inclinations (Fig. 2). The overlying strata are dominated by normal polarity components and north-northwest declinations.

The angular unconformity in section II previously has been interpreted to represent the second unconformity in the Devonian basin (Fig. 1B). However, paleomagnetic directions from sections I and II concur extremely well (Fig. 2 and Table 1), indicating that the two unconformities are in fact the same. Note, for example, the directional similarity between basalt site 34 of section II with normal polarity sites from section I (above unconformities), and south-southwest–directed reverse polarity directions with positive inclinations (sites 31, 32 and 35, Section II) that match sites G1 and G2b from section I (Fig. 2 and Table 1). The unusual paleomagnetic signature of samples from basaltic sites 44 (section II) and 20/21 (section I) provides an important correlation "fingerprint" (Fig. 2). The basalt above the unconformity in section I and II represents the same flow and not two separate flows, as previously thought. Anomalous directional results from these basaltic flows (44 and 20/21) are interpreted as a spot reading during a field reversal (probably reverse [R] to normal [N]; sites 18 [R] → 20/21 [transitional] → 50/I [N]). Remagnetization of both flows is ruled out, because this anomalous, steep, positive, west-southwest direction is not compatible with any Devonian or younger directions from Laurentia. In addition, sites 18 and 19 provide a positive contact test; baked sandstone (site 19) directionally conforms to the overlying basalts (site 20/21), whereas sandstones from site 18 (20 m below 20/21) yield southwesterly declinations and negative inclinations (Fig. 2).

Fold tests were statistically insignificant at the 95% confidence level. However, sites above both unconformities are practically flat lying, whereas sites below unconformities have north-northeast–south-southwest fold axes that are subparallel to the remanence directions. The stratigraphically linked reversal pattern, when combined with the transitional directions in both sections (Fig. 2), clearly indicates a primary, early diagenetic origin of the remanence components.

$^{40}Ar/^{39}Ar$ RESULTS

Plagioclase from the basalt flow at site 44 was dated by $^{40}Ar/^{39}Ar$ furnace step heating at the Massachusetts Institute of Technology (MIT) argon laboratory. The release spectrum yields a near-plateau age of 335.6 ± 3.1 Ma. (Fig. 3). Analytical and statistical details follow those in Hodges and Bowring (1995), except that a newer version (3.1.3) of the MIT Ar isotopic analysis program was used. The plagioclase cooling age is interpreted to date the time of extrusion of the basaltic lava.

DISCUSSION

The paleomagnetic signatures across the Basis–Kap Kolthoff and Kap Kolthoff–Kap Graah unconformities in the eastern and western side of the Devonian basin are broadly similar. Therefore, we argue that they are time correlative and do not represent two different unconformities within the basin. This implies that the cumulate stratigraphic thickness of the basin actually is <6 km, rather than the earlier reported >8 km. A stratigraphic link between the two unconformities at each side of the basin is not depicted in existing maps or profiles (Bütler, 1959; Olsen and Larsen, 1993). Additional mapping is needed to evaluate the validity of the new proposed structural and stratigraphic model of the basin.

Paleomagnetic poles from below (B, Fig. 4) and above (A, Fig. 4) the first Devonian unconformity are significantly different. Compared with

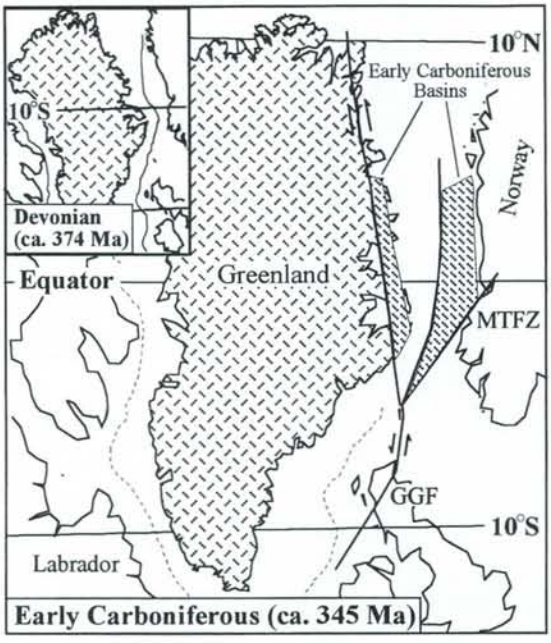

Figure 5. Early Carboniferous reconstruction (inset: mid-Late Devonian reconstruction) based on combined Laurentia and Baltica smooth path (Fig. 4b). Labrador Sea and North Atlantic reconstruction used Bullard et al. (1965) fits, which minimize paleomagnetic pole misfit (see Fig. 4). Paleomagnetic south poles (North American coordinates) used for reconstructions are 8.6°S and 288.1°E (ca. 374 Ma) and 21.5°S and 300.8°E (ca. 345 Ma; based on smooth path in Fig. 4b). GGF—Great Glen fault system; MTFZ—Møre-Trøndelag fault zone. Patterns show proxy Early Carboniferous basins of North Atlantic region.

Laurentian (North America and Scotland) and Baltic poles, pole B partly overlaps Middle to Late Devonian poles (Givetian and Frasnian), whereas pole A plots within the Early Carboniferous (Fig. 3B). The latter relation is at clear variance with the previously postulated Late Devonian, or Frasnian, age (ca. 377–367 Ma; Harland et al., 1990). The paleomagnetic reference poles for this time interval are not well constrained (Fig. 4). Pole A, however, clearly plots in the vicinity of Carboniferous reference poles, and within the 345–329 Ma segment of a combined Laurentia-Baltica apparent polar wander path (Fig. 4B). A Carboniferous age is further confirmed by the ca. 336 Ma $^{40}Ar/^{39}Ar$ age from the lowermost basalt (site 44) in the Kap Graah series.

If this Carboniferous age is representative, it has serious paleontological and evolutionary implications. The tetrapod *Ichthyostega* (Jarvik, 1961), regarded as the earliest well-preserved fossil of animals that walked on land, occurs in the deposits above our sampling sites. *Ichthyostega*, found in the Celsius Bjerg series, had been regarded as having evolved during the mid–Late Devonian (Fammenian) (Jarvik, 1961; Friend et al., 1983).

The East Greenland poles overlap with the Laurentia and Baltic poles after reconstructing the Labrador Sea, and the collective data imply a near-equatorial position of Greenland (Fig. 5) during Late Devonian and Early Carboniferous time. A minor, systematic, easterly offset of both Greenland poles is indicated by our data when compared with published reference poles (Fig. 4); the overall misfit of these poles is, however, minimized in a Bullard et al. (1965) fit. This may indicate that the amount of pre-drift, Labrador Sea extension previously has been underestimated. Alternatively, the fits can be improved by invoking Late Devonian to Early Carboniferous, local, counterclockwise block rotation of the basin. Because Baltica had docked obliquely against Laurentia from the south (Torsvik et al., 1996), the resulting sinistral transpression could have caused strain partitioning between local rotations, folding, and left-lateral faulting. Although we envision the "Devonian" basin of East Greenland as a supradetachment basin (Hartz and Andresen, 1995), rather than a basin controlled by strike-slip faults (Larsen and Bengaard, 1991), such local block rotations are compatible with a link to well-known left-lateral faults within the Caledonian orogen, such as the Great Glen fault in Scotland and/or the Møre-Trøndelag fault zone in west-central Norway (Fig. 5).

ACKNOWLEDGMENTS

Field work was made possible through financial support from Vista, Hydro, Saga, Statoil, and the Norwegian Research Council (grant 100306/431 to Andresen). Torsvik acknowledges additional financial support by Mobil and Phillips (Onoff/3). We thank the Danish Polar Center for logistical support, SIRIUS (the Danish Military dogsled patrol) for letting us use their huts, and Bill Olzewski and Kip Hodges, MIT argon laboratory, for assistance with the isotopic dating. We thank Mark Steltenpohl for valuable comments and Rob van der Voo and Neil Opdyke for reviews.

REFERENCES CITED

Bullard, E. C., Everett, J. E., and Smith, A. G., 1965, The fit of the continents around the Atlantic, *in* A symposium on continental drift: Royal Society of London Philosophical Transactions, ser. A, v. 258, p. 41–51.

Bütler, H., 1959, Das Old Red-Gebiet am Moskusoksefjord: Meddelelser om Grønland, v. 160, p. 182.

Friend, P. F., Alexander-Marrack, P. F., Allen, K. C., Nicholson, J., and Yeats, A. K., 1983, Devonian sediments of East Greenland, VI: Review of results: Meddelelser om Grønland, v. 206, 96 p.

Haller, J., 1971, Geology of the East Greenland Caledonides: New York, Interscience, 415 p.

Harland, W. B., Armstrong, R. L., Cox, A., Craig, L. E., Smith, A. G., and Smith, D. G., 1990, A geologic time scale 1989: Cambridge, United Kingdom, Cambridge University Press, 263 p.

Hartz, E., and Andresen, A., 1995, Caledonian sole thrust of central East Greenland: A crustal-scale Devonian extensional detachment?: Geology, v. 23, p. 637–640.

Hodges, K. V., and Bowring, S. A., 1995, $^{40}Ar/^{39}Ar$ thermochronology of isotopically zoned micas: Insights from the southwestern USA Proterozoic orogen: Geochimica et Cosmochimica Acta, v. 59, p. 3205–3220.

Jarvik, E., 1961, Devonian vertibrates, *in* Raasch, G. O., ed., Geology of the Arctic, Volume 1: Toronto, Ontario, University of Toronto Press, p. 197–204.

Larsen, P. H., and Bengaard, H. J., 1991, The Devonian basin initiation in East Greenland: A result of sinistral wrench faulting and Caledonian extensional collapse: Geological Society of London Journal, v. 148, p. 355–368.

Olsen, H., and Larsen, P-H., 1993, Lithostratigraphy of the continental Devonian sediments in North-East Greenland: Grønland Geologiske Undersøgelser Bulletin, v. 165, 108 p.

Roest, W. R., and Srivastava, S. P., 1989, Sea-floor spreading in the Labrador Sea: A new reconstruction: Geology, v. 17, p. 1000–1003.

Torsvik, T. H., Smethurst, M. A., Meert, J. G., Van der Voo, R., McKerrow, W. S., Brasier, M. D., Sturt, B. A., and Walderhaug, H. J., 1996, Continental break-up and collison in the Neoproterozoic and Palaeozoic—A tale of Baltica and Laurentia: Earth-Science Reviews, v. 40, p. 229–258.

Manuscript received April 4, 1997
Revised manuscript received May 12, 1997
Manuscript accepted May 20, 1997